



UNIVERSITÀ  
DEGLI STUDI  
DI PADOVA

Sede Amministrativa: Università degli Studi di Padova

Dipartimento di Scienze Chimiche

SCUOLA DI DOTTORATO DI RICERCA IN: SCIENZE MOLECOLARI

INDIRIZZO: SCIENZE CHIMICHE

CICLO XXVII

## **Molecular and nanodimensional metal based systems for the therapy against neurodegenerative diseases**

**Direttore della Scuola :** Ch.mo Prof. Antonino Polimeno

**Supervisore:** Prof. Mauro Carraro

**Dottorando:** Antonio Sorarù

**31 Gennaio 2015**







## Summary

**Reactive oxygen species (ROS) are harmful species produced during metabolic processes**, such as photosynthesis and respiration, of living organism. In both case, the substrate (oxygen/water) undergoes several multi electronic reaction, during which some electrons can “escape” from the catalytic cycle and produce ROS, such as superoxide radical anion, hydrogen peroxide, hydroxyl radical and other derivatives. These species are really dangerous, since they are able to oxidize almost all cellular components. **Indeed they can damage lipids, proteins, DNA, affecting cellular functions till cell death.** **Under oxidative stress condition, accumulation of damage due to ROS has been supposed to play a role in several pathologies, and in particular in age-related ones, such as Alzheimer’s disease (AD).** This disease is characterized by an accumulation of neurotoxic senile plaques, mainly made of short peptide monomers, that tend to aggregate into fibrils, called amyloid  $\beta$  peptide ( $A\beta$ ). Although the mechanism involved in the production of these peptides is still unknown, some hypothesis suggest that ROS are produced within the fibrils and are responsible for further  $A\beta$  production.

Nature has developed different catalytic strategies to limit ROS production, and the most important is the enzymatic pathway: superoxide dismutases (SOD) and catalase (CAT) enzymes are able to dismutate, respectively, superoxide and hydrogen peroxide. Nevertheless, **in case of unpaired ROS production it is of huge interest to find new artificial systems that are able to help natural enzymes in their task. In this thesis, four different classes of synthetic enzymes (synzymes) that mimic natural anti ROS systems have been investigated:**

- I. Isostructural **mononuclear manganese complexes**, with general formula  $[Mn(L)X_2]$ , characterized by a pentadentate ligand L, containing different heteroatoms (N, O or S) have been used for the dismutation of hydrogen peroxide and superoxide anion. Their activity, also depending on heteroatoms, and stability were studied, first in organic solvents to have a comparison with literature similar compounds, then in aqueous solution, where only few compounds were known to work. **The sulfur-containing complex  $[Mn(L)(OTf)_2]$  was found to exhibit high dual SOD/CAT-like activity with excellent stability, when used in the presence of a base.**

- II. Isostructural **dinuclear manganese complexes**, with general formula  $[\text{Mn}_2\text{L}_2\text{X}]$ , were widely studied as artificial catalases. A comparison with other dimanganese complexes, in terms of Michealis-Menten parameter,  $K_M$  and  $k_{\text{cat}}$ , was performed. Superoxide dismutase activity was also evaluated, demonstrating the **unique dual SOD/CAT behavior of  $[\text{Mn}_2\text{L}_2\text{X}]$  with respect to other dinuclear complexes**. Finally, the **ligands were modified with mitochondriotropic functionalities**. In particular, two fluorescent rhodamine derivatives and a triphenylphosphonium salt, were taken into account.
- III. Some **multimetallic manganese oxoclusters**, containing 6-13 manganese atoms, were synthesized during a Short Term Scientific Mission in Dublin, in the group of Prof. Wolfgang Schmitt. **The catalase-like activity of these compounds was tested for the first time**. Their  $\text{H}_2\text{O}_2$  dismutation capability was thus demonstrated and their stability in aqueous environment was checked. Preliminary test as SOD mimics were also performed.
- IV. In the end, a completely inorganic compound, a **polyoxometalate (POM) substituted with four ruthenium atoms, with formula  $[\text{Ru}_4\text{O}_4(\text{OH})_2(\text{H}_2\text{O})_4(\gamma\text{-SiW}_{10}\text{O}_{36})_2]^{10-}$** , able to dismutate hydrogen peroxide was studied. Its activity in different biological buffers and media was initially optimized. **Its capability of interaction with A $\beta$  peptides, coupled with its catalase activity, were exploited to control these two major events involved in Alzheimer's disease. Preliminary test on neuronal cells were then performed** (with Dr.ssa de Bartolo (ITM-CNR, Rende, CS)), **confirming the interesting properties of the compound *in vitro* and finding a very low toxicity**. Finally, **encapsulation of POM was achieved in order to enables delivery and targeting in cells**, using polymeric multilayer biocompatible microcapsules in which POM is deposited. The presence of POM and its catalytic activity were confirmed and analyzed.

## Riassunto

Le reazioni biochimiche che coinvolgono il trasferimento di elettroni dall'ossigeno per dare acqua, durante la respirazione cellulare, e dall'acqua per dare ossigeno, durante la fotosintesi, possono portare alla formazione di specie reattive dell'ossigeno (ROS, reactive oxygen species), dovute alla "perdita" di elettroni dal ciclo catalitico. Tra queste specie troviamo inizialmente il superossido  $O_2^-$ , l'acqua ossigenata e il radicale ossidrile. Queste possono reagire con altre molecole per dare origine ad altre specie reattive, per esempio dell'azoto, ma soprattutto **possono danneggiare peptidi, lipidi e DNA e causare ingenti danni alle funzioni cellulari** fino a portare alla morte della cellula stessa. In condizioni di stress ossidativo, **l'accumulo di queste specie sembra giocare un importante ruolo nelle malattie degenerative, come ad esempio il morbo di Alzheimer (AD)**. In questo caso, la malattia è caratterizzata dalla presenza di aggregati proteici in forma di placche, che hanno un effetto neurotossico. Questi accumuli proteici sono costituiti principalmente da peptidi di 40-42 amminoacidi chiamati  $\beta$ -amiloidi ( $A\beta$ ), che tendono ad aggregare, in forma di fibrille. Le cause della formazione e accumulo di questi peptidi non sono ancora del tutto chiare, ma si hanno evidenze sul coinvolgimento delle ROS nella fase di formazione dei peptidi, e sull'aumento della loro produzione, dopo la formazione delle fibre, a causa di reazioni mediate dai metalli intrappolate nelle fibre stesse.

La natura ha sviluppato dei sistemi per proteggersi da queste specie reattive, tra questi citiamo gli enzimi superossido dismutasi (SOD) e catalasi (CAT), capaci rispettivamente di eliminare superossido e acqua ossigenata, che tuttavia in certe situazioni di elevato stress ossidativo possono risultare insufficienti per prevenire i danni.

È quindi di estremo interesse lo studio di composti artificiali capaci di aiutare gli enzimi naturali nel loro compito di eliminare le ROS dall'ambiente biologico. Considerando ciò, **in questa tesi sono state considerate le seguenti quattro classi di composti, utilizzati come enzimi sintetici (*synzymes*), per imitare le funzioni dei sistemi anti ROS naturali:**

- I. Complessi **mononucleari ed isostrutturali di manganese**, di formula generale  $[Mn(L)X_2]$ , caratterizzati da un legante pentadentato, L, contenente differenti eteroatomi (N, O, o S), sono stati studiati nella dismutazione dell'acqua ossigenata e del radicale anione superossido. L'attività è stata inizialmente analizzata in

solvente organico (acetonitrile) per aver dei termini di paragone con altri composti di letteratura. In seguito l'attività è stata studiata anche in acqua, dove solo pochi composti di letteratura sono risultati attivi. **Se utilizzati in presenza di base, i complessi  $[\text{Mn}(\text{L})(\text{OTf})_2]$  contenenti zolfo mostrano una duplice attività SOD/CAT ed un'elevata stabilità.**

- II. **Complessi dinucleari ed isostrutturali di manganese**, di formula generale  $[\text{Mn}_2\text{L}_2\text{X}]$ , sono stati studiati inizialmente per l'eliminazione dell'acqua ossigenata. Un confronto con simili composti di letteratura è stato effettuato tramite il calcolo dei parametri, derivati dall'equazione di cinetica enzimatica di Michalis-Menten,  $K_M$  e  $k_{\text{cat}}$ . È stata anche analizzata la capacità di smaltire il superossido, **dimostrando le caratteristiche uniche di  $[\text{Mn}_2\text{L}_2\text{X}]$  nella duplice attività CAT/SOD, in ambiente acquoso, rispetto ad altri complessi dinucleari.** Infine, modificando i leganti, si è cercato di introdurre nuove funzionalità adatte alla veicolazione del composto in cellula. In particolare, **sono stati utilizzati residui organici noti per la loro affinità verso i mitocondri**, come i derivati della rodamina e i sali di trifenilfosfonio.
- III. Sono stati studiati **oxoclusters multimetallici di manganese**, contenuti 6-13 atomi di metallo, sintetizzati durante un Short Term Scientific Mission (STSM, COST action CM1203) a Dublino, presso il laboratorio del Prof. Wolfgang Schmitt, analizzandone per la prima volta l'attività di dismutazione dell'acqua ossigenata e del superossido, oltre che la stabilità in soluzioni acquose.
- IV. Un composto completamente inorganico, un **poliossometallato (POM) contenete quattro atomi di rutenio, di formula  $[\text{Ru}_4\text{O}_4(\text{OH})_2(\text{H}_2\text{O})_4(\gamma\text{-SiW}_{10}\text{O}_{36})_2]^{10-}$** , è considerato per la sua solubilità in ambiente acquoso e la capacità di dismutare efficacemente l'acqua ossigenata. L'attività è stata analizzata in diversi tamponi e mezzi comunemente usati per analisi di sistemi biologici. **In soluzione, il complesso è capace di ridurre la produzione di ROS e anche di interagire con peptidi amiloidei, evitandone l'aggregazione in fibrille, dimostrandosi quindi promettente nel contrastare due importanti eventi che si verificano durante la malattia di Alzheimer.** In collaborazione con la Dr.ssa de Bartolo (ITM-CNR, Rende, CS) sono state quindi effettuate **prove preliminari in cellule neuronali, per verificare sia la tossicità del composto (che risulta essere nulla anche a**



100µM di concentrazione) che l'effettiva attività anti-ROS e anti-amiloidogenica *in vitro*.

Infine si è studiato l'inserimento del POM all'interno della *shell* di microcapsule polimeriche multistrato, con la prospettiva di controllarne la veicolazione in cellula.



# Table of contents

<b>Summary</b>	I
<b>Table of contents</b>	VII
<b>Abbreviations</b>	XI
<b>1. Introduction</b>	1
1.1. Oxidative stress and related diseases	3
1.2. Mitochondria, respiratory chain and reactive oxygen species (ROS)	9
1.3. Complexes and nanodimensional systems with CAT/SOD mimicking Activity	12
1.4. Amyloid peptides and Alzheimer's disease	16
1.5. Aim of the thesis	19
References	21
<b>2. Antioxidant activity of Manganese complexes</b>	25
2.1. Manganese complexes as artificial catalase (CAT) and superoxide dismutase (SOD): a general introduction	27
2.2. Mononuclear compounds [MnLX <sub>2</sub> ] ( <b>1-3</b> )	34
2.3. Dinuclear complex, [Mn <sub>2</sub> L <sub>2</sub> YClO <sub>4</sub> ] ( <b>4</b> ) a catalytic screening	41
2.4. Mitochondrial toxicity of <b>4</b>	47
2.5. Modification of apical ligand of dinuclear complexes with mitochondriotropic substituent ( <b>5-7</b> )	53
2.6. Conclusions	65
References	67
<b>3. Manganese oxoclusters as artificial antioxidants</b>	71
3.1. Oxoclusters, a brief overview and manganese compounds	73
3.2. Stability and catalytic activity of multi-manganese complexes ( <b>8-16</b> )	74
3.3. Conclusions	80
References	81

<b>4. Polyoxometalates against degenerative diseases</b>	83
4.1. Polyoxometalates: short description and applications in medicine	85
4.2. Catalytic activity and inhibition of Tetranuclear Ruthenium (IV) polyoxometalate $\text{Na}_{10}[\text{Ru}_4\text{O}_4(\text{OH})_2(\text{H}_2\text{O})_4(\gamma\text{-SiW}_{10}\text{O}_{36})_2]$ ( <b>17</b> ) in water solution	90
4.3. Interaction with amyloid peptides	95
4.4. Toxicity in cell and protective effects in the presence of amyloids	106
4.5. Mitochondrial toxicity test	111
4.6. Encapsulation	115
4.7. Conclusions	121
References	122
<b>5. Conclusions</b>	125
<b>6. Experimental Part</b>	131
6.1. Materials and methods	133
6.2. Instruments	134
6.3. Synthetic procedures	135
6.4. Catalytic measurements	150
6.5. Biological tests	151
References	156
<b>Appendix</b>	I
<b>Acknowledgements</b>	





## Abbreviations

A $\beta$ : Amyloid $\beta$ or $\beta$ -Amyloid	M: Metal center (or Molecule in ESI)
ACN: Acetonitrile	MALDI: Matrix-assisted laser desorption ionization
ADP: Adenosine diphosphate	MeOH: Methanol
ATP: Adenosine triphosphate	Mops/MOPS: 3-(N-morpholino)propansulfonic acid
BBB: Blood Brain Barrier	MS: Mass spectrometry
BBS: Borate Buffer Solution	MTT: 3-(4,5-dimethylthiazol-2-yl)-2,5-diphenyltetrazolium bromide
Cat: Catalyst	NAD: Nicotinamide adenine dinucleotide
CAT: Catalase	NMR: Nuclear Magnetic Resonance
CD: Circular dichroism	NP: Nanoparticle
DMAP: Dimethylaminopiperazine	PBS: Phosphate Buffer Solution
DMSO: Dimethylsulfoxide	PEG: Polyethylenglycol
ESI: Electrospray ionization	POM: Polyoxometalate
EtOH: Ethanol	RNS: Reactive nitrogen species
FCCP: Carbonyl cyanide-4-(trifluoromethoxyphenylhydrazone)	ROS: Reactive oxygen species
FT: Fourier Transform	SOD: Superoxide dismutase
GC: Gas Chromatograph	TEA: Triethylamine
Hepes/HEPES: (4-(2-hydroxyethyl)-1-piperazineethanesulfonic acid )	Tf: Triflate
HFIP: 1,1,1,3,3,3-Hexafluoro-2-propanol	TOF: Time of flight
ICP-MS: inductive coupled plasma mass spectrometry	TPP: Triphenylphosphonium
IR: Infrared	Tris: Tris(hydroxymethyl)aminomethane
L: Ligand	UQ: Ubiquinone
$\lambda$ : Wavelength	UV-Vis: Ultraviolet-Visible
LC: Liquid chromatography	





# *1. Introduction*



## 1.1 Oxidative stress and related diseases

Aerobic eukaryotic organisms need oxygen for their bioenergetics activity. Reduction of molecular oxygen during electron transport chain, with production of water, allows ATP (Adenosine triphosphate) synthesis, the energetic fuel of cell. Instead, photosynthesis oxidize water to molecular oxygen using light to produce ATP, that is used to reduce carbon dioxide and produce glucose. Both systems involve a multi-electron transfer that allows these redox reactions. However, they are not perfect, sometimes electron transfer of respiratory chain fails and up to 4% of electrons can escape from the catalytic cycle and produce the so called Reactive Oxygen Species (ROS).<sup>1</sup>

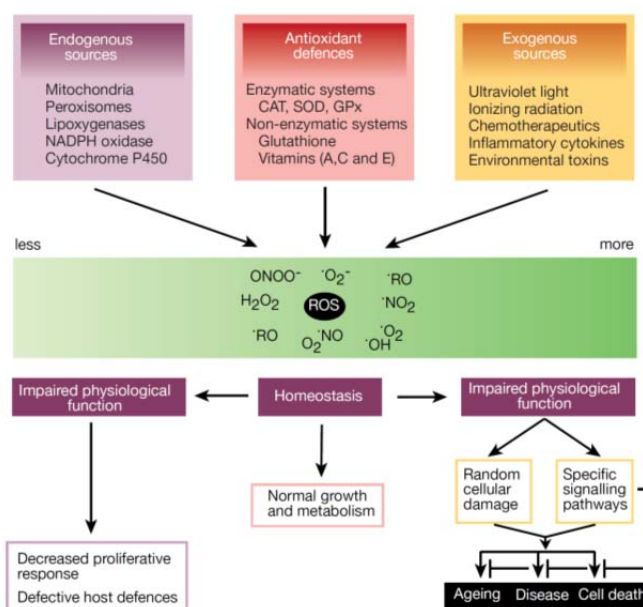
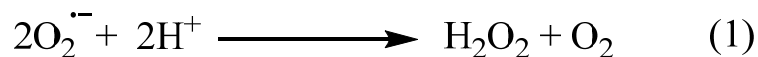


**Figure 1:** Source of cellular ROS and effects due to overproduction or deficiency of ROS.

ROS is a generic terms used to group superoxide anion ( $O_2^{\cdot-}$ ), hydroxyl radical ( $\cdot OH$ ) and hydrogen peroxide ( $H_2O_2$ ), but often it also includes reactive nitrogen species (RNS) such as peroxynitrite ( $ONOO^{\cdot}$ ) and nitric oxide ( $\cdot NO_2$ ).<sup>2</sup> Mitochondria are one of the main producer of ROS: since superoxide anion arises from the first reduction within the respiratory chain, it is called primary ROS. Subsequently, hydrogen peroxide is produced upon dismutation of superoxide, by superoxide dismutase (SOD) enzyme, which is also present in mitochondrial environment. Then hydroxyl radical can be generated from the reaction of  $H_2O_2$  with metal ions, such as  $Fe^{3+}$  and  $Cu^{2+}$ , through the so called Fenton

reaction. Hydroxyl radical is the most reactive species, the most dangerous oxygen species, with a life time of  $10^{-9}$ s (Scheme 1).<sup>3</sup>



**Scheme 1:** Dismutation of superoxide radical: hydrogen peroxide/dioxygen production by SOD (1) and Fenton reaction with formation of hydroxyl radical (2).

Under oxidative stress there is an imbalance between their production and removal that can produce damage to the cell.<sup>2,4,5</sup>

While hydroxyl radical is dangerous for its reactivity, hydrogen peroxide is dangerous because of its diffusion capability, it can indeed damage not only mitochondria, but also other cell functionalities.<sup>1</sup> If we consider that a human adult, at rest, breathes 3.5 ml  $\text{O}_2/\text{kg}/\text{min}$  and if just 1% of this goes to superoxide radical ( $\text{O}_2^{\bullet-}$ ) this leads to 53.66 moles year or about 1.72 kg/year of  $\text{O}_2^{\bullet-}$ . This number is going to increase up to 20-fold under aerobic exercise regime.<sup>6,7</sup>

In particular ROS can damage important cellular component like membrane lipids, proteins, DNA, leading to secondary products which are still dangerous, and also cause cell death. Mitochondrial DNA mutation due to ROS has been implicated in cancer, cardiac disease and type II diabetes.<sup>8</sup> ROS are implicated in several other physiological functions, including the cell signaling, which can be impaired at high concentration (Figure 1).

Due to high oxygen consumption, central nervous system is particularly vulnerable to oxidative injury, also because antioxidant molecules and enzymes concentration is relatively low and there are much more molecule prone to oxidation (for example polyunsaturated lipids).<sup>9</sup> Oxidative damage accumulates during life cycle, with related DNA, lipid, protein damage that have been proposed to play a key role in disease neurodegenerative disease.<sup>2,8,10,11</sup>

ROS can be easily eliminated by the organism, using endogenous anti-oxidant, such as thiols and polyphenols. Glutathione, for example, is a simple molecule, that contain sulfur atoms that can be easily oxidized by ROS. In this way, they are able to limit damages to other molecules, however, once oxidized, they must be reduced again, to display high effectiveness. Enzymes, in particular glutathione peroxidase (GSP) and reductase (GSR), are thus needed to re-generate the reduced of glutathione.<sup>12</sup>

However, the most important antioxidant compounds are two enzymes whose substrate are ROS: superoxide dismutases (SOD) that are able to dismutate superoxide radical to hydrogen peroxide and oxygen and catalase (CAT) that can dismutate hydrogen peroxide into water and oxygen.<sup>13</sup> These enzymes usually contain one or more metal center that catalyze multi electronic reactions. The most common superoxide dismutase are mononuclear, containing only one manganese atom, or dinuclear containing both copper and zinc (Figure 2). In both case there are many histidine residues and an acidic aminoacid, in this case aspartate, that coordinate the metal atoms, while a molecule of water completes the coordination sphere.

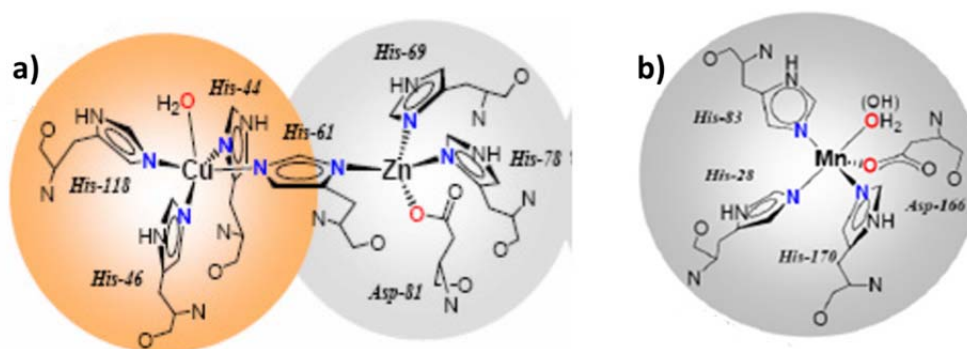
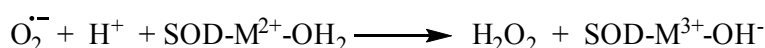
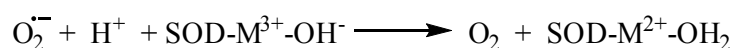


**Figure 2:** Active site of a) Cu-Zn SOD and b) MnSOD.

While Cu-ZnSOD is mostly located in the cytosol, MnSOD is mainly situated in mitochondria. Some eukaryotic species are known to produce an iron containing superoxide dismutase, also located in mitochondria. Both MnSOD and FeSOD contain one metal center and they seem to work through an alternate redox process involving both divalent and trivalent metal ions (Scheme 2).<sup>14</sup>



**Scheme 2:** Alternate redox process for superoxide dismutation by MnSOD.

There are also various species of catalases, the most frequent species contains a Fe-protoporphyrin motif (Figure 3) and it is a tetramer of identical subunits, each bearing a metal center. Below the porphyrin plan there is a tyrosinate that coordinates to the metal

center and an arginine residues, while over it there are a histidine and an asparagine, that play a crucial role in hydrogen peroxide dismutation. There is also a channel, with 30 Å length and 15 Å width, for the access of active site.<sup>15</sup> One defect of these type of catalases is that they are easily inhibited by cyanide and azide anion, like in hemoglobin.

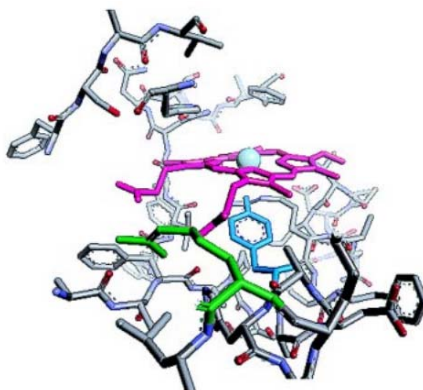


**Figure 3:** Active site of Fe-heme catalase

On the contrary, dimanganese catalase is less sensitive to inhibitors. In Figure 4 is shown the active site of a MnCAT from *L.plantarum*: also in this case metals center are coordinated by histidines residues and acidic residues (glutamate), with two molecules of water and one hydroxyl, involved in the coordination of the two metal centers.<sup>16</sup>

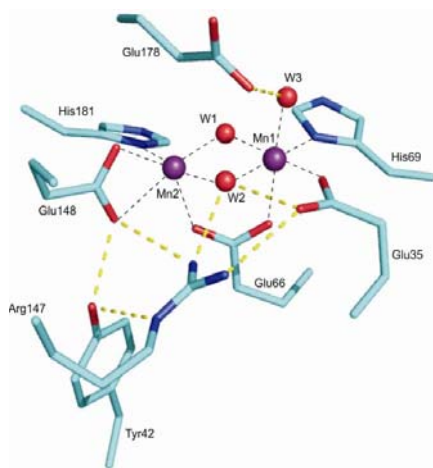
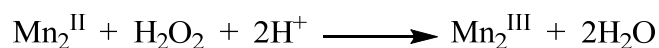
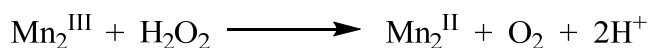


**Figure 4:** Structure of active site of MnCAT of *L.plantarum*,

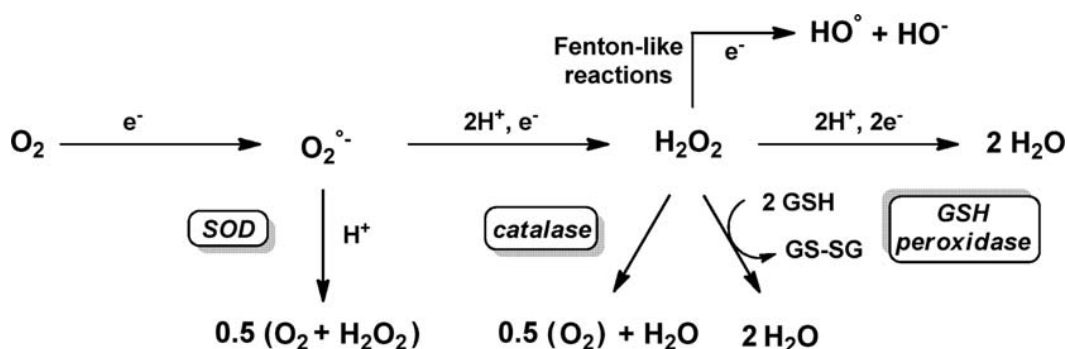
Due to high rate and efficiency of this enzyme, catalytic cycle it is not well known, but it has been supposed that during the catalytic cycle, manganese atoms change their oxidation

state from  $\text{Mn}^{\text{III}}$  to  $\text{Mn}^{\text{II}}$  and vice versa, although a  $\text{Mn}^{\text{IV}}$  intermediate is not completely excluded. Furthermore,  $\text{H}_2\text{O}_2$  binding is followed by a reduction of di manganese center with parallel oxidation of peroxide species and oxygen release. Then another  $\text{H}_2\text{O}_2$  molecule binds with a subsequent reduction to water and re-oxidation of the two manganese atoms (Scheme 3).<sup>17</sup>



**Scheme 3.** Variation of Mn oxidation states, as supposed during catalytic cycle of catalase.

SOD and CAT have a pivotal role in limiting ROS production in cells, SOD reduce dangerous superoxide radical produced during electron transport chain of mitochondrial respiration (and, of course, superoxide formed during other cellular reactions, outside the mitochondria). CAT, above all, has a very important role, indeed it intercept diffusible hydrogen peroxide, produced also by SOD enzyme, that could damage other organelles, and prevent the formation of very dangerous hydroxyl radical (Scheme 4).<sup>18</sup>



**Scheme 4:** Reactive species produced in organisms and method of elimination by glutathione, SOD and CAT enzymes.

It is known that the mutation of Cu-ZnSOD seems to be involved in amyotrophic lateral sclerosis, misfolding and aggregation of the enzyme, in which there is an alteration of metal binding site, induce motor neuron toxicity, with inclusion of proteinaceous residues of the enzyme.<sup>19</sup>

SOD enzyme and its mimicking compounds have shown to have a protective and beneficial role in many disease, both in preclinical and clinical tests. Preclinical studies have confirmed a positive effect of the enzyme for ischemia-reperfusion injury, or against inflammations, Parkinson's disease, cancer and many other pathologies, although in some situations native enzyme administration did not show very high efficiency, due to limitation of blood-brain barrier (BBB) penetration, cell permeability and half-life in circulating system. In addition, this is a very expensive method, so the use of artificial, low mass, superoxide dismutase mimicking systems is much more appealing.<sup>20</sup>

Catalase is a very important enzyme, since it dismutates hydrogen peroxide and avoid its diffusion and the formation of hydroxyl radical that is one of the most dangerous oxygen species, capable of react very rapidly with every biomolecules. Recent research on inhibition of catalase has shown a neat increment of oxidative stress in peroxisomes with an increment of hydrogen peroxide and also a subsequent increment of mitochondrial ROS production.<sup>21</sup> Considering Alzheimer's disease, inhibition of catalase activity comport a more cytotoxic effect of amyloid peptides, that are involved in this pathologies.<sup>22</sup>

Many degenerative pathologies can be linked to short/long term ROS overproduction, for example during aging. Among these, neurodegenerative disease are the most invalidating and with dramatic social consequences. Alzheimer's disease (AD), Parkinson's disease (PD), Huntington's disease (HD), amyloidosis, but also stroke, atherosclerosis, some forms of cancer, can be connected to oxidative stress. In the case of protein-based disease, such as AD, PD, HD and amyloidosis (but also Creutzfeldt-Jacob disease), production of harmful proteinaceous aggregates seems to be related to overproduction of ROS in the arch of life. Alzheimer's disease is the most common age-related neurodegenerative disorders, probably one of the most devastating, both for the patients and the relatives.<sup>23</sup> Many studies have been done on this pathology, however its causes are not really clear yet. Oxidative stress seems to be one of the cause of the disease, also because the typical plaque of AD, made mainly of amyloid peptide, are an important production site of reactive oxygen species. These reactive species can be involved in the production of more amyloid peptides, in a cycle that lead in increased damages due to both oxidative stress and plaque formation.<sup>24</sup> Amyloid peptides seems to be able to interact with mitochondria, disrupting their homeostasis, creating pores. In addition they affect the respiratory chain, in particular with complex I and complex IV, mitochondrial proteins involved in electron



transport chain during oxidative phosphorylation, causing a further increment in ROS production, especially of superoxide anion, affecting also ATP production.<sup>25</sup>

As it will be shown in the next chapters, the use of catalytic antioxidant that mimic natural enzymes such as catalase and superoxide dismutase are of huge interest for the development of new drugs for cellular ROS scavenging.

## 1.2 Mitochondria, respiratory chain and reactive oxygen species (ROS)

Mitochondria play a central role in ROS production, since they are the energetic centers of cell, producing ATP from ADP using generally glucose and oxygen. Mitochondria are also homeostasis regulators, in particular of calcium ions, and play a fundamental role in cell signaling and in the apoptotic process that lead to cell death, due to oxidative stress or aging (Figure 5).<sup>26</sup>

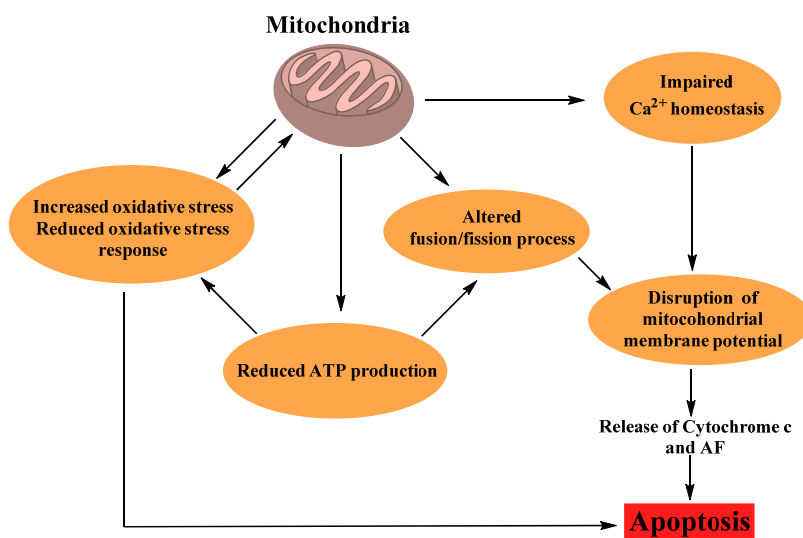


**Figure 5:** Role of mitochondria in oxidative stress and apoptotic process.

These organelles are usually 1-4 $\mu$ m in length and 1-0.2 $\mu$ m width and are made of an external membrane, an intermembrane space, an internal membrane folded in cristae and finally an inner matrix (Figure 6).

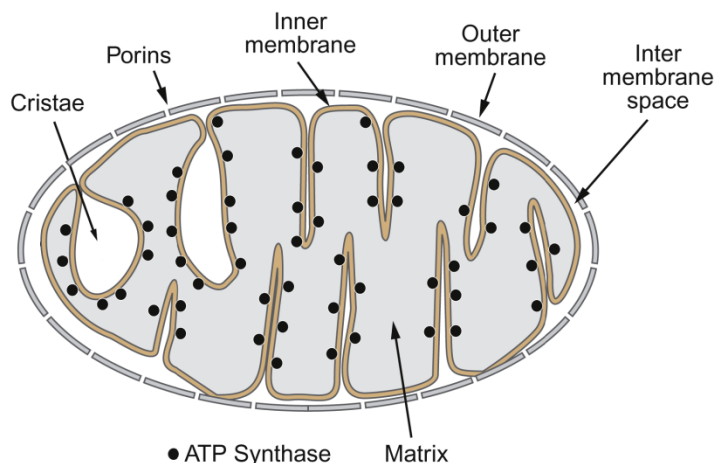


**Figure 6:** Schematic representation of a mitochondrion.<sup>27</sup>

The outer membrane contains many transport proteins, integral proteins and porins, allowing free diffusion of small molecules, with less than 10kDa weight, but limiting heavier molecules crossing. Being freely permeable to ions and metabolites, the intermembrane composition is equivalent to the cytosol. The inner membrane plays a crucial role in mitochondrial respiration, indeed it contains all the proteins needed for the respiratory chain and many transport proteins. Its impermeability to charged species allows the production of the ionic gradients necessary for the ATP synthesis. The matrix is an highly concentrated solution of enzymes, that participate to the oxidative metabolism, substrates, nucleotides cofactors, ions and mitochondrial DNA/RNA, ribosomes that produce several mitochondrial proteins.<sup>28</sup> The proteins involved in the oxidative phosphorylation are usually called “complexes”, there are four complexes, labeled I-IV, whose task is to create the protonic gradient used for the oxidative phosphorylation. The proton electrochemical gradient ( $\Delta\mu_{H^+}$ ,  $\text{kJ}\cdot\text{mol}^{-1}$ ) is a thermodynamic measure of the removal of an ion gradient from equilibrium and has two components: difference in protons concentration, usually 0.5 pH units, and difference in electrochemical potential between the aqueous phases separated by the inner membrane, the membrane potential ( $\Delta\psi$ ). Complexes I, III and IV are called proton translocating complexes, they are directly involved in the gradient generation, while complex II allows electron transport chain when complex I does not work because of damaging or substrate (NADH) deficiency. Ubiquinone (UQ) and cytochrome c (cyt c) are electrons carriers from complex to complex, in the case of ubiquinone two proton are also moved. Last, complex V, also known as ATPsynthase (ATPase), uses the proton gradient so formed to synthesize ATP

from ADP plus phosphate. All these components, together with protons and electrons flows are shown in figure 7.<sup>27</sup>

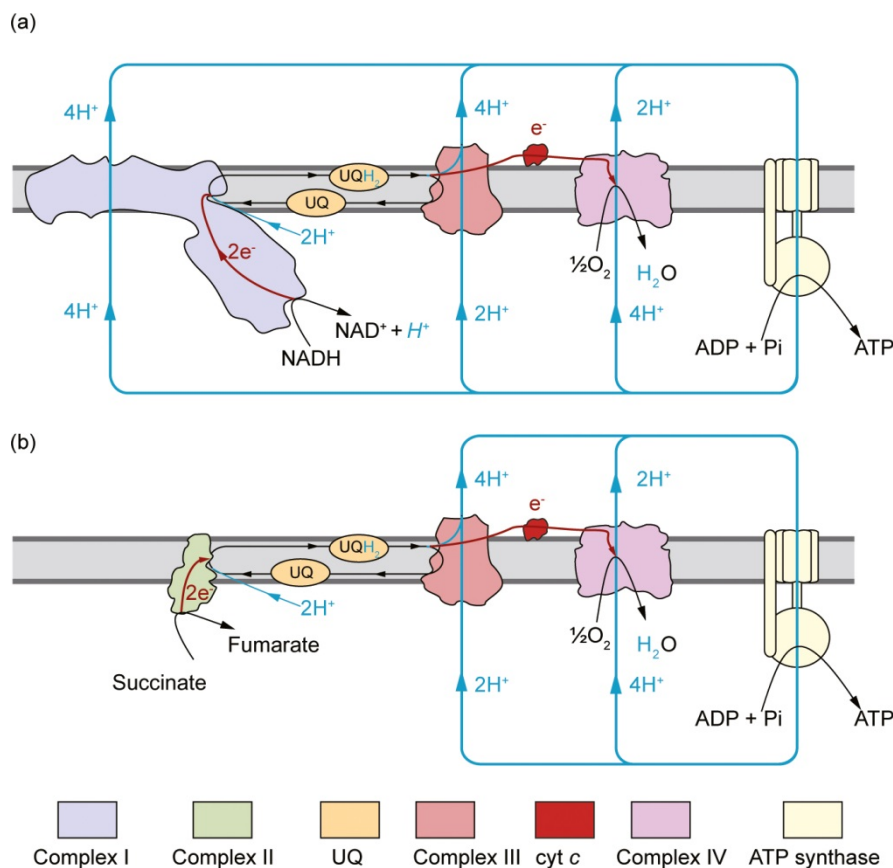


**Figure 7:** Mitochondrial respiratory chain and proton circuits during phosphorylation: a) classical circuit from complex I and b) when complex I is bypassed because environmental condition prevent it function.

As said before, mitochondria are the major producers of reactive oxygen species, indeed ROS can be produced from ubiquinone, cytochromes or iron-sulfur clusters located in complexes I-II-III. In particular, complexes I and III have sufficiently negative potential to produce superoxide radical, however also complex II seems to be able to produce ROS.<sup>29</sup> Production of these species starts with superoxide radical production by a monoelectronic reduction of oxygen, although superoxide anion can dismutate spontaneously to oxygen and hydrogen peroxide, it is usually rapidly dismutated by MnSOD enzyme, that is present in the mitochondrial matrix. Superoxide anion could produce hydrogen peroxide that is less reactive but could easily diffuse out of mitochondrion or interact with active metal centers to give Fenton reaction and produce the dangerous hydroxyl radical, very reactive compound with an half-life time of nanoseconds (Figure 8). Others reactive species, for

example singlet oxygen and nitrogen reactive species (such as nitric oxide and peroxyxynitrite), can be produced in different ways starting from superoxide anion.<sup>30</sup>

It is known that ROS have a role in signaling of cells, indeed at low concentration they are essential for cell living and proliferation, however if their concentration is too high, growing of cells stops and at much higher concentration could lead to cell senescence, cell death and apoptosis.<sup>31</sup>

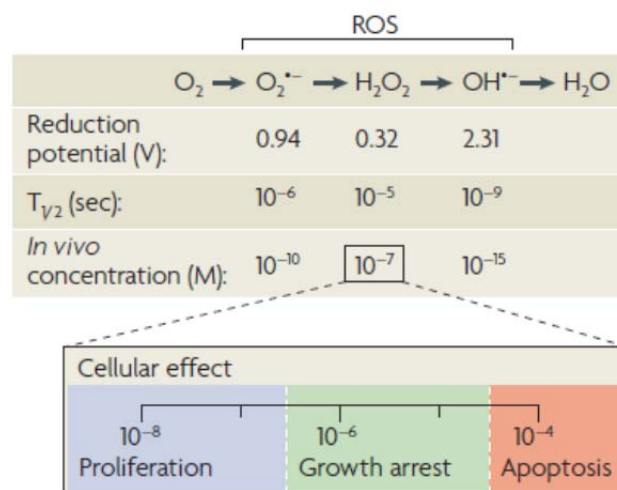


**Figure 8:** Table of reduction potential, half-life time ( $T_{1/2}$ ) and concentration in vivo of common ROS. Effects of ROS concentration at cellular level.

ROS are released into cytosol because of membrane potential and also through channel such as inner membrane anion channel (IMAC) and mitochondrial permeability transition pore (mPTP), but there are others ROS producer, for example mono amine oxidase (MAO), a flavoenzymes that is bound to the outer mitochondrial membrane, or protein p66Shc that plays a crucial role in the oxidative stress response.<sup>32</sup>

### 1.3 Complexes and nanodimensional systems with CAT/SOD mimicking activity

One of the possible solution to limit damages by ROS is the use of antioxidants, natural molecules such as vitamins or polyphenols, but also artificial molecules like fullerene, peptide derivatives or metal complexes.<sup>33</sup> One of the major problems is the high concentration needed of these molecules, indeed they eliminate ROS but usually working in stoichiometric ratio, meaning that one antioxidant molecule scavenges one reactive

specie. Another problem is that these molecules disperse and react in different sites before reaching the target: for this reason, there are many studies whose goal is the selective delivery of these molecules, for example using functional groups able to target mitochondria, also called mitochondriotropic.<sup>34</sup> Among these latter we can find many rhodamine derivatives or phosphonium salts, usually positively charged and containing an hydrophobic domain (usually aromatic) that facilitate mitochondrial uptake (Figure 9).<sup>35</sup>

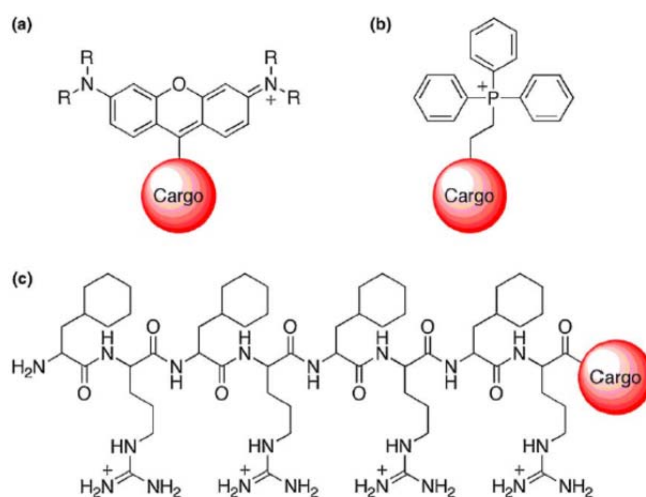


**Figure 9:** Example of functionalized molecule for mitochondrial targeting a) rhodamine derivatives, b) triphenylphosphonium salt and c) peptide derivative containing natural and synthetic aminoacids.<sup>36</sup>

The use of biomimetic catalysts, that try to imitate cellular enzymes as catalase or superoxide dismutase could in principle reduce the concentration needed, indeed they could work in catalytic concentrations and can be easily modified with targeting functionalization. These biomimetic compounds are usually metal complexes containing one or more (often two) metal centers, quite often manganese, iron or other essential metals trying to imitate natural systems.<sup>37</sup>

Several metal ions play a crucial role in biological systems, since they are involved in oxygen transport (copper and iron), multi electronic reactions such as respiratory chain or photosynthetic systems (manganese, iron), structural functions in some proteins for example in zinc-finger proteins (zinc, cobalt), signaling and homeostasis (sodium, calcium, potassium).<sup>38</sup> Many other heavy metals, such as mercury, platinum, ruthenium, cadmium, have toxic effects on biological systems, but some of their complexes are now under investigation as drugs. Indeed, changing the ligands of the metal center allows to modulate activity, toxicity and targeting, so to take advantage of their toxicity against

insane cells or to exploit some characteristics to bind specific proteins involved in diseases. For example copper is an essential element, but over accumulation of copper, typical of Wilson's disease, has toxic effects. It has been demonstrated that reactive metals like iron and copper play a crucial role in Alzheimer's diseases, since they accumulate in senile plaques and, upon coordination with peptide fragments of these plaques, enhance the production of reactive oxygen species.<sup>39</sup>

Coordination metal complexes are widely studied as enzymes mimics for bioinspired reactions. In the literature, many examples of manganese complexes that are able to mimic SOD and CAT activity were reported. However, not only manganese is active in the simulation of biological reactions, but also copper, iron and cobalt complexes. Among potentially toxic heavy metals, iridium and ruthenium compounds are promising for their biomimetic activity and, like platinum or gold, are currently under investigation in medicinal chemistry.<sup>40</sup>

In the last few years, new systems to fight oxidative stress, that differ from classical antioxidant molecules and also from coordination complexes, have appeared. Gold nanoparticles, silica nanoparticles, ceria nanoparticles, polyoxometalates and metal clusters have been studied as possible agents in medicine. Nanoparticles (NPs) of silica and gold are the most studied, and maybe the best known nanosystems used with medicinal aim, indeed there are several studies in which NPs, labelled with tracker molecule, were investigated to establish their toxicity, bioavailability and also their application in drug delivery.<sup>41</sup> Interactions with cytochrome c of zinc oxide NPs have been studied, but also the interactions between amyloid peptides and CdTe NPs have demonstrated to reduce peptides aggregation in fibrils.<sup>42</sup> Completely organic nanoparticles conjugated with fluorescent probe and organic drug, have been studied again against Alzheimer's disease.<sup>43</sup> Recently, ceria nanoparticles have been used as protective agents against ischemic stroke, indeed it is known that cerium could be a good antioxidant, thanks to, redox switching between  $Ce^{3+}$  to  $Ce^{4+}$ , CeNPs were used to eliminate ROS and apoptosis, demonstrating that they could reduce ischemic damages in brain (Figure 10).<sup>44</sup>

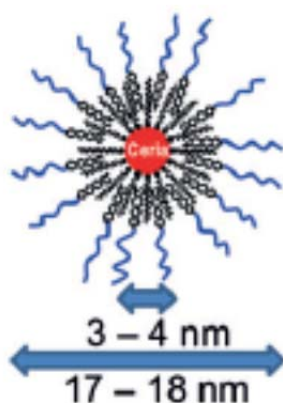


**Figure 10:** Example of phospholipidic-PEG CeNPs with anti ROS activity.

Completely inorganic compound like polyoxometalates, that will be described better in chapter 4, have been used as therapeutic agents. Indeed they can interact with proteins, like albumin,<sup>45</sup> if they are substituted with transition metals they can strongly interact with specific protein domains, and also act anti-aggregating agents of amyloid peptides.<sup>46</sup> Some of this polyoxometalates could act as peptide, hydrolyzer, some example involving proteolysis of human albumin serum have been recently reported.<sup>47</sup> In this field, a polyoxometalate that can degrade amyloid peptide when irradiated with light, has been reported: the POM is able to break oligomeric forms of these peptides, but also to cleave peptide bonds of amyloid leading to smaller fragments (Figure 11).<sup>48</sup>

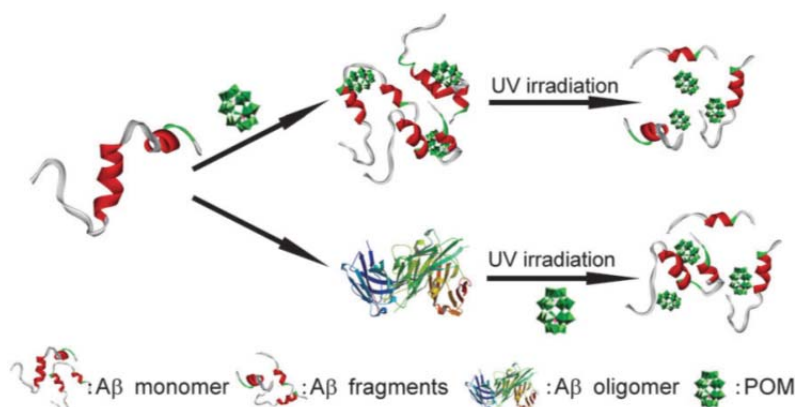


**Figure 11:** Schematic representation of photodegradation of amyloid peptides and oligomers catalyzed by a polyoxometalate (POM).

## 1.4 Amyloid peptides and Alzheimer's disease

Alzheimer's disease (AD) is the most common cause of dementia (50-80%) of worldwide population, affecting about 18 millions of people, whose incidence increases with age. Maybe it is one of the most terrible among neurodegenerative diseases, both for the patients but also for their relatives, characterized by progressive cognitive decline, with impairment of daily living and progressive behavioral disturbance.<sup>49</sup> Although some cases of genetic forms of AD exist, the most common AD is age related, meaning that, with the increase of the life expectancy, the number of people affected by AD is set to increase. Alzheimer's disease was described for the first time in 1907 by Alois Alzheimer, a German psychiatrist and neuropathologist, that followed a 55 years patient affected by dementia. The autopsy revealed the hallmarks of the disease, the extracellular plaques and intraneural neurofibrillary tangles, that Alzheimer discovered to be formed by amyloid peptides.<sup>50</sup> Amyloid term, known in plant science, was used to describe lardaceous deposits in central nervous system, because of their reactivity to iodine staining, similar to cellulose-like material, in the middle of 1800. The true nature of amyloid was determined later, through a lot of hypothesis, till when X-rays diffraction of amyloid, dissolved every doubt about their structure and composition. Amyloid are proteinaceous deposit that gives Congo red birefringence, or a typical X-ray diffractive pattern of  $\beta$ -sheet pleated, with the chemical nature of fibrils with a diameter of 8-10nm.<sup>51</sup> Other proteins are associated with fibrils and amyloid diseases and are involved in many pathologies such as Alzheimer's, Parkinson's, Huntington's, type II diabetes, amyloidosis (Table 1).<sup>52</sup>

**Table 1:** Proteins associated with fibrils and amyloid diseases.\*

Protein	Disease	Ref.
$\alpha$ -Synuclein	Parkinson's (PD)	53
Amyloid- $\beta$	Alzheimer's (AD)	54
Huntingtin	Huntington's (HD)	53a,55
IAPP	Type II diabetes	56
Lysozyme	Hereditary systematic amyloidosis	57
Tau	AD, frontotemporal dementia	53a-b,58
SAA	Secondary systematic amyloidosis	57b
ABri	Familial British dementia	59
Gelsolin	Finish-type familial amyloidosis	60
Medin	Aortic medial amyloid	61

\*Term "amyloid" has been extended to intracellular protein deposit (Tau,  $\alpha$ -Synuclein). The proteins listed are also considered "amyloid" on the basis of positive staining with amyloid-binding dyes and/or the presence of fibrillar morphology (adapted from ref. 52).



Concerning Alzheimer's disease (almost all consideration are similar to other pathologies with their own protein involved in), it is characterized by the occurrence of a 40-42 AA peptides called  $\beta$ -Amyloids. They are generally produced by the cleavage of the Amyloid Precursor Protein (APP) by  $\beta/\gamma$  secretase enzymes, mainly into A $\beta$ 40, less toxic, while A $\beta$ 42 is predominant in senile plaque. They are characterized by an hydrophobic portion, whereby amino acids involved are lysine, leucine, valine and phenylalanine (KLVFF in one letter symbols<sup>†</sup>), that tends to form  $\beta$ -sheet secondary structures, these could lead to formation of oligomeric species and finally to fibrils. Both peptides can self-assemble into amyloid fibrils with facile conversion in physiological conditions and fibril seeds can incredibly increase further fibril formation. A typical fibrillation kinetics involves the formation of monomeric species that are able to produce oligomeric soluble forms, that can finally aggregate into fibrils (Figure 12).<sup>62</sup>

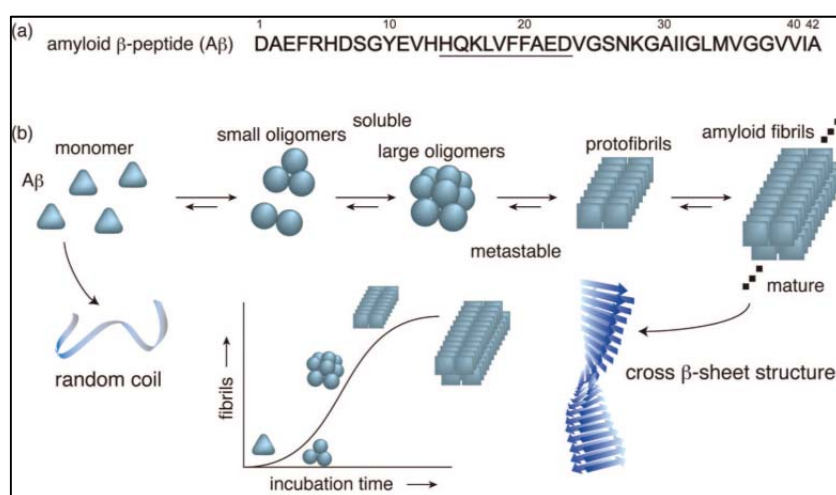


**Figure 12:** a) Amino acidic sequences of A $\beta$ 42, with the hydrophobic region that tends to forms beta-sheet; b) Kinetics of fibrillation of  $\beta$ -Amyloid from monomeric species to final mature fibrils.

Usually A $\beta$ 42 are faster in nucleation and fibrillation than A $\beta$ 40, for this they are more toxic. The toxicity is due to many effects of beta amyloid oligomers and fibril:

- Alteration of membranes, cellular and mitochondrial, resulting in alteration of their homeostasis;
- Interaction with DNA and membrane receptors with consequent dysfunction;<sup>63</sup>
- Induction of oxidative stress due to accumulation of redox active metals, such as Fe<sup>III</sup> and Cu<sup>II</sup>, but also accumulation of other important metal, for example Al<sup>III</sup> and Zn<sup>II</sup>.<sup>64</sup>

<sup>†</sup> For aminoacids nomenclature, three letter and one letter symbols, see the table in Appendix, pag. I.

Recent studies have thus focused on two sides: the first is to limit oligomers/fibril formation to avoid plaque deposition, the second is to reduce damages due to oxidative stress.

Inhibition of fibrils formation is one of the goal of research, and many small molecules having this function have been studied, most of them are called beta-sheet breaker, because their interaction breaks secondary  $\beta$ -sheet structure.<sup>65</sup> These molecules could be short peptides, complementary to KVLFF sequence, or hydrophobic molecule that are able to avoid fibrillation, like curcumin or resveratrol, that have also antioxidant properties.<sup>66</sup> Also fullerene has been studied to inhibit fibrils formation thanks to hydrophobic interaction, while nanoparticles and inorganic compounds like polyoxometalates have been studied for their electrostatic interactions with positively charged domains of peptides.<sup>46,48</sup>

The other important phenomenon that should be contrasted is the increase of oxidative stress due to accumulation of metals that can perform redox process with formation of reactive oxygen species (ROS). It was been noticed that antioxidant molecules can slow the course of the disease, probably because they slow down the damages due to high oxidative stress. Metal chelators, able to subtract metal ions, seemed to improve somehow the situation, indeed metals play a role also in fibrillation: the coordination of  $A\beta_{42}$  to metals can promote oligomerization and fibril formation, in addition to an increase in ROS production (Figure 13).<sup>64c,67</sup>

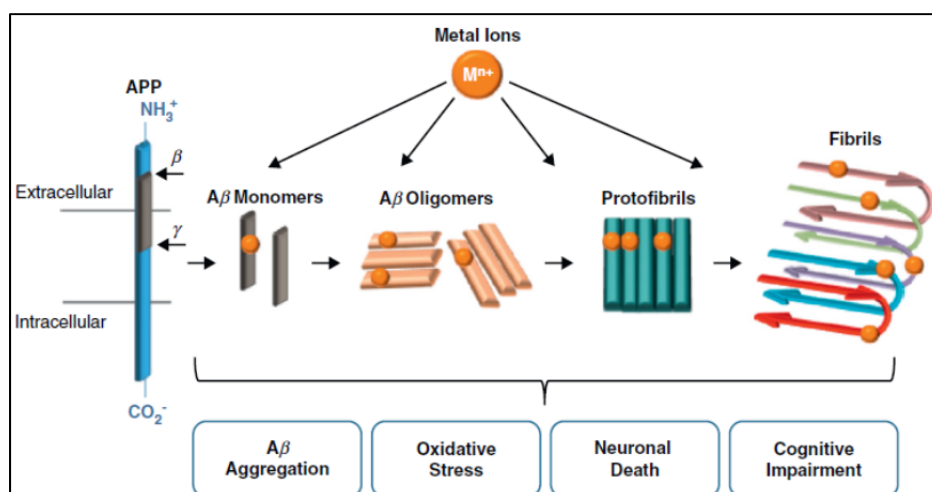


**Figure 13:** Generation of  $A\beta$  species and the potential involvement of metal ions associated, in Alzheimer's disease. Metal ions are shown to interact with  $A\beta$  species, facilitating aggregation and enhancing reactive oxygen species (ROS) generation, which can lead to oxidative stress and neuronal death.

As said before, A $\beta$  can interact with mitochondria, with the membranes, disrupting their homeostasis, but also with electron transport chain complexes inducing an increasing in ROS production. These ROS increase the oxidative stress and could also induce an increase in amyloid production. It is not still well known if ROS production is a consequence of amyloid effects or if ROS accumulated during the life could generate the amyloid accumulation.<sup>68</sup> It is however clear that a drug with dual anti ROS/anti amyloidogenic activity would be a powerful method to get better activity and better knowledge of such phenomena.

## 1.5 Aim of the thesis

The aim of this thesis is the study of organic or inorganic compounds, containing active metal center, able to fight against degenerative diseases. We have seen that reactive oxygen species are involved in many degenerative pathologies like Alzheimer's or Parkinson's diseases, but also in cancer, stroke, ischemia and other age-related syndromes. Natural defense sometimes are not enough, so it is important to help nature in the fight against oxidative stress. Coordination complexes able to eliminate superoxide anion or hydrogen peroxide have been considered in this thesis work, their catalytic activity has been tested and in some case also their toxicity. Tailored modification for targeting and delivery was also considered. A complete inorganic compound has been studied as artificial *synzyme* with high robustness in oxidative conditions and some peculiarity for protein interaction. Also in this case targeting and delivery methodologies was considered. Toxicity of this total inorganic compound has been investigated as its anti ROS efficiency. Finally some multimetallic oxoclusters were taken in account as ROS scavengers, these compounds were synthesized during a Short Term Scientific Mission (STSM) in Dublin, under supervision of Prof. Wolfgang Schmitt. Preliminary results about catalytic reactivity and stability in water will be presented with some perspective of application.



## References

- <sup>1</sup> Venditti P., Di Stefano L., Di Meo S., *Mitochondrion*, **2013**, 13, 71.
- <sup>2</sup> Holbrook N.J., Finkel T., *Nature*, **2000**, 408-239.
- <sup>3</sup> Hlavatá L., Ježek P., *Int. J. Biochem. Cell B.*, **2005**, 37, 2478.
- <sup>4</sup> Harman D., *Proc. Natl. Acad. Res.*, **1981**, 78, 7124-7128.
- <sup>5</sup> Pizzitelli M., Walton P.A., *Front. Physiol.*, **2012**, 3, 1.
- <sup>6</sup> Valentine J. S., Foote C.S., Greenberg A., Liebman J. F., *Active oxygen in biochemistry*, 1<sup>st</sup> Edition, **1995**.
- <sup>7</sup> Harman D., *Proc. Natl. Acad. Res.*, **1981**, 78, 7124.
- <sup>8</sup> Moraes C.T., Fukui H., *Trends Neurosci.*, **2008**, 31, 5, 251.
- <sup>9</sup> a) M. Sayre L.M., Perry G., Smith M.A., *Chem. Res. Toxicol.*, **2008**, 21, 172; b) Signorelli S.S., Neri S., Di Pino L., Costa M.P., Pennisi G., Digrandi D., Ierna D., *Clin. Exp. Med.*, **2001**, 1, 9.
- <sup>10</sup> a) Morris M.R., Frank P., Novak R.F., *Chem. Res. Toxicol.*, **1989**, 2, 2, 76; b) Valko M., Rhodes C.J., Moncol J., Izakovic M., Mazur M., *Chem. Biol. Interact.*, **2006**, 160, 1.
- <sup>11</sup> a) M. Sayre L.M., Perry G., Smith M.A., *Chem. Res. Toxicol.*, **2008**, 21, 172–188; b) Signorelli S.S., Neri S., Di Pino L., Costa M.P., Pennisi G., Digrandi D., Ierna D., *Clin. Exp. Med.*, **2001**, 1, 9–12.
- <sup>12</sup> Murphy M.P., *Antioxid. Redox Signal.*, **2012**, 16, 476.
- <sup>13</sup> Fridovich I., *Science*, **1978**, 201, 875.
- <sup>14</sup> a) Chan V.W.F., Bjerrum M.J., Borders C.L., *Arch. Biochem. Biophys.*, **1990**, 279, 195; b) Stallings W.C., Patridge K.A., Strong R.K., Ludwig M.L., *J. Biol. Chem.* **1985**, 260, 16424; c) Sinet P.M., Lavelle F., Michelson A.M., Jerome H., *Biochem. Biophys. Res. Commun.*, **1975**, 67, 904; d) McAdam M.E., Levelle F., Fox R.A., Fielden E.M., *Biochem J.* **1977** 165, 81–87, e) Miller A.F., *FEBS Lett.*, **2012**, 586, 585.
- <sup>15</sup> Alfonso-Prieto M., Biarnés X., Vidossich P., Rovira C., *J. Am. Chem. Soc.*, **2009**, 131, 11751.
- <sup>16</sup> Shank M., Barynin V., Dismukes G.C., *Biochemistry*, **1994**, 33, 15433.
- <sup>17</sup> a) Signorella S., Hureau C., *Coordin. Chem. Rev.*, **2012**, 256, 1229; b) De Boer J.W., Browne W.R., Feringa B.L., Hage R., *C. R. Chimie*, **2007**, 10, 341; c) Wu A.J., Penner-Hahn J.E., Pecoraro V.L., *Chem. Rev.*, **2004**, 104, 903; d) Boelrijk A.E.M., Dismukes G.C., *Inorg. Chem.*, **2000**, 39, 3020.
- <sup>18</sup> a) Batinic-Haberle I., Clair D.St., Vujaskovic Z., Salvemini D., Tovmasyan A., Spasojevic I., Miriyala S., *Biochim. Biophys. Acta*, **2012**, 1822, 794; b) Miller A.F., *FEBS Letters*, **2012**, 586, 585.
- <sup>19</sup> Hart P.J., Hasnain S.S., Cohlberg J.A., Padua S., Hayward L.J., Tiwari A., Valentine J.S., Doucette P.A., Strange R.W., Holloway S.P., Taylor A.B., Whitson L.J., Seetharaman S.V., Antonyuk S.V., Cao X., *J. Biol. Chem.*, **2008**, 280, 23, 16169.
- <sup>20</sup> Cuzzocrea S., Riley D.P., Salvemini D., *Nat. Rev.*, **2002**, 1, 367.
- <sup>21</sup> Pizzitelli M., Walton P.A., *Front. Physiol.*, **2012**, 3, 1.
- <sup>22</sup> Milton N.G.N., *Neurotoxicology*, **2001**, 22, 767.
- <sup>23</sup> Oddo S., Green K.N., LaFerla F.M., *Nat. Rev.*, **2007**, 8, 499.
- <sup>24</sup> a) Larsson N.G., Bratic A., *J. Clin. Invest.*, **2013**, 123, 3, 951; b) Ugalde C., Martín A.M., Arenas J., Marín-Buera L., Moreno-Lastres D., Morán M., *Free Radical Bio. Med.*, **2012**, 53, 595.
- <sup>25</sup> Avila J., Perry G., Martín-Maestro P., García-Escudero V., *Oxid. Med. Cell. Longev.*, **2013**, 1.
- <sup>26</sup> Radi E., Gallus G.N., Formichi P., Da Pozzo P., Cardaioli E., Federico A., *J. Neur. Sci.*, **2012**, 322, 254.
- <sup>27</sup> Nicholls D.G., Ferguson S.J., *Bioenergetics4*, **2013**, Academic Press
- <sup>28</sup> Voet D., Voet J.G., Pratt C.W., *Fundamentals of Biochemistry: Life at the Molecular Level*, 2nd Edition, **2007**.
- <sup>29</sup> a) Venditti P., Di Stefano L., Di Meo S., *Mitochondrion*, **2013**, 13, 71; b) Orr A.L., Quinlan C.L., Perevoshchikova I.V., Brand M.D., *J. Biol. Chem.*, **2012**, 287, 42921.
- <sup>30</sup> Bonini M.G., Consolareo M.E.L., Hart P.C., Mao M., Luelsdorf A., de Abreu P., Master A.M., *IUBMB Life*, **2014**, 66, 3, 167.
- <sup>31</sup> Giorgio M., Trinei M., Migliaccio E., Pelicci P.G., *Nature Rev. Mol. Cell. Biol.*, **2007**, 8, 722.
- <sup>32</sup> Martínez-Reyes I., Cuezva J.M., *Biochim. Biophys. Acta*, **2014**, 1837, 1099.
- <sup>33</sup> a) D'souza G.G.M., Cheng S.M., Weissig V., *Mitochondrion*, **2004**, 3, 229; b) Murphy P.M., Smith R.A.J., Lin T.K., Kelso G.F., Coulter C.V., *Free Radical Bio. Med.*, **2000**, 28, 10, 1547.
- <sup>34</sup> Ichas F., Ghosez L., De Giorgi F., Quinart A., Schuler M., Dessolin J., *Eur. J. Pharmacol.*, **2002**, 447, 155.
- <sup>35</sup> Kagan V.E., Fink M.P., Wipf P., Davoren J.E., Hoye A.T., *Accounts Chem. Res.*, **2008**, 41, 1, 87.
- <sup>36</sup> Chang J.C., Srikun D., Dickinson B.C., *Curr. Opin. Chem. Biol.*, **2010**, 14, 50.
- <sup>37</sup> Haberle I.B., Clair D.S., Vujaskovic Z., Salvemini D., Tovmasyan A., Spasojevic I., Miriyala S., *Biochim. Biophys. Acta*, **2012**, 1822, 794.
- <sup>38</sup> Lippard S.J., Berg J.M., *Principle of Bioinorganic Chemistry*, **1994**, University Science Book.
- <sup>39</sup> Jomova K., Valko M., *Toxicology*, **2011**, 283, 65.

- <sup>40</sup> Scott E.L., Orvig C., *Chem. Rev.*, **2009**, 109, 4885.
- <sup>41</sup> a) Palantavida S., Guz N.V., Sokolov I., *Part. Part. Syst. Charact.*, **2013**, 30, 804; b) Herd H., Daum N., Jones A.T., Huwer H., Gandehari H., Lehr C.M., *ACS Nano*, **2013**, 7, 3, 1961; c) Zhao Y.L., Li Z., Kabehie S., Botros Y.Y., Stoddart J.F., Zink J.I., *J. Am. Chem. Soc.*, **2010**, 132, 13016.
- <sup>42</sup> a) Šimšiková M., Antalík M., Kaňuchová M., Škvarla J., *Int. J. Biol. Macromol.*, **2013**, 59, 235-241; b) Yoo S.I., Yang M., Brender J.R., Subramanian B., Sun K., Joo N.E., Jeong S.H., Ramamoorthy A., Kotov N.A., *Angew. Chem. Int. Ed.*, **2011**, 50, 5110-5115.
- <sup>43</sup> a) Le Droumaguet B., Souguir H., Brambilla D., Verpillot R., Nicolas J., Taverna M., Couvreur P., Andrieux K., *Int. J. Pharma.*, **2011**, 416, 453-460; b) Brambilla D., Verpillot R., Le Droumaguet B., Nicolas J., Taverna M., Kóňa J., Lettiero B., Hashemi S.H., De kimpe L., Canovi M., Gobbi M., Nicolas V., Scheper W., Moghimi S.M., Tvaroška I., Couvreur P., Andrieux K., *ACS Nano*, **2012**, 6, 7, 5897.
- <sup>44</sup> Kim C.H., Kim T., Choi I.Y., Soh M., Kim D., Kim Y.J., Jang H., Yang H.S., Kim J.Y., Park H.K., Park S.P., Park S., Yu T., Yoon B.W., Lee S.H., Hyeon T., *Angew. Chem. Int. Ed.*, **2012**, 51, 11039.
- <sup>45</sup> a) Nadjo L., Keita B., Yao J., Zhang G., Ma Y., Zheng L., *Phys. Chem. Chem. Phys.*, **2010**, 1299. b) Miron S., Craescu C.T., Nadjo L., de Oliveira P., Keita B., Kortz U., Bassil B.S., Yao J., Zhang G., Ma Y., Zheng L., *Eur. J. Inorg. Chem.*, **2009**, 5189. c) Nadjo L., de Oliveira P., Miron S., Craescu T.C., Keita B., Zhang G., *Biomacromolecules*, **2008**, 9, 812.
- <sup>46</sup> Qu X., Wang E., Ren J., Li M., Geng J., *Angew. Chem. Int. Ed.*, **2011**, 60, 4184.
- <sup>47</sup> a) Parc-Vogt T.N., Bartik K., Proost P., Ly H.G.T., Moelants E., Stroobants K., *Chem. Eur. J.*, **2013**, 19, 2848; b) Parc-Vogt T.N., Proost P., Moelants E., Absillis G., Stroobants K., *Chem. Eur. J.*, **2014**, 20, 3894.
- <sup>48</sup> Li M., Xu C., Ren J., Wang E., Qu X., *Chem. Comm.*, **2013**, 49, 11394.
- <sup>49</sup> Scarpini E., Scheltens P., Feldman H., *Lancet Neurol.*, **2003**, 2, 539.
- <sup>50</sup> Vilatela M.E.A., López-López M., Yescas-Gómez P., *Arch. Med. Res.*, **2012**, 43, 622.
- <sup>51</sup> Sipe J.D., *Amyloid Proteins*, **2005**, Wiley-VCH.
- <sup>52</sup> Rochet J.C., Lansbury P.T.Jr., *Curr. Op. Struc. Biol.*, **2000**, 10, 60.
- <sup>53</sup> a) Goedert M., Spillantini M.G., Davies S.W., *Curr. Op. Neurobiol.*, **1998**, 8, 619; b) Goedert M., *Philos. Trans. R. Soc. Lond. B Biol. Sci.*, **1999**, 354, 1101; c) Galvin J.E., Lee V.M., Schmidt M.L., Tu P.H., Iwatsubo T., Trojanowski J.Q., *Adv. Neurol.*, **1999**, 80, 313.
- <sup>54</sup> a) Teplow D.B., *Amyloid: Int. J. Exp. Clin. Invest.*, **1998**, 5, 121-142; b) Selkoe D.J., *Nature*, **1999**, 399(suppl), A23-A31.
- <sup>55</sup> a) Perutz M.F., *Trends Biochem. Sci.*, **1999**, 24, 58-63; b) Ross C.A., *Neuron*, **1997**, 19, 1147-1150.
- <sup>56</sup> Clark A., Charge S.B., Badman M.K., MacArthur D.A., de Koning E.J., *Biochem. Soc. Trans.*, **1996**, 24, 594.
- <sup>57</sup> a) Kelly J.W., *Curr. Op. Struc. Biol.*, **1998**, 8, 101-106; b) Kelly J.W., *Curr. Op. Struc. Biol.*, **1996**, 6, 11.
- <sup>58</sup> Goedert M., Crowther R.A., Spillantini M.G., *Neuron* **1998**, 21, 955.
- <sup>59</sup> a) Vidal R., Frangione B., Rostagno A., Mead S., Revesz T., Plant G., Ghiso J., *Nature* **1999**, 399, 776; b) Lansbury P.T. Jr., Kosik K.S., *Chem. Biol.*, **1999**, 7, 1, R9.
- <sup>60</sup> Kiuru S., *Amyloid: Int. J. Exp. Clin. Invest.*, **1998**, 5, 55.
- <sup>61</sup> Häggqvist B., Näslund J., Sletten K., Westermark G.T., Mucchiano G., Tjernberg L.O., Nordstedt C., Engström U., Westermark P., *Proc. Natl. Acad. Sci. USA*, **1999**, 96, 8669.
- <sup>62</sup> Takahashi T., Mihara H., *Acc. Chem. Res.*, **2008**, 41, 10, 1309.
- <sup>63</sup> Chew L.Y., Mu Y., Long H.W., Zhao L.N., *Int. J. Mol. Sci.*, **2012**, 13, 7303.
- <sup>64</sup> a) R.F. Brissos, S. Garcia, A. Presa, P. Gamez, *Comments Inorg. Chem.*, **2011**, 32, 219; b) Barnham K.J., Bush A.I., *Curr. Op. Chem. Biol.*, **2008**, 12, 222; c) Hureau C., Faller P., *Biochimie*, **2009**, 1212.
- <sup>65</sup> a) Nowick J.S., Eisenberg D., Zhao M., Liu C., Cheng P.N., *Nat. Chem.*, **2012**, 4, 927; b) Ran C., Moore A., Sun H., Tian X., Li Z., Tian Y., Zhang X., *J. Am. Chem. Soc.*, **2013**, 135, 44, 16397; c) Kotov N.A., Ramamoorthy A., Jeong S.H., Joo N. E., Sun K., *Angew. Chem. Int. Ed.*, **2011**, 50, 5110; d) Kanai M., Sohma Y., Sato T., Taniguchi A., Sasaki D., Araya T., Arai T., *Angew. Chem. Int. Ed.*, **2014**, 53, 8236; e) Lee H.H., Choi T.S., Lee S.J.C., Lee J.W., Park J., Ko Y.H., Kim W.J., Kim K., Kim H.I., *Angew. Chem. Int. Ed.*, **2014**, 53, 7416.
- <sup>66</sup> a) Yang F., Lim G.P., Begum A.N., Ubeda O.J., Simmons M.R., Ambegokar S.S., Chen P., Kaye R., Glabe C.G., Frautschy S.A., Cole G.M., *J. Biol. Chem.*, **2005**, 18, 5892; b) Mu Y., Chew L.Y., Benoit J., Chiu S.W., Zhao L.N., *J. Phys. Chem. B.*, **2012**, 116, 7428; c) Shi J., Dong H., Gong Q., Li F., *Curr. Pharma. Des.*, **2012**, 18, 27; d) Liu R., Huang L., Zhao M., Sun X., Du X., Zhang X., Wang Y., Yang S., Wang X., Feng Y., *Neurotoxicology*, **2009**, 30, 986.
- <sup>67</sup> a) Barnham K.J., Cappai R., Smith D.G., *Biochim. Biophys. Acta*, **2007**, 1768, 1976; b) Szalai V.A., Kaupp L.J., Karr J.V., *J. Am. Chem. Soc.*, **2004**, 126, 13534; c) Perry G., Smith M.A., Wang X., Su B., Zhu X., *Cell. Mol. Life Sci.*, **2007**, 64, 2202.

---

<sup>68</sup>a) Varadarajan S., Yatin S., Aksenova M., Butterfield D.A., *J. Struc. Biol.*, **2000**, 130, 184; b) Pinho C.M., Teixeira P.F., Glaser E., *Biochim. Biophys. Acta*, **2014**, 1837, 1069; c) Benzi G., Moretti A., *Neurobiol. Aging*, **1995**, 16, 4, 661.





## *2. Antioxidant activity of Manganese complexes*



## 2.1 Manganese complexes as artificial superoxide dismutase (SOD) and catalase (CAT) enzymes: a general introduction

Many studies have been done to create mimicking systems of natural SOD and CAT enzymes. In particular, they describe the use of mononuclear manganese compounds with one metal center able to dismutate superoxide anion, and dinuclear manganese complexes able to eliminate hydrogen peroxide. There are only few compounds reported in literature that are able to perform both reactions, and usually mononuclear compounds form dimeric structure to dismutate hydrogen peroxide. There are several parameters to evaluate SOD activity. The first analysis is the redox potential of the species, indeed optimal SOD activity requires a potential close to 0.36V vs. Normal Hydrogen Electrode (NHE), an intermediate value between superoxide reduction potential (0.89V) and oxygen reduction potential (-0.16V, pH 7). Natural SODs are in a range of potentials between 0.2-0.45V (Figure 14).<sup>1</sup>

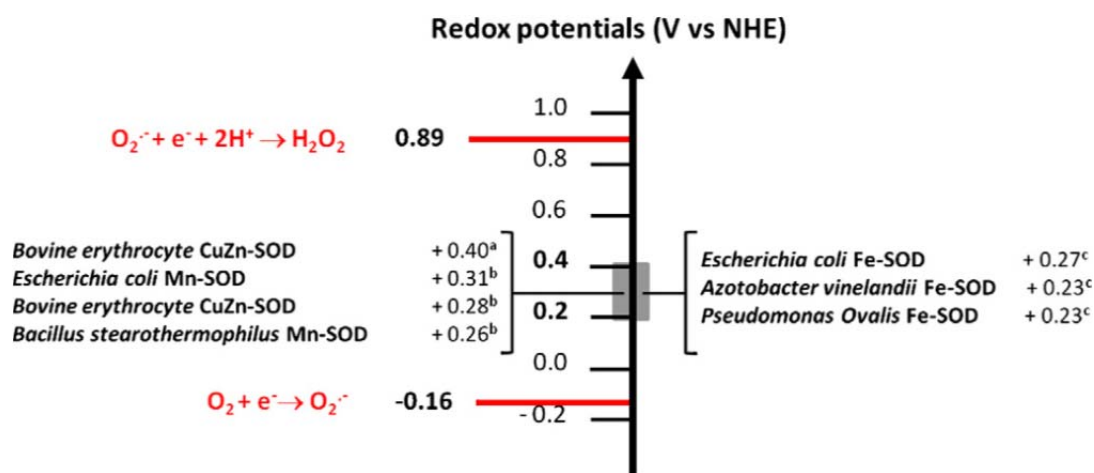


**Figure 14:** Redox potential of natural SODs at pH 7 (a<sup>2</sup>,b<sup>3</sup>,c<sup>4</sup>).

Direct methods are available to estimate kinetic constant of superoxide dismutation, among these techniques we found pulse radiolysis and stopped flow analysis, in which superoxide anion is formed *in situ* and the kinetic of superoxide dismutation is followed by UV-Vis measurements. Considering indirect methods what is usually measured is the IC<sub>50</sub>, the concentration at which SOD mimic inhibits 50% of superoxide production, measured thanks to a sacrificial molecular probe (the absorbance of reduced specie is followed to evaluate superoxide production). For example, EPR spectroscopy exploits a spin-trap

sacrificial compound (usually DMPO). The most common method is known as McCord-Friedovich (McCF), whereby superoxide is generated in buffer solution with a xanthine/xanthine oxidase system and the reduction of the sacrificial compound (nitro blue tetrazolium (NBT) or cytochrome c) is used to convert  $O_2^-$  to dioxygen, while the formation of their reduced species is followed by UV-Vis spectroscopy.<sup>5,6</sup> From  $IC_{50}$ , that depends on the molecular probe and its concentration, it is possible to calculate the catalytic rate constant,  $k_{McCF}$  (Figure 15) with which it is possible to have a good comparison between the SOD mimics.

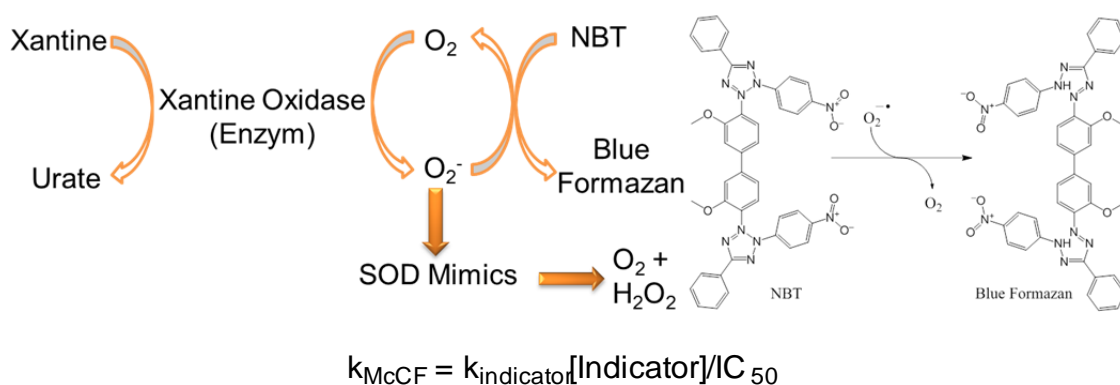


**Figure 15:** Scheme of indirect method with xanthine/xanthine oxidase system, NBT as indicator and formula needed to calculate the kinetic constant of superoxide elimination. On the right, reduction of NBT and formation of blue formazan, followed at 550nm.

Three other characteristics are needed to have a good SOD mimicking complex: it should be able to cycle from  $Mn^{II}$  to  $Mn^{III}$ , the ligand should be stable in both oxidation states and there must be at least one coordination site for binding superoxide. There are many ligand systems for manganese atoms that match all these properties, starting from porphyrins, to macrocyclic ligands, Salen/Shiff's base ligands like and acyclic multidentate ligands (Figure 16).<sup>1</sup>

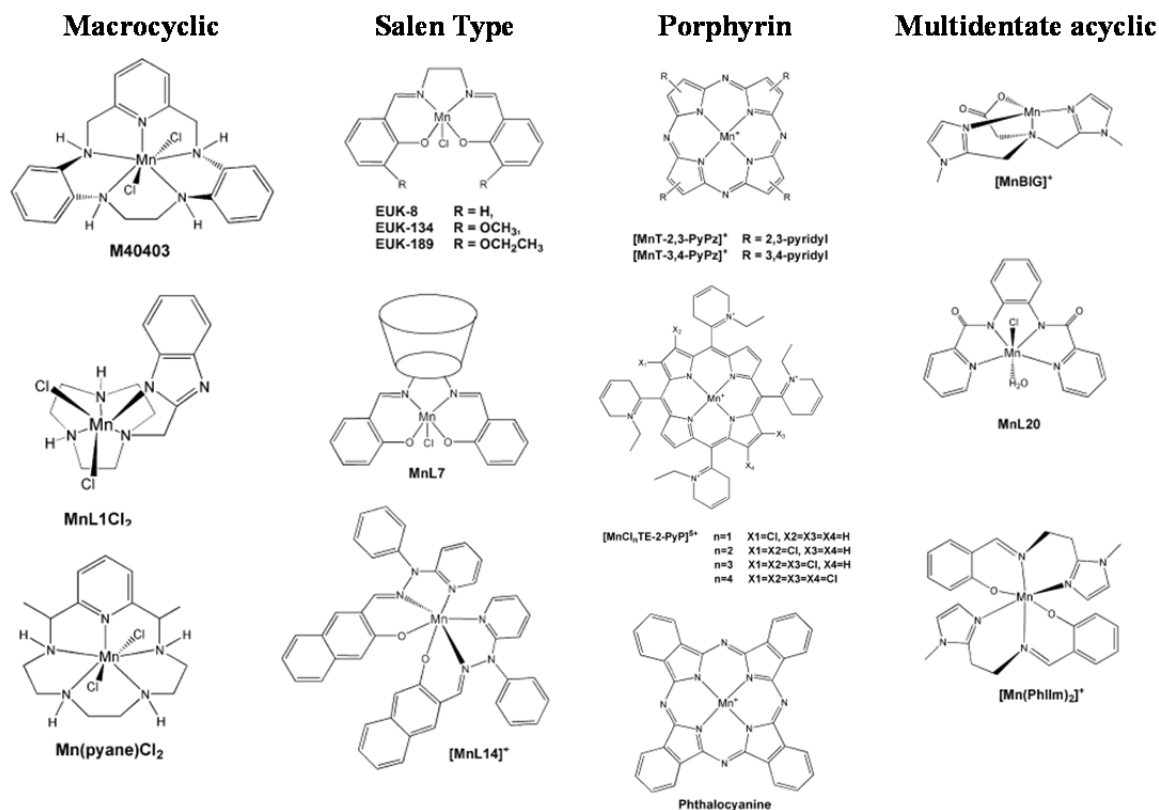
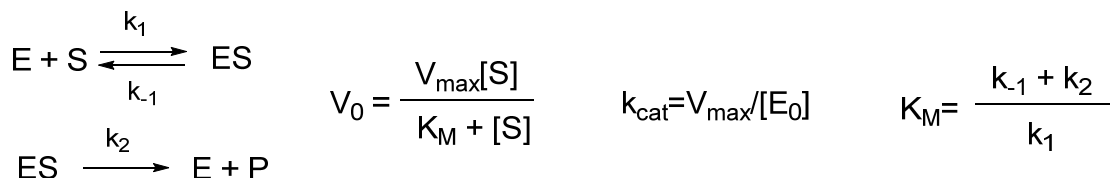


**Figure 16:** Some example of macrocyclic, Salen type, porphyrins and multidentate acyclic manganese complexes with SOD activity.

Many other factors should also be considered for a successful biological application, like lipophilicity, that should favors internalization in mitochondria, and maintenance of the activity *in vitro* and *in vivo*. To date, however, only few molecules, for example M4040X family have been tested *in vivo*.<sup>7</sup>

Elimination of superoxide anion by dismutation is not enough, indeed hydrogen peroxide is formed during the reaction and, in the presence of iron or other reactive metals, it can undergoes Fenton reactions leading to formation of harmful hydroxyl radicals. For this reason, SOD mimics should be used together with CAT mimics or, even better, they should present a dual activity Many dinuclear manganese complexes have been synthesized in the last ten years, trying to imitate natural manganese catalase. Comparison among complexes is usually done considering second order kinetic constant of hydrogen peroxide dismutation. When the kinetic constants, calculated at increasing H<sub>2</sub>O<sub>2</sub> concentrations, exhibits a saturation behavior, Michaelis–Menten parameters can also be calculated. In the last case, a saturation behavior with a limiting maximum rate, and two constants, K<sub>M</sub>, the

affinity constant (it is the substrate concentration at which the reaction rate is half of  $V_{max}$ ), and  $k_{cat}$ , the unimolecular rate constant for ES dissociation into pristine enzyme and products (the higher is the value, the higher is the number of catalytic cycle performed by the catalyst), can be achieved (Scheme 5).<sup>8</sup>



**Scheme 5:** Michaelis-Menten equilibria, equation for the initial rates and kinetic constants  $k_{cat}$  and  $K_M$ .

These two parameters allow to compare artificial catalases with the natural one, indeed Michaelis-Menten behavior is typical of enzymatic systems. In this system, the intermediate, ES, specie is considered to be in a steady state. It is possible to obtain an equation with a maximum rate value ( $V_{max}$ ) and the Michaelis constant ( $K_M$ ), from which it is possible to calculate  $k_{cat}$ , that depends on enzyme concentration. These parameters allow the comparison with other similar systems known in literature. Furthermore  $k_{cat}/K_M$  ratio gives an idea of catalyst efficiency, the higher is the ratio, the higher is the catalytic efficiency: for natural enzymes  $k_{cat}$  is often very high while  $K_M$  is very low. In table 2 are reported some values of  $k_{cat}$  and  $K_M$  of different literature compound able to dismutate hydrogen peroxide.

**Table 2:** Artificial Mn systems with catalase-like activity compared in terms of efficiency parameters and reaction conditions.

Entry <sup>ref.</sup>	Catalyst	$k_{cat}(s^{-1})$	$K_M(mM)$	Solvent T(°C)
<i>DiMn catalysts that disproportionate H<sub>2</sub>O<sub>2</sub> with saturation kinetics<sup>a</sup></i>				
1 <sup>9</sup>	[Mn <sub>2</sub> (μ-OAc) <sub>2</sub> (X <sup>1</sup> -hppnO)] <sup>+</sup>	3.4-23	150-600	DMF, 25
2 <sup>10</sup>	[Mn <sub>2</sub> (μ-OAc)(μ-OMe)(X <sup>2</sup> -hppentO)] <sup>+</sup>	1.31-2.8	88-170	DMF, 10
3 <sup>11</sup>	[Mn(X <sup>3</sup> -salpnO) <sub>2</sub> ]	4.2-21.9	10-120	CH <sub>3</sub> CN, 25
4 <sup>12</sup>	[Mn <sub>2</sub> (μ-O)(OAc)(OH)(benzimpnO)] <sup>+</sup>	2.7	6	MeOH:H <sub>2</sub> O, 25
5 <sup>13</sup>	[Mn <sub>2</sub> (μ-OAc)(μ-OMe)(X <sup>4</sup> -salpentO)S <sub>2</sub> ] <sup>+</sup>	0.75-7.9	16-78	DMF, 25
6 <sup>14</sup>	[Mn <sub>2</sub> (μ-OAc) <sub>2</sub> (bphpmp)] <sup>+</sup>	2.48	83	NR, 25
7 <sup>15</sup>	[Mn <sub>2</sub> (X <sup>5</sup> -bphba)Cl <sub>2</sub> ] <sup>+</sup>	0.017-0.075	20-151	H <sub>2</sub> O, 25
8 <sup>16</sup>	[Mn <sub>2</sub> (etsalim) <sub>4</sub> (Hetsalim) <sub>2</sub> ] <sup>2+</sup> + 5 equiv. OH <sup>-</sup>	0.038	21	EtOH, 25
9 <sup>17</sup>	[Mn(bpia)(μ-OAc)] <sub>2</sub> <sup>2+</sup>	0.237	45	DMF, 25
10 <sup>18</sup>	[Mn <sub>2</sub> (μ-O) <sub>2</sub> (μ-OAc)(Me <sub>3</sub> -tacn)(OAc) <sub>2</sub> ]	5.5	-	Ac. buffer, pH 4.6, 20
11 <sup>18</sup>	[Mn <sub>2</sub> (μ-O) <sub>2</sub> (μ-OAc)(Me <sub>3</sub> -tacn)(bipy)] <sup>2+</sup>	13.2	-	Ac. buffer, pH 4.6, 20
12 <sup>19</sup>	[Mn <sub>2</sub> (μ-Cl) <sub>2</sub> (tpa) <sub>2</sub> ] <sup>2+</sup>	107	3100	CH <sub>3</sub> CN, 25
13 <sup>20</sup>	[Mn(μ-O)(salpn)] <sub>2</sub>	250	250	Cl <sub>2</sub> CH <sub>2</sub> /CH <sub>3</sub> CN, 25

	Catalyst	$k_{cat}(s^{-1})$	Solvent T(°C)
<i>DiMn catalysts that disproportionate H<sub>2</sub>O<sub>2</sub> with second order kinetics<sup>b</sup></i>			
<b>14</b> <sup>21</sup>	[Mn <sub>2</sub> (bpmp)(μ-OAc) <sub>2</sub> ] <sup>+</sup>	0.29	DMF, 20
<b>15</b> <sup>22</sup>	[Mn <sub>2</sub> (pmpemp)(μ-OAc) <sub>2</sub> ] <sup>+</sup>	14.5	CH <sub>3</sub> CN, 0
<b>16</b> <sup>23</sup>	[Mn <sub>2</sub> (μ-O) <sub>2</sub> (tpa) <sub>2</sub> ] <sup>3+</sup>	0.065	CH <sub>3</sub> CN, 0
<b>17</b> <sup>23</sup>	[Mn <sub>2</sub> (μ-O) <sub>2</sub> (bpg) <sub>2</sub> ] <sup>+</sup>	0.29	CH <sub>3</sub> CN, 0
<b>18</b> <sup>23</sup>	[Mn <sub>2</sub> (μ-O) <sub>2</sub> (pda) <sub>2</sub> ] <sup>-</sup>	1.6	CH <sub>3</sub> CN, 0
<b>19</b> <sup>24</sup>	[Mn <sub>2</sub> (μ-O) <sub>2</sub> (X <sup>6</sup> -bispicMe <sub>2</sub> en) <sub>2</sub> ] <sup>2+</sup>	14-35	Phosphate buffer 7.5, 30

a: saturation kinetics, rates described by Michaelis-Menten model;

b: second order kinetics =  $k_{cat}[cat][H_2O_2]$

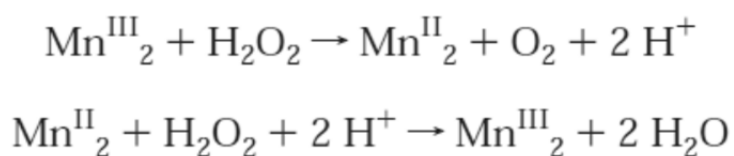
S = solvent, X<sup>1</sup>= OMe, Cl; X<sup>2</sup>= OMe, H, Br; X<sup>3</sup>= 5-OCH<sub>3</sub>, H, 5-NO<sub>2</sub>; X<sup>4</sup>= OMe, Me, H, Cl Br, NO<sub>2</sub>;

X<sup>5</sup>= OMe, Me, H, NO<sub>2</sub>; X<sup>6</sup>= H, OEt, Me, Cl, NO<sub>2</sub>.

These kinetics are usually followed monitoring the oxygen evolution, measuring the volume of oxygen evolved, the pressure produced or by using a Clark electrode, sensible to oxygen concentration.

Mn complexes can be characterized by EPR, electrochemistry and IR spectroscopy. Although NMR analysis is not possible due to manganese paramagnetism, quite often crystal structures are available. While there is a huge number of ligands that coordinate two manganese atoms to give catalase mimics, only few mononuclear compounds have shown a dual activity. Noteworthy, the formation of dinuclear species, in particular for salen complexes, has been suggested also in in such cases.

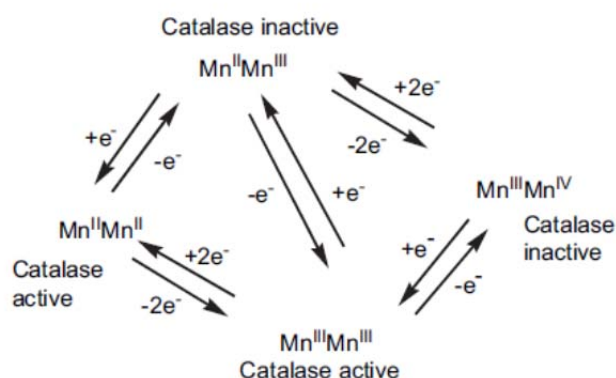
In the catalytic cycle, the two manganese atoms run from oxidation state +II to +III, sometimes also oxidation state +IV is involved (Scheme 6).<sup>25</sup>



**Scheme 6:** Catalytic cycle of dimanganese core of catalase mimicking systems

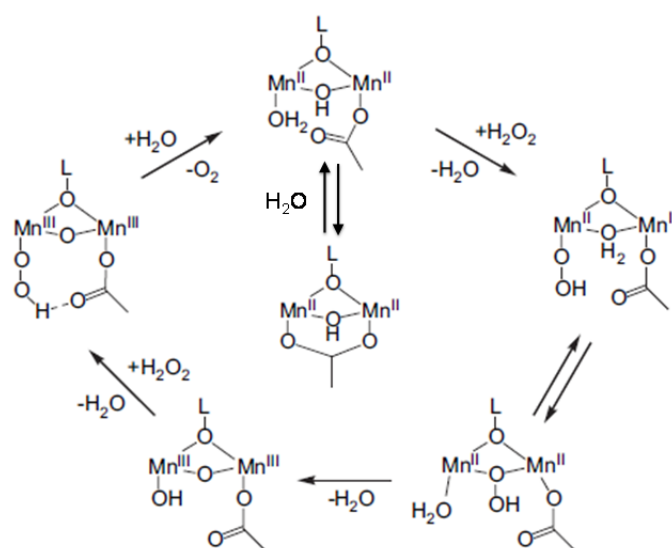
There are many example of catalase mimics in literature, containing alkoxo, phenoxo,oxo and carboxylate. Since the ligand change Mn environment and distance, the structure affect the reactivity behavior of Mn centers, which can go from Mn<sub>2</sub><sup>II</sup> to Mn<sub>2</sub><sup>III</sup> but could also reach Mn<sub>2</sub><sup>IV</sup>, for example with salophen ligands. While Mn<sup>III</sup>Mn<sup>IV</sup> state is inactive towards hydrogen peroxide dismutation for natural enzymes (Scheme 7), artificial catalase usually are active at such oxidation state with some exception that work in higher oxidation states.

Mn<sup>II</sup>Mn<sup>III</sup> oxidation state is also inactive in natural catalase, while Mn<sub>2</sub><sup>II</sup> is very sensible to anionic inhibitors like azide (N<sub>3</sub><sup>-</sup>), phosphate (HPO<sub>4</sub><sup>2-</sup>) and halides like chloride and fluoride (Cl<sup>-</sup>, F<sup>-</sup>).<sup>26</sup>



**Scheme 7:** Scheme of interconversion between different oxidation states in Mn-catalase enzymes. Mono-electronic reactions lead to inactive form of catalase, with mixed oxidation states.

The proposed catalytic cycle for artificial catalase is quite similar to the natural one, indeed the dimanganese core cycles from Mn<sup>II</sup>Mn<sup>II</sup> to Mn<sup>III</sup>Mn<sup>III</sup> oxidation state with respectively reduction of hydrogen peroxide to water and oxidation to oxygen. In the proposed cycle, a water molecule replace one coordination site of manganese left free by the bridging ligand. Water is then replaced by hydrogen peroxide and after two proton exchanges, water is released and manganese core oxidized to III-III; hydrogen peroxide coordinates again and oxygen is released with the reduction of manganese core to II-II, then the cycle starts again (Scheme 8).<sup>12</sup>



**Scheme 8:** Proposed catalytic for artificial catalase systems with carboxylate apical ligands.



Ligands can also be divided in binucleating, in which one ligand coordinates two metal centers, and non-binucleating in which two or more ligands coordinate the two manganese atoms (Figure 17).<sup>27</sup>

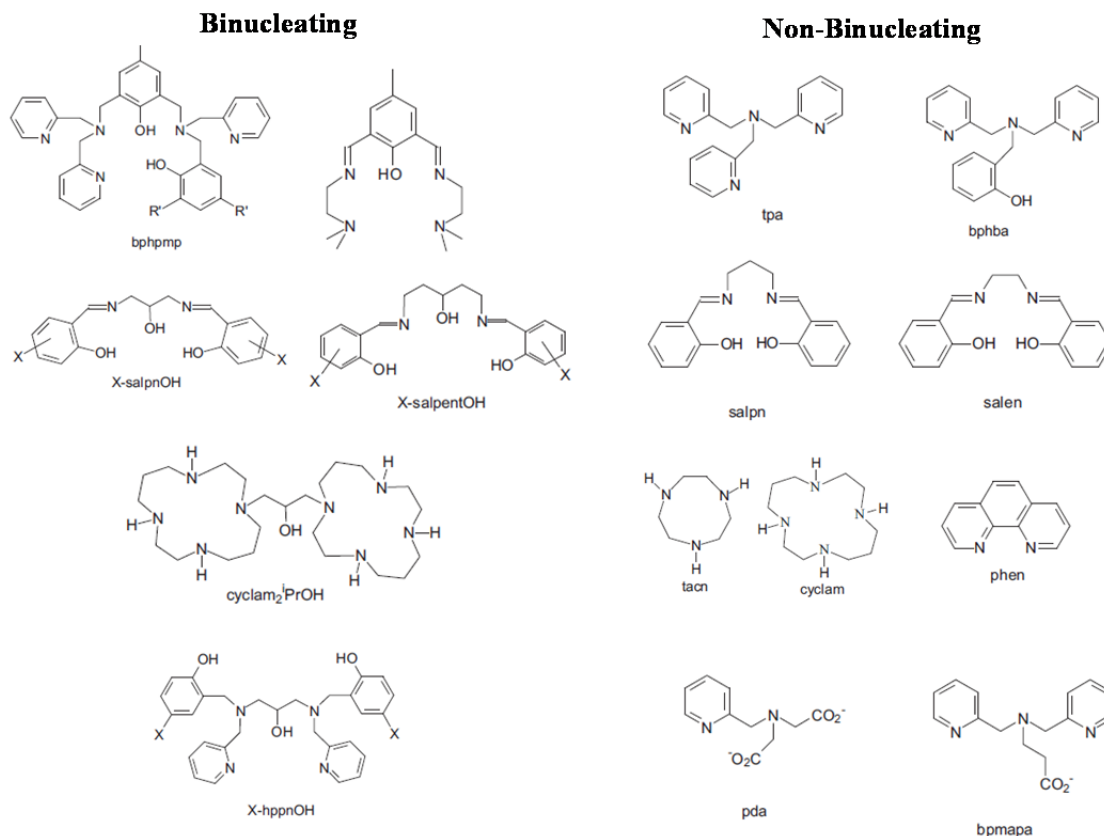


**Figure 17:** Some common binucleating and non-binucleating ligands of artificial dinuclear catalase and their abbreviation.

Obviously, all these complexes should have a labile position where coordinate hydrogen peroxide, very often this is occupied by a bridging carboxylate. It has been demonstrated that the presence of a carboxylate ligand could change drastically the reactivity of some complexes, indeed if the ligands stabilize the  $Mn_2^{II}$  form, catalase activity predominates, while if  $Mn_2^{III}$  state is stabilized, catalase activity disappears and the epoxidation of organic substrates is favored.<sup>26</sup>

In the following chapters will be presented the results obtained with some mononuclear manganese complexes, with both CAT and SOD activity, and with a dinuclear manganese complex with high catalase activity, including its modification for mitochondrial targeting and preliminary toxicity tests on isolated mitochondria.

## 2.2 Mononuclear compounds [MnLX<sub>2</sub>] (1-3)

Herein a series of seven-coordinate Mn<sup>II</sup> complexes with linear pentadentate ligands **1-3** (Figure 18) and their potential as catalytic antioxidants is presented. The series comprises isostructural ligands with both hard nitrogen and oxygen donors (NMe)<sub>2</sub>Py<sub>3</sub> (**1**), (NTos)<sub>2</sub>Py<sub>3</sub> (**1'**) and O<sub>2</sub>Py<sub>3</sub> (**2**) as well as a soft sulfur-containing analogue S<sub>2</sub>Py<sub>3</sub> (**3**).<sup>28</sup>

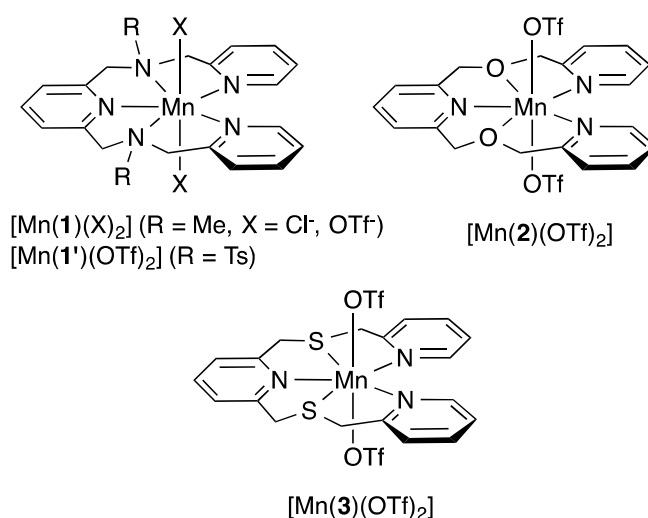


**Figure 18:** Seven coordinate Mn(II) complexes containing linear pentadentate ligands with N, O and S donors (**1-3**).

The synthesis and characterisation of the ligands and metal complexes, by the group of prof. George Britovsek (Imperial College London) are provided in the Experimental part. A seven-coordinate geometry was confirmed for complexes [Mn(**1**)Cl<sub>2</sub>] and [Mn(**2**)(OTf)<sub>2</sub>] in the solid state (see Figures 19) and is comparable to the structure of the macrocyclic Mn<sup>II</sup> complex called M40403 (see page 29).<sup>29</sup> In all cases, a distorted pentagonal bipyramidal coordination geometry is observed with the pentadentate ligand that chelate the manganese atoms and two apical ligands, chloride or triflate, that complete the coordination sphere of manganese.

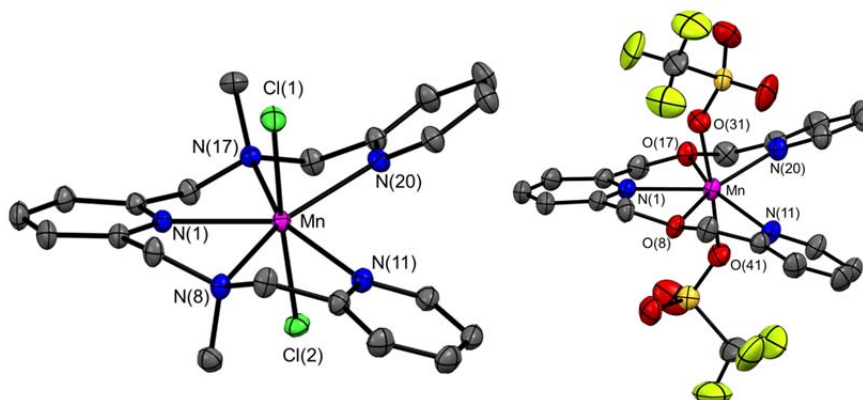


**Figure 19:** Molecular structure of [Mn(1)Cl<sub>2</sub>] (left) and molecular structure of [Mn(2)(OTf)<sub>2</sub>] (right).

Triflate ligands are generally weakly coordinating and are easily displaced in acetonitrile or aqueous solutions to give complexes of the type [Mn(L)(S)<sub>2</sub>](OTf)<sub>2</sub> with coordinated solvent ligands (S = acetonitrile or water) and uncoordinated triflate anions. The Mn<sup>II</sup> complexes studied here are high spin over the temperature range from 233 and 343 K in acetonitrile solution, with magnetic moment values of 5.9-6.0 μ<sub>B</sub>. NMR spectroscopy is normally not useful for Mn<sup>II</sup> complexes due to the extreme line-broadening caused by the paramagnetic Mn<sup>II</sup> center. Cyclic voltammograms in acetonitrile are featureless between -1.5 V and +1.5 V (vs. Ag/AgNO<sub>3</sub>), as was noted for related dicationic seven-coordinate Mn<sup>II</sup> complexes.<sup>30</sup> All complexes are essentially colourless and the UV-Vis spectra are featureless at wavelengths above 300 nm, indeed charge transfer and d-d transitions are not expected in the visible region for these Mn<sup>II</sup> complexes and the only absorptions seen are due to π-π\* transitions in the region of 260-280 nm (Figure 20).<sup>31</sup>

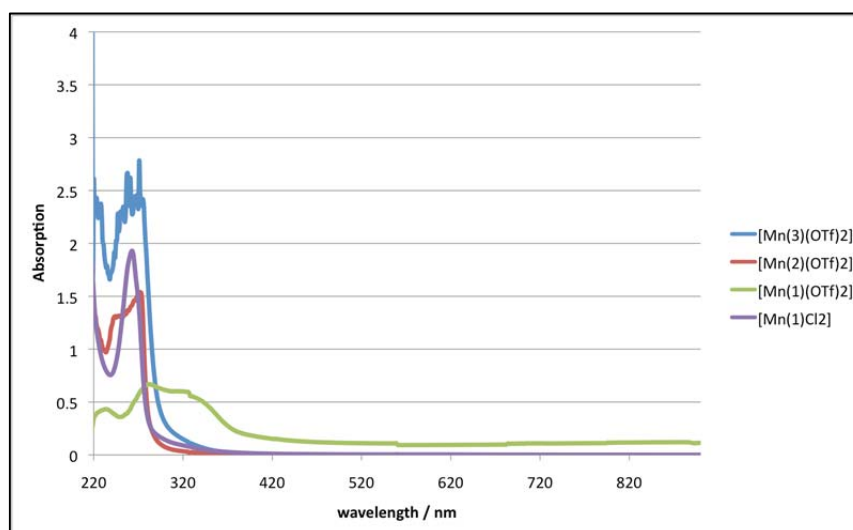


**Figure 20:** UV-Vis spectra of 0.1mM manganese(II) complexes in CH<sub>3</sub>CN at 298 K.

Catalase-like activity of the complexes was initially evaluated in aqueous acetonitrile (in order to have a comparison with literature compounds), in the presence of excess H<sub>2</sub>O<sub>2</sub> (550 equivalents) by monitoring continuous oxygen evolution. The observed catalytic performances have been examined by determining the initial rate (R<sub>0</sub>), O<sub>2</sub> yield and turnover number (TON, defined as mole of dioxygen evolved per mole of catalyst). The results are collected in Table 3 and compared with literature data on salen-type complexes, which decompose irreversibly in water after several minutes.<sup>27,32</sup>

**Table 3:** CAT-like activity of mononuclear Mn complexes<sup>‡</sup>.

Compound	R <sub>0</sub> <sup>a</sup> (μM/min)	% O <sub>2</sub> yield (μM)	TON
Salen-type complexes <sup>b,27,32</sup>	260-29	0.7-3.3 (36-167)	4-17
[Mn( <b>2</b> )(OTf) <sub>2</sub> ] <sup>c</sup>	18	6.3 (1038)	17
[Mn( <b>1</b> )(OTf) <sub>2</sub> ] <sup>c</sup>	29	8.7 (1426)	24
[Mn( <b>1</b> )(Cl) <sub>2</sub> ] <sup>c</sup>	5	0.6 (107)	2
[Mn( <b>1'</b> )(OTf) <sub>2</sub> ] <sup>c</sup>	8	2.4 (397)	7
[Mn( <b>3</b> )(OTf) <sub>2</sub> ] <sup>c</sup>	128	14 (2310)	39
[Mn( <b>3</b> )(OTf) <sub>2</sub> ] <sup>d</sup>	317	100(16500)	275
[Mn( <b>3</b> )(OTf) <sub>2</sub> ] <sup>e</sup>	25	12 (1950)	33

a)Initial reaction rate calculated as μMO<sub>2</sub>/min; b)[Mn]=10μM, [H<sub>2</sub>O<sub>2</sub>]=10mM, 50mM phosphate buffer (pH 7-8), 3 min, 25 °C; c)[Mn]=60μM, [H<sub>2</sub>O<sub>2</sub>]=33mM, CH<sub>3</sub>CN, 2 h, 25 °C; d) addition of NaOH sol. (10μL 1M), CH<sub>3</sub>CN, 5h; e)[Mn]=60μM, [H<sub>2</sub>O<sub>2</sub>]= 3mM, 50mM borate buffer (pH 9.2), addition of 600μM imidazole, 75 min, 25 °C.

From Table 3, it can be observed that the activity is strongly affected by the nature of the ligands, increasing in the order (NTos)<sub>2</sub>Py<sub>3</sub> (**1'**) < O<sub>2</sub>Py<sub>3</sub> (**2**) < (NMe)<sub>2</sub>Py<sub>3</sub> (**1**) < S<sub>2</sub>Py<sub>3</sub> (**3**) for the bis(triflato) complexes, while the dichlorido complex [Mn(**1**)Cl<sub>2</sub>] is the least active. In comparison with previously reported results, these complexes display good catalyst stability as oxygen evolution is detected up to 2 hours of reaction and turnovers up to 39 can be obtained (Figure 21).

<sup>‡</sup> A “health warning” has to be applied when comparing activities determined for different catalysts systems by different groups of researchers in different labs.

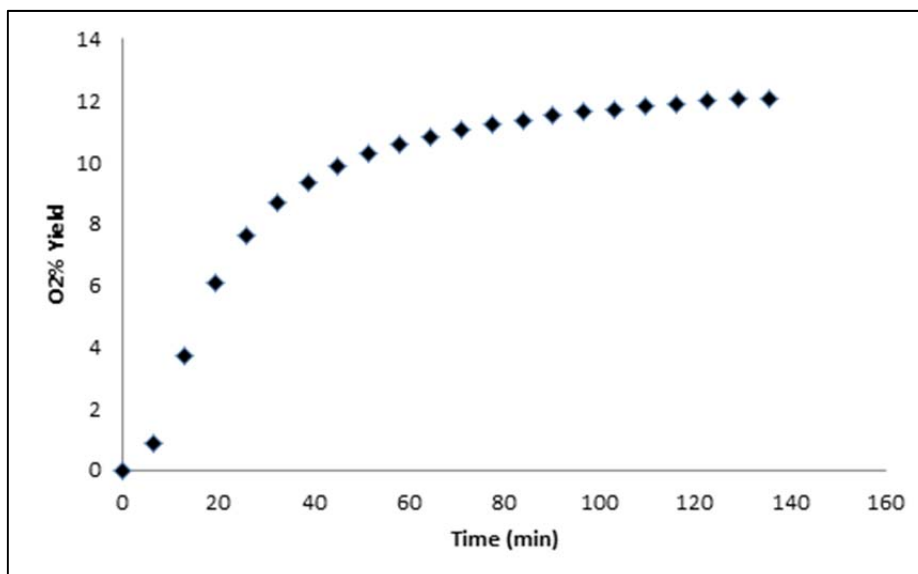


**Figure 21:** H<sub>2</sub>O<sub>2</sub> (33 mM) dismutation by [Mn(3)(OTf)<sub>2</sub>] (60 μM) in 12ml CH<sub>3</sub>CN at 25.0 °C.

In all cases, the dismutation activities level off after approximately 20 minutes, but no precipitation or color change was observed at the end of the reaction. FTIR analysis of the recovered catalysts showed only little changes and no complex degradation (Figure 22).<sup>33</sup>

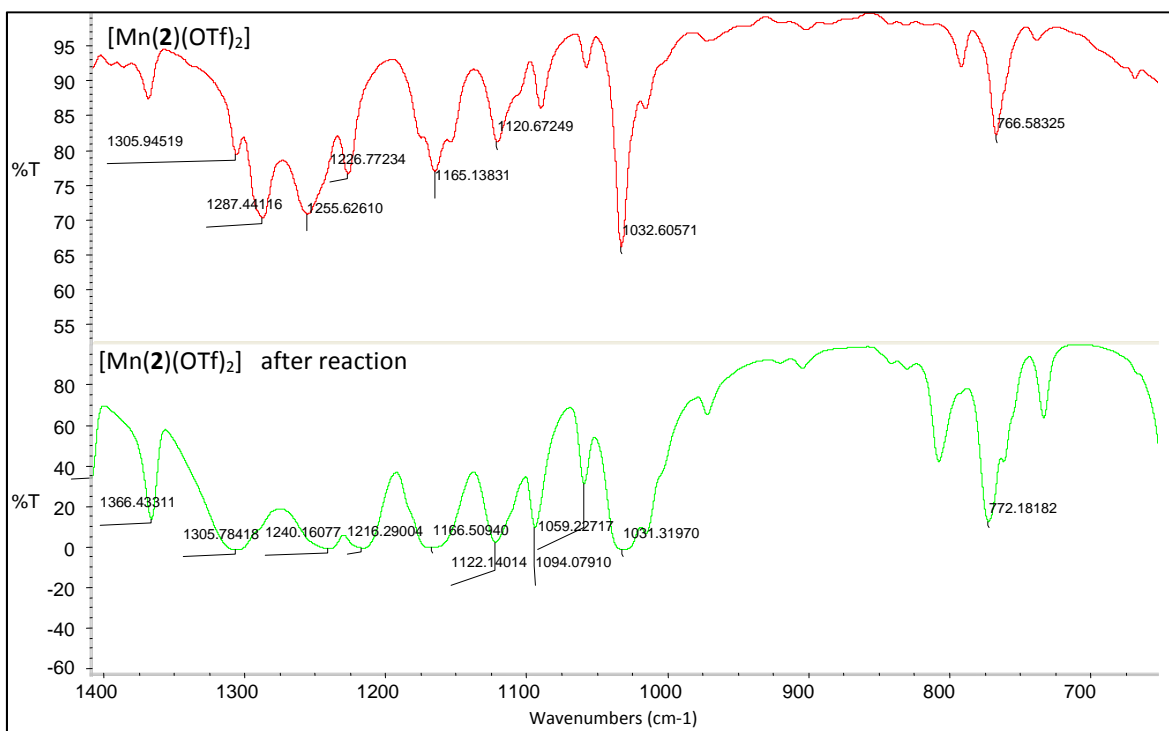


**Figure 22:** Comparison between FTIR spectra of [Mn(2)(OTf)<sub>2</sub>] before (red)/after (green) H<sub>2</sub>O<sub>2</sub> dismutation reaction in CH<sub>3</sub>CN.

The kinetic profiles at different  $[\text{Mn}(\mathbf{3})(\text{OTf})_2]$  concentrations show a well-behaved first order dependence within the range of 30-90  $\mu\text{M}$  (Figure 23). This observation is consistent with the involvement of a single-site catalyst in the rate-determining step of the process. The reaction mechanism is believed to involve the formation of a high valent  $\text{Mn}=\text{O}$  intermediate, followed by a rate limiting attack of  $\text{H}_2\text{O}_2$ , finally ending in  $\text{O}_2$  release.<sup>34</sup>

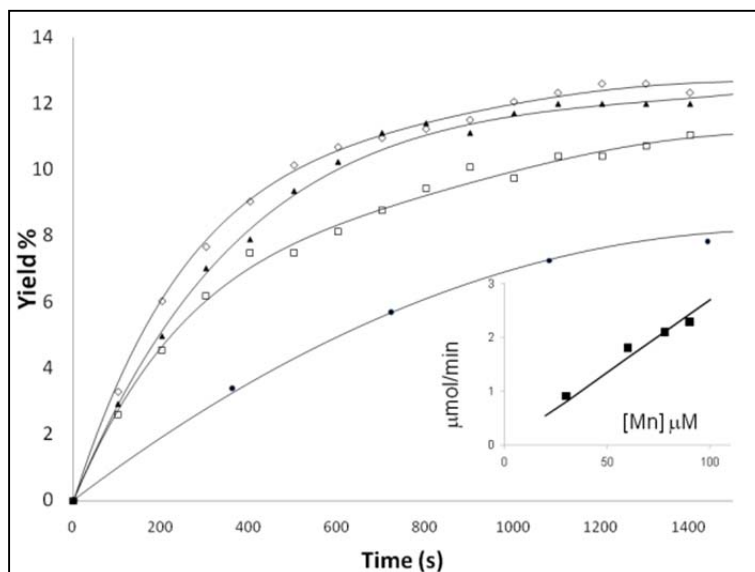


**Figure 23:** Yield of oxygen evolution *versus* time at different  $[\text{Mn}(\mathbf{3})(\text{OTf})_2]$  concentrations ( $\bullet$  30  $\mu\text{M}$ ,  $\square$  60  $\mu\text{M}$ ,  $\blacktriangle$  78  $\mu\text{M}$ ,  $\diamond$  90  $\mu\text{M}$ ) in  $\text{CH}_3\text{CN}$ , 25  $^\circ\text{C}$ . Inset: initial rate of  $\text{O}_2$  evolution *versus*  $[\text{Mn}(\mathbf{3})(\text{OTf})_2]$  concentration.

The progressive addition of water resulted in a decrease of the activity of  $[\text{Mn}(\mathbf{3})(\text{OTf})_2]$ . Since more water is produced from the dismutation reaction, this may explain the inhibition at longer reaction times. More importantly, the pH of the solution appears to have a major influence on the stability of the catalyst system. The addition of small amounts of acid ( $\text{HCl}$ , 0.1M, 10  $\mu\text{L}$ ) resulted in an immediate loss of CAT activity, whereas the addition of a base ( $\text{NaOH}$ , 1M, 10  $\mu\text{L}$ ) generated a very active ( $R_0 = 317 \mu\text{M}/\text{min}$ ) and remarkably stable catalyst performance ( $\text{TON}=275$ ) and resulted in 100% oxygen evolution within 5 hours (Figure 24).

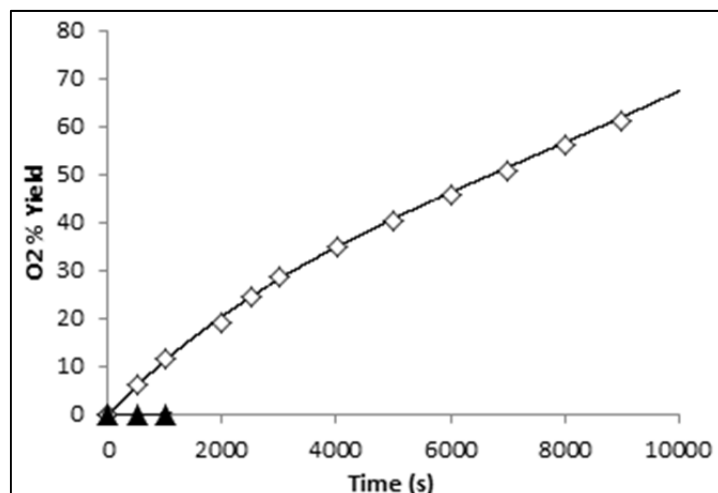


**Figure 24:** Yield of oxygen evolution *versus* time using [Mn(3)(OTf)<sub>2</sub>] (60 μM), H<sub>2</sub>O<sub>2</sub> 33mM in CH<sub>3</sub>CN, 25 °C with the addition of 10 μl NaOH 1M ◊ and 10 μl of HCl 0.1M ▲.

Further investigations have shown that the reaction can also be carried out in an aqueous borate buffer solution at pH 9.2 with minimal catalyst deactivation, but only when an additional coordinating base such as imidazole is added (see Table 3). On the contrary, the addition of imidazole in acetonitrile did not increase the reactivity. The beneficial effect of added base in the H<sub>2</sub>O<sub>2</sub> dismutation reaction was also noted by others authors.<sup>35,36,§</sup>

The novel seven-coordinate Mn(II) complexes of ligands **1-3** also show SOD-like activity in aqueous environment. The SOD reactivity of all complexes was evaluated using the NBT (nitro blue tetrazolium chloride) method, which allows monitoring of the catalytic removal of O<sub>2</sub><sup>-•</sup> generated in a xanthine/xanthine oxidase system.<sup>37</sup> SOD activities were determined as IC<sub>50</sub> (50% inhibition of NBT reduction) and the results are collected in Table 4. Overall, the Mn<sup>II</sup> complexes with ligands **1-3** show similar or lower activity, if compared to the reference complexes EUK-113 and the salen complexes.<sup>33,38,39</sup> The sulfur-containing complex [Mn(3)(OTf)<sub>2</sub>] provides the best SOD-like activity within the series with a kinetic constant close to that of M40403, known as the best only-SOD mimetic complex. The tosylated complex [Mn(1')(OTf)<sub>2</sub>] was inactive under these conditions, probably due to the low solubility in water. The

§ In phosphate buffer (pH 9) the catalyst is also active but less stable and performing with R<sub>0</sub> 18 μM/min and final yield of 3%. In this case, the addition of imidazole in acetonitrile did not increase the reactivity.

sulfur donors in ligand **3** are believed to generate a stronger ligand field with increased complex stability under the experimental conditions.

**Table 4:** SOD-like activity of mononuclear Mn complexes.

Compound	IC <sub>50</sub> (μM)	k <sub>MCCF</sub> (M <sup>-1</sup> s <sup>-1</sup> )
Mn-SOD of <i>Thermus thermophilus</i> <sup>40</sup>	ND	2 x 10 <sup>9</sup>
M40403 <sup>41</sup>	ND	2 x 10 <sup>7</sup>
EUK-113 <sup>a,33,39</sup>	0.13-0.7	ND
Salen complexes <sup>a, 39</sup>	0.004-0.75	ND
[Mn( <b>3</b> )(OTf) <sub>2</sub> ] <sup>b</sup>	0.75	8 x 10 <sup>6</sup>
[Mn( <b>2</b> )(OTf) <sub>2</sub> ] <sup>b</sup>	1.41	4 x 10 <sup>6</sup>
[Mn( <b>1</b> )(OTf) <sub>2</sub> ] <sup>b</sup>	1.51	4 x 10 <sup>6</sup>
[Mn( <b>1</b> )(Cl) <sub>2</sub> ] <sup>b</sup>	2.57	2 x 10 <sup>6</sup>
[Mn( <b>1'</b> )(OTf) <sub>2</sub> ] <sup>b</sup>	inactive	/
Ligand <b>3</b> <sup>c</sup>	inactive	/

a) Cytochrome 1.0 mM, 1200 units/mL catalase, 50 mM xanthine and sufficient xanthine oxidase to produce a rate of reduction of cytochrome c of 0.025 absorbance unit (at 550nm) per minute; b) Xanthine 50μM, NBT 100μM, Xanthine oxidase 0.005U/ml in phosphate buffer 50 mM pH 7.4, catalyst 0.6-1.8μM. c) Various concentrations: 0.6-1.8μM and 6μM.

As a remark, the mononuclear complexes reported have good SOD and CAT activity, in particular the sulfur containing complex **3** is the best of the series and it is able to dismutate hydrogen peroxide in water solution. This is particularly interesting if we consider that, in previous observations with a pentadentate SNNNS manganese complex, sulfur donors were found to inhibit antioxidant activity.<sup>42</sup> In contrast, the [Mn(**3**)(OTf)<sub>2</sub>] complex with an alternating NSNSN binding motif, shows dual CAT and SOD activity, surpassing the nitrogen and oxygen-based complexes.

Even if the condition are still not really near to physiological environment, this study opens new perspectives in the design of new manganese complexes as ROS scavengers. Future studies will be directed to identify the key intermediates involved in these dismutation reactions and establish structure-reactivity relationships.



### 2.3 Dinuclear complex $[\text{Mn}_2\text{L}_2\text{XClO}_4]$ (**4**): a catalytic screening

Feringa et al., in 2005, presented a catalyst, able to dismutate hydrogen peroxide, which was proposed as a molecular propeller to move silica nanoparticles dispersed in organic solvents like acetonitrile, dichloromethane and glycerol.<sup>43</sup> We have thus synthesized the same catalyst,  $[\text{Mn}_2\text{L}_2\text{X}]$ , and deeply studied its potential as artificial catalase and SOD mimicking system.

The ligand used is a dipyridylaminophenolate (**L**, Figure 25), characterized by two pyridyl rings, a tertiary amino group and a phenolate, so it is a tetradentate ligand, with three nitrogen atoms and an oxygen atom. This ligand is easily synthesized starting from dipyridylketone after five steps, that are described in the experimental part.

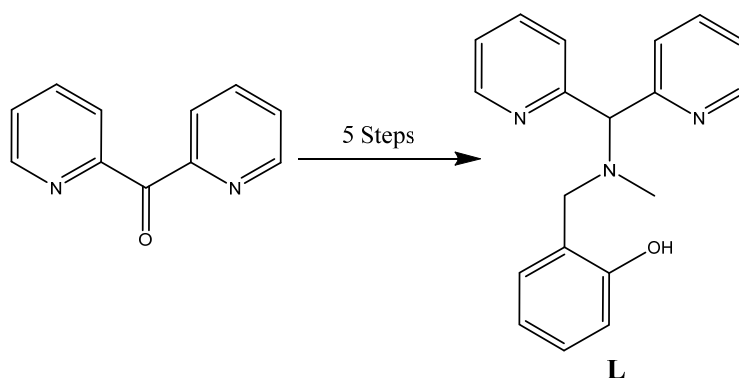


**Figure 25:** Starting material and structure of the ligand **L**.

It is a non-binucleating ligand, indeed two of them coordinate two manganese centers, while an apical bridging carboxylate complete the coordination sphere of the metals. Different catalyst  $[\text{Mn}_2\text{L}_2\text{X}]$  (**4**), were synthesized adding manganese perchlorate, a bridging ligand (benzoic acid (Bz) or 4-formyl benzoic acid (BzCHO), as in the original paper, acetate (Ac) and also chloride (Cl)) and trimethylamine to a methanol solution of **L**. The solution is left cool down after heating and a solid was recovered and washed with methanol and diethyl ether. The acetate complex was obtained in crystalline form (Figure 26).

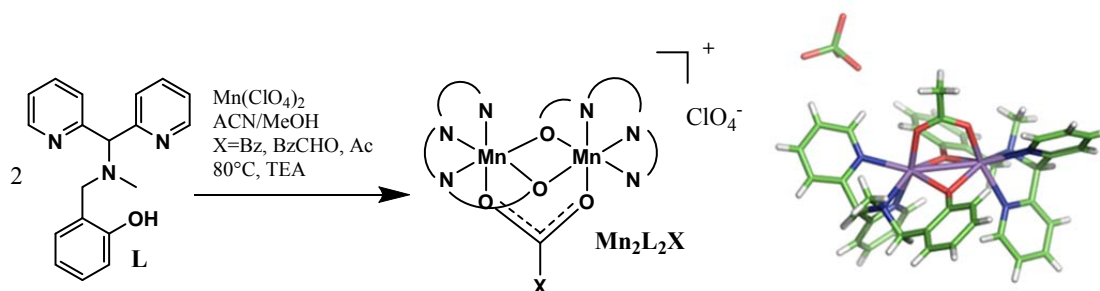


**Figure 26:** Synthesis and structure of  $[\text{Mn}_2\text{L}_2\text{X}]$  (4), with  $\text{X}=\text{CH}_3(\text{Ac})$ ,  $\text{C}_6\text{H}_5(\text{Bz})$  or  $\text{C}_6\text{H}_4\text{CHO}$  (BzCHO), carbon atoms in green, nitrogen atoms in blue, oxygen atoms in red, manganese atoms in purple and hydrogen atoms in white. (Perchlorate anion can also be recognized in the crystal structure).

Compared with other literature dinuclear compounds (Table 5), that have Mn-Mn distances higher than  $3.4\text{\AA}$ , in this case the distance is lower. Considering the acetate complex, it is characterized by a distance Mn-Mn of  $3.123\text{\AA}$ , a little bit higher than the benzoate complex, that has an Mn-Mn distance of  $3.106\text{\AA}$ . In natural compound the distances between manganese atoms are usually from  $2.9$  to  $3.6\text{\AA}$ , depending on the oxidation state of the metal centers and on the type of the ligands.<sup>44</sup>

**Table 5:** Bond distances (in  $\text{\AA}$ ) obtained by X-Ray analysis.

Complex	Mn-Mn	Mn-N(tertiary amine)	Mn-N (aromatic ring)	Mn-X
$[\text{Mn}_2(\mu\text{-Cl})_2(\text{tpa})_2]^{2+}$	$3.5519^{45}$	2.285	2.250-2.231-2.238	
$[\text{Mn}(\text{bpia})(\mu\text{-OAc})_2]^{2+}$	$4.128^{46}$	2.402	2.330-2.305	2.213
$[\text{Mn}_2(\text{X}^5\text{-bphba})\text{Cl}_2]^+$	$3.411^{47}$	2.367	2.348-2.254	2.203
$[\text{Mn}_2\text{L}_2\text{Bz}]^+$	$3.106^{43}$	2.285	2.358-2.297	2.133
$[\text{Mn}_2\text{L}_2\text{Ac}]^+$	3.123	2.351	2.377-2.277	2.129

The reactivity of dinuclear  $\text{Mn}_2\text{L}_2\text{Bz}$  was initially evaluated in  $\text{CH}_3\text{CN}$ , as in the original literature report. Accordingly to the original study,  $\text{H}_2\text{O}_2$  decomposition to oxygen and water occurs at a fast rate ( $k = 1.51 \cdot 10^{-3} \text{ s}^{-1}$ ), with no catalyst degradation, as confirmed by FTIR analysis. Then, the behavior of these complex in pure water and different buffers (phosphate buffer, MOPS/KOH and Hepes/HCl buffers at pH 7.4, borate buffer at higher pH) was widely studied, in order to get the mechanistic insight, and to optimize their activity in biological buffers and to evaluate the activity in the presence of typical CAT inhibitors. A first comparison was carried out measuring the evolved oxygen when using  $60\mu\text{M}$  of  $\text{Mn}_2$  complex and  $\text{H}_2\text{O}_2$   $33\text{mM}$  at  $25.0\text{ }^\circ\text{C}$ . Initial rate of dismutation and endpoint of reactions were compared to have an idea of the activity of the complex. As reported in table 6 below, in acetonitrile the initial rate is quite high but the reaction stops at about 50%, the same happens in water, with a lower initial rate and a similar endpoint. In water,

catalytic H<sub>2</sub>O<sub>2</sub> decomposition by Mn<sub>2</sub>L<sub>2</sub>Bz produces, within the first minutes (5 min), a drop of the solution pH, from an initial value of 7.0 to 5.5. The pH variation is likely responsible of the catalytic activity depletion in the long term. Indeed, the oxygen evolution activity can be restored at pH=6.2, upon addition of a base. Even if no H<sup>+</sup> production is considered in the proposed mechanism,<sup>48</sup> spontaneous acidification of the reaction mixture was observed in previous literature reports, where aggregation of Mn-based complexes, to form dimers and tetramers was described under catalytic regime.<sup>49</sup> The drop of activity under acidic conditions was proven by the observation, by positive ESI-MS, of the free ligand (m/z=306), while the expected peak (m/z=867) was no longer present in 5·10<sup>-4</sup>M HCl. Due to such behavior, buffer solutions were used in all the other experiments to avoid fall of the pH and of the reactivity.

**Table 6:** Initial rate and H<sub>2</sub>O<sub>2</sub> conversion of catalyst with benzoate as apical ligand (Cat 60μM, H<sub>2</sub>O<sub>2</sub> 33mM, 25°C) in acetonitrile, water, borate buffer (BBS), phosphate buffer (PBS), HEPES and MOPS.

	Compound	Solvent	R <sub>0</sub> (μMO <sub>2</sub> /s) <sup>a</sup>	Endpoint (O <sub>2</sub> mM) <sup>b</sup>
1	Mn <sub>2</sub> L <sub>2</sub> Bz	CH <sub>3</sub> CN	37	7.6 (46%)
2	Mn <sub>2</sub> L <sub>2</sub> Bz	H <sub>2</sub> O	12	8.3 (50%)
3	Mn <sub>2</sub> L <sub>2</sub> Bz	BBS (pH7.8)	38	16.5 (100%)
4	Mn <sub>2</sub> L <sub>2</sub> Bz	PBS (pH7.4)	93	6.3 (39%)
5	Mn <sub>2</sub> L <sub>2</sub> Bz	HEPES	51	1.7 (10%)
6	Mn <sub>2</sub> L <sub>2</sub> Bz	MOPS	74	2.2 (14%)

a) Initial reaction rate; b) maximum O<sub>2</sub> produced, when the reaction kinetic level off.

The initial rate was higher in buffered solutions, especially in phosphate solution, however the endpoint of reactions was lowered, indeed in phosphate buffer only 40% of conversion was reached, while in HEPES and MOPS, only 10% or a little bit higher conversion was reached. Only borate buffer allowed a quantitative dismutation. Although buffer anions affected the reactivity, FTIR spectra confirmed the higher stability of the complex, in buffered solutions, after the reaction. In addition, while synthetic catalases are very sensitive to pH, and most of them are reported to work efficiently only at pH > 9, the activity of Mn<sub>2</sub>L<sub>2</sub>X (60μM, H<sub>2</sub>O<sub>2</sub> 33mM) was maintained, in borate buffer, in the range 7.8-8.9, a range which approaches that of natural MnCATs, which display high efficiency in the pH range 7-10.<sup>50</sup>

Catalytic activity of the three complexes, and also chloride complex, in borate buffer at pH 7.8 was screened to check how the nature of the ligands influences the dismutation (Figure 27).

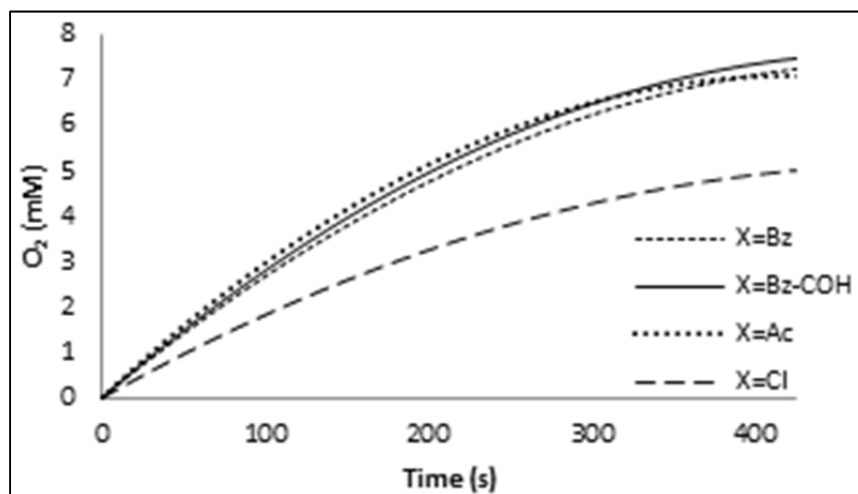


**Figure 27:** Oxygen evolution *versus* time with different  $\text{Mn}_2\text{L}_2\text{X}$  complexes  $60\mu\text{M}$ ,  $\text{H}_2\text{O}_2$   $33\text{mM}$ ,  $50\text{mM}$  BBS at pH 7.8,  $25^\circ\text{C}$ .

$\text{Mn}_2\text{L}_2\text{Bz}$ ,  $\text{Mn}_2\text{L}_2\text{BzCHO}$  and  $\text{Mn}_2\text{L}_2\text{Ac}$  have, more or less, the same kinetic profile, and yield quantitative conversion of  $\text{H}_2\text{O}_2$ . However, the presence of the carboxylate bridge is not necessary for the catalase activity. Indeed,  $\text{Mn}_2\text{L}_2\text{Cl}$  has a slower initial rate but still good values and quantitative dismutation. The low sensitivity to the bridging motif may allow the synthesis of new multifunctional compounds, also taking advantage of the aldehydic function of  $\text{Mn}_2\text{L}_2\text{BzCHO}$ , without affecting the catalase activity.

The dependence between initial reaction rate and [4] indicates a well-behaved first order kinetic dependence in the wide range of concentration explored (Figure 28). This is consistent with the integrity of the dinuclear Mn core as the active site enabling  $\text{H}_2\text{O}_2$  decomposition, and rules out any aggregation/dissociation equilibria occurring before the rate determining step of the process. The same linear trend has been observed in both organic and aqueous solvents. The stability of the dinuclear structure was confirmed by the mass spectra collected after the reaction.

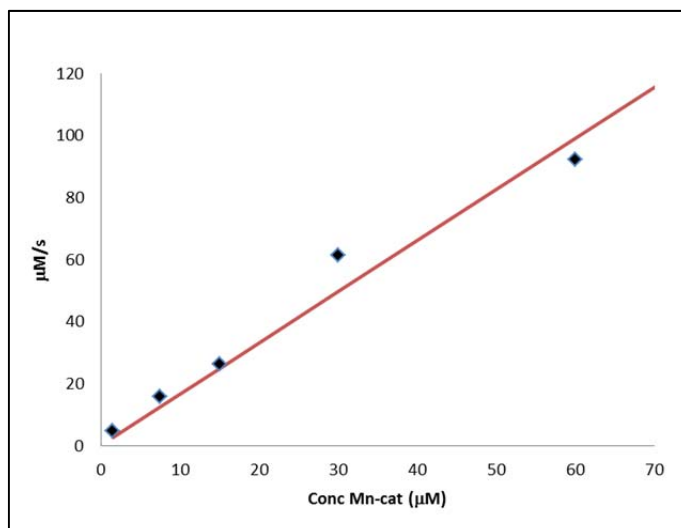


**Figure 28:** Graph of initial rate vs. **4** concentration, typical first order behavior.

Stability was also checked by FTIR spectra of catalyst before and after reaction with hydrogen peroxide in aqueous solution, there are no changes in the spectrum after  $H_2O_2$  dismutation (Figure 29), confirming the stability and the robustness of the catalyst in aqueous solution.

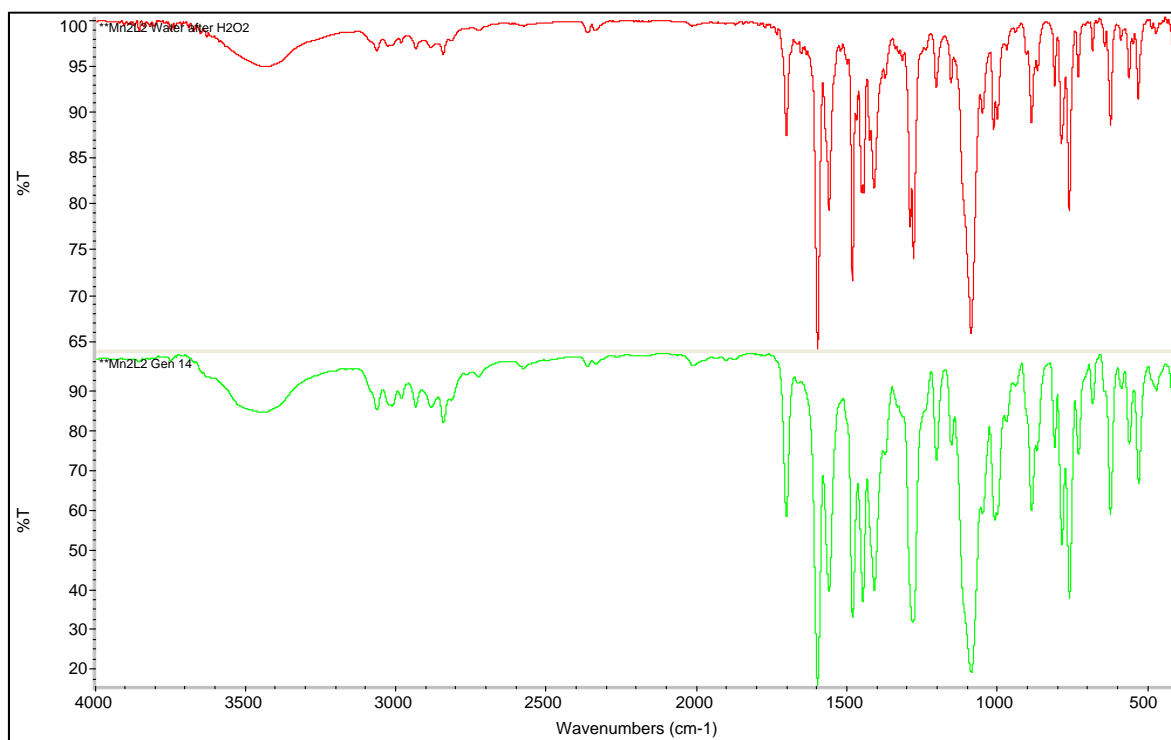


**Figure 29:** FTIR spectra of  $Mn_2L_2BzCHO$  before (green) and after (red) reaction with  $H_2O_2$ .

The CAT-like activity of the  $\text{Mn}_2\text{L}_2\text{Bz}$  has been further investigated to allow a comparison with the natural enzyme and with synthetic analogs proposed in the literature up to now. The initial rates of oxygen evolution were determined in borate buffer (50mM) at pH 7.8 and in  $\text{CH}_3\text{CN}$  at  $25^\circ\text{C}$  by setting up different  $\text{H}_2\text{O}_2$  decomposition experiments in the presence of  $[\text{Mn}_2\text{L}_2\text{X}] = 7.5\mu\text{M}$ , and varying the initial  $\text{H}_2\text{O}_2$  concentration in a wide range so that  $[\text{H}_2\text{O}_2]_0 = 22-700\text{mM}$ . Data were analyzed collecting values of oxygen evolution rate,  $R_0$  ( $\mu\text{MO}_2/\text{s}$ ), for each  $[\text{H}_2\text{O}_2]_0$  conditions. Fitting of these experimental values, according to the Michaelis-Menten equation, results in well-behaved saturation curves from which the kinetic parameters as  $V_{\text{max}}$  ( $\mu\text{MO}_2/\text{s}$ ),  $k_{\text{cat}}$  ( $\text{s}^{-1}$ ),  $K_{\text{M}}$  (mM) and  $k_{\text{cat}}/K_{\text{M}}$  ( $\text{s}^{-1}\text{M}^{-1}$ ) could be extracted. Table 7 collects Michaelis-Menten parameters of the different literature complexes. Several Mn-based systems have been proposed as artificial catalases. A large part of these are based on dinuclear  $\text{Mn}^{\text{II}}$  complexes, with close structural analogy to  $[\text{Mn}_2\text{L}_2\text{Bz}]$ , and some representative examples are reported.

**Table 7:** Summary of most active Mn complexes with CAT-like activity.

#	Catalyst	$k_{\text{cat}}$ ( $\text{s}^{-1}$ )	$K_{\text{M}}$ (mM)	$k_{\text{cat}}/K_{\text{M}}$ ( $\text{M}^{-1}\text{s}^{-1}$ )	Solvent T( $^\circ\text{C}$ )
1	$\text{Mn}_2\text{L}_2\text{Bz}$	37	470	80	BBS, pH 7.8, 25
		21	360	58	$\text{CH}_3\text{CN}$ , 25
2 <sup>11</sup>	$[\text{Mn}(\text{X}^3\text{-salpnO})_2]$	4.2-21.9	10-120	42-220	$\text{CH}_3\text{CN}$ , 25
3 <sup>12</sup>	$[\text{Mn}_2(\mu\text{-O})(\text{OAc})\text{-}(\text{OH})(\text{benzimpnO})]^+$	2.7	6	450	$\text{MeOH}:\text{H}_2\text{O}$ , 25
4 <sup>15</sup>	$[\text{Mn}_2(\text{X}^5\text{-bphba})\text{Cl}_2]^+$	0.017-0.075	20-151	1-3	$\text{H}_2\text{O}$ , 25
5 <sup>19</sup>	$[\text{Mn}_2(\mu\text{-Cl})_2(\text{tpa})_2]^{2+}$	107	3100	35	$\text{CH}_3\text{CN}$ , 25
6 <sup>20</sup>	$[\text{Mn}(\mu\text{-O})(\text{salpn})_2]$	250	250	1000	$\text{Cl}_2\text{CH}_2/\text{CH}_3\text{CN}$ , 25

There are numerous catalase mimicking system that have quite high  $k_{\text{cat}}$  and low  $K_{\text{M}}$ , so they are really efficient, however they are hardly ever reported in aqueous environment (entry 2-3-5-6), indeed, the few compounds that are reported in water have low  $k_{\text{cat}}$  and high  $K_{\text{M}}$ , being their efficiency ( $k_{\text{cat}}/K_{\text{M}}$ ) not so good (entry 4), and they may require high pH. Furthermore most of these compounds, when used in water, almost always works only few minutes than degrade.

Considering the primary role of catalase enzymes against oxidative stress and degenerative diseases, it is important to transfer catalytic activity from lab conditions into aqueous biological environment.

A central point of the research was the combined SOD/CAT mimicking activity enabled by a single synthetic catalyst. The interplay of both anti-oxidant mechanisms is not possible for a natural enzyme, due to its specificity properties, but it can be obtained with a synthetic catalysts. The SOD capacities of  $\text{Mn}_2\text{L}_2\text{Bz}$  under examination has been evaluated using the same method described above for the mononuclear compounds. The dinuclear complex shows a quite good activity, 2 orders of magnitude ( $k_{\text{McFC}} 3.3 \cdot 10^7 \text{ M}^{-1}\text{s}^{-1}$ ) lower than the best artificial SOD mimic (M40401,  $k_{\text{McFC}} 1.6 \cdot 10^9 \text{ M}^{-1}\text{s}^{-1}$ ), that is the nearest to the natural SOD, but without catalase activity. However, the complex shows higher reactivity than a lot of reported mononuclear complexes with only SOD-activity. Up to date it is the best dinuclear complex known and the best one with double CAT/SOD activity. Compared with the compounds **1-3**, it has higher reactivity as SOD mimic, and it has also higher CAT activity, working better also near physiological conditions (Table 8).

**Table 8:** Summary of most active Mn complexes with SOD-like activity.

	Compound	$k_{\text{McCF}} (\text{M}^{-1}\text{s}^{-1})$
<b>1</b> <sup>1</sup>	MnSOD	$8 \cdot 10^8$
<b>2</b> <sup>1</sup>	M40401	$1.6 \cdot 10^9$
<b>3</b> <sup>1</sup>	$[\text{MnCl}_4\text{TE-2-PyP}]^{5+}$	$4.08 \cdot 10^8$
<b>4</b> <sup>1</sup>	<b><math>\text{Mn}_2\text{L}_2\text{Bz}</math></b>	<b><math>3.3 \cdot 10^7</math></b>
<b>5</b> <sup>28</sup>	$[\text{Mn}(\mathbf{3})(\text{OTf})_2]$	$8 \cdot 10^6$
<b>6</b> <sup>1</sup>	$[\text{Mn}(\text{TMIMA})_2]^{2+}$	$3.6 \cdot 10^6$
<b>7</b> <sup>1</sup>	EUK-8	$6.0 \cdot 10^5$

Xanthine 50 mM, NBT100  $\mu\text{M}$ , xanthine oxidase 0.005 U/ml in phosphate buffer 50 mM pH 7.8.

## 2.4 Mitochondrial toxicity

Focusing on dinuclear compound **4** structure, formed by two tetradentate ligands, made of 3 aromatic rings, these hydrophobic portion could, in principle, easily cross mitochondrial membrane, also because the overall charge of the complex is slightly positive (+1). Having both SOD- and CAT-like activities, it is able to eliminate superoxide anion and also hydrogen peroxide, so it is really interesting as possible agent to reduce anomalous ROS production in mitochondria. Its activity was thus checked in some representative aqueous media, not only containing the buffer but also some salts like EGTA, used to chelate calcium, potassium chloride, needed to regulate the osmotic pressure of the solution, and

usually phosphate. In table 9 are reported some values of initial rate, endpoint and turnover number (TON) of the catalyst in different buffers, more or less complex, for example KH (Krebs-Henseleit) is a typical carbonate buffer containing many compounds, like magnesium sulfate, calcium chloride, glucose, sodium chloride, potassium chloride and potassium phosphate. The values of initial rate, as said before, depend on buffer type and pH, in particular the complex buffer containing EGTA, MOPS and phosphate was found to lower the initial rate and the TON. The same behavior was observed when the pH is lowered. In the last three lines of the table, some experiments in the presence of typical catalase inhibitors, cyanide, 3-amino-1,2,4-triazole and azide, have been performed in borate buffer, the best condition for  $[\text{Mn}_2\text{L}_2\text{Bz}]$  compound. It is possible to see that only cyanide anion has an inhibitory effect on the complex, with a reduced initial rate and halved production of oxygen.

**Table 9:** Initial rate and oxygen production of  $[\text{Mn}_2\text{L}_2\text{Bz}]$  in different buffer at different pH and in the presence of catalase inhibitors.

Compound	Buffer	$R_0$ $\mu\text{M}\text{O}_2/\text{s}$	EndPoint $\mu\text{molO}_2$	Time	TON
$[\text{Mn}_2\text{L}_2\text{Bz}]$	BBS pH 7.8	39	198	1h	275
$[\text{Mn}_2\text{L}_2\text{Bz}]$	PBS pH 7.8	95	77	1h	107
$[\text{Mn}_2\text{L}_2\text{Bz}]$	PBS pH 7.4	25	81	1h	113
$[\text{Mn}_2\text{L}_2\text{Bz}]$	KH pH 7.4	32	75	1h	104
$[\text{Mn}_2\text{L}_2\text{Bz}]$	MOPS Mito pH 7.4	17	26	1h	36
<b>In the presence of catalase inhibitors</b>					
$[\text{Mn}_2\text{L}_2\text{Bz}]$	BBS pH 7.8 $\text{NaN}_3$	34	198	1h	275
$[\text{Mn}_2\text{L}_2\text{Bz}]$	BBS pH 7.8 ATZ	24	198	1h	275
$[\text{Mn}_2\text{L}_2\text{Bz}]$	BBS pH 7.8 KCN	11	95	1h	132

The initial idea was to evaluate the effects of the complex on mitochondria, monitoring the different events: (i) during normal respiration, analyzing the basal respiration, (ii) during the phosphorylation process, when oxygen consumption increase and (iii) under uncoupled respiration, when the presence of an additive, carbonyl cyanide-4-(trifluoromethoxyphenyl)hydrazone (FCCP), induces increase of mitochondrial respiration due to disruption of the protonic gradient into mitochondria. Finally, we have monitored the effects on mitochondria in which the respiratory chain was interrupted by the addition of antimycin A, an antibiotic that also increase ROS production. However, the endogenous



catalase contribution was always much higher than the activity induced by **4**. In addition, among common inhibitors, only cyanide was found to inhibit the enzymes, but also inhibited also our complex. Within such *scenario* it was impossible to appreciate any effect of the catalyst on the rate of oxygen evolution, in the presence of added H<sub>2</sub>O<sub>2</sub>, also using the oxygraph.

Only the toxicity on the isolated mitochondria was thus evaluated, analyzing oxygen consumption rate, with a Clark electrode, during the different metabolic events i-iii.

In a typical experiment, isolated mitochondria were injected in a reactor containing the a buffer solution at pH 7.4, where different concentration of complex were added. Oxygen consumption after the addition of mitochondria was registered, being the initial consumption due to basal respiration of the organelles (State2 or St2), from this rate it is possible to understand if the complex has had an uncoupling effects on respiration. Adenosine diphosphate (ADP) was then added and an increase of the respiratory rate was observed, indeed mitochondria started to produce ATP from ADP, since more oxygen was needed and an increase of oxygen consumption was observed, this was the rate during the phosphorylation (State3 or St3). After all ADP has been consumed, oxygen consumption returned on the level of basal respiration (State4 or St4). Finally after stabilization, FCCP was added, this compound leaded to the maximum oxygen consumption rate (StateUn or StUn). An example of these experiments is show in figure 30, there are many curves of oxygen consumption in the presence of different concentration of [Mn<sub>2</sub>L<sub>2</sub>Bz] (FerBz in the figure).

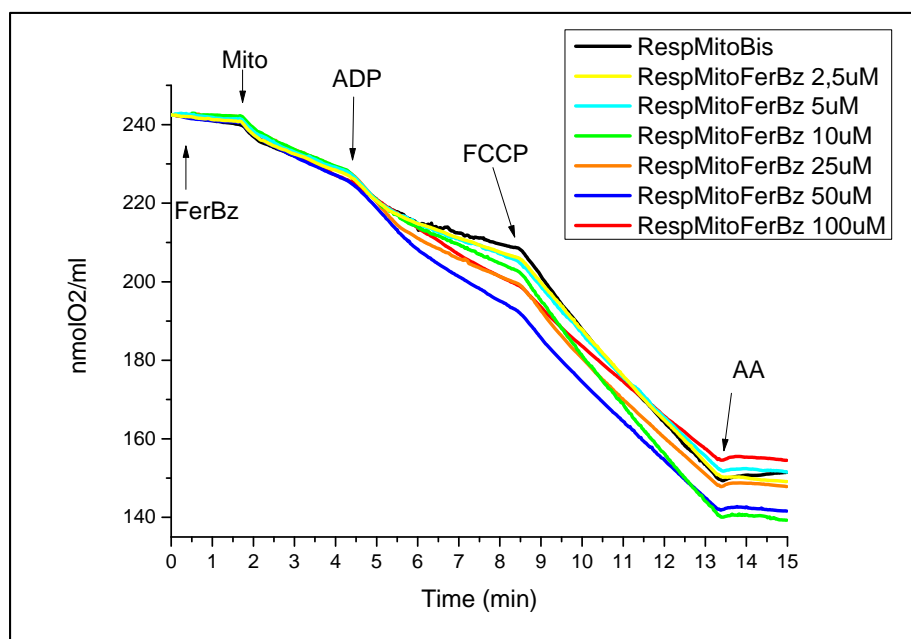


**Figure 30:** Mitochondrial oxygen consumption, mitochondria alone in black, and in the presence of  $[\text{Mn}_2\text{L}_2\text{Bz}]$  100 $\mu\text{M}$  (red line), 50 $\mu\text{M}$  (blue line), 25 $\mu\text{M}$  (orange line), 10 $\mu\text{M}$  (green line), 5 $\mu\text{M}$  (cyan line) and 2.5 $\mu\text{M}$  (yellow line).

The complex showed a little uncoupling effect at about 50 $\mu\text{M}$  concentration, with an increase of basal respiration (St2), that can be easily seen also from the figure, probably it fostered the passage of some protons, leading to an increase of oxygen consumption to equilibrate again the protonic gradient. A toxic effect above 100 $\mu\text{M}$  is easily visible from the rate of oxygen consumption reported in table 10, where it is clear the lowering of phosphorylation rate (St3). It is possible that at high concentration (100 $\mu\text{M}$ )  $[\text{Mn}_2\text{L}_2\text{Bz}]$ , interferes with ATPase, the protein involved in the ADP phosphorylation, leading to a decrease of the oxygen consumption.

**Table 10:** Rate of oxygen consumption ( $\text{nmolO}_2 \cdot \text{mg protein}^{-1} \cdot \text{ml}^{-1}$ ) with standard deviation (average of three measurement) at different states and with different concentration of complex  $[\text{Mn}_2\text{L}_2\text{Bz}]$ .

$[\text{Mn}_2\text{L}_2\text{Bz}], \mu\text{M}$	0	2.5	5	10	25	50	100
St 2	4.1 $\pm$ 0.7	4.5 $\pm$ 0.6	5.1 $\pm$ 0.8	5.19 $\pm$ 0.7	5.3 $\pm$ 0.9	6.5 $\pm$ 1.6	6.6 $\pm$ 1.4
St 3	12.8 $\pm$ 3.0	15.3 $\pm$ 5.1	15.6 $\pm$ 3.8	15.37 $\pm$ 4.0	14.6 $\pm$ 3.0	13.2 $\pm$ 2.3	8.1 $\pm$ 1.8
St 4	3.2 $\pm$ 0.3	3.6 $\pm$ 0.1	4.09 $\pm$ 0.5	4.6 $\pm$ 0.2	4.9 $\pm$ 0.8	6.0 $\pm$ 0.3	6.1 $\pm$ 0.3
St Un	13.0 $\pm$ 2.2	15.7 $\pm$ 3.3	19.7 $\pm$ 6.9	21.9 $\pm$ 7.3	19.3 $\pm$ 6.4	16.2 $\pm$ 4.9	15.7 $\pm$ 5.2
St 3/St 2	3.2 $\pm$ 0.6	3.4 $\pm$ 0.8	3.0 $\pm$ 0.3	2.9 $\pm$ 0.4	2.8 $\pm$ 0.2	2.1 $\pm$ 0.3	1.2 $\pm$ 0.1
St Un/St 2	3.2 $\pm$ 0.5	3.5 $\pm$ 0.9	3.8 $\pm$ 0.9	4.1 $\pm$ 0.9	3.6 $\pm$ 0.8	2.5 $\pm$ 0.7	2.4 $\pm$ 0.7

Another parameter that can be considered is the ratio between rate of state3 and state2 (or state4),  $St3/St2$ , also called Respiratory Control Ratio (RCR) that gives an idea of the “health” of mitochondria, indeed if this ratio is equal or higher than 3, this means mitochondria are functioning well. What is possible to see is that the ratio in the presence of  $[Mn_2L_2Bz]$  is more or less near 3 until  $25\mu M$ , while there is a neat decrease at  $50\mu M$  or higher, so mitochondria are quite healthy under  $50\mu M$  of our complex.

Furthermore to better understand the effects of  $[Mn_2L_2Bz]$  on mitochondria a Calcium Retention Capacity (CRC) experiment was performed. Although mitochondria can accumulate calcium, it is not an infinite process, indeed the over-accumulation of calcium could induce the so called mitochondrial permeability transition, in which the formation of a pore (permeability transition pore or PTP), cause the catastrophic loss of integrity of the inner mitochondrial membrane. In CRC experiment several addition of calcium to isolated mitochondria in the presence of a fluorescence probe for calcium (Calcium Green™) detection were performed. When calcium was added there was an increase of fluorescence and a subsequent decrease because calcium is confiscated by mitochondria. This can happen several times until a certain concentration is reached, that is called calcium retention capacity, at which mitochondria release all the calcium accumulated with a clear increase of fluorescence, the release of the calcium is due to the formation of the permeability transition pore (PTP). These events seems to be involved in many pathologies, apoptosis and also seem to be caused by oxidative stress. CRC was analyzed at different concentrations of  $[Mn_2L_2Bz]$  (Figure 31), and also in the presence of a protective agent, cyclosporin A, that postpones the pore opening (Figure 32), to evaluate the effects of our compound.

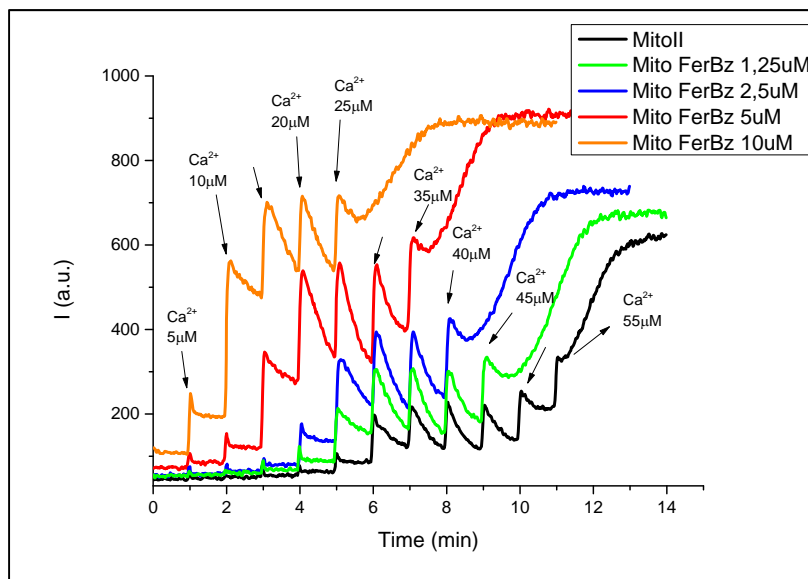


**Figure 31:** CRC graph of isolated mitochondria in the absence (black line) and in the presence of different concentration of  $[\text{Mn}_2\text{L}_2\text{Bz}]$ : 10  $\mu\text{M}$  (orange line), 5  $\mu\text{M}$  (red line), 2.5  $\mu\text{M}$  (blue line) and 1.25  $\mu\text{M}$  (green line). The arrows indicate the addition of calcium chloride and the total concentration added.

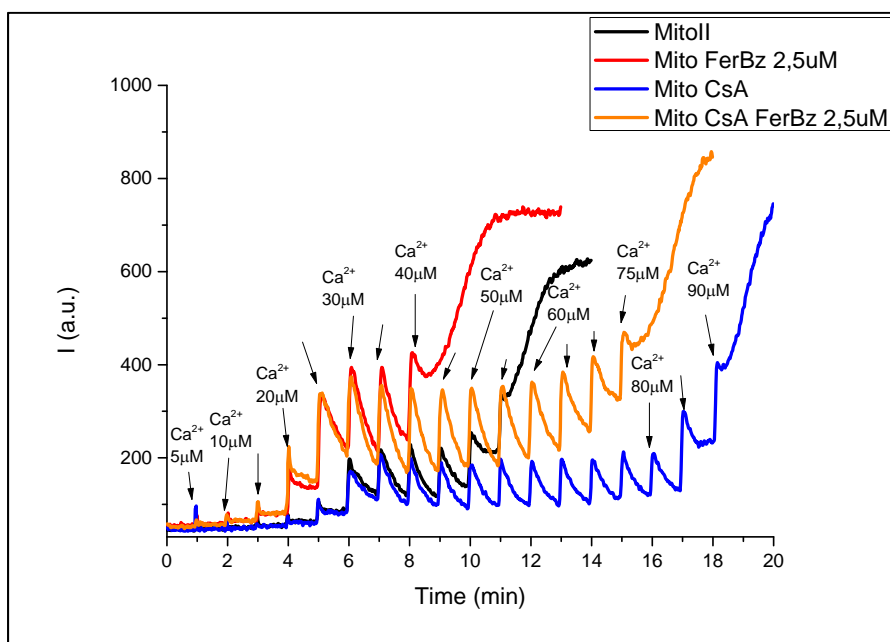


**Figure 32:** CRC graph of isolated mitochondria in the presence of cyclosporin A and  $[\text{Mn}_2\text{L}_2\text{Bz}]$  (blue and orange lines) compared with blank experiment without cyclosporin A (red and black lines).

In the following table are resumed the concentration of calcium chloride added until there is the opening of the pores.

**Table 11:** Calcium concentration at which there is pores opening in the presence of different [Mn<sub>2</sub>L<sub>2</sub>Bz] concentration and in the presence of cyclosporin A (on the right).

[Mn <sub>2</sub> L <sub>2</sub> Bz]	Without Cyclosporin A					With Cyclosporin A (1μM)	
	0 μM	1.25 μM	2.5 μM	5 μM	10 μM	0 μM	2.5 μM
Opening, μM di Ca <sup>2+</sup>	55	45	40	35	25	90	75

The higher is the [Mn<sub>2</sub>L<sub>2</sub>Bz] concentration, the earlier is the pore opening. Also in the presence of cyclosporin A, the opening of the pore is still earlier (75μM) than the control experiment (90μM). The complex interacts with the pore on the inner membrane, that is proved by the anticipation of the pore opening in the presence of the complex and this can be a confirm that it enters into mitochondria. Furthermore, it has been recently supposed that the transition pore could be formed by two ATP synthase (ATPase) proteins,<sup>51</sup> this could be a further indication of the interaction with ATP synthase, that at higher concentration of complex (50μM) lead to an inhibition of phosphorylation rate. Further studied should be performed to understand if this anticipation of pore opening, and interaction with ATPase, at high complex concentration, could have a role in complex activity or negative effects of toxicity.

## **2.5 Modification of apical ligand of dinuclear complexes with mitochondriotropic substituent (5-7)**

One of the biggest issue when using drugs is their selective delivery/targeting to specific cell functionalities. Targeting and delivery systems are widely studied to improve the effects of the drugs, they are also important to implement the antioxidant efficiency of the catalyst. In our case, the aim is to target mitochondria, indeed most of ROS are produced into these organelles, so it is important to carry the catalyst near or, better, into mitochondria. Suitable functionalities were thus anchored on the antioxidant, in order to assist their penetration into cellular and mitochondrial membranes. In particular, since the latters are usually negatively charged, almost all the targeting agents are positively

charged.<sup>52</sup> Among literature examples, peptides represent one appealing possibility for building recognition motifs. Indeed, target peptides can be recognized by a certain sequences of aminoacids with a suitable secondary structure.<sup>53</sup> Targeting peptides were also designed to incorporate antioxidant moieties. The SS peptide is characterized by alternating aromatic residues such as dimethyltyrosine, that originates the antioxidant activity, and basic residues, like arginine and lysine, that provide the net positive charge to specifically target mitochondria (Figure 33 left).<sup>54</sup> Another example of peptides are the XJB Gramicidin S analogs, based on a sequence of AA (usually hydrophobic, like leucine, valine, proline or phenylalanine), of membrane active gramicidin antibiotics, conjugated with TEMPO as radical scavengers (Figure 33 right).<sup>55</sup>

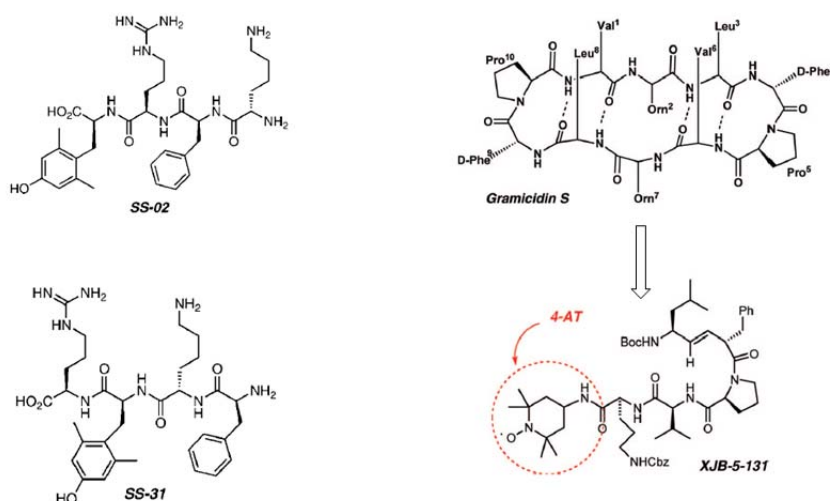


**Figure 33:** SS peptide with antioxidant activity for targeting mitochondria (on the left), and Gramicidin S and an example of derivative containing TEMPO radical as ROS radical trap (on the right).

Another kind of targeting molecule are the lipophilic cations, among containing a nonpolar framework and a positive charge, which are able to pass through the membranes, exploiting the negative membrane potential (about -180mV) of mitochondria. Among these compounds, Rhodamine is widely used to target mitochondria, since it contains a positive charge and it can be easily modified, furthermore it is luminescent, and its optical properties could also be tuned and exploited for fluorescence imaging. Phthalocyanines were linked with two rhodamine residues to target mitochondria and used for photodynamic therapy and induce apoptosis.<sup>56</sup> Conjugation of an anti-inflammatory compound, like dieckol, with rhodamine increases its activity thanks to rhodamine

trafficking.<sup>57</sup> Although the precursors are cheap, some rhodamine derivatives are quite expensive, depending on their desired features, such as quantum yield of fluorescence, lipophilicity and charge (Figure 34). The cheapest is rhodamine B (Rho B, 0.45€/g), whose synthesis is easy and cheap. More complex rhodamine are more expensive, rhodamine123 (Rho 123, 1650€/g) is the most expensive commercial one.<sup>58</sup>

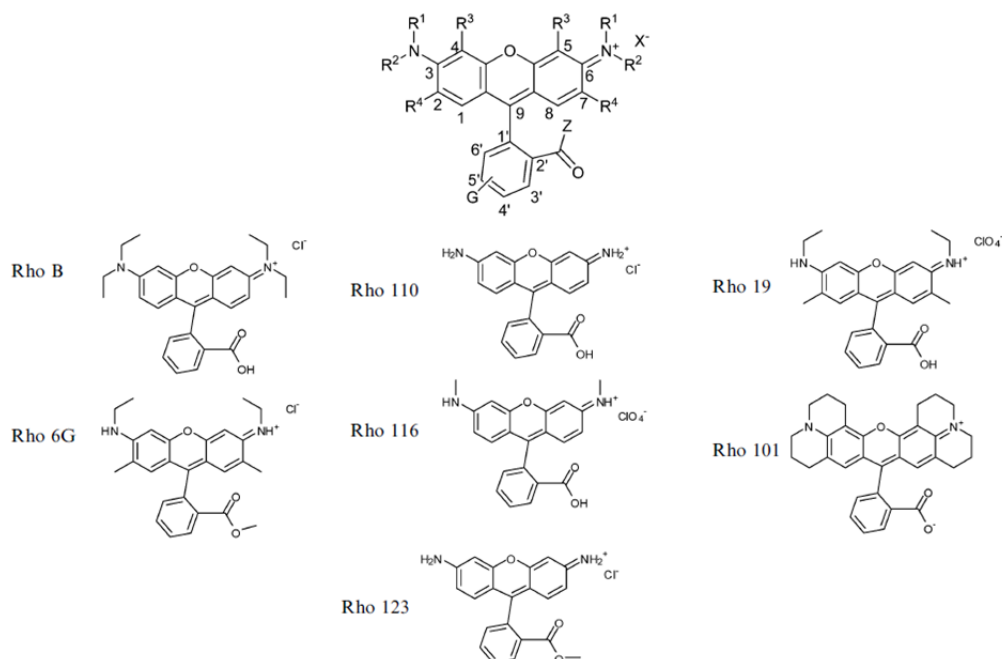


**Figure 34:** General structure of rhodamines and some commercially available compounds.

Another type of mitochondriotropic substituent are triphenylphosphonium salts (TPP), that are easily synthesized starting from a bromine compound and triphenylphosphine. With rhodamine, TPP compound represent the majority of non-peptidic mitochondrial targeting agents.<sup>59</sup> Classical antioxidant molecules, like polyphenols and vitamins, especially vitamin E, were functionalized with TPP pendants to target mitochondria, but also some SOD mimicking catalysts, such as salen compounds were functionalized with TPP salts to selectively drive them into mitochondria (Figure 35).<sup>60</sup>

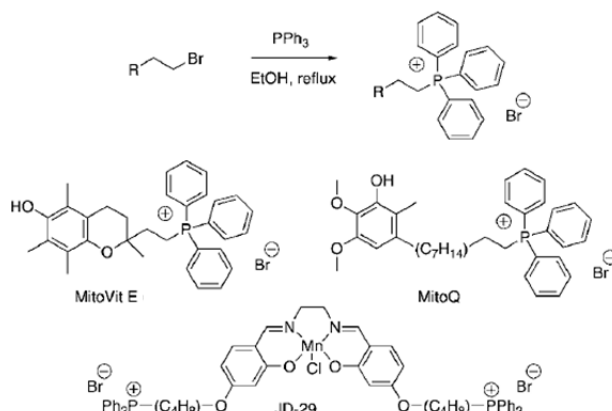


**Figure 35:** Scheme of TPP salts synthesis from an alkyl bromide and triphenylphosphine (PPh<sub>3</sub>) and three examples of antioxidants conjugated with TPP: vitamin E, MitoQ and SOD-like Mn catalyst.

A lot of other targeting agents exist, for example sulfonyl-urea compounds, anthracyclines, resveratrol and its analogues, some kind of porphyrins, curcumin and other lipophilic compounds (Figure 36).<sup>52</sup>

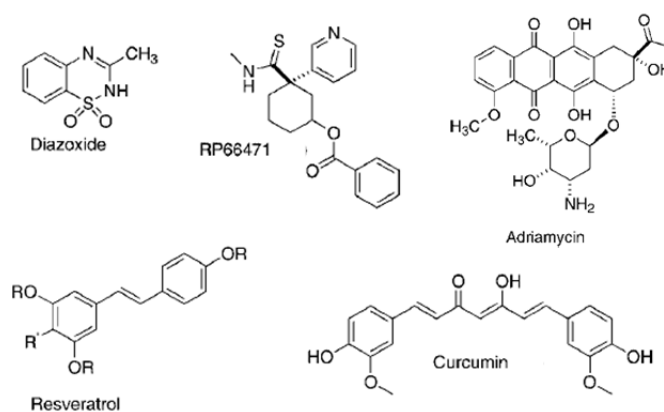
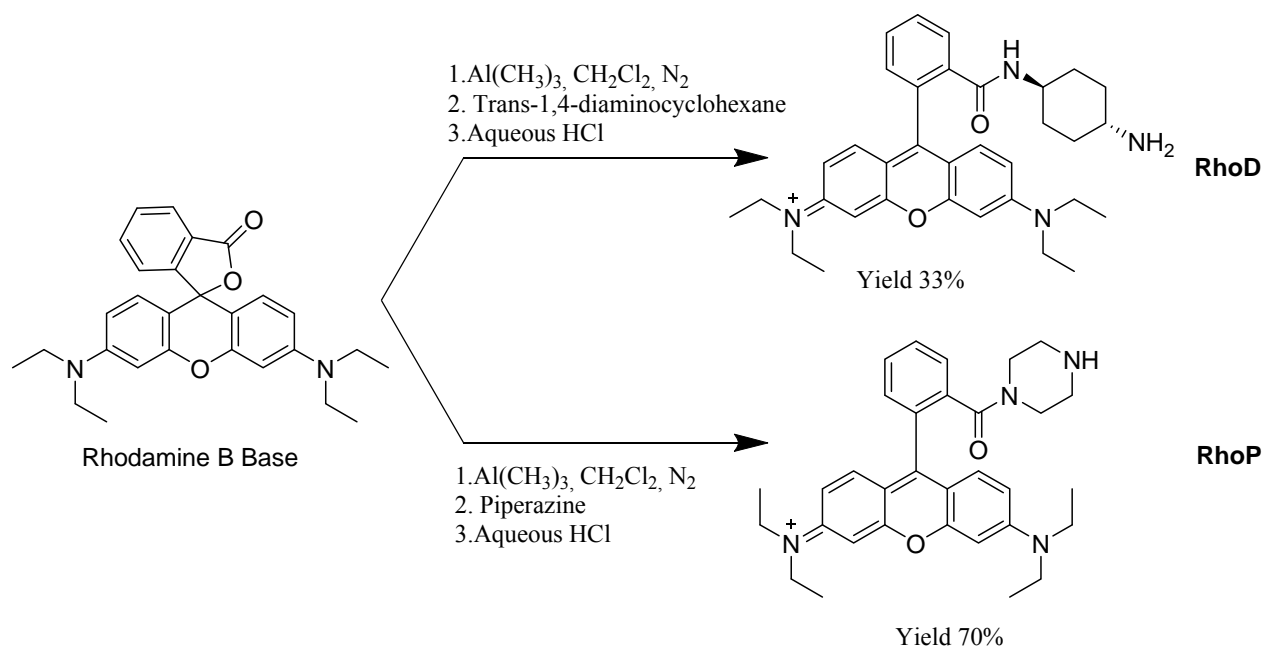


**Figure 36:** Other examples of targeting antioxidant molecules, clockwise from upper left: two sulfonyl-urea derivatives, an anthracycline, curcumin and resveratrol molecules.

Herein, the conjugation of the dinuclear manganese complex with rhodamine and TPP salts has been obtained exploiting the carboxylic bridging ligand of the dinuclear complex **4**. Two rhodamine B derivatives were thus synthesized with two semi-rigid spacers between a carboxylate and the aromatic region of the rhodamine. A TPP salts of bromovaleric acid was also used to synthesize a complex with a mitochondriotropic pendant. Rhodamine B was chosen because of its cheapness and good quantum yield (0.53 for cationic form).

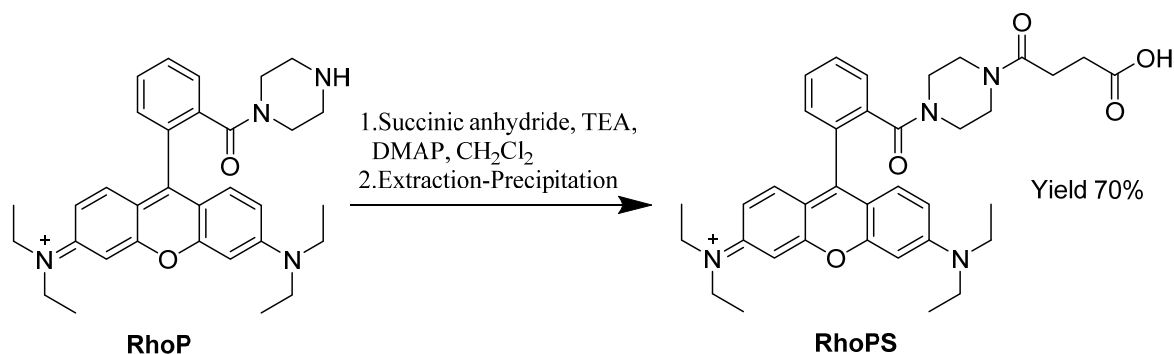


The first step was the functionalization of rhodamine B base with a semi-rigid spacer, such as piperazine or *trans*-1,4-diaminocyclohexane amide.<sup>61</sup> Rhodamine B Base can be easily synthesized starting from rhodamine B by basification. Lactone form is obtained in high yield (>90%). Both diamino-spacers react with the lactone in the presence of trimethylaluminium, in dry dichloromethane under nitrogen (Scheme 9).



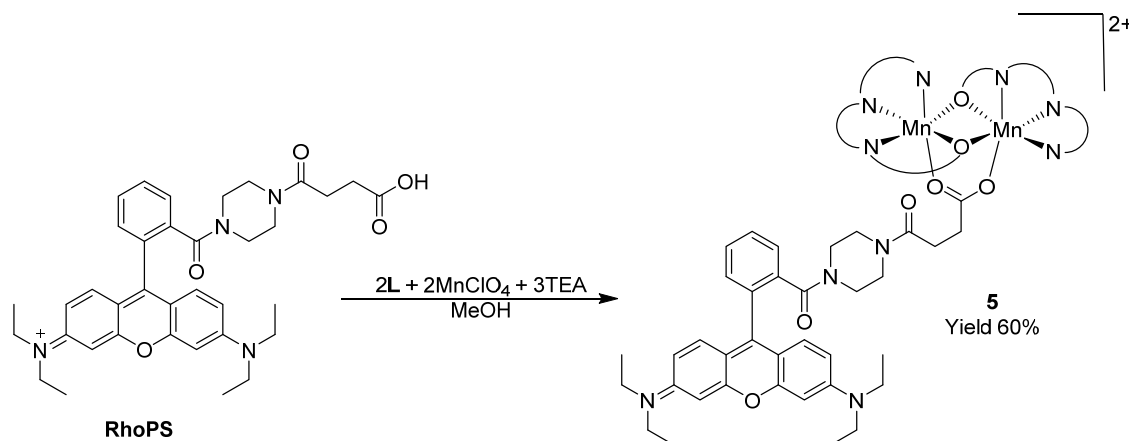
**Scheme 9:** Synthesis of rhodamine *trans*-1,4-diaminocyclohexane amide (**RhoD**) and rhodamine piperazine amide (**RhoP**) starting from rhodamine B Base.<sup>61</sup>

In the next step, a carboxylic acid, required for Mn coordination, has to be introduced. So **RhoP** has been reacted with succinic anhydride forming amido bond and leaving an available carboxylic functionality (Scheme 10).



**Scheme 10:** Synthesis of rhodamine 4-(3-carboxypropionyl)piperazine amide (**RhoPS**).<sup>61a</sup>

Finally, it was possible to synthesize the catalyst **5** using **RhoPS** instead of benzoic acid (Scheme 11). The product did not crystallize but after the addition of trimethylamine a reddish-pink solid precipitated. Solid was abundantly washed with methanol and diethyl ether. The paramagnetic product **5** was characterized by FTIR, UV-Vis and MALDI-TOF MS.



**Scheme 11:** Synthesis of **5**.

In particular, FTIR analysis (Figure 37) confirmed the formation of the complex, upon comparison of the region around 1100cm<sup>-1</sup>, with the comparison of typical bands of the catalyst, but also the reduction of carboxylate signals at about 1600-1700cm<sup>-1</sup>, expected after coordination to the manganese atoms.

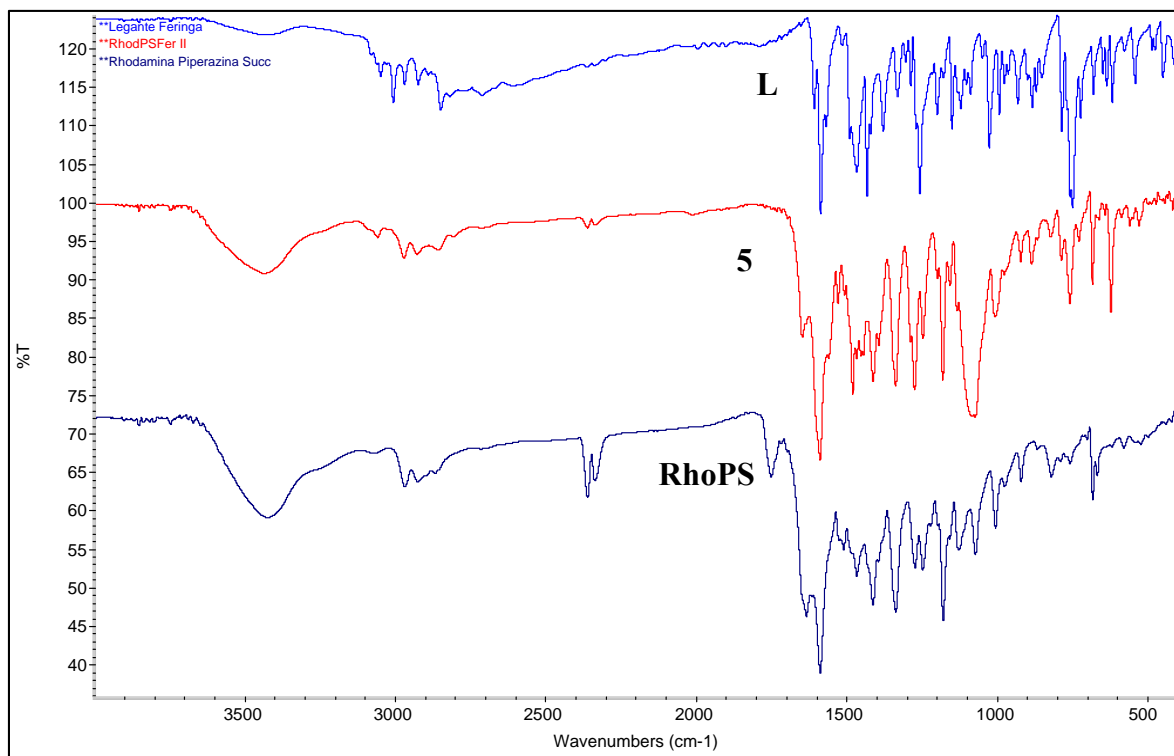


**Figure 37:** FTIR spectra of tetradentate ligand **L** (upper spectrum, blue), rhodamine derivatives carboxylate **RhoPS** (below, dark blue) and final complex **5** (in the middle, red).

Mass spectrum analysis confirmed the formation of the products, indeed with a MALDI-TOF instrument the molecular peaks was clearly visible ( $m/z$  1329 [ $M^+$ ]), together with other molecular fragments ( $m/z$ : 611-817-970-1161), due to spacer breaking at different points (Figure 38). Also ESI-MS confirmed the formation of the complex by molecular peaks double charged at about  $m/z$  664.2.

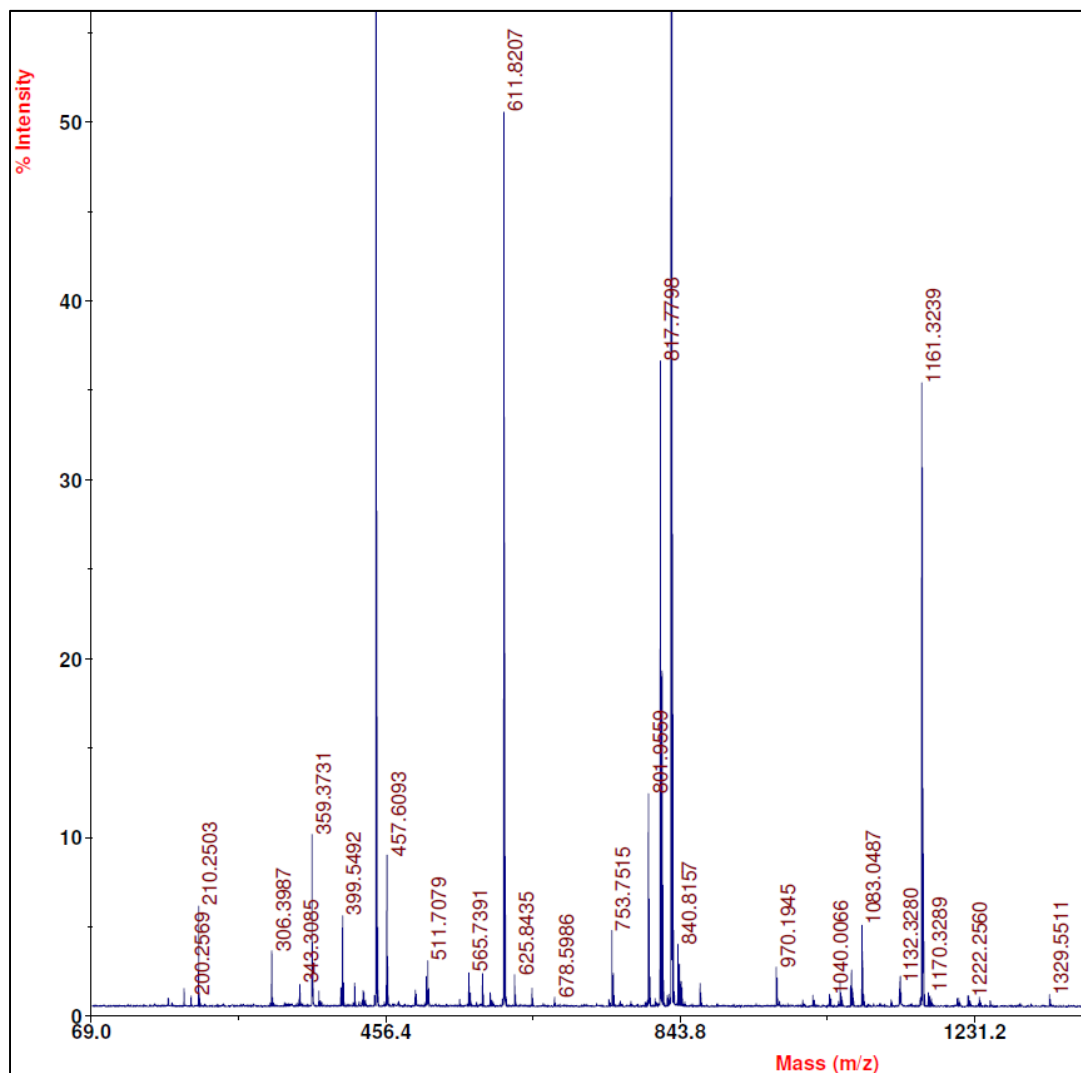


**Figure 38:** MALDI-TOF spectra of compound **5**.

UV-Vis analysis of **5** showed that the rhodamine spectral features have been retained and catalyst bands are clearly visible at about 250nm (Figure 39). Also the fluorescence of rhodamine is retained, with a decreased intensity of emission in ethanol.

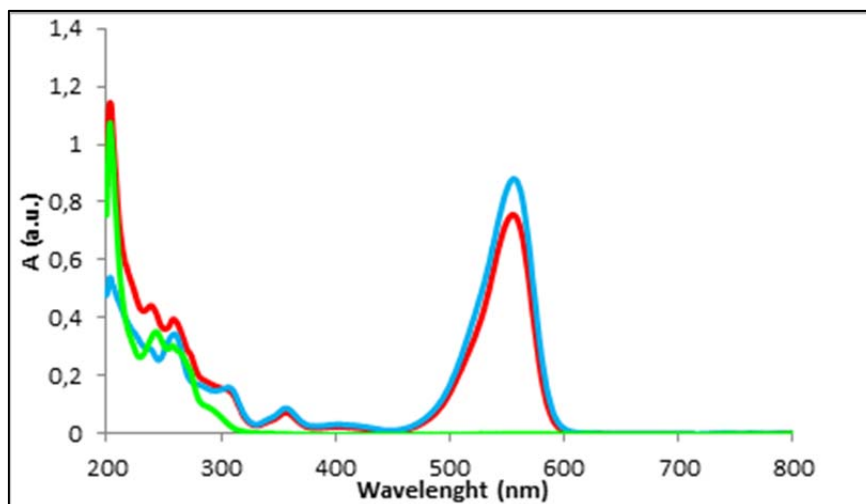
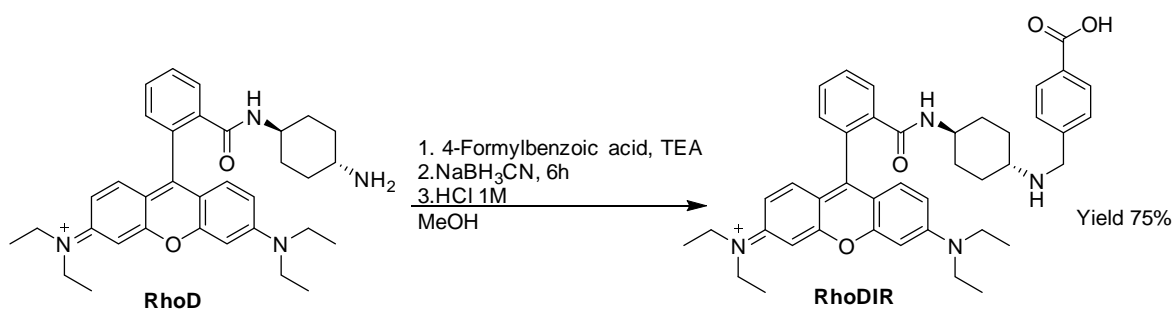


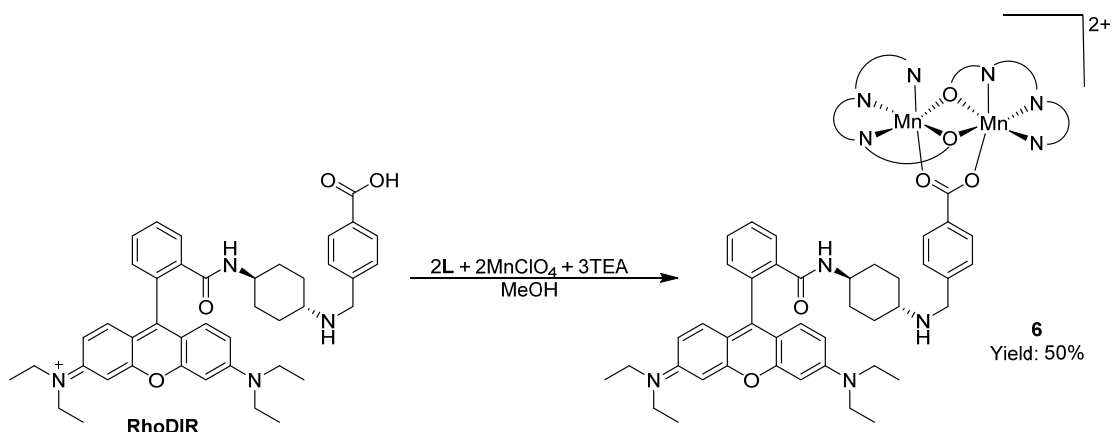
**Figure 39:** UV-Vis spectra of original complex **4** (green), rhodamine ligand **RhoPS** (blue) and complex **5** (red)  $10^{-5}$  M in EtOH.

In the case of **RhoD**, 4-formylbenzoic acid was attached by reaction between aldehyde and amine of diamine cyclohexane. To increase the stability of the bonds to aqueous conditions, the resulting imino bond has been reduced in situ with sodium cyanoborohydride and the product **RhoDIR** was purified by a chromatographic column (Scheme 12).



**Scheme 12:** Synthesis of rhodamine-*trans*-1,4-diminocyclohexane amide-4-carboxybenzyl (**RhoDIR**).

As in the previous synthesis of **5**, it was possible to synthesize the catalyst with the new rhodamine derivative. Product **6** is obtained after precipitation and washed with methanol and diethyl ether (Scheme 13).



Product **6** was characterized by FTIR, UV-Vis, ESI-MS and MALDI-TOF MS. Also in this case FTIR confirm the formation of the complex, indeed a band at about  $1100\text{cm}^{-1}$  appeared, but also some peaks at  $1700\text{cm}^{-1}$  disappeared, due to carboxylate coordination (Figure 40).

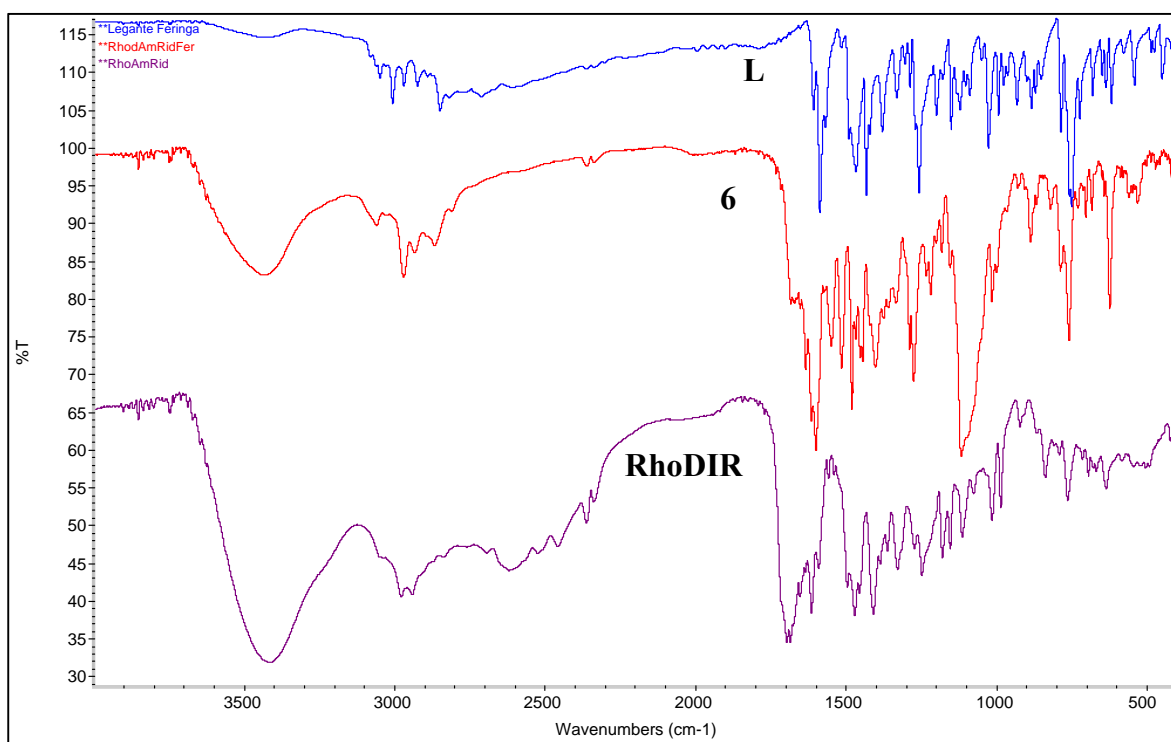
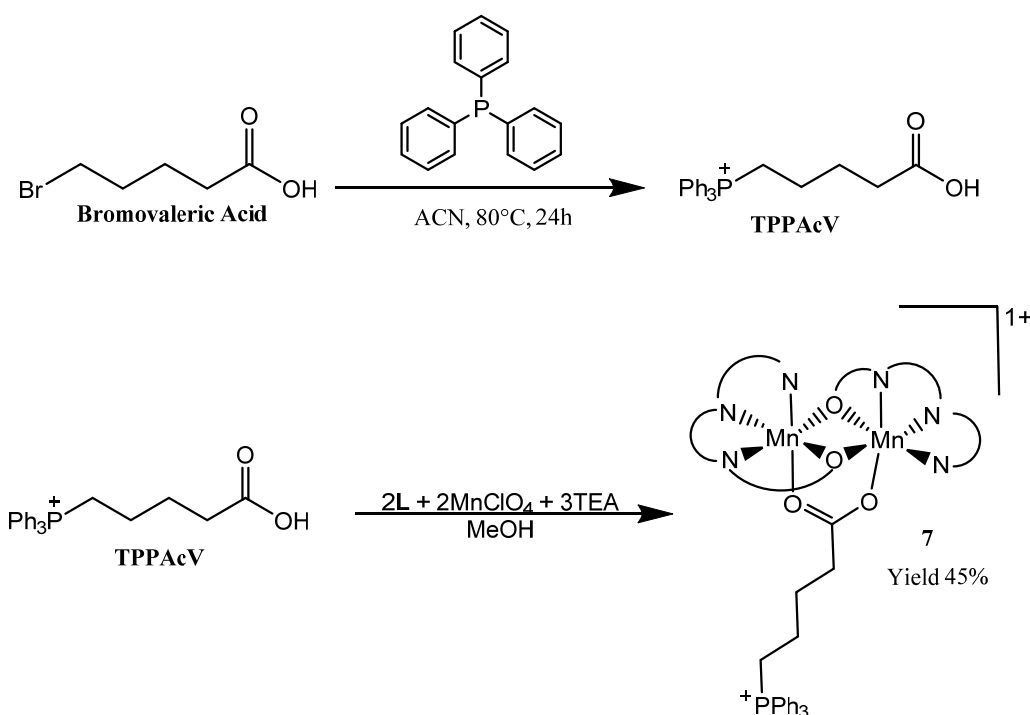


**Figure 40:** FTIR spectra of tetradentate ligand **L** (upper spectrum, blue), rhodamine derivatives carboxylate **RhodIR** (below, dark violet) and final complex **6** (in the middle, red).

Mass spectrum analysis confirms the formation of the products, indeed with a MALDI-TOF instrument the molecular peaks was clearly visible ( $m/z$  1390 [ $M^+$ ]), but also other

molecular fragments ( $m/z$ : 359-442-830-963), in which the carboxylate is broken at different point.

The last compound with a mitochondriotropic function is a TPP-based carboxylate, obtained from reaction of commercially available bromovaleric acid with triphenylphosphine.<sup>62</sup> The carboxylate was then reacted with the ligand, in the presence of trimethylamine and manganese perchlorate. The white precipitate was washed with methanol and diethyl ether (Scheme 14).



**Scheme 14:** Synthesis of triphenylphosphine derivative (TPPAcV) of valeric acid (upper reaction) and synthesis of catalyst 7.

FTIR and mass analysis confirmed the structure of the complex. FTIR showing the shift of the carboxylate band from about  $1750\text{cm}^{-1}$  to  $1600\text{cm}^{-1}$  and the peak at  $1100\text{cm}^{-1}$  typical of the complex (Figure 41). While ESI-MS analysis confirm the presence of the complex by its molecular peak at  $m/z$  540.1 [ $\text{M}^{2+}$ ] and its fragmentation peaks due to ligand, carboxylate and rupture of carboxylic acid ( $m/z$  306.2, 363.2, 763.1).

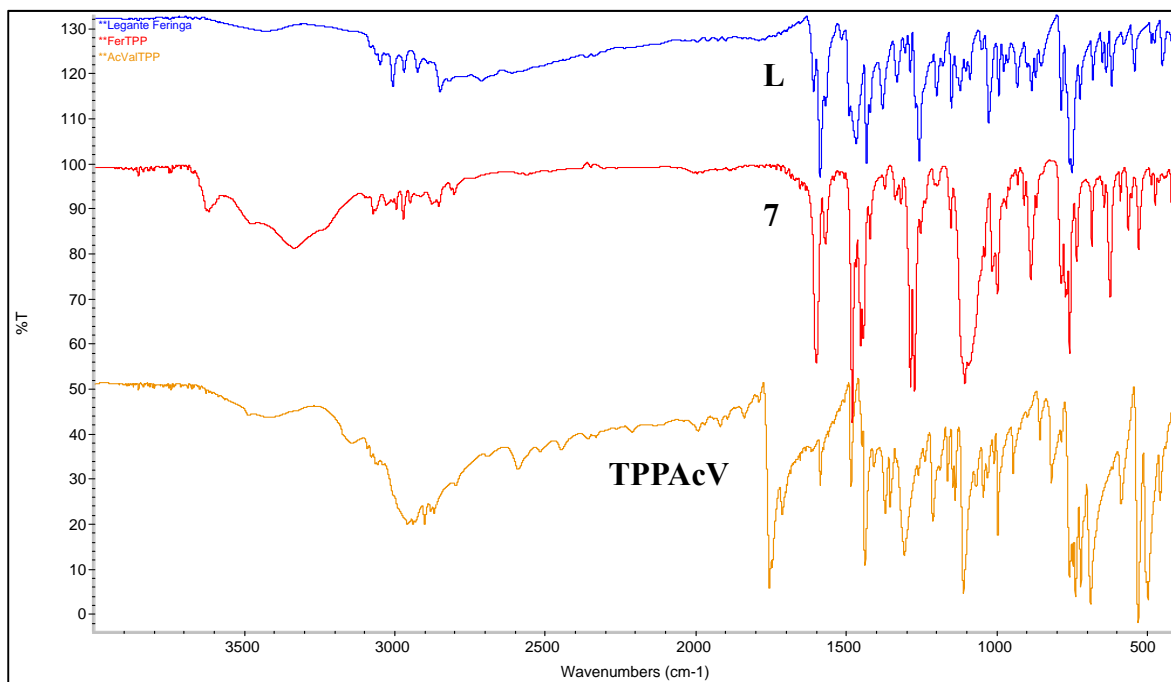


**Figure 41:** FTIR spectra of tetradentate ligand **L** (upper spectrum, blue), TPP Valeric acid **TPPAcV** (below, orange) and final complex **7** (in the middle, red).

Finally, the catalytic activity of these compounds to dismutate  $\text{H}_2\text{O}_2$  was tested in borate buffer solution (BBS), that was found to be the best systems, at pH 7.8. It was also possible to evaluate the effect of the apical ligand on the initial rate of oxygen production. The kinetics are shown below (Figure 42).

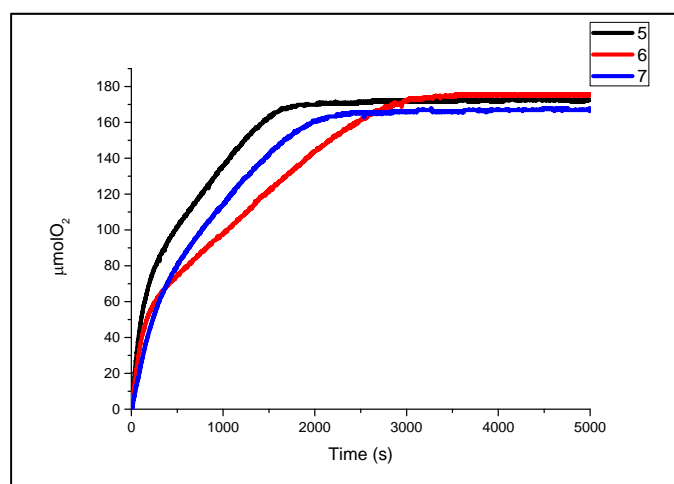


**Figure 42:** Kinetics trace of hydrogen peroxide dismutation by compound **5** (black line), **6** (red line) and **7** (blue line). Kinetics were performed in the same condition used for the original compound **4**, borate buffer solution 50mM at pH 7.8 and  $\text{H}_2\text{O}_2$  33mM.



How it is possible to see from kinetic traces piperazine compound **5**, was the most reactive, with higher initial rate of dismutation of  $52\mu\text{MO}_2/\text{s}$ , while TPP complex was the less reactive with an initial rate of about  $21\mu\text{MO}_2/\text{s}$  and diaminocyclohexane derivative had an intermediate value ( $33\mu\text{MO}_2/\text{s}$ ). This meaning that changing the apical ligand could influence initial rate of dismutation. However, despite the differences of  $R_0$ , all of them reached complete dismutation in about one hour, the reactivity of initial complex was indeed retained. Further studies should be performed to better understand the effects of complex apical ligands, indeed while considering acetate, benzoate and 4-formylbenzoate, no differences occurred between the complexes, in the presence of carboxylate that contains positive charge, basic group or more hydrophobic group, some differences have appeared. Maybe with the optimization of the apical ligand it will be possible to further increase the initial rate of dismutation of the complex but also its activity at pH lower than 7.8, to get closer to physiological pH.

The last study to do is to check the effective entrance of these compound into mitochondria, in particular the rhodamine derivatives could be follow by fluorescence, while TPP compound entrance could be monitored on isolated mitochondria with a TPP ion selective electrode.

## **2.6 Conclusions**

In conclusion to this part, two kind of manganese-containing catalysts that are able to mimic SOD and CAT enzymes have been studied. The mononuclear compounds are the first examples of mononuclear complexes that are able to dismutate superoxide anion and hydrogen peroxide in aqueous solution, being their activity dependent on the heteroatoms on the ligands ( $\text{S} > \text{O} > \text{N}$ ).

Then a dinuclear complex of manganese was thoroughly studied as antiROS compound. Starting for literature knowledge of its reactivity for  $\text{H}_2\text{O}_2$  dismutation, we deeply studied its activity, finding the best buffer solution (borate buffer near physiological pH) to perform catalytic test, then we obtained Michaelis-Menten parameter that allows us to compare the activity with other literature compounds. This catalyst is the best, till now,

that is able to eliminate hydrogen peroxide in aqueous solution, with complete conversion of the substrate without loss of reactivity, while most of the literature compounds work only few minutes. Stability was indeed confirmed by FTIR, mass analysis and recharging experiments. Toxicity studies on isolated mitochondria revealed no toxicity till 50 $\mu$ M concentrations and a possible interaction with ATPase and induction of anticipating permeability transition pore opening. Modification of apical bridging carboxylate with mitochondriotropic pendants like rhodamine derivatives and triphenylphosphonium salts was achieved, products were characterized and catalytic activity was confirmed to be maintained and similar to original compound. Unfortunately, no crystal structure of these compound was obtained. As perspective, the positive effects on cell protection against oxidative stress and selective delivery and also the toxicity will be studied.

## References

- <sup>1</sup> Iranzo O., *Bioorg. Chem.*, **2011**, 39, 73.
- <sup>2</sup> Fee J.A., DiCorleto P.E., *Biochemistry*, **1973**, 12, 4893.
- <sup>3</sup> Lawrence G.D., Sawyer D.T., *Biochemistry*, **1979**, 18, 3045.
- <sup>4</sup> Barrette W.C.J., Sawyer D.T., Fee J.A., Asada K., *Biochemistry*, **1983**, 22, 624.
- <sup>5</sup> McCord J.M., Fridovich I., *J. Biol. Chem.*, **1969**, 244, 6049.
- <sup>6</sup> Flohe L., Otting F., *Methods Enzymol.*, **1984**, 105, 93.
- <sup>7</sup> Salvemini D., Riley P.D., Cuzzocrea S., *Nature Rev.*, **2002**, 1, 367.
- <sup>8</sup> Voet D., Voet J.G., Pratt C.W., *Foundamentals of Biochemistry: Life at the Molecular Level*, 2nd Edition, **2007**.
- <sup>9</sup> Signorella S., Tuchagues J.P., Moreno D., Palopoli C., in Hughes J.G., Robinson A.J., (Eds.), *Inorganic Biochemistry Research Progress*, Nova Sci. Publ. Inc., New York, **2008**.
- <sup>10</sup> Biava H., Palopoli C., Duhayon C., Tuchagues J.P., Signorella S., *Inorg. Chem.*, **2009**, 48, 3205.
- <sup>11</sup> Velasco A., Bensiek S., Pecoraro V.L., *Inorg. Chem.* **1998**, 37, 3301.
- <sup>12</sup> Boelrijk A.E.M., Dismukes G.C., *Inorg. Chem.*, **2000**, 39, 3020.
- <sup>13</sup> a) Moreno D., Palopoli C., Daier V., Shova S., Vendier L., González-Sierra M., Tuchagues J.P., Signorella S., *Dalton Trans.* **2006**, 5156; b) Biava H., Palopoli C., Shova S., Gaudio M.D., Daier V., González-Sierra M., Tuchagues J.P., Signorella S., *J. Inorg. Biochem.*, **2006**, 100, 1660; c) Palopoli C., Chansou B., Tuchagues J.P., Signorella S., *Inorg. Chem.* **2000**, 39, 1458; d) Palopoli C., González-Sierra M., Robles G., Dahan F., Tuchagues J.P., Signorella S., *Dalton Trans.*, **2002**, 3813; e) Daier V., Biava H., Palopoli C., Shova S., Tuchagues J.P., Signorella S., *J. Inorg. Biochem.*, **2004**, 98, 1806.
- <sup>14</sup> Karsten P., Neves A., Bertoluzzi A.J., Strähle J., Maichle-Mössmer C., *Inorg. Chem. Commun.*, **2002**, 5, 434.
- <sup>15</sup> Reddig N., Pursche D., Kloskowski M., Slinn C., Baldeau S.M., Rompel A., *Eur. J. Inorg. Chem.*, **2004**, 879.
- <sup>16</sup> Godbole M.D., Kloskowski M., Hage R., Rompel A., Mills A.M., Spek A.L., Bouwman E., *Eur. J. Inorg. Chem.*, **2005**, 304.
- <sup>17</sup> Triller M.U., Hsieh W.Y., Pecoraro V.L., Rompel A., Krebs B., *Inorg. Chem.*, **2002**, 41, 5544.
- <sup>18</sup> Bossek U., Saher M., Weyhermüller T., Weighardt K., *Chem. Soc. Chem. Commun.*, **1992**, 1780.
- <sup>19</sup> Shin B.K., Kim M., Han J., *Polyhedron*, **2010**, 29, 2560.
- <sup>20</sup> a) Larson E.J., Pecoraro V.L., *J. Am. Chem. Soc.* **1991**, 113, 3810. ; b) Larson E.J., Pecoraro V.L., *J. Am. Chem. Soc.* **1991**, 113, 7809.
- <sup>21</sup> Kaizer J., Csonka R., Speier G., *React. Kinet. Catal. Lett.*, **2008**, 94, 157.
- <sup>22</sup> Dubois L., Xiang D.F., Tan X.S., Latour J.M., *Eur. J. Inorg. Chem.*, **2005**, 1565.
- <sup>23</sup> Dubois L., Pécaut J., Charlot M.F., Baffert C., Collomb M.N., Deronzier A., Latour J.M., *Chem. Eur. J.* **2008**, 14, 3013.
- <sup>24</sup> Delroisse M., Rabion A., Chardac F., Tétard D., Verlhac J.B., Fraisse L., Séris J.L., *J. Chem. Soc., Chem. Commun.* **1995**, 949.
- <sup>25</sup> Whittaker M.M., Barynin V.V., Antonyuk S.V., Whittaker J.W., *Biochemistry*, **1999**, 38, 9126.
- <sup>26</sup> De Boer J.W., Browne W.R., Feringa B.L., Hage R., *C. R. Chimie*, **2007**, 10, 341.
- <sup>27</sup> Signorella S., Hureau C., *Coord. Chem. Rev.*, **2012**, 256, 1229.
- <sup>28</sup> Grau M., Rigodanza F., White A.J.P., Sorarù A., Carraro M., Bonchio M., Britovsek G.J.P., *Chem. Commun.*, **2014**, 4607.
- <sup>29</sup> Aston K., Rath N., Naik A., Slomczynska U., Schall O.F., Riley D.P., *Inorg. Chem.*, **2001**, 40, 1779.
- <sup>30</sup> a) Lonnon D.G., Ball G.E., Taylor I., Craig D.C., Colbran S.B., *Inorg. Chem.*, **2009**, 48, 4863, b) Liu G.F., Dürr K., Puchta R., Heinemann F.W., van Eldik R., Ivanovic-Burmazovic I., *Dalton Trans.*, **2009**, 6292.
- <sup>31</sup> Geiger R.A., Chattopadhyay S., Day V.W., Jackson T.A., *J. Am. Chem. Soc.*, **2010**, 132, 2821.
- <sup>32</sup> Miller A.F., *FEBS Letters*, **2012**, 586, 585.
- <sup>33</sup> Doctrow S.R., Huffiman K., Bucay Marcus C., Tocco G., Malfroy E., Adinolfi C.A., Kruk H., Baker K., Lazarowych N., Mascarenhas J., Malfroy B., *J. Med. Chem.*, **2002**, 45, 4549.
- <sup>34</sup> Abashkin Y.G., Burt S.K., *Inorg. Chem.*, **2005**, 44, 1425.
- <sup>35</sup> Jiang X., Liu H., Zheng B., Zhang J., *Dalton Trans.*, **2009**, 8714.
- <sup>36</sup> Deary M.E., Durrant M.C., Davies D.M., *Org. Biomol. Chem.*, **2013**, 11, 309.
- <sup>37</sup> Serbest K., Özen A., Ünver Y., Er M., Degirmencioglu I., Sancak K., *J. Mol. Struct.*, **2009**, 922, 1.
- <sup>38</sup> Fekl U., van Eldik R., *Eur. J. Inorg. Chem.*, **1998**, 389.
- <sup>39</sup> Noritake Y., Umezawa N., Kato N., Higuchi T., *Inorg. Chem.*, **2013**, 52, 3653.
- <sup>40</sup> Bull C., Niederhoffer E.C., Yoshida T., Fee J.A., *J. Am. Chem. Soc.*, **1991**, 113, 4069.

- <sup>41</sup> Salvemini D., Wang Z.Q., Zweier J.L., Samouilov A., Macarthur H., Misko T.P., Currie M.G., Cuzzocrea S., Sikorski J.A., Riley D.P., *Science*, **1999**, 286, 304.
- <sup>42</sup> Dürr K., Yalalov D.A., Heinemann F.W., Tsoгоеva S.B., Ivanovic-Burmazovic I., *Z. Naturforsch.*, **2010**, 65b, 258.
- <sup>43</sup> Vicario J., Eelkema R., Browne W.R., Meetsma A., La Crois R.M., Feringa B.L., *Chem. Comm.*, **2005**, 3936.
- <sup>44</sup> Shank M., Barynin V., Dismukes G.C., *Biochemistry*, **1994**, 33, 15433.
- <sup>45</sup> B.K. Shin, M. Kim, J. Han, *Polyhedron*, **2010**, 29, 2560
- <sup>46</sup> M.U. Triller, W.Y. Hsieh, V.L. Pecoraro, A. Rompel, B. Krebs, *Inorg. Chem.*, **2002**, 41, 5544.
- <sup>47</sup> N. Reddig, D. Pursche, M. Kloskowski, C. Slinn, S.M. Baldeau, A. Rompel, *Eur.J. Inorg. Chem.*, **2004**, 879.
- <sup>48</sup> a) Wu A. J., Penner-Hahn J. E., Pecoraro V. L., *Chem. Rev.*, **2004**, 104, 903-938; b) Boelrijk A.E.M., Dismukes G.C., *Inorg. Chem.*, **2000**, 39, 3020; c) Whittaker M.M, Barynin V.V., Antonyuk S.V., Whittaker J., *Biochemistry (N. Y.)*, **1999**, 38, 9126.
- <sup>49</sup> a) Morris M.R., Frank P., Novak R.F., *Chem. Res. Toxicol.*, **1989**, 2 (2), 76; b) Lessa J.A., Horn A., Erika J., Bull S., Rocha M.R., Benassi M., Catharino R.R., Eberlin M.N., Casellato A., Noble C.J., Graeme I., Hanson R., Schenk G., Silva G.C., C. Antunes O.A., Fernandes C., *Inorg. Chem.* **2009**, 48, 4569.
- <sup>50</sup> Amo T., Atomi H., Imanaka T., *J.Bacteriol*, 2002, **184**, 3305; b) Allgood G.S., Perry J.J., *J.Bacteriol*, 1986, **168**, 563.
- <sup>51</sup> Giorgio V., von Stockum S., Antoniel M., Fabbro A., Fogolari F., Forte M., Glick G.D., Petronilli V., Zoratti M., Szdabó I., Lippe G., Bernardi P., *PNAS*, **2013**, 110, 15, 5887.
- <sup>52</sup> Hoye A.T., Davoren J.E., Wipf P., Fink M.P., Kagan V.E., *Acc. Chem. Res.*, **2008**, 41, 1, 87.
- <sup>53</sup> a) Duby G., Boutry M., *Plant Science*, **2002**, 162, 477; b) Eilers M., Hwang S., Schatz G., *EMBO J.*, **1988**, 7, 1139; c) Neupert W., *Annu. Rev. Biochem.*, **1997**, 66, 863; d) Matsuura S., Arpin M., Hannum C., Margoliash E., Sabatini D.D., Morimoto T., *Proc. Natl. Acad. Sci. U.S.A.*, **1981**, 78, 4368; d) Rosenblum J.S., Gilula N.B., Lerner R.A., *Proc. Natl. Acad. Sci. U.S.A.*, **1996**, 93, 4471.
- <sup>54</sup> a) Zhao K., Zhao G.M., Wu D., Soong Y., Birk A.V., Schiller P.W., Szeto H.H., *J. Biol. Chem.*, **2004**, 279, 4682; b) Winterbourn C.C., Parsons-Mair H.N., Gebicki S., Gebicki J.M., Davies M.J., *Biochem. J.*, **2004**, 381, 241.
- <sup>55</sup> a) Wipf P., Xiao J., Jiang J., Belikova N.A., Tyurin V.A., Fink M.P., Kagan V.E., *J. Am. Chem. Soc.*, **2005**, 127, 12460; b) Jiang J., Kurnikov I., Belikova N.A., Xiao J., Zhao Q., Amoscato A.A., Braslau R., Studer A., Fink M.P., Greenberger J.S., Wipf P., Kagan V.E., *J. Pharm. Exp. Ther.*, **2007**, 320, 1050 c) Kanai A., Zabbarova I., Amoscato A., Epperly M., Xiao J., Wipf P., *Org. Biomol. Chem.*, **2007**, 5, 307.
- <sup>56</sup> Zhao Z., Chan P.S., Li H., Wong K.L., Wong R.N.S., Mak N.K., Zhang J., Tam H.L., Wong W.Y., Kwong D.W.J., Wong W.K., *Inorg. Chem.*, **2012**, 51, 812.
- <sup>57</sup> Kwak J.H., He Y., Yoon B., Koo S., Yang Z., Kang E.J., Lee B.H., Han S.Y., Yoo Y.C., Lee K.B., Kim J.S., *Chem. Comm.*, **2014**, 50, 86, 13045.
- <sup>58</sup> Beija M., Afonso C.A.M., Martinho J.G.M., *Chem. Soc. Rev.*, **2009**, 38, 2410.
- <sup>59</sup> a) Dessolin J., Schuler M., Quinart A., De Giorgi F., Ghosez L., Ichas F., *Eur. J. Pharmacol.*, **2002**, 447, 155; b) Murphy M.P., *Trends Biotechnol.*, **1997**, 15, 326; c) Muratovska A., Lightowers R.N., Taylor R.W., Wilce J.A., Murphy M.P., *Adv. Drug Delivery Rev.*, **2001**, 49, 189, d) Sheu S.S., Nauduri D., Anders M.W., *Biochem. Biophys. Acta*, **2006**, 1762, 256.
- <sup>60</sup> a) Ross M.F., Kelso G.F., Blaikie F.H., James A.M., Cochemé H.M., Filipovska A., Da Ros T., Hurd T.R., Smith R.A.J., Murphy M.P., *Biochemistry*, **2005**, 70, 222; b) Smith R.A.J., Porteous C.M., Coulter C.V., Murphy M.P., *Eur. J. Biotechnol.*, **1999**, 263, 709; c) Adlam V.J., Harrison J.C., Porteous C.M., James A.M., Smith R.A.J., Murphy M.P., Sammut I.A., *FASEB J.*, **2005**, 19, 1088; d) James A.W., Sharpley M.S., Manas A.R.B., Frerman F.E., Hirst J., Smith R.A.J., Murphy M.P., *J. Biol. Chem.*, **2007**, 282, 14708.
- <sup>61</sup> a) Francis M.B., Nguyen T., *Org. Lett.*, **2003**, 5, 18, 3245; b) Grissom C.B., Lee M., *Org. Lett.*, **2009**, 11, 12, 2499.
- <sup>62</sup> de los Angeles Rey M., Martínez-Pérez J.A., Fernández-Gacio A., Halkes K., Fall Y., Granja J., Mouriño A., *J. Org. Chem.*, **1999**, 64, 3196.





### *3. Manganese oxoclusters as artificial antioxidants*

Most of the work described in this chapter was performed during a Short Term Scientific Mission within COST action 1203, in the laboratory of Prof. Wolfgang Schmitt, at the Trinity College Dublin in Ireland, from June 23<sup>rd</sup> to September 7<sup>th</sup> 2014.





### **3.1 Manganese oxoclusters, a brief overview**

The increase of number of metal centers have been taken into account in order to amplify the activity of the artificial CAT/SOD mimicking systems. In this chapter, polynuclear 3d manganese oxoclusters have been considered as catalase and superoxide dismutase synzymes. Oxoclusters are a class of compound characterized by the presence of a multimetallic structure in which metals are linked by oxygen bridge and coordinated by organic polydentate ligands. Early transition metals clusters (e.g. Zr, Hf, Ti), mixed clusters (e.g. Ti-Zr, Ag-Zr, Ti-Y Cu-Y), lanthanide (e.g. La-Zn, Ba-Ce, Sm-Ti) and also middle transition metals clusters (Fe, Cr, Mn) have been synthesized during these years.<sup>1, 3</sup> They are usually discrete and globally neutral species, featuring different nuclearities (3-14 metals), connectivity modes (corner, edge or face sharing of the polyhedra) and coordination number of metal atoms (depending on metal atom).<sup>2</sup> The interest for these polynuclear 3d metal complexes is due to various reasons: they might exhibit high-spin (S) ground states and magnetic anisotropy, thus working as nanoscale magnetic particles,<sup>3</sup> or they can be used as building blocks for hybrid inorganic-organic materials,<sup>4</sup> and as precursors for the nucleation of nanostructured metal oxides or secondary building units (SBU) for MOFs (Metal organic frameworks).<sup>5</sup>

There has been considerable interest in manganese complexes over the last 20 years mainly owing to their utility in the fields of bioinorganic chemistry and magnetic materials.<sup>6</sup> Mn is an essential redox active metal, used by nature as catalyst in important biological reactions, it is also present in many enzyme active site.<sup>7</sup> Manganese oxoclusters are of particular interest for two main reasons. They share some features with the natural catalase, in which two manganese atoms are bridged by two oxygens and a carboxylate, and with the oxygen evolving catalyst (OEC) of photosynthetic system, in which there are four manganese and a calcium ions linked by oxygen bridges ( $Mn_4CaO_5$ , Figure 43).<sup>8</sup> Their magnetic properties as single-molecule magnets (SSM) are really interesting in material science,<sup>9</sup> indeed SMMs are regarded as the elementary units in both ultimate high-density magnetic storage devices and for the design of quantum computers.<sup>10</sup> In literature there are many examples of multi manganese oxoclusters that have been studied, mainly for their electronic and magnetic properties, that are very often related to their symmetry and nuclearity, but nothing about their catalytic activity has been reported yet.

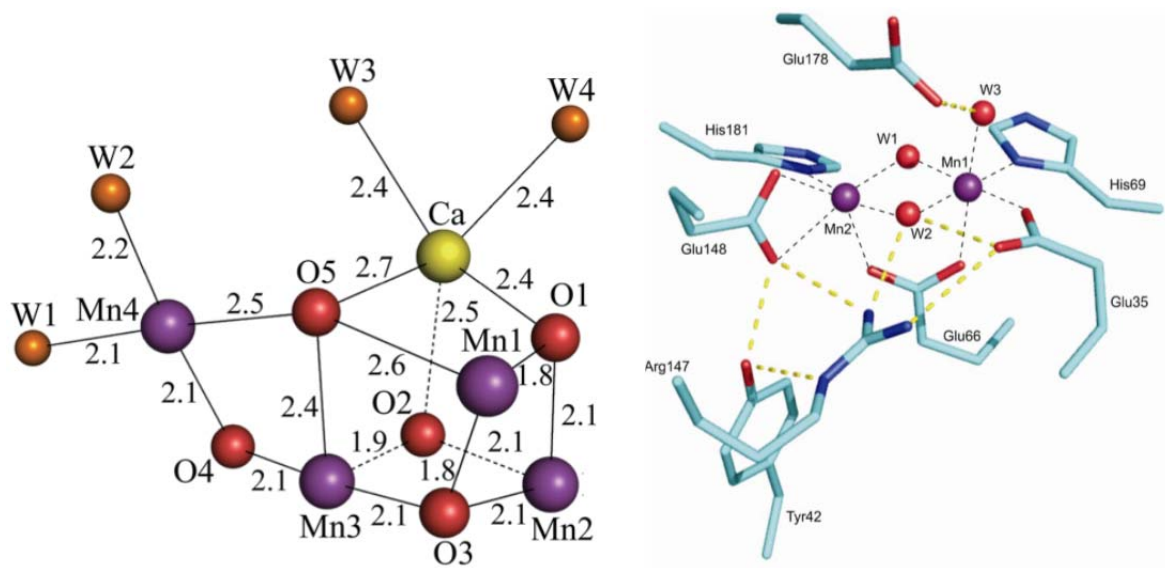


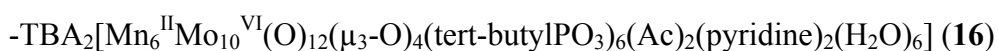
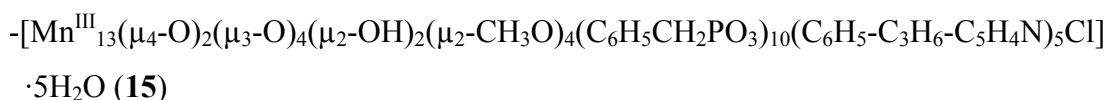
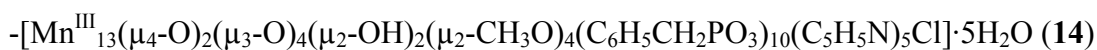
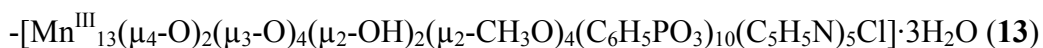
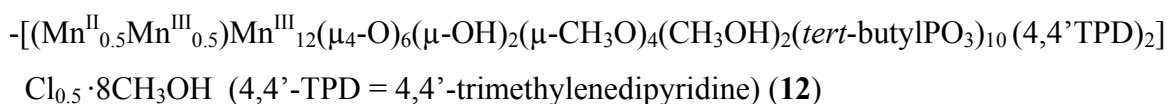
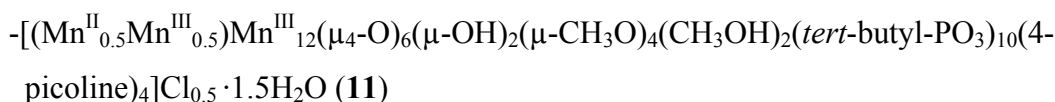
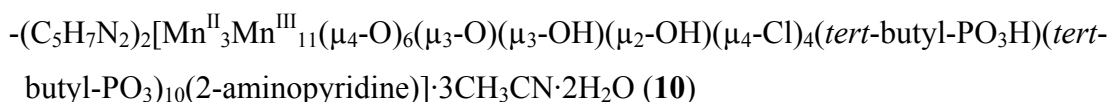
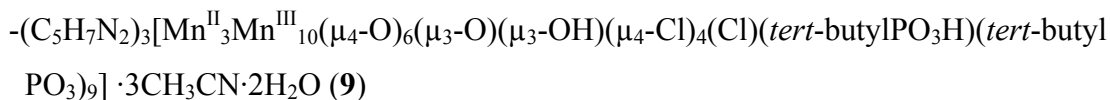
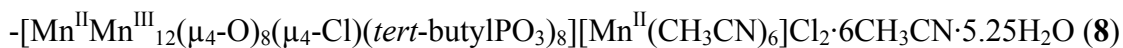
**Figure 43:** Catalytic center of photosynthetic OEC containing 4 Mn atoms (left) and Mn catalase of *L.plantarum* containing 2 Mn atoms.

For all these motives, in the next section, the preparation of different multi-metallic compounds of Mn has been taken into account, trying to discover novel catalysts that have catalase and superoxide dismutase mimicking activity.

### 3.2 Catalytic activity and stability of multi-manganese complexes (8-16)

Mn-based oxoclusters containing 13 and 6 metal centers in different oxidation states have been prepared following literature procedures.<sup>11</sup> These compounds are usually made of 6-13 manganese ions connected by oxygen and/or chloride atoms and coordinated by organic phosphonate ligands (*tert*-butyl-, phenyl- and benzyl-); metal centers are usually present as Mn<sup>III</sup>, but it is also possible to have Mn<sup>II</sup> atoms. These compounds show interesting magnetic properties and are stable in acetonitrile, DMF and DMSO. In a typical synthesis (more details can be found in the Experimental Part, chapter 6), an organic phosphonate ligand is dissolved in organic solvent, usually methanol or acetonitrile, in the presence of manganese (+II) and manganese (+VIII) salts, whose amount differs from cluster to cluster, and an organic base is added. After few hours the solution is filtered and left to crystallize at room temperature for 1-2 weeks. The oxoclusters synthesized are listed below. They are all characterized by high nuclearity, 6, 13 or 14 manganese atoms, organic phosphonate ligands, mainly *tert*-butylphosphonates and an organic base, like

trimethylamine or pyridine and derivatives, that sometimes could also coordinate the metals. A molybdate oxocluster, containing 6 manganese, was also prepared.



In figure 44 are reported all the structures of these clusters: it is interesting to notice the different spatial arrangement of manganese atoms in the structures, depending on the type of phosphonate used, the ratio of  $\text{Mn}^{\text{II}}/\text{Mn}^{\text{VII}}$  added, the presence of bases and the molar ratio of the ligands. Molybdate-based species are of particular interest, considering that they contain a more extended inorganic domain that can make the cluster more resistant to oxidative conditions, while the occurrence of many metal centers could support multi-electronic reactions.

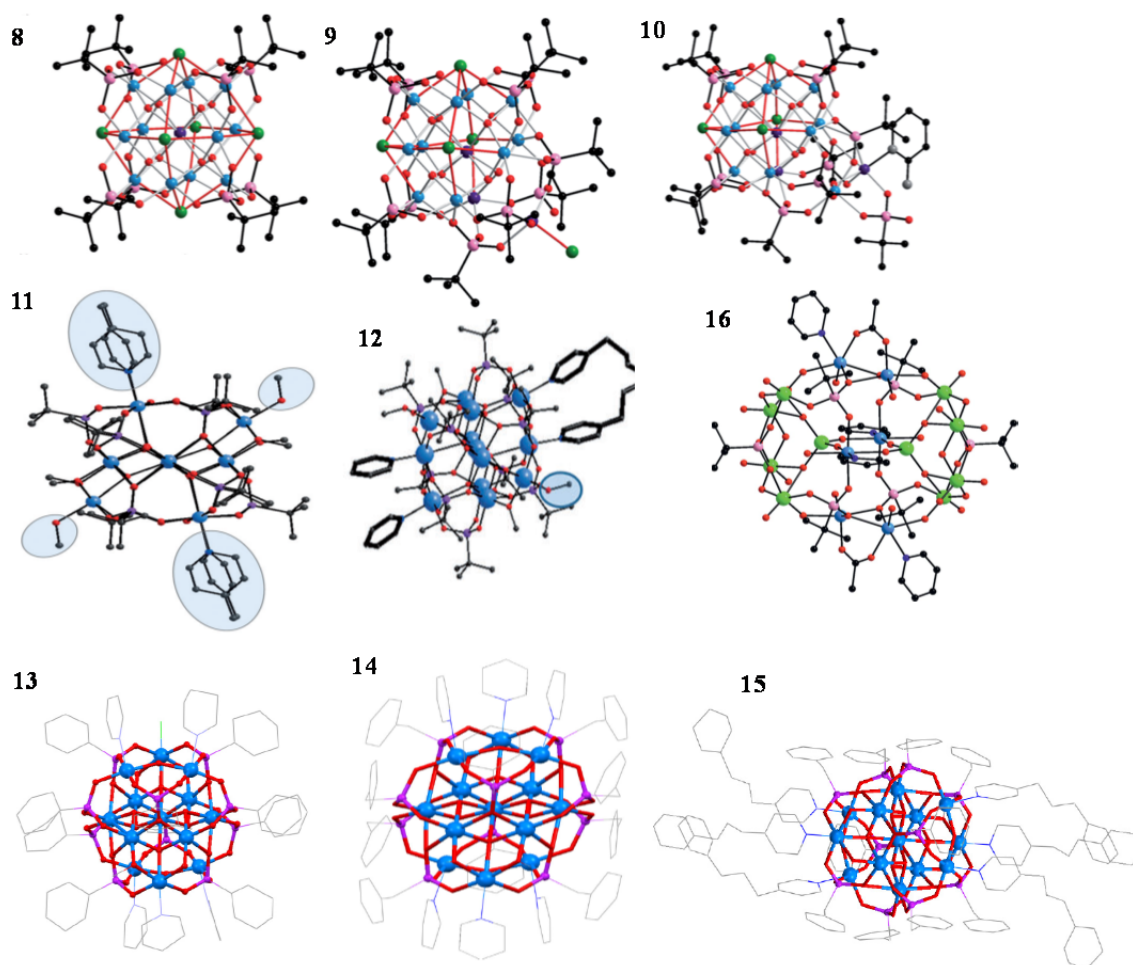


**Figure 44:** Structure of the clusters synthesized **8-16**, in particular from the top left: compound **8-9-10**. In the middle from the left: **11-12-16**. And lower from left: **13-14-15**. Legend: in blue manganese atoms, in red oxygen atoms, light green (compound **16**) molybdenum atoms, dark green chloride atoms and carbon atoms in black.

Compounds **8-12** are formed by *tert*-butylphosphonates ligands and have 13-14 Mn atoms, the bases used are different and also the Mn<sup>II</sup> content is different. Also compound **16** has *tert*-butylphosphonates ligands, but there are only 6 manganese atoms in the structure. The others oxoclusters, **13-15** are synthesized with phenyl and benzyl phosphonates with different bases but all are formed by 13 Mn<sup>III</sup> atoms.

All these compound were tested as catalase mimics: interestingly for almost all of them, reactivity in acetonitrile falls down rapidly, while in aqueous solution they often reach the complete dismutation of H<sub>2</sub>O<sub>2</sub> in few hours (Figure 45).

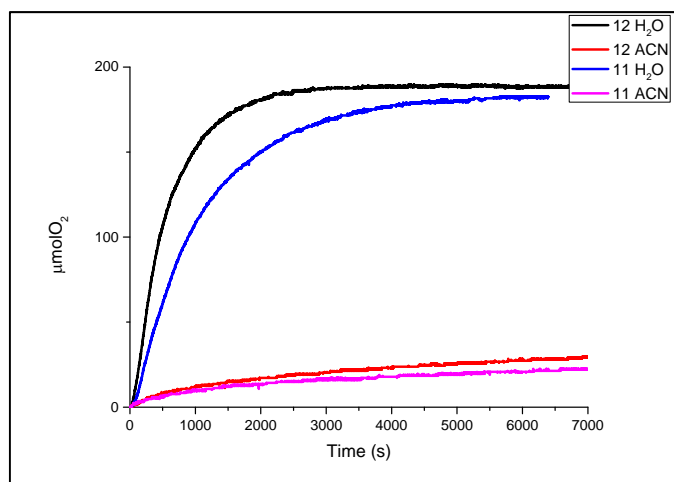


**Figure 45:** Example of differences in reactivity in acetonitrile (pink-red lines) and in water (blue-black lines) of two manganese oxoclusters with similar structure (**11-12**).

This behavior is common for the compound with 13 manganese atoms, while molybdate compound (**16**), with only 6  $\text{Mn}^{\text{II}}$  atoms, has still low activity in acetonitrile but is basically inactive in pure water. Compound **8-10** have similar structural features. Indeed, they are obtained lowering the molar ratio between chloride anion and phosphonate ligands, with respect to oxocluster **8**, leading to less symmetric compounds (Figure 46). These changes slightly affect the reactivity, being the less symmetric compound the most reactive one (Figure 46 left).

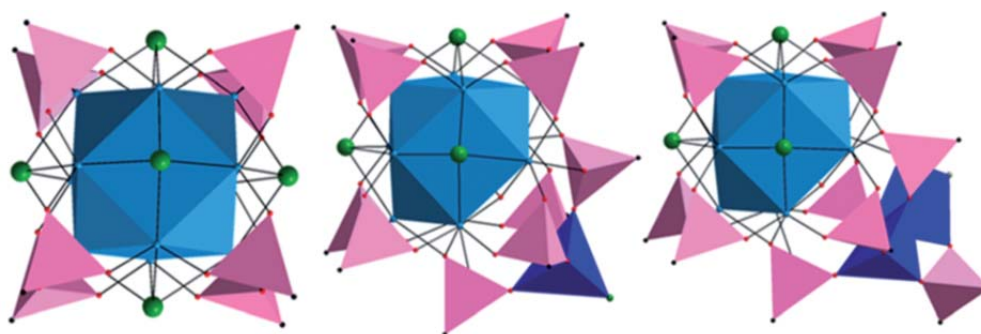


**Figure 46:** Schematic representation of compounds **8** (left), **9** (middle) and **10** (right) in which manganese atoms cluster is in blue, while phosphonate ligands are in pink. Dark blue is the “external” manganese portion of clusters **9** and **10**.<sup>11a</sup>

Compounds **13-15** contain hindered aromatic phosphonates. They are less reactive, with only a small difference between phenyl-based clusters (**13**) and benzyl-based clusters (**14**), probably due to phosphonate ligand, being the former more reactive than the latter. For the

compound **15**, the introduction of a different coordinating base (4-(3-phenylpropyl)pyridine) is responsible for a better reactivity (Figure 47). Being the coordination environment similar to that of compound **14**, this effect may be due to a different aggregation state in solution.

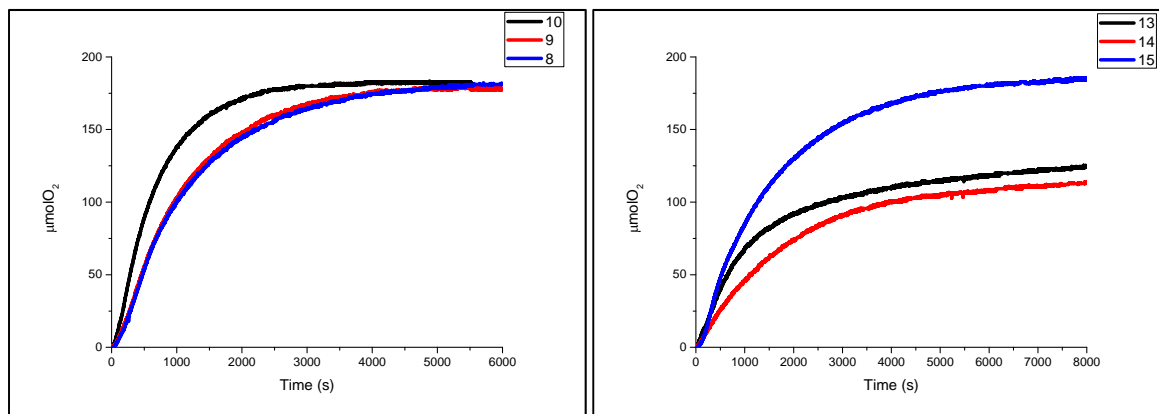


**Figure 47:** Kinetics trace of similar clusters, on the left compounds **8-9-10**, on the right compounds **13-14-15**.

The mixed Mn/Mo cluster (**16**) shows an opposite behavior, with a very low activity for H<sub>2</sub>O<sub>2</sub> dismutation in water, while in acetonitrile it is active, even if not so fast. The low reactivity, in this case, can be due to stabilization of Mn in a lower oxidation state (Mn<sup>II</sup>, while previous clusters contain mainly Mn<sup>III</sup> atoms). Cluster reactivity are resumed in table 12, highlighting that the compound **12** was the most active one, with an initial dismutation rate of 17.5 μMO<sub>2</sub>/s in aqueous solution, Again, the use of different base (in **11**), affects the reactivity of isostructural clusters.

**Table 12:** Number of manganese atoms and initial rate of hydrogen peroxide dismutation in water of oxoclusters **8-16**.

Cluster N.	N. Mn atoms	R <sub>0</sub> μMO <sub>2</sub> /s <sup>a</sup>
<b>8</b>	13	7.6 (-)
<b>9</b>	13	9.7 (0.4)
<b>10</b>	14	14.6 (1.2)
<b>11</b>	13	12.3 (0.9)
<b>12</b>	13	17.5 (1.7)
<b>13</b>	13	7.5 (0.6)
<b>14</b>	13	4.6 (-)
<b>15</b>	13	9.5 (-)
<b>16</b>	6	- (1.6)

a: Initial rate in acetonitrile inside brackets.

The different coordination environment is particularly important if considering that, in concentrated aqueous solution, the oxoclusters have the tendency to precipitate after few hours. Solids were analyzed by FTIR and mass spectroscopy, upon re-dissolving them in acetonitrile or DMF. IR spectra reveals some changes in the cluster structures, and suggest the loss of the coordinating base.

The reactivity in buffered solution was also tested: in phosphate buffer solution (PBS), catalysts was much less efficient, probably because of the competition between phosphonate ligands and phosphate. Indeed, solids precipitated from phosphate buffer (50mM, pH 7.4) showed major changes in IR spectrum (Figure 48 reports the representative behavior of compound **13**). Unfortunately, mass spectra did not give any information about structure changing or modification, while recrystallization attempts were not successful.

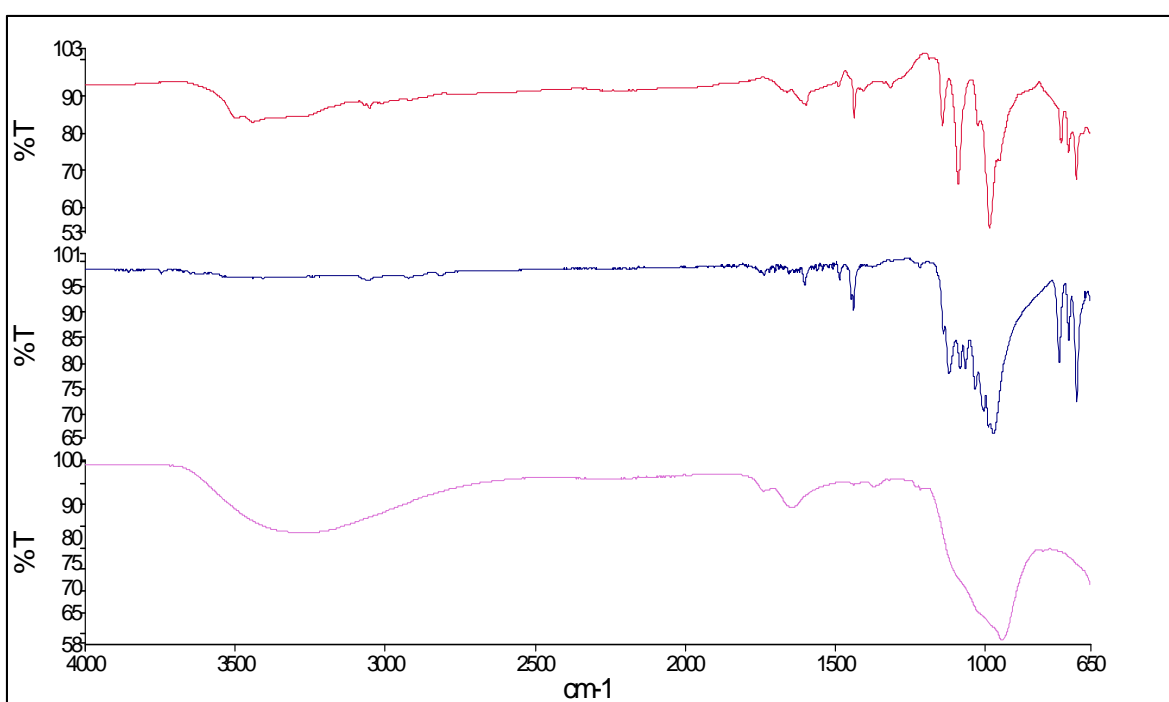


**Figure 48:** Example of IR spectra of compound **13**, a  $Mn_{13}$  cluster, before (blue line, middle) and after dissolution and precipitation in water (red line, top) and phosphate buffer (pink line, bottom).

Finally, the SOD activity of these oxocluster was analyzed, using borate buffer at pH 7.8. Preliminary tests have shown a good activity against superoxide anion formation, with an  $IC_{50}$  lower than  $1\mu M$ , with an hypothetical kinetic constant higher than  $10^6 M^{-1}s^{-1}$ . The Mo/Mn mixed cluster was instead much less reactive.

### **3.3 Conclusions**

New multimetallic compounds have been prepared and used for hydrogen peroxide dismutation. The anti ROS activity of manganese oxoclusters, in aqueous solution, is herein demonstrated for the first time. From a comparison of reactivity, it is evident that Mn(III) is required to dismutate H<sub>2</sub>O<sub>2</sub>, while in the presence of only Mn(II), the activity is extremely reduced.

Despite the high nuclearity, however, the clusters are slower than the dinuclear compound presented above. In addition, in water their structure changes and a major drawback is represented by the need to avoid phosphate buffers. Further experiments should thus be performed to assess the nature of the active species, and to exclude manganese release from the cluster. To increase the solubility and stability in water, different synthetic procedures, involving different/hydrophilic ligands have already been considered, but this will require further experiments. Activity in other buffered solutions, containing Tris, Mops, Hepes, carbonate buffer will also be explored to optimize the reactivity.



## References

- <sup>1</sup> a) Hubert-Pfalzgraf L.G., Liliane G., *J. Mater. Chem.*, **2004**, 14, 3113; b) Hubert-Pfalzgraf L.G., *Coord. Chem. Rev.*, **1998**, 178-180, 967; c) Brethon A., Hubert-Pfalzgraf L.G., *J. Sol-Gel Sci. Techn.*, **2006**, 39, 159; d) Brethon A., Hubert-Pfalzgraf L.G., Daran J.C., *Dalton Trans.*, **2005**, 1, 250; e) Hubert-Pfalzgraf L.G., Daniele S., *Compte Rendu Chim.*, **2004**, 7, 521-527; f) Losada G., Mendiola M.A., Sevilla M.T., *Inorg. Chim. Acta*, **1997**, 255, 125; g) Zhang K.L., Shi Y.J., You X.Z., Yu K.B., *J. Mol. Struct.*, **2005**, 743, 73; h) Long D.L., Kögerler P., Farrugia L.J., Cronin L., *Chem. Asian J.*, **2006**, 1, 352.
- <sup>2</sup> a) Faccioli F., Bauer M., Pedron D., Sorarù A., Carraro M., Gross S., *Eur. J. Inorg. Chem.*, **2015**, 2, 210.
- <sup>3</sup> a) Sessoli R., Gatteschi D., Hendrickson D.N., Christou G., *MRS Bull.*, **2000**, 25, 66; b) Aubin S.M.J., Gilley N.R., Pardi L., Krzystek J., Wemple M.W., Brunel L.C., Maple M.B., Christou G., Hendrickson D.N., *J. Am. Chem. Soc.*, **1998**, 120, 4991; c) Thomas L., Lionti L., Ballou R., Gatteschi D., Sessoli R., Barbara B., *Nature*, **1996**, 383, 145; d) Oshio H., Nakano M., *Chem. Eur. J.*, **2005**, 11, 5178; e) Christou G., *Polyhedron*, **2005**, 24, 2065; f) Brechin E. K., *Chem. Commun.*, **2005**, 5141.
- <sup>4</sup> a) Schubert U., *Chem. Soc. Rev.*, **2011**, 40, 575; b) Carraro M., Gross S., *Materials*, **2014**, 7, 3956; c) Gross S., *J. Mater. Chem.*, **2011**, 21, 15853; d) Sliem M.A., Schmidt D.A., Bétard A., Kalidindi S.B., Gross S., Havenith-Newen M., Devi A., Fischer R.A., *Chem. Mater.*, **2012**, 12, 4274.
- <sup>5</sup> a) Guillerm V., Gross S., Serre C., Devic T., Bauer M., Férey G., *Chem. Commun.*, **2010**, 46, 767; b) Dan-Hardi M., Serre C., Frot T., Rozes L., Maurin G., Sanchez C., Férey G., *J. Amer. Chem. Soc.*, **2009**, 131, 10857.
- <sup>6</sup> Wang M., Ma C., Wen H., Chen C., *Dalton Trans.*, **2009**, 994.
- <sup>7</sup> a) Mukhopadhyay S., Mandal S.K., Bhaduri S., Armstrong W.H. *Chem. Rev.*, **2004**, 104, 3981; b) Nugent J., *Biochim. Biophys. Acta*, **2001**, 1503, 1; c) Yoder D.W., Hwang J., Penner-Hahn J.E., *Met. Ions Biol. Syst.*, **2000**, 37, 527; d) Barynin V.V., Whittaker M.M., Antonyuk S.V., Lamzin V.S., Harrison P.M., Artymiuk P.J., Whittaker J.W., *Structure*, **2001**, 9, 725; e) Whittaker J.W., *Met. Ions Biol. Syst.*, **2000**, 37, 587.
- <sup>8</sup> a) Signorella S., Hureau C., *Coord. Chem. Rev.*, **2012**, 256, 1229-1245; b) Umena Y., Kawakami K., Shen J.R., Kamiya N., *Nature*, **2011**, 473, 55.
- <sup>9</sup> Glaser T., *Chem. Comm.*, **2011**, 47, 116.
- <sup>10</sup> a) Gatteschi D., Sessoli R., *Angew. Chem., Int. Ed.*, **2003**, 42, 268; b) Tejada J., Chudnovsky E.M., del Barco E., Hernandez J.M., Spiller T.P., *Nanotechnology*, **2001**, 12, 181.
- <sup>11</sup> a) Zhang L., Clérac R., Heijboer P., Schmitt W., *Angew. Chem. Int. Ed.* **2012**, 51, 3007; b) Schmitt W., Heijboer P., Venkatesan M., Onet C.I., Clérac R., Zhang L., *Chem. Eur. J.*, **2012**, 18, 13984; c) Camelia Ioana Onet, *PhD Thesis*, **2013**, School of Chemistry, University of Dublin, "Hybrid Organic-Inorganic Materials: Synthesis, solid state characterization and solution studies of organoarsenate and -phosphonate functionalized clusters networks"; d) Zhang L., Marzec B., Clérac R., Chen Y., Zhang H., Schmitt W., *Chem. Comm.*, **2013**, 49, 66.



## *4. Polyoxometalates against degenerative disease*



#### 4.1 Polyoxometalates: short description and applications in medicine

Polyoxometalates (POMs) are interesting polynuclear multicharged oxyanionic compounds of variable sizes (from Ångstrom to tens of nanometers) that are easily synthesized in aqueous solution using early transition metals (V, Mo and W are the most common) in high oxidation state ( $d^0$ - $d^1$ ) in controlled pH, concentration and temperature conditions.<sup>1</sup>

Sc	Ti	V	Cr	Mn	Fe	Co	Ni	Cu	Zn
Y	Zr	Nb	Mo	Tc	Ru	Rh	Pd	Ag	Cd
La	Hf	Ta	W	Re	Os	Ir	Pt	Au	Hg

Two are the fundamental parameters to have these structures:

1. Cationic radii able to host an octahedral coordination;
2. Empty d orbitals able to form terminal double bond metal oxygen.

Commonly they are formed by octahedral  $MO_6$  (sometimes pentahedral  $MO_5$  or tetrahedral  $MO_4$ ) where one or at least two oxygen (Lipscomb's principle<sup>2</sup>) form a double bond with the metal. Terminal oxygens are essential for the formation of discrete structure and avoid the formation of widespread structure like in metal oxides.

Polyoxometalate could be divided in isopolyanion (A) or heteropolyanion (B) depending on chemical composition:



Where M is the transition metal in high oxidation state and X is another d-group metal or a non-metal atom (P, Si, As, Sb, Bi).

One of the most studied and famous class of these compounds are the  $\alpha$ -Keggin, with a general formula  $[X^{n+}M_{12}O_{40}]^{(8-n)-}$  with  $M = Mo^{VI}$  or  $W^{VI}$  and  $X = Si^{IV}$ ,  $Ge^{IV}$ ,  $P^V$ ,  $As^V$  and  $Sb^V$ . The heteroatom is in the center of the structure with a tetrahedral coordination  $XO_4$  surrounded by 12 octahedral metal centers  $MO_6$  of molybdenum or tungsten that are usually divided in triplets  $M_3O_{13}$  in which each octahedral unit shares the edge. These triplets are linked by the corner of octahedral units, the particular disposition gives a  $T_d$  symmetry to the POM structure (Figure 49).

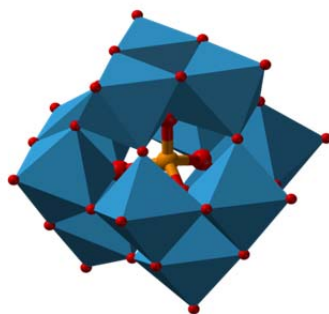


**Figure 49:** Polyhedric structure of  $\alpha$ -Keggin polyanion  $[\text{PW}_{12}\text{O}_{40}]^{3-}$ : Octahedra  $\text{WO}_6$  in blue and internal tetrahedral heteroatom P (orange).

The structure described is the most stable and is labelled as  $\alpha$  form, many isomers less stable, characterized by the rotation of  $60^\circ$  of one ( $\beta$  isomer), two ( $\gamma$  isomer), three ( $\delta$  isomer) or four ( $\epsilon$  isomer) triplets  $\text{M}_3\text{O}_{13}$  around their symmetry axes.<sup>3</sup> These compounds are called saturated because of their low anionic charge, high stability and high symmetry. It is possible to synthesize lacunary structures in which one or more tetrahedral units  $\text{MO}_4^{4+}$  are removed from the saturated structure, generating monovacant ( $\text{XM}_{11}\text{O}_{39}$ ), divacant ( $\text{XM}_{10}\text{O}_{36}$ ) and trivacant ( $\text{XM}_9\text{O}_{34}$ ) structures (Figure 50).<sup>4</sup>

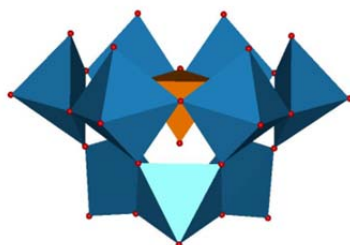


**Figure 50:** Polyhedric representation of a trivacant polyanion  $[\alpha\text{-PW}_9\text{O}_{34}]^{9-}$ : Octahedra  $\text{WO}_6$  in blue and internal tetrahedral heteroatom P (orange).

Exploiting the nucleophilic oxygen of the lacuna it is possible to insert different functionalities, for example other metal centers such as  $\text{Fe}^{\text{II/III}}$ ,  $\text{Mn}^{\text{II/III}}$ ,  $\text{Co}^{\text{II/III}}$ ,  $\text{Ru}^{\text{II/III/IV}}$ .<sup>5,6,7,8</sup> These compounds are synthesized starting from the lacunary POM and metal precursors (M'L).

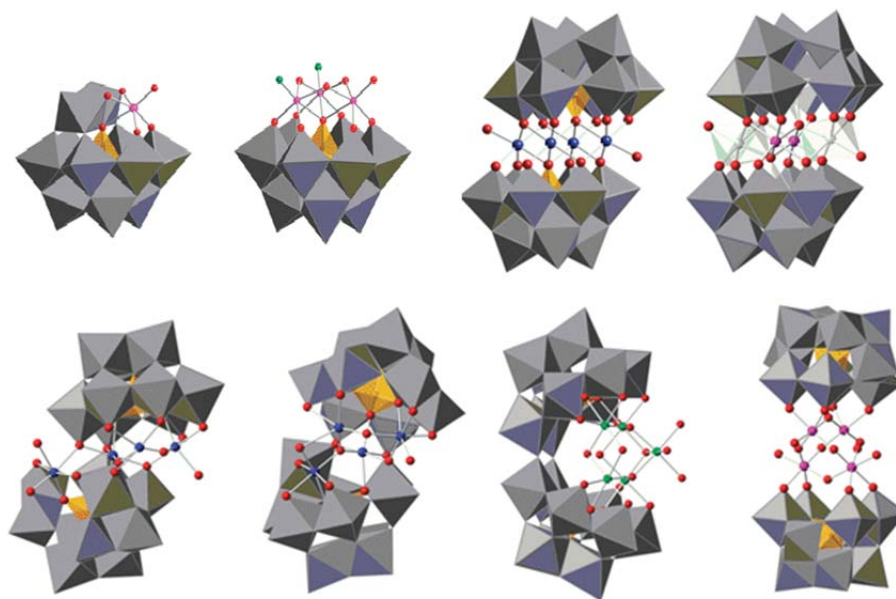


**Figure 51:** Example of transition metal substituted polyoxometalates.

The simplest case of TMSP is when a single metal  $M'$  is coordinated in the lacunary site of a monovacant POM (Figure 51, first structure on the top-left). The lacunary polyoxometalates can also act as a inorganic polydentate ligand coordinating more metal atoms usually stabilized by sandwich-like or dimeric/trimeric structures.<sup>9</sup> The resulting transition metal substituted POMs display coordination analogies with porphyrins and enzymes, and in some cases, a biomimetic activity has also been recorded. This feature, coupled with high robustness to oxidative conditions is of great interest for catalytic applications.<sup>10</sup>

Due to their redox properties, POMs can oxidize several organic substrates, including biological targets.<sup>11</sup> This feature, coupled with the possibility to interact with positively charged domains of proteins and enzymes,<sup>12,13,14</sup> makes POMs interesting inorganic nanodrugs candidates with antitumoral,<sup>15</sup> antiviral,<sup>16</sup> antibacterial<sup>17</sup> activity. There are also evidences of POM containing Lewis acid sites acting as proteases, so they are able to cut and disassemble complex protein.<sup>18</sup>

Some literature data have demonstrated that they are able to penetrate cell's membranes, characterized by a negative surface, even if they are also negatively charged species. POM cytotoxicity depends on POM composition.<sup>19</sup> Considering HeLa cells, one of the most used type,  $IC_{50}$  of 80-90 $\mu$ M were usually found, although Mn or V substituted POMs have an  $IC_{50}$  lower than 10 $\mu$ M.

A major disadvantage, that has hampered their clinical development, is the lack of hydrolytic stability, resulting in the formation of smaller toxic species.<sup>20</sup> Nevertheless, a second generation of POMs (TMSP and POMs decorated with organic pendants) is nowadays well developed, and there are several examples of stable POMs with enhanced activity, which are promising for their antitumoral properties. Other problems are the high molecular weight of POMs and their inorganic composition, while usually drugs are organic and with low molecular weight. These characteristics can be a problem in the blood flux and to cross the blood brain barrier (BBB).<sup>21</sup> On the other hand, the use of cargo macromolecules, in particular starch,<sup>22</sup> liposomes,<sup>23</sup> chitosan<sup>24</sup> or carboxymethylchitosan (CMC)<sup>25,26</sup> has shown that it is possible to improve cellular uptake and stability of POM, while reducing their toxicity.

Concerning the interaction with proteins, the formation of adducts with serum protein was extensively studied in the last years. In particular interaction with serum albumin, bovine (BSA) or human (HSA), was deeply studied, also because albumin is the most abundant protein in blood plasma (40mg/ml) where it is important for interception, transport and transfer of bioactive molecules, aminoacids, lipids, drugs and metal ions. Moreover albumin facilitates hematic flux to organs, especially to liver, intestine, kidney and brain. It is clear how the study of POM albumin interaction is important for their use in medicinal application.<sup>12</sup>

Common techniques to study this interaction are fluorescence, circular dichroism (CD), calorimetry (ITC and DSC) and UV-Vis spectroscopy. Fluorescence is the preferred one, indeed quenching of tryptophan (but sometimes also quenching of tyrosine or phenylalanine) allows to obtain Stern-Volmer binding constant, which are mainly static, due to electrostatic interactions of POM with the protein. Different polyoxometalates were studied, Keggin, Wells-Dawson and also POM substituted with transition metals or lanthanides. In this last case, using europium POM, an increase of POM's fluorescence (up to 5 times) in the presence of albumin was observed, due to the favorable competition of albumin with water molecules on the lanthanide (Figure 52).<sup>13</sup> Usually, the binding constant falls between values of  $5 \cdot 10^4$  e  $10^7 \text{ M}^{-1}$ , depending on POM's structure, charge and pH of the solution (usually around 7.4). Similar results are obtained by means of isothermal titration calorimetry (ITC) from which thermodynamic parameters could be obtained. Circular dichroism is used to investigate changes in secondary structure of the protein, indeed interaction with the polyoxometalate could drastically alter the CD signal, meaning that the protein structure is strongly altered.



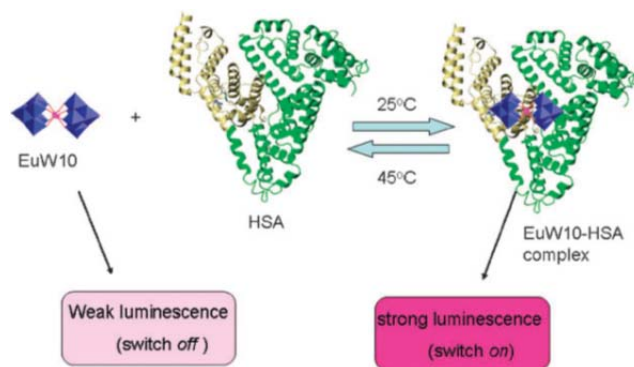


**Figure 52:** Interaction of HSA with europium polyoxometalate, albumin-POM adduct enhance POM intrinsic fluorescence.<sup>13</sup>

Recent studies have shown that polyoxometalates can also interact with amyloid peptides and display anti-amyloidogenic activity. This interaction was confirmed by fluorescence, dichroism and ITC methods. In particular, the aggregation of the peptide in fibrillary structures was monitored using fluorescent probes (for example thioflavin T, ThT) that increase their fluorescence intercalating the aggregated peptide (forming  $\beta$ -sheet secondary structure). CD analysis demonstrated the  $\beta$ -sheet breaker activity of POM. The interaction efficiency depend on POM charge, dimensions and on presence of other transition metals, which may allow to establish a specific coordination. This interaction is mainly electrostatic, in the A $\beta$ 40-42 domain, where positive charged residues such as lysine, histidine and arginine, are localized.<sup>27</sup>

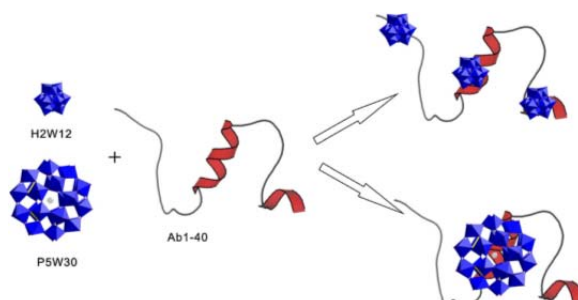


**Figure 53:** Two different POMs ( $\text{H}_2\text{W}_{12}\text{O}_{40}^{6-}$  and  $\text{NaP}_5\text{W}_{30}\text{O}_{110}^{14-}$ ), with different charge and shape, that interact with an amyloid peptide (A $\beta$ 1-40).<sup>27</sup>

Recently a polyoxometalate containing a nickel atom was used as anti-amyloidogenic compound, in order to avoid amyloid aggregation, thanks to electrostatic interaction with the peptide, but also coordination of nickel atom by histidine residues, showing also an indirect anti-ROS effect. Indeed, the coordination of amyloids to POM, avoid interaction of these peptide with iron haem, interaction that could increase ROS production.

Furthermore, studies of stability and blood brain barrier (BBB) penetrations, have demonstrated that POM could pass through BBB, remaining intact, and suggesting its extracellular distribution into the brain.<sup>28</sup>

#### 4.2 Catalytic activity and inhibition of Tetranuclear Ruthenium (IV) polyoxometalate $\text{Na}_{10}[\text{Ru}_4\text{O}_4(\text{OH})_2(\text{H}_2\text{O})_4(\gamma\text{-SiW}_{10}\text{O}_{36})_2]$ (17) in water solution

The polyoxometalate studied is a tetraruthenium substituted polyoxometalate, firstly synthesized in our research group in 2008, and known for its oxygenic activity: indeed it is able to oxidize water and also to dismutate hydrogen peroxide. Its molecular formula is  $\text{Na}_{10}[\text{Ru}_4\text{O}_4(\text{OH})_2(\text{H}_2\text{O})_4(\gamma\text{-SiW}_{10}\text{O}_{36})_2]$  (RuPOM, 17) and it is characterized by an adamantane-like tetraruthenium core that can perform multi-electronic reactions, stabilized by two dilacunary decatungstosilicate anions  $[\text{SiW}_{10}\text{O}_{36}]^{8-}$  (Figure 54).<sup>29</sup>

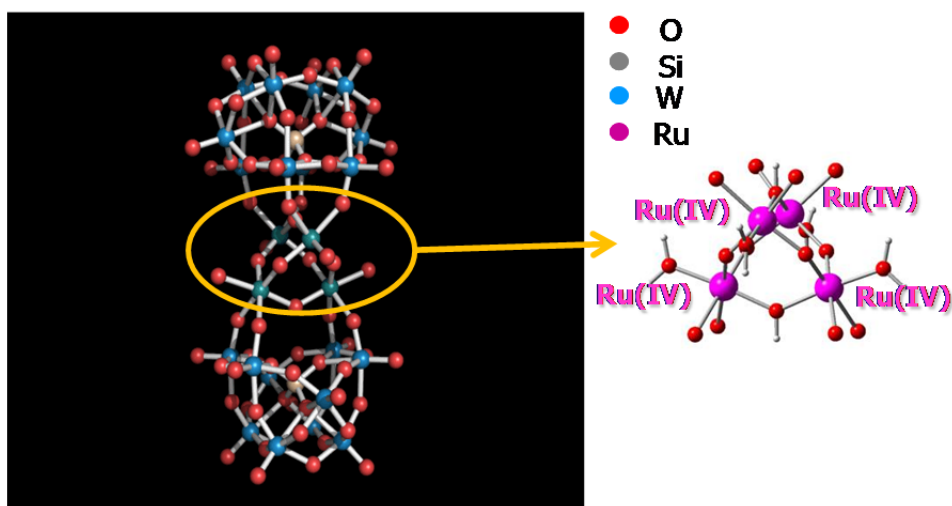


**Figure 54:** Structure of  $\text{Na}_{10}[\text{Ru}_4\text{O}_4(\text{OH})_2(\text{H}_2\text{O})_4(\gamma\text{-SiW}_{10}\text{O}_{36})_2]$  (RuPOM, 17), in evidence the tetraruthenium core. It is possible to see from the image the two  $[\text{SiW}_{10}\text{O}_{36}]^{8-}$  polyoxometalate scaffolds. in red oxygen atoms, in blue tungsten atoms and in grey silicon atoms. Ruthenium atoms are in green (magenta in the scheme on the right).

The oxidation state of ruthenium atoms in the core is  $\text{Ru}^{\text{IV}}$ , while during the catalytic cycle all ruthenium atoms are supposed to oxidation state +V.<sup>30</sup> It has a high negative charge (-10) and is resistant to oxidative and hydrolytic conditions. For the aim of this thesis, the  $\text{H}_2\text{O}_2$  dismutation is an added value that characterizes this POM. In particular, the high

charge could promote interaction with amyloid peptides, while the catalytic activity and robustness are attractive features in the field of ROS elimination.

RuPOM can act as artificial catalase, in particular in phosphate buffer (50mM) it can reach a TON of 2200 with a bimolecular rate constant  $k$  of  $36.8\text{M}^{-1}\text{s}^{-1}$ .<sup>31</sup> An even higher catalytic activity can be observed at higher pH, as shown by the increasing initial rates,  $R_{0\text{pH}7.8} > R_{0\text{pH}7.4} > R_{0\text{pH}7.0}$  calculated from the kinetics curves (Table 13, Figure 55).

**Table 13:** Initial rate of hydrogen peroxide dismutation at different pH,  $\text{H}_2\text{O}_2$  33mM,  $15\mu\text{M}$  RuPOM in 12ml PBS 50mM,  $\mu\text{molO}_2$  are calculated after 1h of reaction.

pH	$R_0 \mu\text{MO}_2/\text{s}$	$\mu\text{molO}_2$
7.0	7.11	157
7.4	11.87	164
7.8	26.4	172

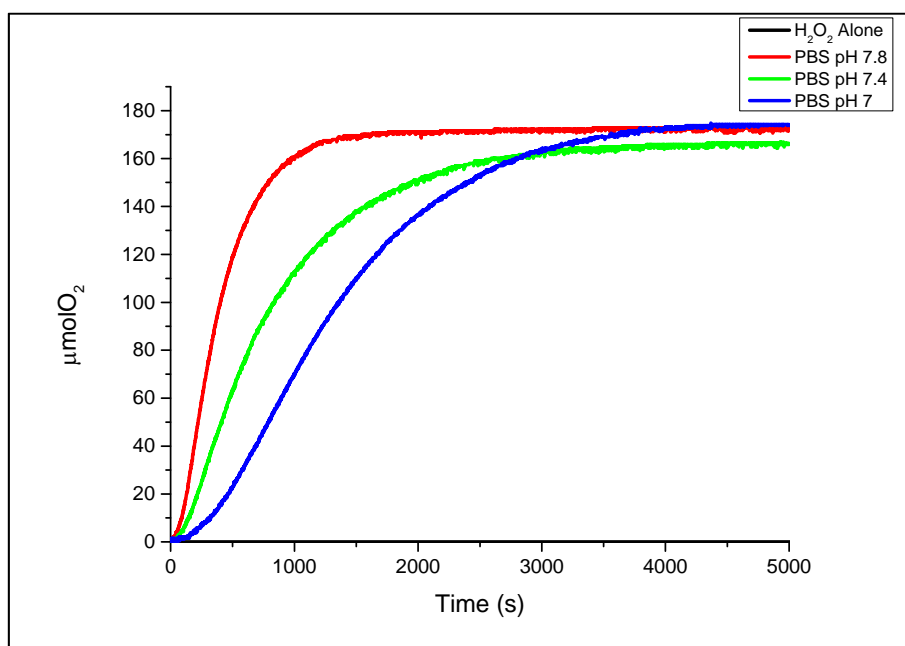


**Figure 55:** Kinetics trace of  $\text{H}_2\text{O}_2$  dismutation by RuPOM at different pH, red pH 7.8, green pH 7.4, blue pH 7.0. No oxygen evolution was registered without catalyst.

In addition, the initial rates of oxygen evolution were determined by setting up different  $\text{H}_2\text{O}_2$  decomposition experiments in the presence of  $15\mu\text{M}$  RuPOM, and varying the initial  $\text{H}_2\text{O}_2$  concentration in a wide range ( $[\text{H}_2\text{O}_2]_0=8\text{-}165\text{mM}$ ). All experiments were performed in phosphate buffer (50mM) at pH 7.0 and  $25^\circ\text{C}$ .

Data were analyzed collecting values of oxygen evolution rate,  $R_0$  ( $\mu\text{molH}_2\text{O}_2/\text{s}$ ), for each  $[\text{H}_2\text{O}_2]_0$  conditions. Fitting these experimental values, according to the Michaelis-Menten

equation, results in a well-behaved saturation curve (Figure 56) from which the kinetic parameters as  $R_{\max}$  ( $\mu\text{molH}_2\text{O}_2/\text{s}$ )  $k_{\text{cat}}$  ( $\text{s}^{-1}$ )  $K_M$  (mM) and  $k_{\text{cat}}/K_M$  ( $\text{s}^{-1}\text{M}^{-1}$ ) (Table 14) can be extracted.

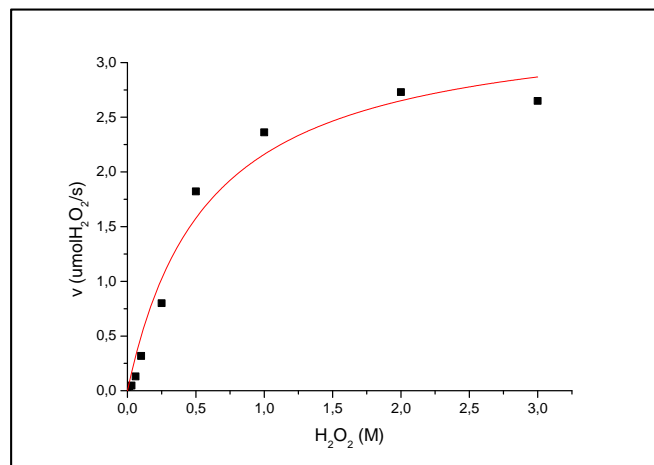


**Figure 56:** Michealis-Menten graph ( $R_0$  vs  $[\text{H}_2\text{O}_2]$ ).

**Table 14:** Kinetics parameter obtained by Michaelis-Menten equation.

$R_{\max}$ ( $\mu\text{mol H}_2\text{O}_2/\text{s}$ )	3.43
$k_{\text{cat}}$ ( $\text{s}^{-1}$ )	19
$K_M$ (mM)	590
$K_{\text{cat}}/K_M$ ( $\text{s}^{-1}\text{M}^{-1}$ )	32

In other buffered solution, the activity of RuPOM can change drastically, depending on the buffer nature (Figure 57). Indeed, if a coordinating buffer is used, such as Tris or Hepes, catalase activity could be quite inhibited. Mops, that has some similarity with Hepes, does not affect much the activity of RuPOM.

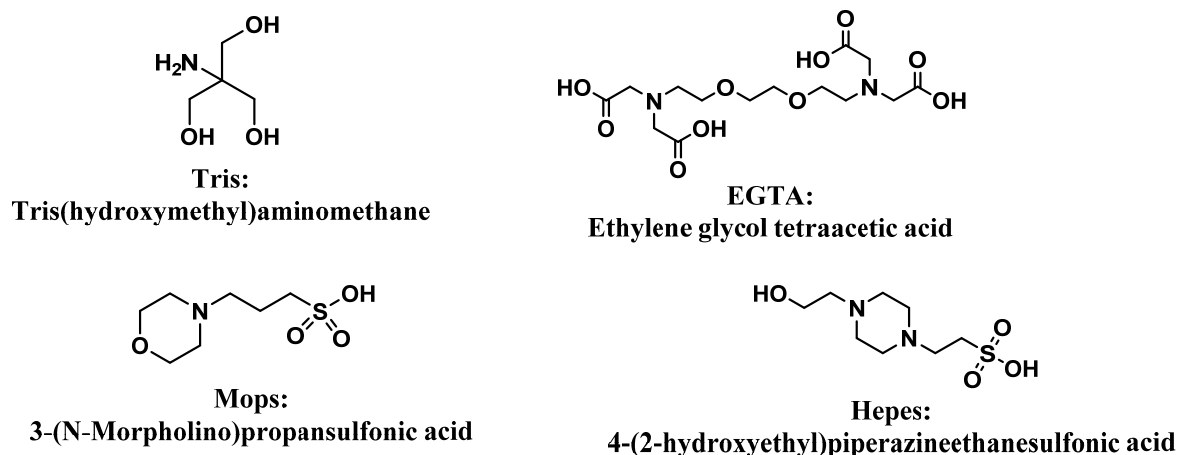


**Figure 57:** Some buffer molecules commonly used in biological assay (Tris, Mops and Hepes) and an additive to selectively remove calcium ions (EGTA).

The addition of salts can influence the kinetics, how shown before for dimanganese complex **4**, but in the case of RuPOM the addition of salts seems to increase the activity of the compound. Indeed in Mops buffer solution containing EGTA the kinetic is faster, if also KCl and phosphate are added, the rate of dismutation further increases. Finally, if a physiological buffer with carbonate, sulfate, chloride, potassium, sodium, calcium and glucose is considered, (Krebs-Henseleit: pH 7.4, NaCl 118mM, NaHCO<sub>3</sub> 25mM, KCl 4.7mM, KH<sub>2</sub>PO<sub>4</sub> 2.15mM, MgSO<sub>4</sub> 0.6mM, CaCl<sub>2</sub> 1.69mM and glucose 2gr/l), it is possible to see that the activity is fully maintained (Figure 58).

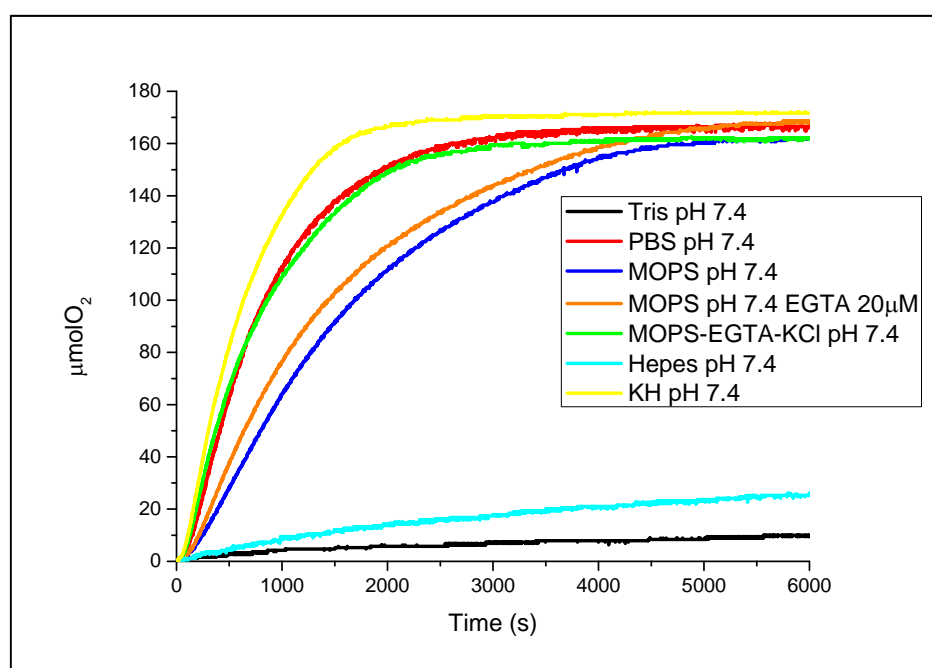


**Figure 58:** Kinetic traces of H<sub>2</sub>O<sub>2</sub> dismutation by RuPOM, in different buffer but at the same pH. KH stands for Krebs-Henseleit buffer solution.

The inhibitory effects of some classical catalase inhibitors such as cyanide, azide and aminotriazole were also tested on RuPOM, in order to assess the possibility of using RuPOM to assist a deactivated native enzyme. Unfortunately, like natural catalase, all these compounds partially or completely inhibit the catalyst. Azide is the least efficient inhibitor but it is able to slow the dismutation about 8 times with a conversion of only 20% after one hour, while the most powerful azide and cyanide inhibit the dismutation about 42 and 475 times respectively, with a conversion of 4% and 2% after one hour (Figure 59).

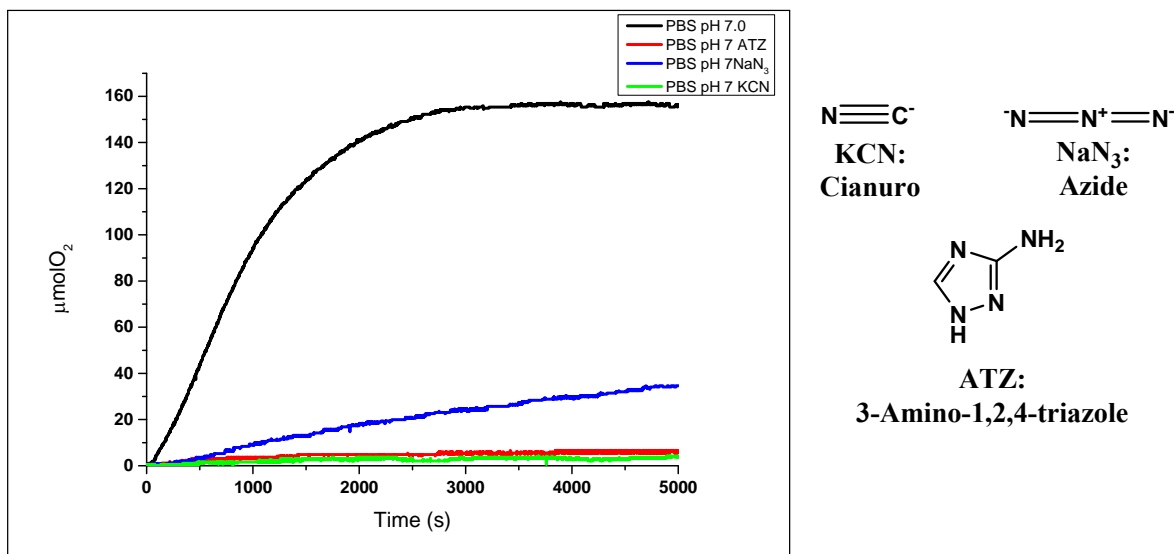


**Figure 59:** Kinetic traces of H<sub>2</sub>O<sub>2</sub> dismutation by RuPOM in the presence of different catalase inhibitors: aminotriazole (ATZ in red), cyanide (KCN in green) and azide (NaN<sub>3</sub> in blue) whose structure are shown on the right, compared with a non-inhibited kinetic (black line).

A comparison of RuPOM with natural catalase was done, but natural catalase is much more efficient in terms of initial rate and also catalytic efficiency, even at a concentration 10 time lower than that of RuPOM (Figure 60).

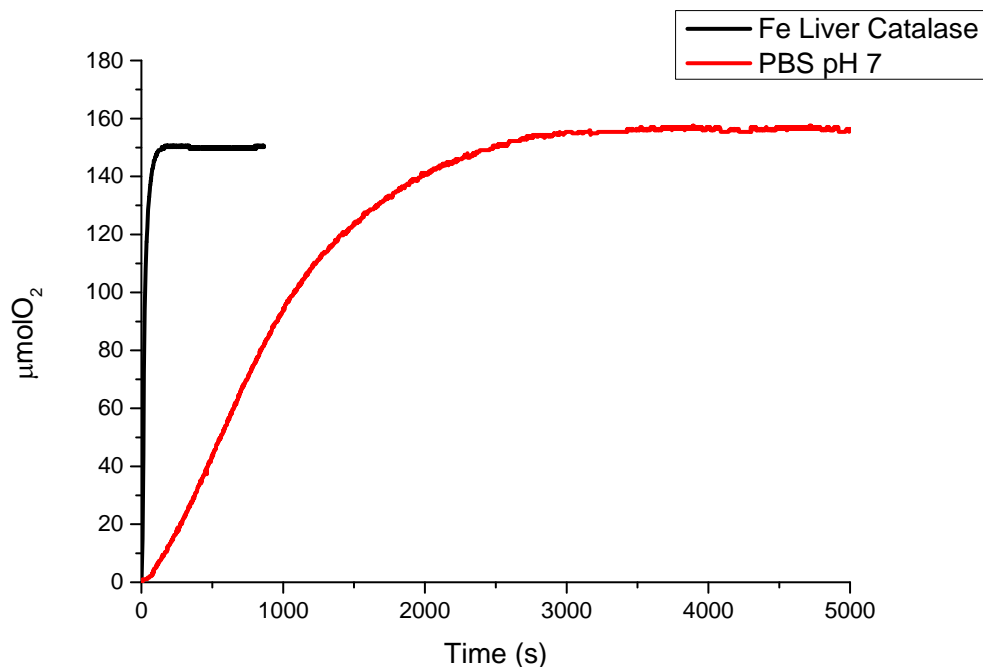


**Figure 60:** Kinetic traces of H<sub>2</sub>O<sub>2</sub> dismutation by 15 μM RuPOM (in red) and by 1.5 μM of commercially available natural iron-catalase (in black), in phosphate buffer at pH 7.0 and 33mM H<sub>2</sub>O<sub>2</sub>.

In the following table 15, some values of initial rate and turnover number (TON after an hour), of RuPOM, in different buffer solution, are reported, to have a global vision of buffer, inhibitors and pH effects.

**Table 15:** Initial rate, TON and buffers used for H<sub>2</sub>O<sub>2</sub> (33mM) dismutation by RuPOM 15μM at different pH and in the presence of inhibitors (30mM). TON is calculated as mole of H<sub>2</sub>O<sub>2</sub> reacted per mole of catalyst after 1h. Comparison with bovine liver Fe catalase 1.5μM.

	Compound	Buffer	R <sub>0</sub> uMO2/s	Time	TON
pH 7	Fe-Catalase	PBS	549.96	250s	16670
	RuPOM	PBS	7.11	1h	1744
	RuPOM	Tris	0.35	1h	64
	RuPOM	Mops	5.65	1h	1511
	RuPOM + KCN	PBS	0.015	1h	311
	RuPOM + NaN <sub>3</sub>	PBS	0.93	1h	61
	RuPOM + ATZ	PBS	0.17	1h	41
pH 7.4	RuPOM	Mops+KCl+EGTA+Pi	14.16	1h	1778
	RuPOM	Tris	0.53	1h	86
	RuPOM	Hepes	0.74	1h	211
	RuPOM	Krebs-Henseleit	17.43	1h	1889
pH 7.8	RuPOM	PBS	26.40	1h	1911
	RuPOM	BBS	15.78	1h	1822

SOD-mimicking activity of the polyanion was then investigated, using NBT and Xanthine/Xanthine oxidase assay, as described before for monomanganese and dimanganese complexes. In the presence of RuPOM, however there is a lower production of oxidized NBT, due to a moderate superoxide dismutation activity of POM. IC<sub>50</sub> is about 11μM, and the kinetic constant is  $5.4 \cdot 10^5 \text{M}^{-1} \text{s}^{-1}$ . Although the latter is four orders of magnitude lower than natural SOD, it is still meaningful for a catalase-like catalyst.

### 4.3 Interaction with amyloid peptides

Alzheimer's disease (AD) is the most common age-related neurodegenerative disease. It is characterized by protein deposits called amyloid plaques that consist of aggregates of the small amyloid β peptide (Aβ).<sup>32</sup> Although there are many hypothesis about this pathology, the amyloid cascade hypothesis explains how amyloid peptides are produced and how they

accumulate generating plaques, in particular it seems that short amyloid peptides can aggregate in oligomeric forms that assemble into fibrillar structure and produce precipitation of tangles of protein.<sup>28,33</sup> Fibrillogenesis of A $\beta$  can be divided in two steps: nucleation and elongation. Proteins rearrange in anomalous way: the hydrophobic portions, normally not exposed, become accessible and available to form soluble oligomers packed as layered  $\beta$ -sheets. During fibrillogenesis,  $\beta$ -sheets are perpendicularly aligned along fibril axis. Fibrils have a diameter of 6-10nm, and are composed by protofilaments made of polypeptide (Figure 61a-c).<sup>34</sup> Then, through a cascade reaction, insoluble fibrils are formed and finally plaques deposit, with further neurological damages.

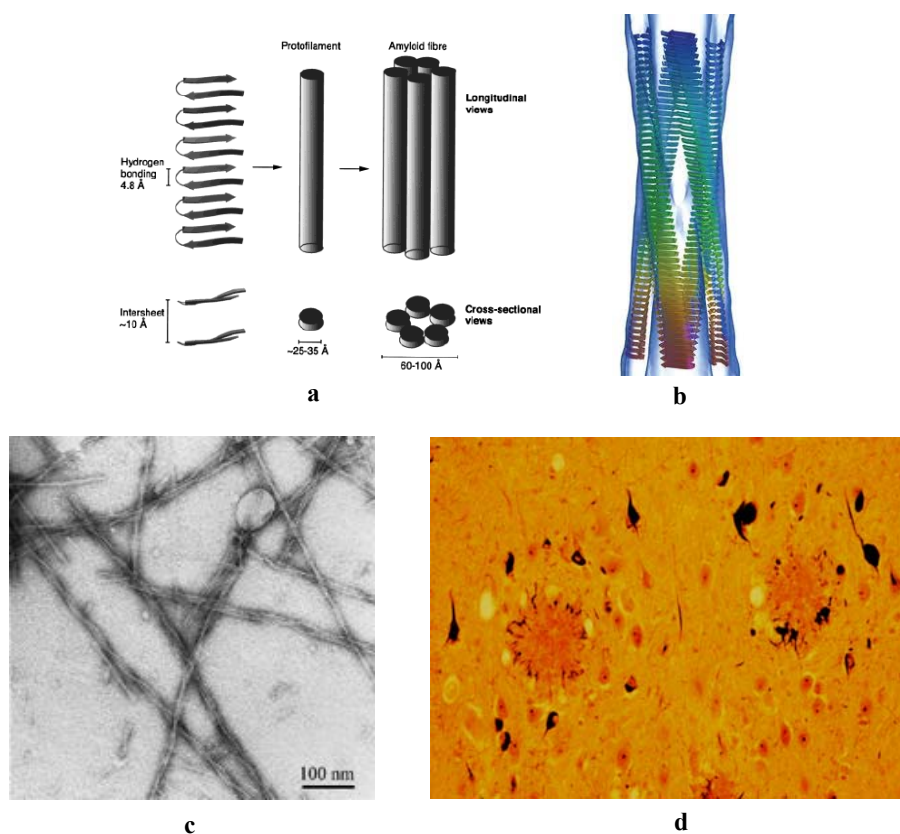


**Figure 61:** a) Scheme of fibrillation of amyloid peptides, b) model of fibrils; c) TEM image of partially formed fibrils and d) image of amyloid plaque in brain tissue.<sup>35</sup>

The oligomeric form seems to be more toxic than fibrils, since they can interact and permeabilize cellular and mitochondrial membranes, forming channels into membranes and disrupting cell or mitochondrial homeostasis.<sup>36</sup> Total and mitochondrial-associated amyloid A $\beta$  of various length increase with age.

Although there is a link between mitochondrial dysfunction and plaques formation, the upstream cause is still unclear.<sup>37</sup> In addition, amyloid peptide impact on mitochondrial



functions, inhibiting enzymes involved in the electron transport chain (complex I and IV),<sup>38</sup> thus causing impairment of oxidative phosphorylation and anomalous ROS production.<sup>39,40</sup>

Moreover, metal dysregulation play a key role in pathogenesis of Alzheimer, indeed metal ions, such Zn<sup>2+</sup>, Cu<sup>2+</sup> and Fe<sup>3+</sup>, foster amyloid aggregation and become, once coordinated by asparagines, methionine, tyrosine and histidine of A $\beta$ , a primary font of reactive oxygen species (ROS) *via* Fenton reaction.<sup>41,42,43,44</sup> Hydrogen peroxide treatment of neurons<sup>45</sup> and deficiency of mitochondrial enzyme MnSOD were shown to increase A $\beta$  production and deposition.<sup>46</sup> Within this *scenario*, ROS production is involved in all phases of the disease.<sup>47,48</sup>

A $\beta$  peptides are made of 40-42 aminoacids, and contain an hydrophobic region with a KVLFF<sup>49</sup> amino acidic motif (AA16-20), which is main responsible to foster  $\beta$ -sheet formation and the subsequent oligomerization and fibrillation. There are also four main aminoacids, three histidines and one aspartate, that can bind metal atoms. For the tests in solution, three peptides of different length are usually studied, 1-40, 1-28, and 1-16 because of their good solubility and less tendency to aggregate, while amyloids 1-42 are mainly used for biological tests rather than chemical experiments because their aggregation is extremely fast (Figure 62).<sup>50</sup>

A $\beta$ 42 (A $\beta$ 1-42): DAEFRHDSGY<sup>10</sup>EVHHQKLVFF<sup>20</sup>AEDVGSNKGA<sup>30</sup>IIGLMVGGVV<sup>40</sup>IA  
 A $\beta$ 40 (A $\beta$ 1-40): DAEFRHDSGY<sup>10</sup>EVHHQKLVFF<sup>20</sup>AEDVGSNKGA<sup>30</sup>IIGLMVGGVV<sup>40</sup>  
 A $\beta$ 28 (A $\beta$ 1-28): DAEFRHDSGY<sup>10</sup>EVHHQKLVFF<sup>20</sup>AEDVGSNK  
 A $\beta$ 16 (A $\beta$ 1-16): DAEFRHDSGY<sup>10</sup>EVHHQK

**Figure 62:** Amino acid sequence of most abundant amyloid peptides A $\beta$ 40 and A $\beta$ 42, and two most studied shorter fragments, A $\beta$ 28 and A $\beta$ 16 used for their higher solubility respect to longer peptides. Coordinating amino acids are colored, in red the four main coordinating.<sup>50</sup>

In the last years, research has focused on the inhibition of peptide aggregation to prevent fibril deposit and then the related dysfunction. Crystallographic structures of amyloid-like fibrils suggest that steric zipper interface between highly ordered parallel and antiparallel beta sheet is an essential element of fibril formation, so that diverse beta-sheet breakers have been investigated.<sup>51</sup> Examples include the use of short peptides and aromatic/hydrophobic molecules. Among the molecules that have been tested as inhibitors of fibrillation, we find fullerene,<sup>52</sup> quinones,<sup>53</sup> isopeptide,<sup>54</sup> or recently cucurbit[7]uril.<sup>55</sup>

Metal mediated aggregation represents another major contribution towards fibrillogenesis. As confirmed by NMR studies, indeed three histidine residues (His6, His13 and His14) can interact with metal centers, which can, in turn, assist further aggregation between peptide chains.<sup>56</sup> A competition with these binding site is thus another possible strategy to inhibit the aggregation. Being His present on the initial fragment, shorter A $\beta$  fragments, such as 1-28 can also be used for studying the interaction with metals.<sup>57</sup> In the last few years polyoxometalates were also tested as anti-amyloidogenic compounds, showing that they are able to prevent fibril formation, as confirmed by thioflavin assay, CD measurement, enzyme digestion, fluorimetric titration and ITC analysis.<sup>27,58</sup> As for the interaction with other proteins and enzymes, the anti-fibrillation effect is mainly due to the ionic interaction with positively-charged aminoacids (mainly His13–Lys16 region, HHQK cluster), with a stoichiometry depending on charge and dimensions of the POM. PC12 cells incubated with A $\beta$  and Dawson-POM mixtures (A $\beta$ :POMs =5 $\mu$ M:10 $\mu$ M) were shown to increase their survival up to 90%, being POM cytotoxicity negligible at the same concentration.<sup>58a</sup>

Moreover, transition metal substituted Dawson POMs ([P<sub>2</sub>MW<sub>17</sub>O<sub>61</sub>]<sup>8-</sup> with M=Ni<sup>II</sup> or Co<sup>II</sup>) can selectively interact with histidines residues of amyloid peptide (HHQK),<sup>59</sup> showing a higher binding constant (up to 6.44 times) than non-substituted Dawson POM, with 1:1 stoichiometry. In this case the POMs were tested *in vivo*, and they were found to be beneficial for inhibiting the peroxidase activity of haem-binding  $\beta$ -Amyloid. In addition, the authors suggested that the POM could distribute extracellularly in the brain, where A $\beta$  aggregates predominately exist, being able to cross the BBB and remaining intact.<sup>59</sup>

The use of anti-aggregation agents, has shown to be only scarcely useful to limit neurodegenerative affects. Chelation therapy, used to scavenge redox active transition metals in the brain,<sup>60</sup> or the administration of antioxidant molecules (polyphenols) are also pivotal to limit ROS damages.<sup>53,61</sup> As already demonstrated in the previous chapter, catalytic ROS scavenger would be more useful thanks to their prolonged activity. Within this *scenario*, multitask compounds represent a major goal. For example, salen Mn complexes with superoxide (SOD) activity were used as ROS scavenger and were also shown to inhibit lysozyme aggregation.<sup>62</sup>

RuPOM has been studied to assess its dual activity, the ability to inhibit A $\beta$  fibrillation and, at the same time, to reduce oxidative stress.<sup>63</sup>

First of all, the interaction of RuPOM with amyloid peptide 1-40 was studied exploiting the intrinsic fluorescence of tyrosine, exciting at 270nm and recording the fluorescence at 305nm. Amyloids were titrated with RuPOM, and the fluorescence was corrected in order to take in account dilution and absorbance of POM. Plotting POM concentration vs F<sub>0</sub>/F (Initial fluorescence divided by observed fluorescence) allows to calculate Stern-Volmer constant of the static quenching occurring with the interaction (Figure 63).

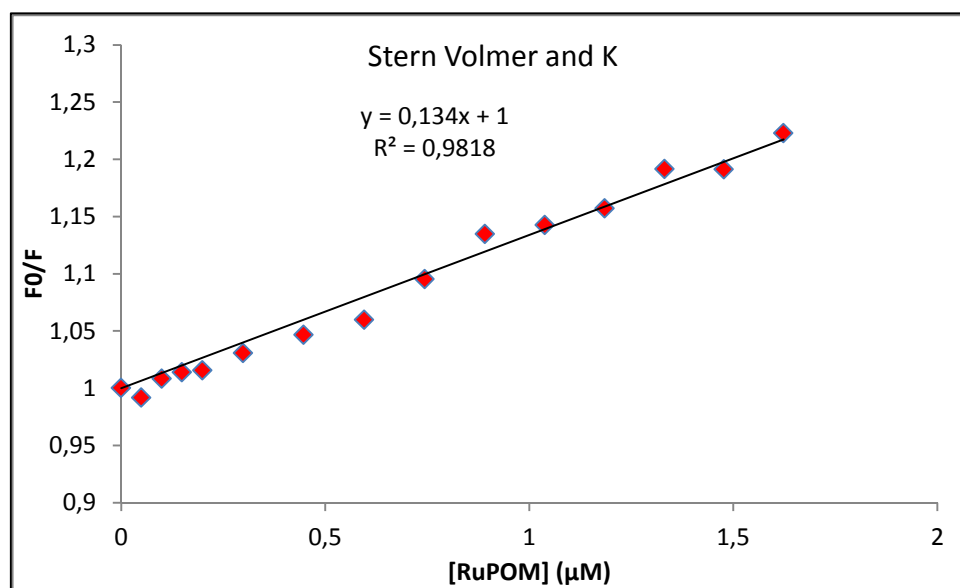


**Figure 63:** Stern-Volmer graph of A $\beta$  1-40 titrated with RuPOM.  $\lambda_{\text{ex}} = 270\text{nm}$ ;  $\lambda_{\text{em}} = 306\text{nm}$ .

The plot gives a Stern-Volmer binding constant value,  $K_{\text{SV}}$ , of about  $1,3 \cdot 10^5 \text{ M}^{-1}$ , which is in agreement with the literature values found for other POMs, around  $10^5$ - $10^6 \text{ M}^{-1}$  depending on POM structure and charge.<sup>58</sup>

After fluorescence studies, circular dichroism (CD) analysis was performed over time to evaluate the effect of RuPOM on  $\beta$ -sheet formation. It is known that A $\beta$  forms beta sheet after incubation at 37°C for 1-2 weeks. As for other polyoxoanions, RuPOM incubated at 37°C for 2 weeks is able to avoid the formation of beta sheet of amyloid 1-40 and also the formation of fibrillary species. Indeed while A $\beta$  incubated at 37°C for 14 days, without POM shows the classical change of conformation from random coil to  $\alpha$ -helix and finally to  $\beta$ -sheet secondary structure, that is responsible for oligomerization and fibril formation. In the presence of POM, instead, there is no formation of  $\beta$ -sheet, as it is possible to see from CD curves (Figure 64).

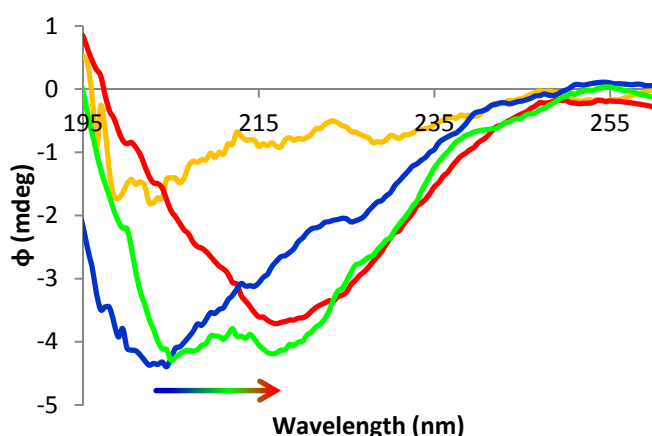


**Figure 64:** CD spectra of A $\beta$  1-40 with (yellow, after 14 days) and without RuPOM at t=0 (blue line), t=7 days (green line) t=14 days (red line); RuPOM has no CD signal (not shown).

Considering fragment 1-40 alone it is possible to observe the conformation change from t=0 random coil (blue line), to alpha helix (t=7 days, green line) and finally to beta sheet, (t=14 days, red line). In particular, the minimum moves from 200nm (random coil), to about 215nm, as expected for the typical  $\beta$ -sheet curve. Yellow line indicates amyloid incubated 14 days at 37°C in the presence of 1 equivalents of RuPOM. As expected, the dichroic signal was lower and during the incubation we did not see any change due to conformation evolution.

A parallel TEM analysis of peptide incubated, confirms the inhibition of fibrillation, as it is possible to see after 14 day incubation with and without 1eq of RuPOM. Amyloid 1-40 alone, after 14 days incubation, shows quite long and ordered fibrillar structures with length up to 2 $\mu$ m and pre-fibrillar aggregates are also visible (Figure 65 left), instead amyloid 1-40 incubated in the presence of POM shows disordered aggregates (Figure 65 right).

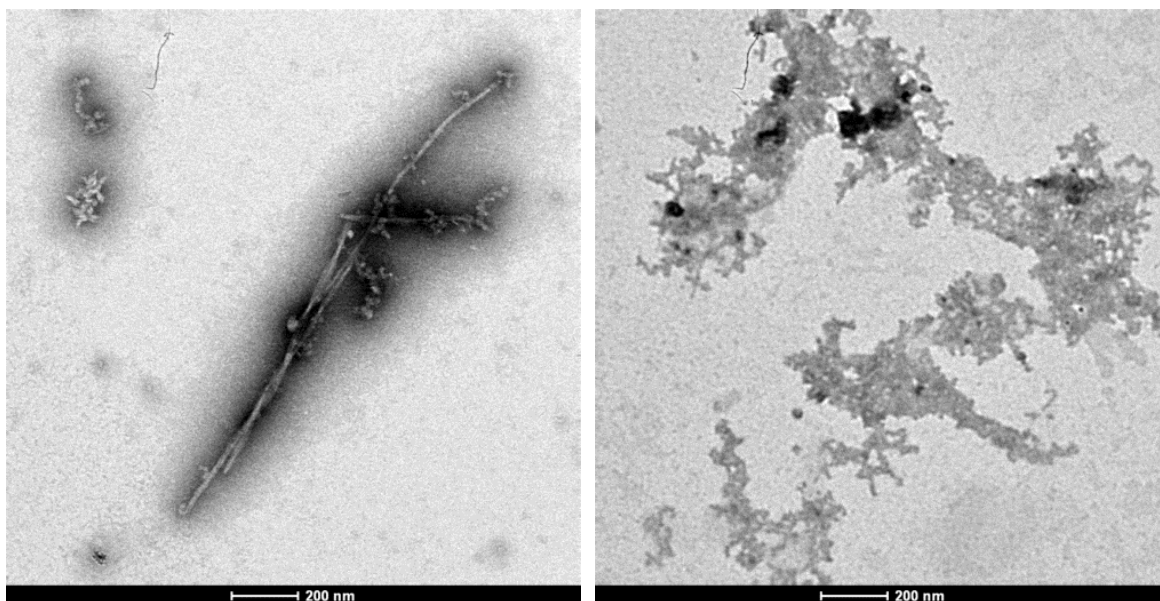


**Figure 65:** TEM micrographs of A $\beta$  1-40 (80 $\mu$ M) without (left) and with 1eq. of RuPOM (right).

So RuPOM has good anti-fibrillar properties and also the capability to avoid formation of beta-sheet from random coil peptide. The common ThioflavinT (ThT) experiments, based on ThT fluorescence increase during the aggregation of  $\beta$ -sheet structures, could not be performed, because RuPOM interaction with ThT and competitive absorbance do not permit to follow the increase of fluorescence during amyloid incubation. So it was impossible to track the kinetics of fibril formation with this technique. As said before, A $\beta$ 42 shows an even higher tendency to fibrillogenesis, so it is quite difficult to follow fibrillation kinetic. After four days of incubation of A $\beta$ 42 (80 $\mu$ M), treated with hexafluoropropanol to disaggregate the peptide, it is possible to see the variation of the dichroic signal at 220nm, that become more negative, and also at about 200nm, that become bigger. In the presence of 0.1eq. (8 $\mu$ M) of RuPOM, the band at 220nm keeps, more or less, the same intensity, while there is a significant change in the region <200nm, where the Cotton effect becomes negative after 4 days incubation with POM (Figure 66). This experiment proves the capability of RuPOM to avoid or to slow the production of beta sheet and so the fibrillation of these peptides.

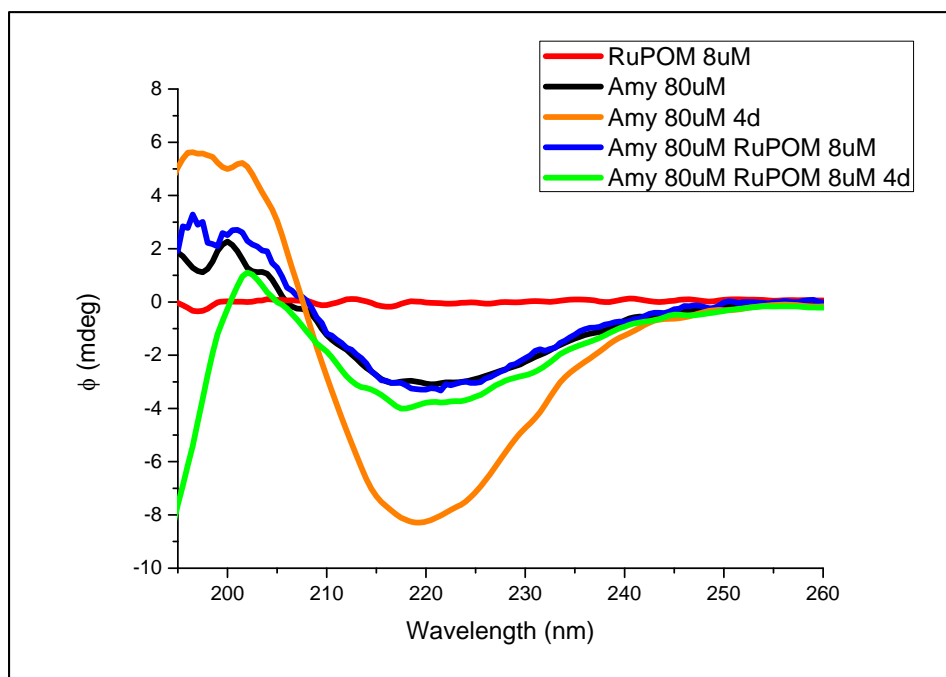


**Figure 66:** CD spectra of A $\beta$ 1-42 (Amy, 80 $\mu$ M) incubated without RuPOM (black line t=0, orange line after 4 days) and with 8 $\mu$ M RuPOM (red line RuPOM alone, blue line t=0 and green line after 4 days).

To better understand the nature of this interaction with amyloidogenic peptides, an  $^1\text{H}$ -NMR study was made on a shorter peptide. Due to the low solubility and extremely high tendency of the A $\beta$  1-40 and 1-42 to aggregate, the 1-28 peptide chain has been initially chosen as a model fragment to establish the interactions between the POM and the peptide chain. As shown before, this fragment has the following aminoacidic sequence, DAEFRHDSGYEVHHQKLVFFAEDVGSNK, and it contains three His residues that could be important for metal coordination. In addition, it is more stable in water and display a lower propensity to aggregate in solution. The  $^1\text{H}$ -NMR spectrum of A $\beta$ 28 (200 $\mu$ M) was recorded, than 0.2 equivalent of RuPOM were added from a concentrated stock solution. The first effect observed was a general broadening of all signals, even if with sub-stoichiometric RuPOM. Interestingly, the same broadening effect is reported in the literature for the addition of 0.2 equivalents of zinc or cadmium solution suggesting the occurrence of equilibria involving proton exchange.<sup>64</sup> We have focused our attention on the signals above 6.7 ppm, where aromatic residues display well resolved signals: 7.78-7.73 ppm and 6.88-6.96 ppm for histidine (His), 7.01 and 6.73 ppm for tyrosine (Tyr), 7.12 ppm for phenylalanine (Phe). In particular, His signals have a much lower intensity or disappear, already after addition of 0.2 RuPOM equivalents, thus suggesting the

occurrence of a strong interaction between His and RuPOM (Figure 67). With 0.4 equivalents of RuPOM added, the broadening of the spectrum becomes even more pronounced, with disappearance of most of the signals (not shown).

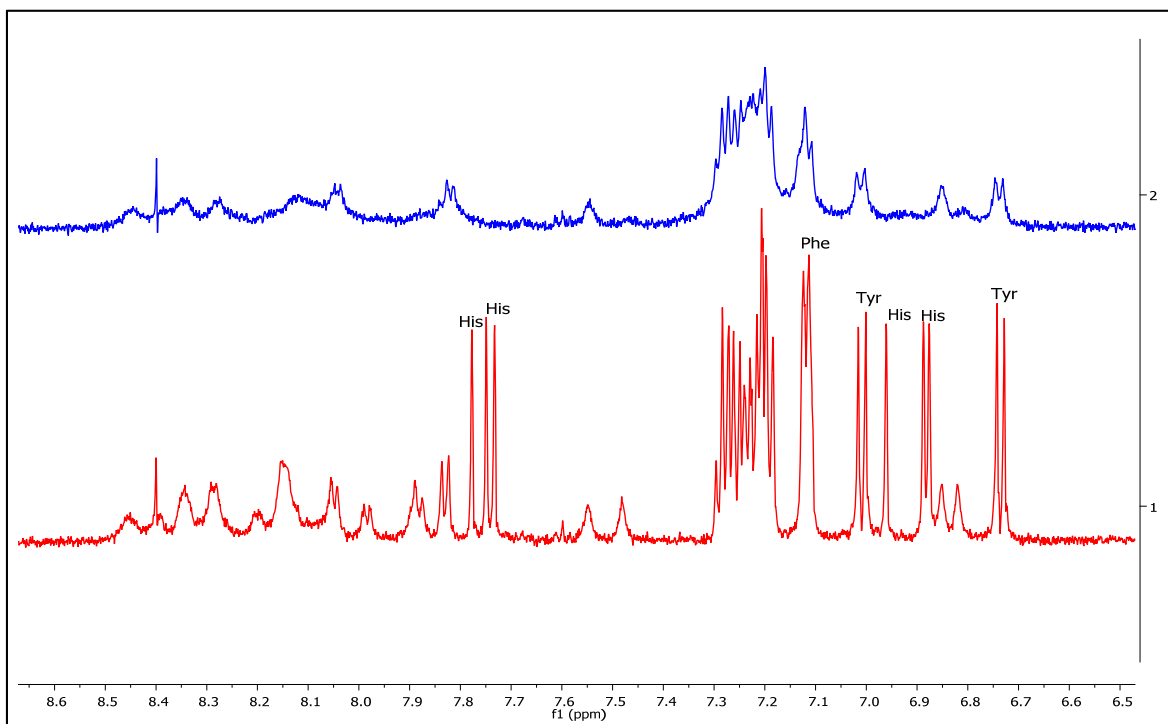


**Figure 67:** Aromatic region  $^1\text{H}$ -NMR spectra of  $\text{A}\beta$  1-28 with (top) and without (bottom) RuPOM.

NMR experiment confirms the interaction of RuPOM with the amyloid peptide. Beside histidine residues of  $\text{A}\beta$ 28, also acidic residues like aspartic or glutamic acids could coordinate. In addition, the general broadening could be due to electrostatic interaction between the positive residues of peptide and the negative charge of POM. Future investigations will be performed with longer peptide 1-40 to have a more complete idea on the coordination mode.

To achieve the goal of the dual activity, RuPOM should retain its activity once coordinated to  $\text{A}\beta$ . So, the effect of amyloid on the CAT activity was tested, using the same fragment 1-28. Oxygen evolution was monitored at 1:1 and 1:2 ratio of RuPOM and  $\text{A}\beta$ 28 ( $\text{A}\beta$  concentration was fixed at  $10\mu\text{M}$ , while RuPOM concentration was 5 and  $10\mu\text{M}$ ). The corresponding experiments without amyloids were also performed. Although coordination of peptide to catalytic active site reduces the reactivity of POM (Figure 68), a complete  $\text{H}_2\text{O}_2$  dismutation can still be achieved, so that anti-ROS properties of RuPOM are partially maintained, especially with 1:1 amyloid/POM ratio.

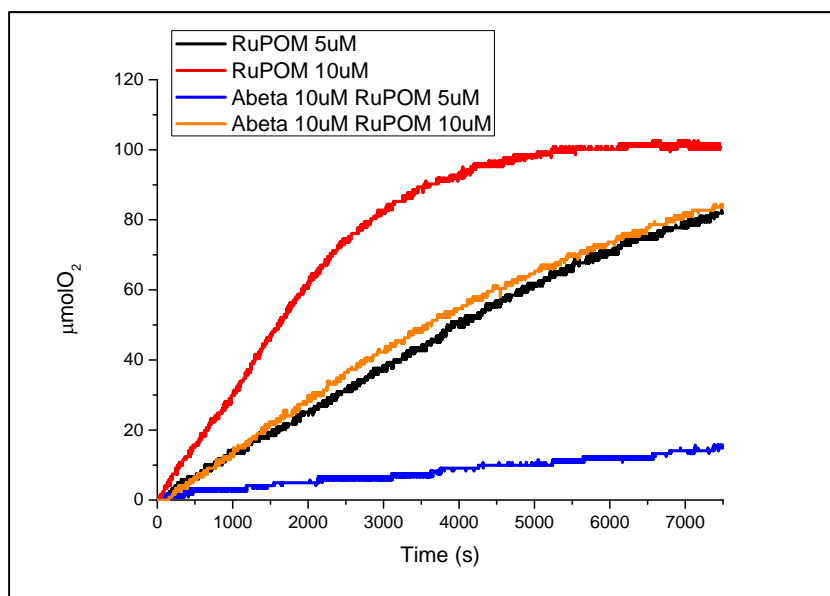


**Figure 68:** Kinetics trace of  $\text{H}_2\text{O}_2$  evolution in the absence and in the presence of amyloid 1-28 ( $10\mu\text{M}$ ) and in the presence of 5- $10\mu\text{M}$  of RuPOM.

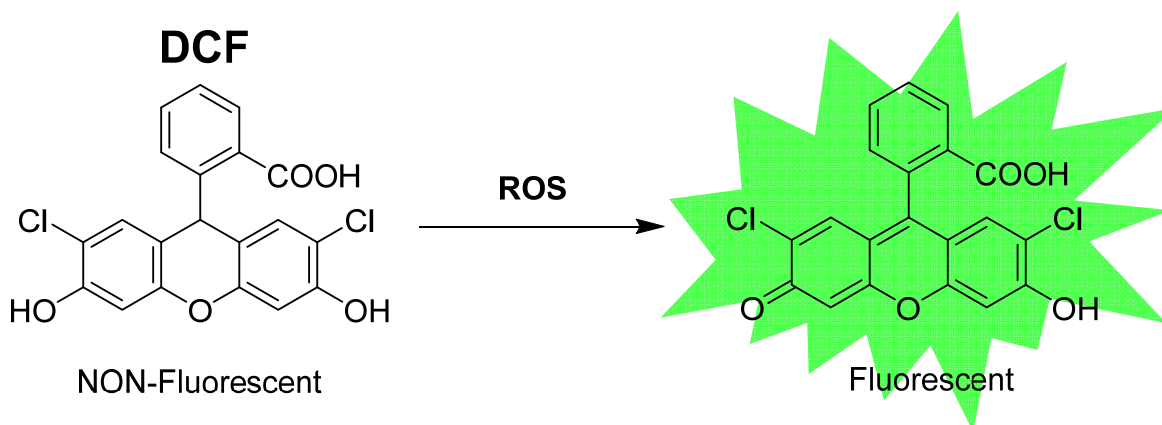
In Table 16, kinetic data have been collected. Entries 2 and 4 show that the initial rate in the presence of amyloid peptides are about 50% lower, that the complete conversion of hydrogen peroxide to oxygen and water is achieved in a longer time, especially at lower catalyst concentration. The turnover number (TON) remains high, while obviously TOF values decrease because of lowering of the reaction rates.

**Table 16:** Initial rate, TON, TOF and yield of  $\text{H}_2\text{O}_2$  disproportion by RuPOM at different concentration alone and in the presence of  $\text{A}\beta_{28}$ .

#	RuPOM	$\text{A}\beta$ 1-28	$R_0$ $\mu\text{molO}_2/\text{s}$	TON (2h)	TOF $\text{s}^{-1}$ (2h)	Yield (Time)
1	$5\mu\text{M}$	-	0.01435	5333	0.74	>99(4.5h)
2	$5\mu\text{M}$	$10\mu\text{M}$	0.00689	933	0.13	80 (25h)
3	$10\mu\text{M}$	-	0.03033	3300	0.46	>99 (2h)
4	$10\mu\text{M}$	$10\mu\text{M}$	0.01482	2766	0.38	>99 (4.5h)

Furthermore, we have studied the anti-ROS effect of RuPOM, using 2',7'-dichlorofluorescein diacetate ( $\text{H}_2\text{DCF}$ ) a molecular probe commonly used to monitor oxidative stress *in vitro*. Once the diacetate form enters into the cell it is cleaved by esterase enzyme, being thus trapped within the cell. When ROS are present, the non-fluorescent  $\text{H}_2\text{DCF}$  is oxidized to DCF, becoming fluorescent (Scheme 15).<sup>65</sup>





**Scheme 15:** Scheme of oxidation of 2',7'-dichlorofluorescein ( $H_2DCF$ ) in the presence of ROS with the formation of the fluorescent form (DCF) ( $\lambda_{ex}$ : 490nm,  $\lambda_{em}$ : 525nm).

In a typical experiment,  $H_2DCF$  ( $5\mu M$ ) and  $H_2O_2$  ( $50\mu M$ ) were mixed, in the presence of POM. In this case we used RuPOM and a nickel containing POM ( $[P_2NiW_{17}O_{61}]^{8-}$  NiPOM), known in literature to have antiamyloidogenic properties and some indirect effects that limit ROS production thanks to  $A\beta$  coordination, however it has not anti-ROS activity (CAT-like) as RuPOM. The activity of RuPOM in limiting the production of DCF was compared with NiPOM (and with a blank experiment) following the increase of fluorescence at 525nm (Figure 69,  $\lambda_{ex}$ : 490nm).

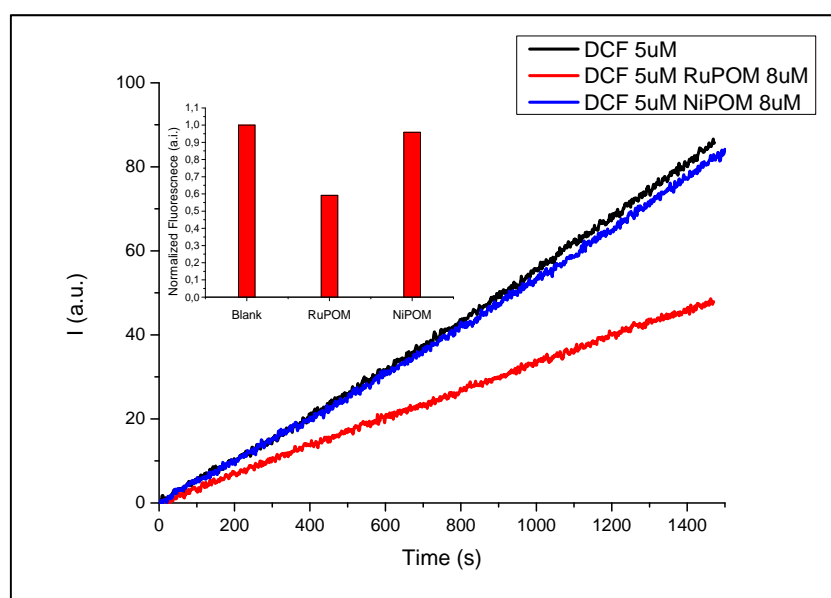


**Figure 69:** Increasing of DCF ( $5\mu M$ ) fluorescence in the presence of  $H_2O_2$  ( $50\mu M$ ): alone (black line), with  $8\mu M$  RuPOM (red line) or NiPOM (blue line). Inset: histogram of normalized intensity after 1400s.

In the presence of RuPOM, the increase of fluorescence due to DCF formation is slower, meaning that part of hydrogen peroxide was scavenged by RuPOM before forming radical species. Instead, in the presence of NiPOM there is a continuous increase of fluorescence, as for the POM-free experiment. Increase of DFC fluorescence, using different H<sub>2</sub>O<sub>2</sub> concentration was also performed, with a plate reader, with and without RuPOM and NiPOM for a longer time (20h). While with 5-50μM of H<sub>2</sub>O<sub>2</sub> (1-10eq.) there are little differences with respect to blank experiment (no H<sub>2</sub>O<sub>2</sub>), in the presence of 500μM (100eq.) of H<sub>2</sub>O<sub>2</sub> it is possible to obtain a strong fluorescence enhancement (Figure 70, left). Such H<sub>2</sub>O<sub>2</sub> concentration was thus chosen to evaluate RuPOM effect. Indeed, the extent of DCF oxidation can be decreased of about 80% with respect to either POM-free or Ni-POM experiments (Figure 70, right).

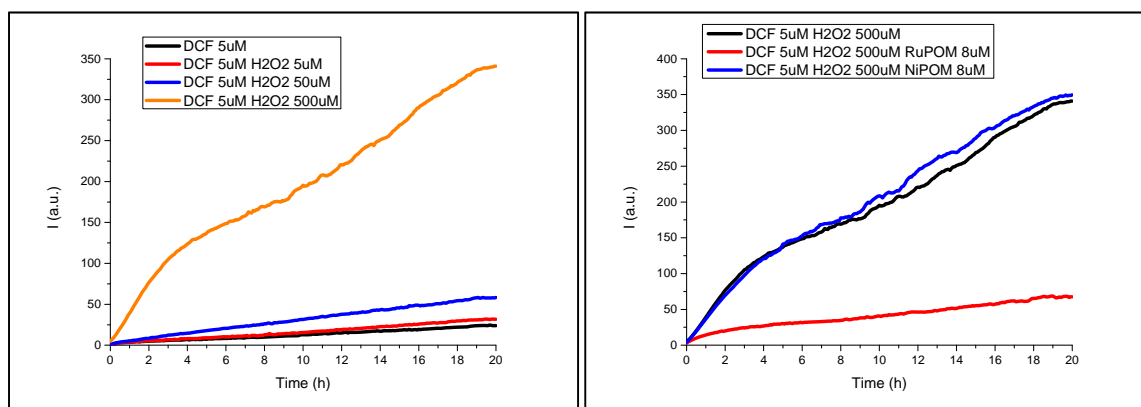


**Figure 70:** 5μ DCF oxidation in the presence of 5-500μM H<sub>2</sub>O<sub>2</sub> (left) and in the presence of 500μM H<sub>2</sub>O<sub>2</sub> and 8μM of POM (right).

These experiments confirm protective effect of RuPOM against reactive oxygen species. In the next chapter cytotoxicity studies will be presented, including the DCF experiment *in vitro*.

#### 4.4 Toxicity in cell and protective effects in the presence of amyloids

In collaboration with Dr. Loredana de Bartolo and Dr. Sabrina Morelli (ITM-CNR Rende, CS) some biological tests were performed on neuronal cells culture. Since the aim of this part of thesis work is to use RuPOM against Alzheimer's disease, toxic effect of POM and its anti-ROS/anti-amyloidogenic effects in the presence of amyloid peptides were

evaluated. So all the tests have been done in the presence of amyloid 1-42, A $\beta$ 42, checking the toxicity of this peptide alone and comparing the results in the presence of RuPOM. Neuronal cells were grown on polycaprolactone-polyurethane (PCL-PU) membranes to recreate a neuronal bio-artificial system.

First of all, toxicity of RuPOM on neuronal cells was evaluated, monitoring cell viability in the presence of different concentrations of compound (Figure 71).

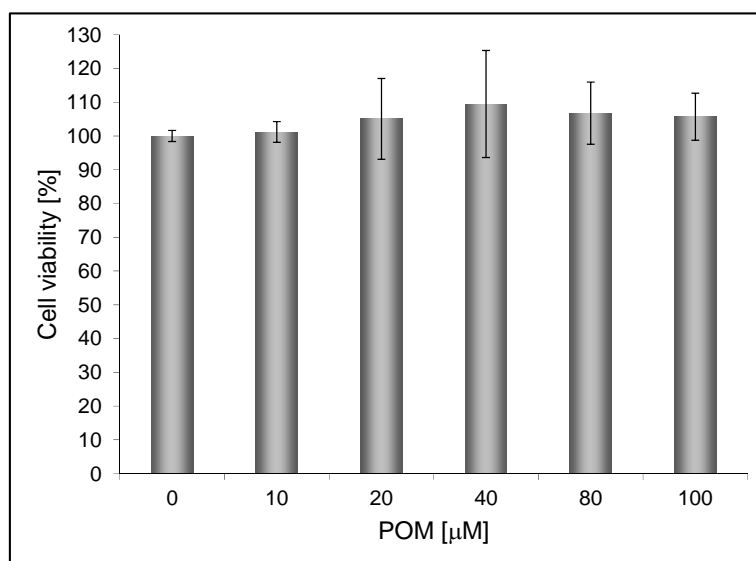


**Figure 71:** Viability of neuronal cells in PCL membrane system after 24 hrs of treatment with various concentrations of RuPOM (colorimetric MTT assay).

How it is possible to see, RuPOM has no toxicity on neuronal cells culture and viability of cells remains near control values at concentration as high as 100 $\mu$ M. A further study was performed monitoring the overall activity of endogenous enzymes as an indirect method to evaluate cell viability. In particular, specific fluorimetric assays allow to evaluate natural catalase (CAT) and glutathione peroxidase (GPx) activity. Although these should eliminate ROS from cellular environment, in case of severe oxidative stress their activity is not enough to prevent cellular damages, resulting, in turn, in a generally lower cellular activity. While in control experiments, without H<sub>2</sub>O<sub>2</sub>, enzymes have quite high activity, in the presence of hydrogen peroxide there is a reduction of their reactivity. The reference NiPOM shows no effects on such behavior. On the contrary, RuPOM is able to protect the enzymes against ROS induced damages (Figure 72).

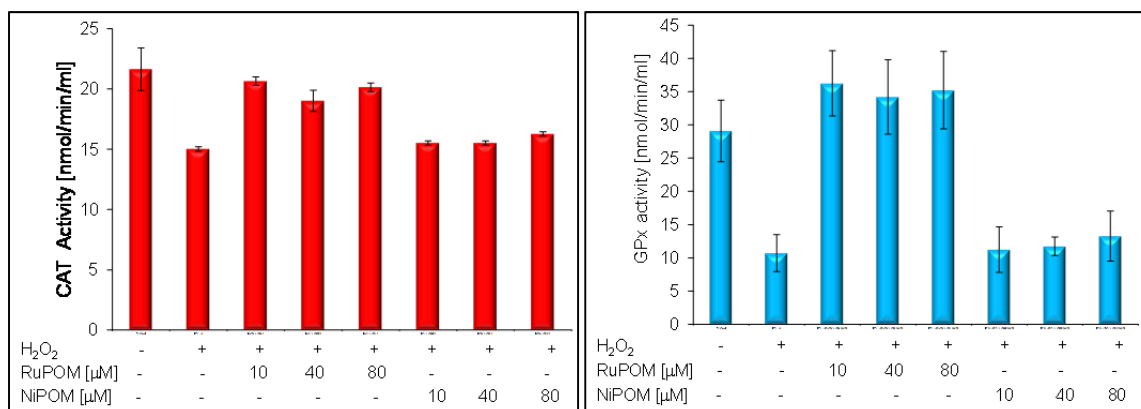


**Figure 72:** Quantitative determination of antioxidant enzyme activities: (left) catalase (CAT) and (right) Glutathione peroxidase (GPx) in cells under oxidative stress with and without POMs.

From these experiments, it is clear that there RuPOM could be a great help in the ROS detoxification in cells under high oxidative stress conditions.

Then, the effects of POM on neuronal cells treated with A $\beta$ 42 were studied. So, viability of cells treated with amyloid peptides, incubated alone or in the presence of RuPOM at different concentration, was evaluated with an MTT assay (see Experimental Part), showing the protective activity of RuPOM against amyloid cytotoxicity (Figure 73 left) and confirming the non-toxicity of RuPOM. Furthermore, antioxidant properties were evaluated using DCF as probe of ROS production in the presence of A $\beta$ . Neuronal cell incubated with A $\beta$ 42, without and in the presence of three different RuPOM concentration, were analyzed by Laser Scanning Confocal Microscopy (LSCM), exploiting the fluorescence of oxidized DCF. In the presence of amyloid peptide there is a great fluorescence increase, meaning that there is an high ROS production (Figure 73 right), with RuPOM, fluorescence intensity is lower, near to control values, meaning that it has a protective effect against A $\beta$ -mediated oxidative stress.

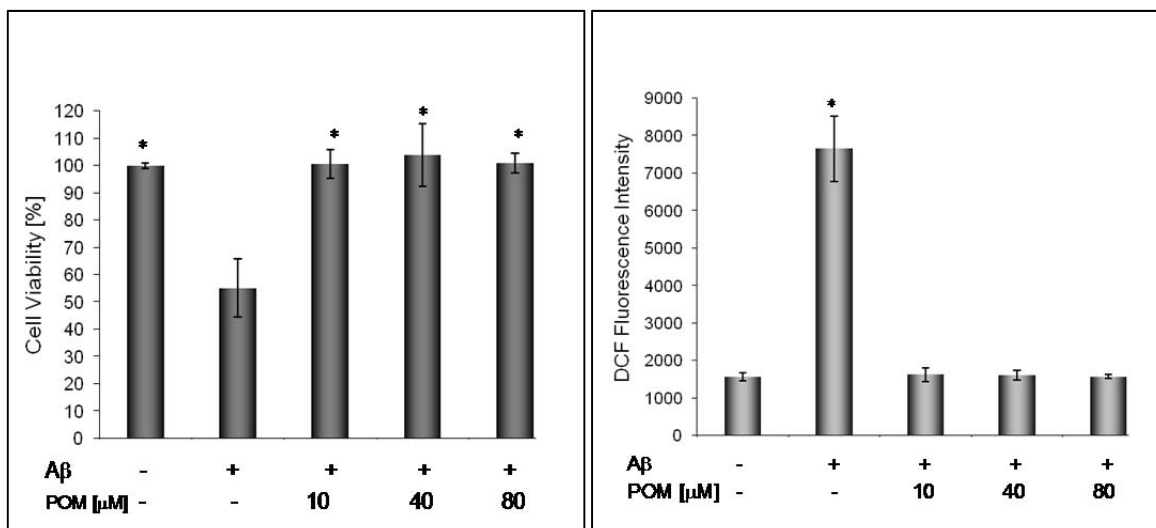


**Figure 73:** Aβ42 (5 μM) incubated with or without RuPOM added to neuronal cells; the cell viability was measured using MTT assays (left). Quantitative analysis of fluorescence intensity of DCF produced in neuronal cells incubated with Aβ42 (5 μM) alone or with a mixture of Aβ42 and RuPOM for 24h (right).

Cytotoxicity of amyloids, and protective effects of RuPOM were also evaluated checking apoptotic cells by monitoring fluorescence signals due to activation of caspase 3 (Casp3) and phosphorylated Jun protein kinase (p-JNK).<sup>§</sup> The percentage of apoptotic cells was calculated by the ratio of apoptotic nuclei (caspase-3 positive nuclei and p-JNK positive nuclei) over total nuclei (DAPI-stained nuclei) counted at different culture conditions (Figure 74).

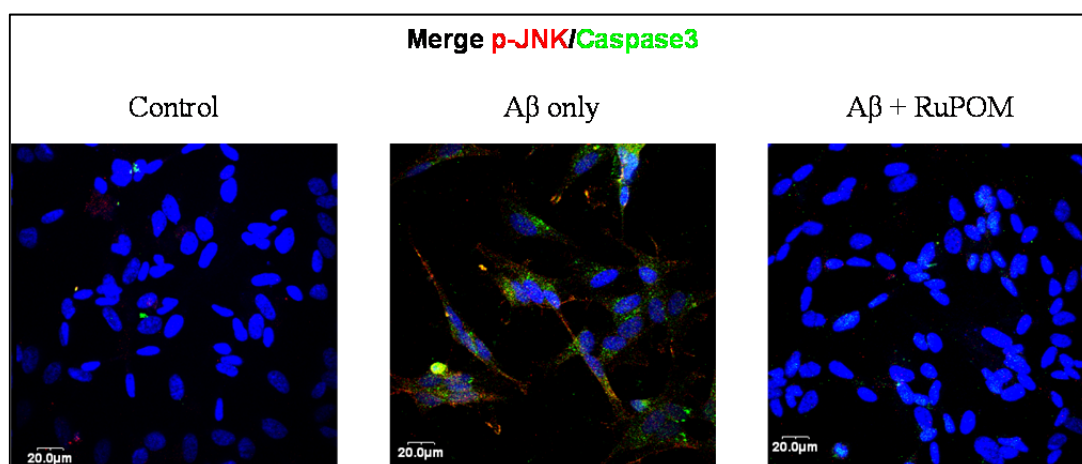


**Figure 74:** Confocal laser micrographs of neuronal cells without treatment (left), incubated for 24h with Aβ 5 μM) alone (middle) and co-treated with Aβ and RuPOM 10 μM (right). Cells were stained for p-JNK (red), caspase-3 (green) and nuclei (blue).

<sup>§</sup> The apoptosis of cells was determined by analysis of active N-terminal c-Jun protein kinase (p-JNK) and Caspase-3, expressed in dead cells. Since p-JNK and Caspase-3 are involved in the apoptotic process, it is possible exploit their production to calculate the percentages of apoptotic cells in a culture. Using two different fluorimetric assays, the presence of Caspase-3 and p-JNK could be evaluated in cells incubated in the presence of β-amyloid peptide and with or without POM.

How it is possible to see from histogram, obtained by fluorescence measurements in figure 75, in the presence of only amyloid peptide, percentage of apoptotic cells revealed by Casp3/JNK is very high. Instead if RuPOM is present, activation and cleavage of these two proteins, that are involved in the apoptotic process, is much lower, similar to control experiment, meaning that there is a protective effect of RuPOM on cell apoptosis induced by amyloid peptides.

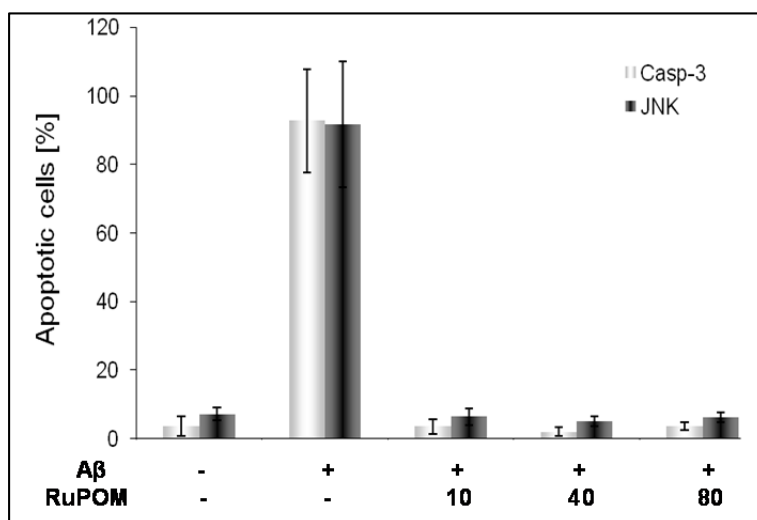


**Figure 75:** Quantitative analysis of p-JNK (full bar) and Caspase-3 (empty bar) activity. The percentage of apoptotic cells was calculated by the ratio of apoptotic nuclei (caspase-3 positive nuclei and p-JNK positive nuclei) over total nuclei (DAPI-stained nuclei) counted at different culture conditions.

Finally mitochondrial function in cells was evaluated measuring mitochondrial membrane potential (MMP), using a potential-sensing fluorescence probe, in the presence of amyloids and amyloids and RuPOM. It is clear from the graph (Figure 76) that in the presence of amyloid peptides MMP decrease, meaning that mitochondria are damaged by Aβ. On the contrary if RuPOM is present, MMP returns at normal values also in the presence of amyloids. So another protective effects of POM is proved. In the next chapter, considering the importance of mitochondria in ROS production the study will focus on the effects of RuPOM on isolated mitochondria.

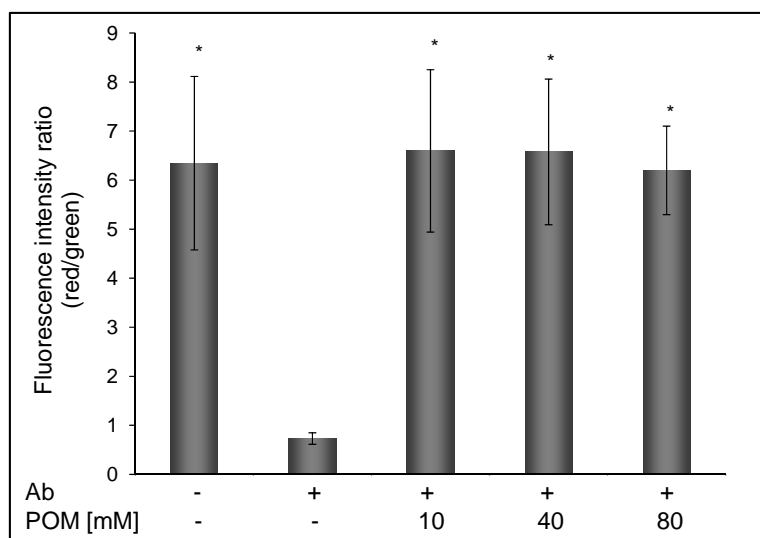


**Figure 76:** Mitochondrial membrane potential in neuronal cells measured with potential-sensing fluorescent probe, JC-1 ( $\lambda_{\text{ex}}$ :514nm,  $\lambda_{\text{em}}$ :529nm). The fluorescence intensity of both mitochondrial JC-1 monomers and aggregates ( $\lambda_{\text{ex}}$ :585 nm,  $\lambda_{\text{em}}$ :590 nm) in the presence of A $\beta$  alone or in a mixture with RuPOM at different concentrations.

#### 4.5 Mitochondrial toxicity test

Likewise dimanganese complex **4**, it was not possible to evaluate a positive effect of RuPOM on isolated mitochondria, whose respiration was artificially blocked by selected inhibitors. So, the toxic effects of the polyanion was studied, as discussed above, analyzing the respiration of mitochondria, as oxygen consumption rate, in the presence of different concentrations of RuPOM.

Respiration of isolated mitochondria at different RuPOM concentrations was analyzed using Mops buffer (20mM) at pH 7.4, containing potassium chloride (120mM), EGTA (10 $\mu$ M), phosphate (1mM), an example of experiments is shown in figure 77.

RuPOM effects starts already at 5 $\mu$ M and become more evident at  $\geq 10\mu$ M, and can be summarized as follows:

- (i) The rate of oxygen consumption during phosphorylation process (State3/St3), is lowered, suggesting a small inhibitory effect on mitochondrial respiration
- (ii) There is an increase of basal respiration (State2/St2 or State4/St4, after phosphorylation), suggesting a slight uncoupling effect of RuPOM (meaning that it disrupts a little bit the protonic gradient of the mitochondria)

- (iii) RuPOM seems to inhibit phosphorylation rate (State3 rate), indeed oxygen consumption decreases increasing RuPOM concentration.
- (iv) Considering Respiratory Control Ratio (RCR, ratio between State3 and State2, St3/St2), it is possible to notice that already at 5 $\mu$ M there is a decrease of the value, meaning that mitochondria are not in good conditions.

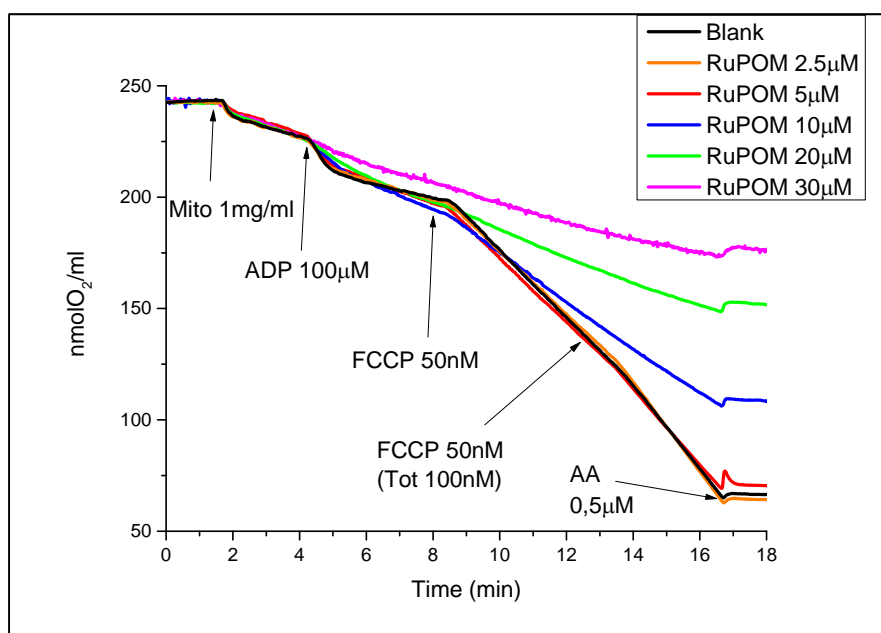


**Figure 77:** Graph of mitochondrial respiration in the presence of different RuPOM concentration (2.5-30 $\mu$ M), effects of RuPOM can be seen at  $\geq 10\mu$ M (blue line).

At concentration of 30 $\mu$ M it is almost impossible to discriminate between the different respiration states and at 100 $\mu$ M there is no differences in oxygen consumption (Table 17).

**Table 17:** Table of oxygen consumption rates (nmolO<sub>2</sub>·mg protein<sup>-1</sup>·ml<sup>-1</sup>) with different RuPOM concentrations (average value and standard deviation on three measurements).

RuPOM $\mu$ M	0	5	10	30	100
St 2	4.17 $\pm$ 0.09	5.19 $\pm$ 1.01	4.44 $\pm$ 0.51	4.61 $\pm$ 0.53	3.50 $\pm$ 0.02
St 3	13.48 $\pm$ 6.66	6.09 $\pm$ 1.70	9.65 $\pm$ 3.13	4.69 $\pm$ 0.67	3.50 $\pm$ 0.02
St 4	4.76 $\pm$ 1.82	5.77 $\pm$ 1.18	5.21 $\pm$ 1.42	4.61 $\pm$ 0.53	3.50 $\pm$ 0.02
St Un	14.44 $\pm$ 3.16	2.26 $\pm$ 0.93	7.81 $\pm$ 2.93	4.43 $\pm$ 0.22	3.50 $\pm$ 0.02
St 3/St 2	3.22 $\pm$ 1.51	1.24 $\pm$ 0.52	2.14 $\pm$ 0.43	1.02 $\pm$ 0.03	1.00 $\pm$ 0.00
St Un/St 2	3.04 $\pm$ 0.07	0.42 $\pm$ 0.09	1.73 $\pm$ 0.45	0.95 $\pm$ 0.06	1.00 $\pm$ 0.00

To better understand the effects of the RuPOM transmission electron microscopy analysis (TEM) of isolated mitochondria, incubated 5 and 50 minutes with RuPOM 5 $\mu$ M (also



without for control experiment) was performed. Mitochondria incubated with RuPOM seem to be swelled and there are much more mitochondria broken after 50 minutes incubation with RuPOM. However, also mitochondria incubated alone, after 50 minutes, were not completely intact (Figure 78). Staining of samples with uranyl acetate was necessary to mark and define the mitochondria for TEM analysis, but this treatment strongly interferes with the recognition of RuPOM. However TEM images suggest that probably RuPOM could act on mitochondrial pores, leading to organelle's rupture.

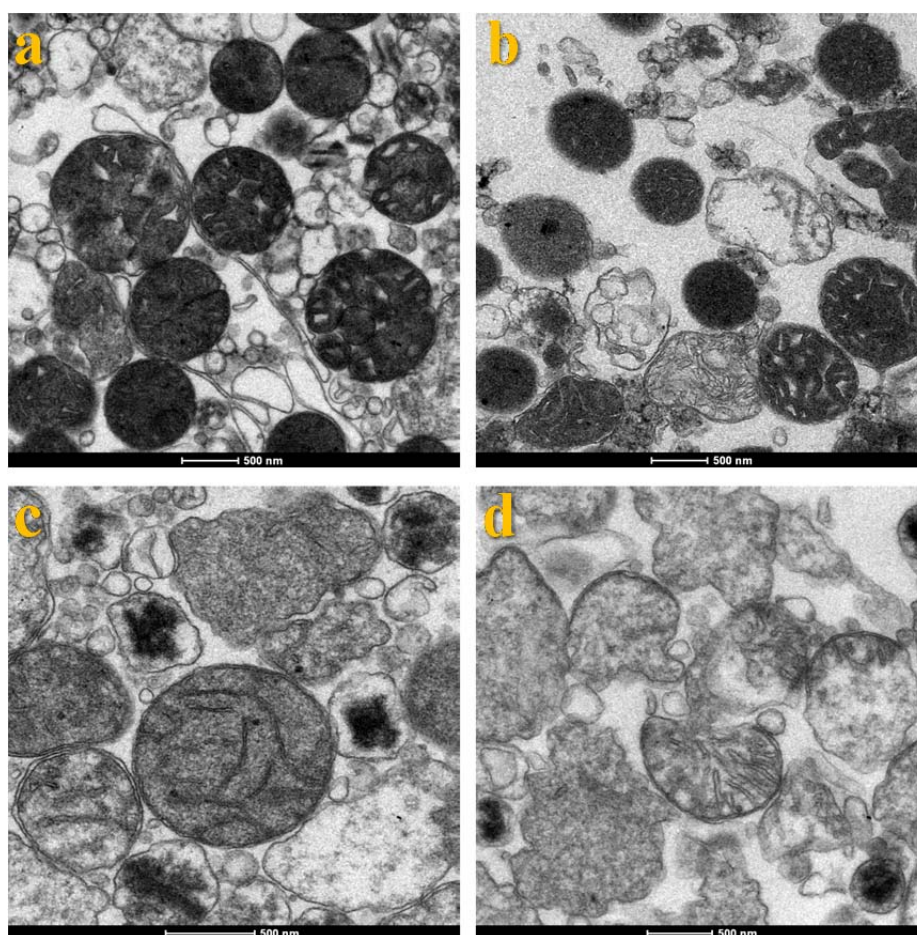


**Figure 78:** TEM of isolated mitochondrial after control incubation of 5 minutes(a) and 50 minutes(b) without POM and mitochondria incubated in the presence of 5 $\mu$ M RuPOM for 5 minutes(c) and 50 minutes(d).

Calcium Retention Capacity (CRC) analysis have been performed to evaluate the effects of RuPOM on the mitochondrial permeability pores and confirm some swelling effects. CRC analysis were done in the absence and in the presence of RuPOM at different concentrations, also with cyclosporin A that postpones pore opening. Effectively RuPOM anticipates pore opening already at 2.5 $\mu$ M concentration, at 10 $\mu$ M concentration of RuPOM pore opens at half calcium concentration with respect to the control (Figure 79).

An interesting observation is that these pores are in the inner mitochondrial membrane, so that this could be an indication of POM entering also in mitochondria, despite their negative charge. With cyclosporin A, the pores opening occurs at higher calcium concentrations, and in the presence of RuPOM and cyclosporin A the pores opening is postponed to  $[Ca^{2+}]$  of  $85\mu M$  instead of  $40\mu M$  that is however lower than the control experiment without RuPOM ( $180\mu M$ ) (Figure 80).

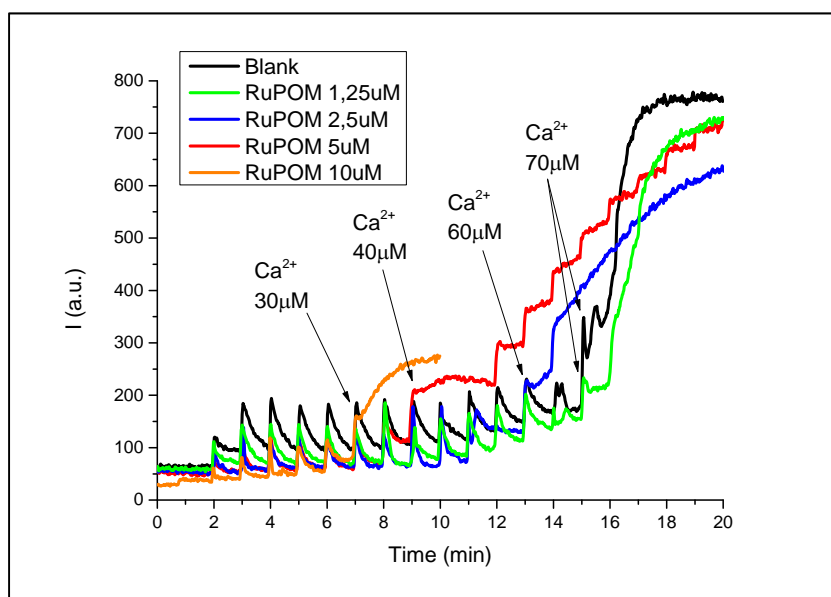


**Figure 79:** CRC graph of isolated mitochondria in the absence (black line) and in the presence of different concentrations of RuPOM:  $10\mu M$  (orange line),  $5\mu M$  (red line),  $2.5\mu M$  (blue line) and  $1.25\mu M$  (green line). The arrows indicate the additions of calcium chloride and the total concentration added.

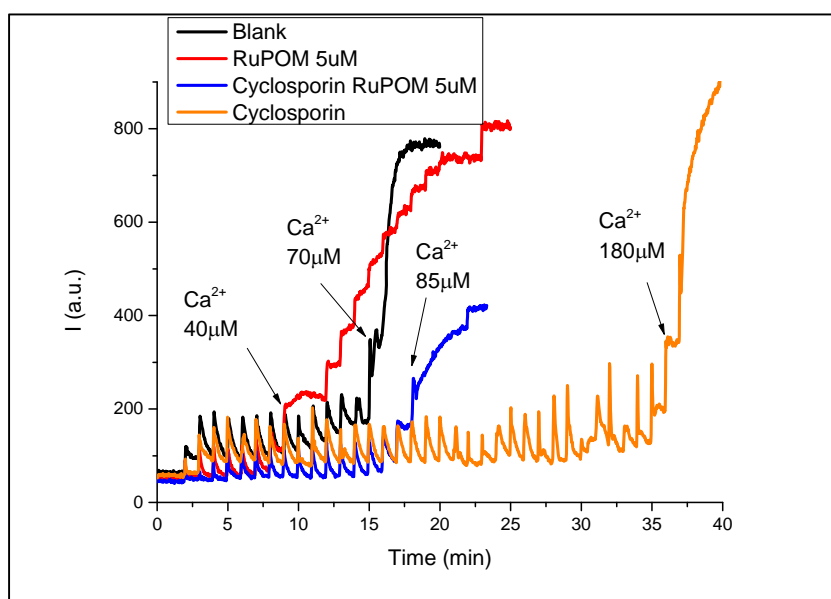


**Figure 80:** CRC graph of isolated mitochondria in the presence of cyclosporin A with/without RuPOM (blue and orange lines) compared with blank experiment without cyclosporin A (red and black lines).

In the following table 18 are resumed the concentration of calcium chloride added until there is the opening of the pores.

**Table 18:** Calcium concentrations at which there is pores opening in the presence of different RuPOM concentrations and in the presence of cyclosporin A (on the right).

RuPOM	Without Cyclosporin A					With Cyclosporin A (1 $\mu$ M)	
	0 $\mu$ M	1.25 $\mu$ M	2.5 $\mu$ M	5 $\mu$ M	10 $\mu$ M	0 $\mu$ M	5 $\mu$ M
Opening, $\mu$ M di Ca <sup>2+</sup>	70	70	60	40	30	180	85

## 4.6 Encapsulation

In this final part, the engineering of a suitable carrier system for POM delivery into cells was investigated, with the aim to enable tissue targeting and controlled POM release.

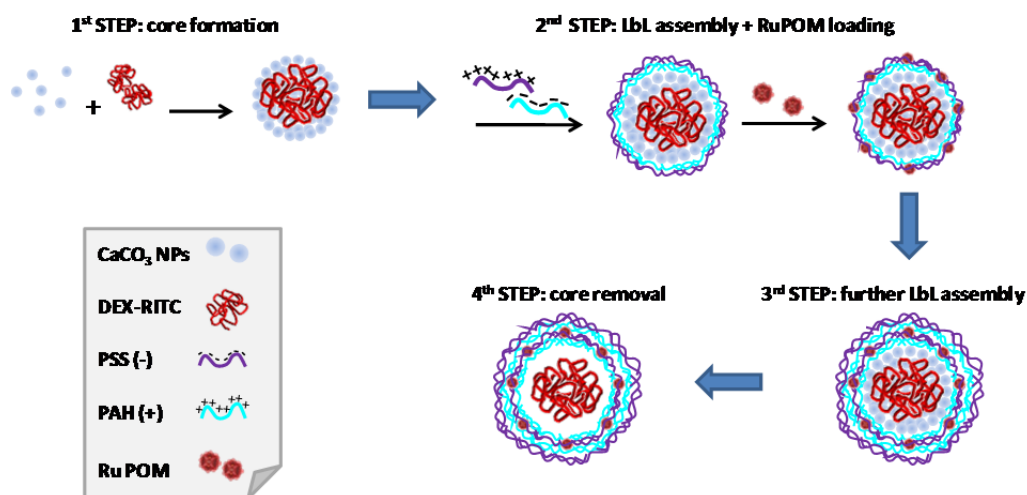
In collaboration with Dr.ssa L.L. del Mercato (NLL, Lecce) RuPOM was encapsulated into biocompatible polymeric multilayer capsules (PMC). These microcapsules were prepared by a layer-by-layer deposition of charged polymer on a templating core of calcium carbonate, formed in situ around a dextran core. After removal of the template CaCO<sub>3</sub> by EDTA treatment, these capsules display a typical “core-shell” structure. The core dictates the volume of the capsule and is the place where macromolecules or nanoparticles can be encapsulated. The shell is stable after the removal of the template and its function is to temporarily protect the core and its content, but it could also be modified with molecules for biological targeting or loaded with ionic species to be sandwiched between the layers.<sup>66</sup>

In more complex systems, core and shell could be loaded with different molecular functions, including fluorescent probes, to enable their localization. The layers are permeable to small molecules, and designed to permit the release of the encapsulated species, better if after an external stimulus (change of pH or radiations) or after biodegradation.<sup>25,67</sup>

For RuPOM delivery capsules were prepared as follows (Scheme 16):

- 1) Dextran labelled with fluoresceine isothiocyanate (FITC) was settled in the core.

- 2) Alternated layers of negative polystyrene sulfonate (PSS) and positive polyallylammonium (PAH) were used to build up the shell.
- 3) A single layer of RuPOM is usually introduced in the middle of the shell, after a positive polymer (PAH) and before a layer of negative polymer (PSS) that saturates the positive sites.



**Scheme 16:** Synthetic steps for capsule formation.

In the first case capsules with dextran (labelled with fluorescein isothiocyanate) in the core were synthesized, and RuPOM was embedded between two double layer of polymers with the following composition  $(PSS/PAH)_2RuPOM(PSS/PAH)_2$ . These capsules, as observed by optical/fluorescence microscopy a diameter near  $3\mu m$  (Figure 81).

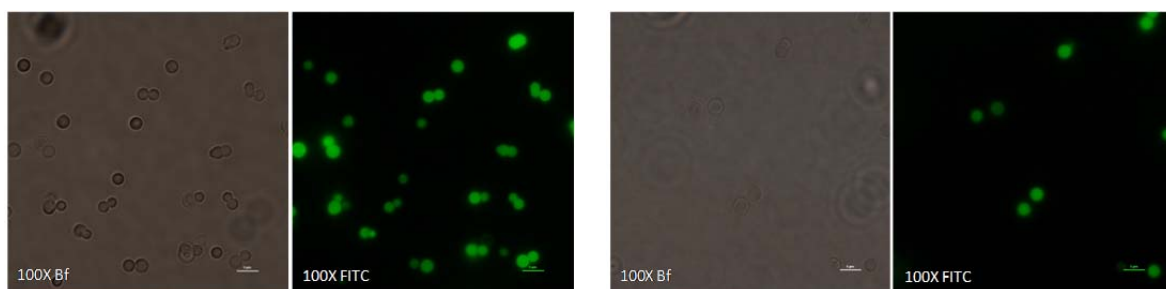


**Figure 81:** Images of multilayer microcapsules at optical microscope and at fluorescence microscope (with a filter at 488nm), with a core of FITC-dextran and with different polymeric coating, with PSS and PAH (on the left) and with dex-S and pArg (one the right).

The uptake of RuPOM can be easily calculated from UV-Vis measurement, measuring the absorbance ( $\lambda:270nm$ ,  $\epsilon_{270}:74846M^{-1}cm^{-1}$ ) of the POM solution before encapsulation, and

of the supernatant solution and washing solutions after encapsulation. The spectrum of capsules confirms the uptake of RuPOM (Figure 82).

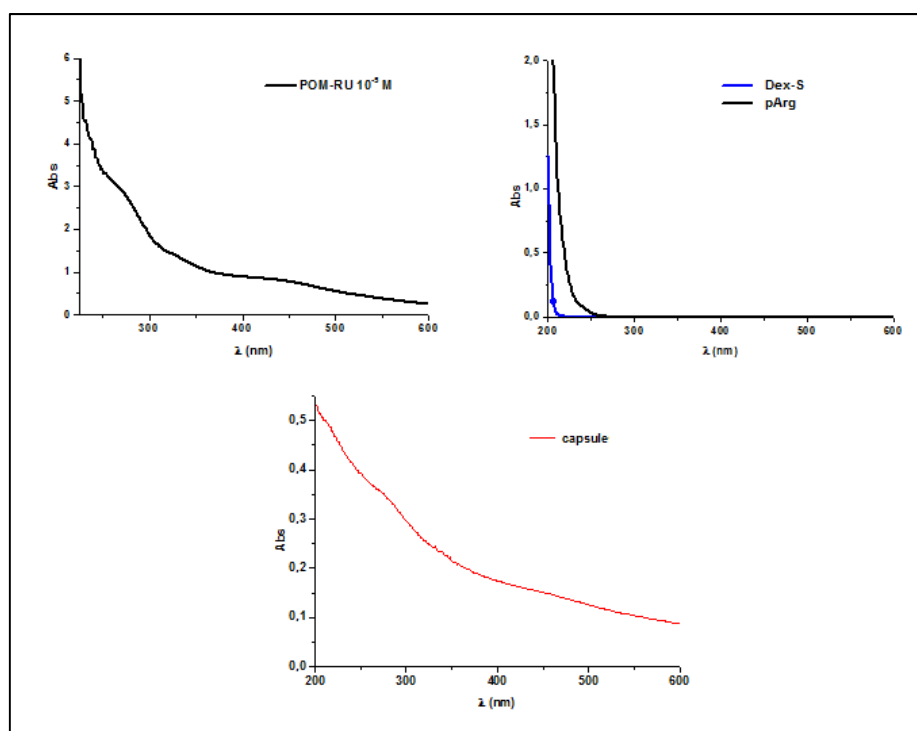


**Figure 82:** Absorption spectra of RuPOM alone (top left), polymers Dex-S and pArg alone (top right) and capsules Dex-FTIC(Dex-S/pArg)<sub>2</sub>RuPOM(Dex-S/pArg)<sub>2</sub> (bottom).

ESEM, TEM and EDAX analysis confirm both the dimensions and the RuPOM presence into the capsules, as it is possible to see from the mapping of the heavy elements distribution within the capsule outer shells. This is highlighted by the bright contour profiles of EDAX/ESEM superimposable images indicating that the tungsten sites of the POM catalyst are localized at the peripheral rim of the spherical micro-structure, with an even distribution and in agreement with the fabrication planning (Figure 83).

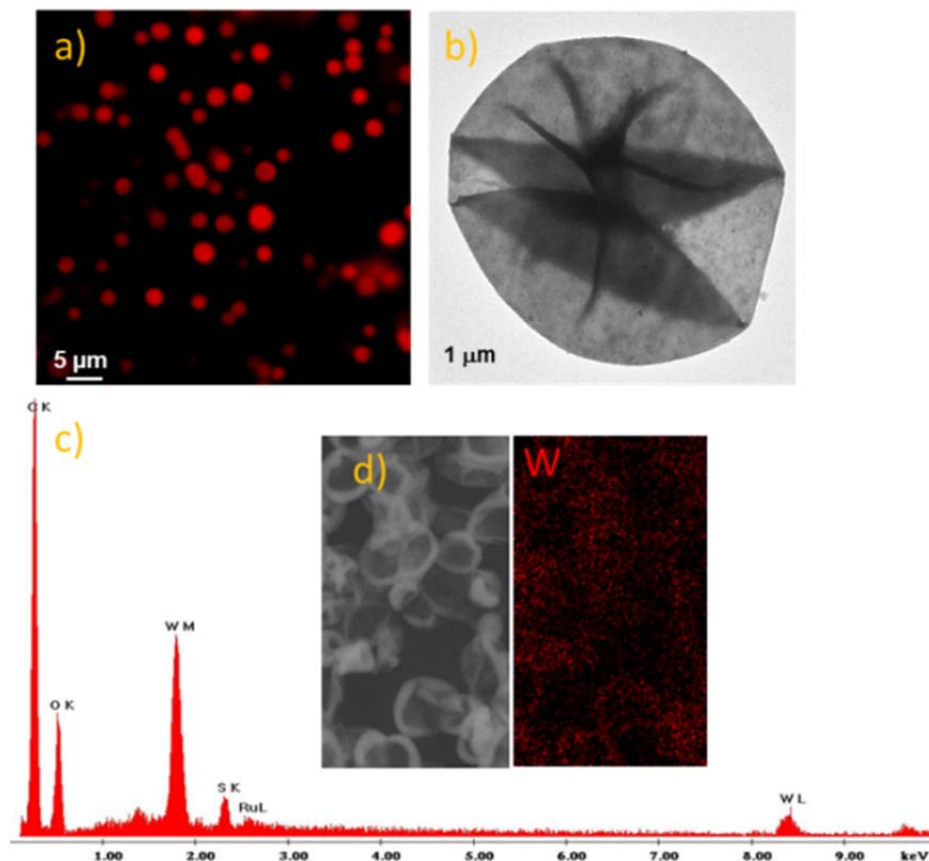


**Figure 83:** a) Fluorescence microscopy image of capsules, b) TEM image of a capsule, c) EDAX microanalysis and d) image and W maps obtained by ESEM/EDAX.

ICP-MS measurements confirmed RuPOM concentration, equal to 0.046% (w/w), obtained by UV-Vis analysis. The W/Ru ratio found,  $4.5 \pm 0.7$ , corresponding to about 0.6 fmol per capsule, (calculated value  $W/Ru=4$ ). FTIR analysis of capsules (Figure 84) confirms POM encapsulation, indeed typical W-O-W stretching ( $780-800\text{cm}^{-1}$ ) and Si-O stretching ( $940\text{cm}^{-1}$ ) of RuPOM are clearly visible in the spectrum, while they are not present in blank capsules without RuPOM.

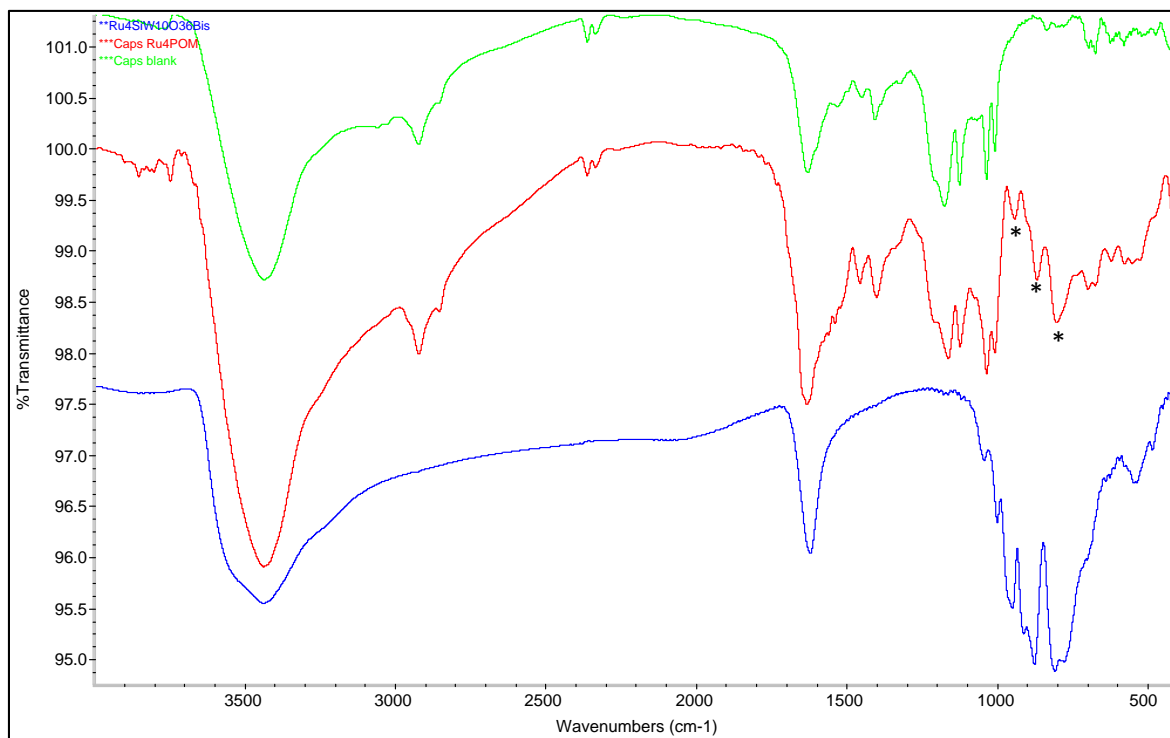


**Figure 84:** FTIR spectra of blank capsules (green), RuPOM containing capsules (red) and RuPOM alone (blue).

So, the confinement of the RuPOM cargo is assessed by three lines of evidence: FTIR spectra, inductively coupled plasma mass spectrometry (ICP-MS) and environmental scanning electronic microscopy (ESEM), coupled with energy dispersive X-ray (EDAX) analyses.

RuPOM containing capsules retain the catalytic activity for hydrogen peroxide dismutation, however the reaction is much slower than the homogenous one, this is probably due to coverage of POM by the polymers, that although it is permeable, slow down the dismutation process. Furthermore there is a inhibitory effect of polyallylammonium (PAH), as it is possible to see from kinetics experiments carried out with RuPOM in the presence of different PAH concentrations (0.2 and 0.02mg/ml). The higher is the PAH concentration, the higher is the inhibitory effect of the polymer.

It was possible to estimate a POM activity into capsules, that resulted to be equal to 7% compared to free POM solution, at the same nominal concentration, 3.6 $\mu$ M, considering the initial rate. While in the presence of homogeneous POM and PAH 0.02mg/ml and 0.2mg/ml the POM activity was respectively 48% and 5% of initial rate.

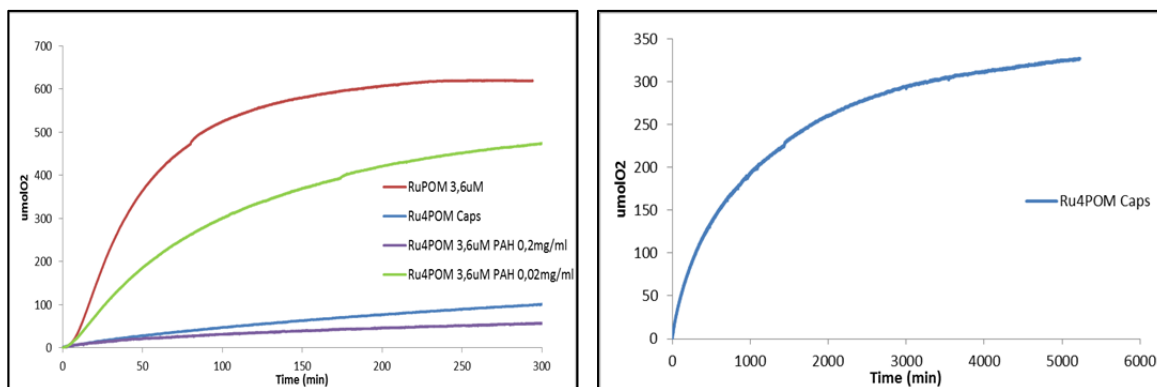


**Figure 85:** Kinetics of H<sub>2</sub>O<sub>2</sub> (0.1M) dismutation by RuPOM capsules (blue) and by an homogenous equimolar solution of RuPOM (3.6µM, in red). Comparison with homogenous solutions of RuPOM containing 0.2-0.02mg/ml PAH (green-violet).

FTIR analysis of capsules after the dismutation reaction, separated by centrifugation and washed with water, confirm the stability of the capsules and the maintenance of RuPOM into the system (Figure 86).

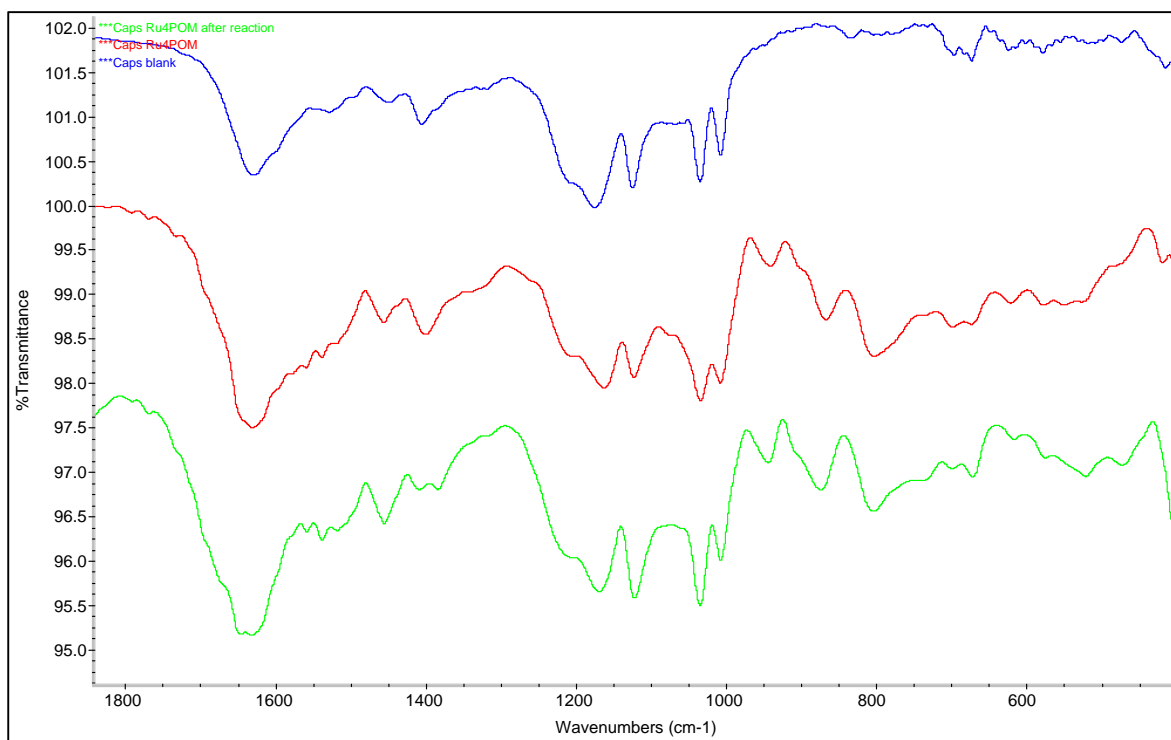


**Figure 86:** Zoom of FTIR analysis of blank capsules (blue), RuPOM containing capsules (red) and RuPOM containing capsules after the reaction with H<sub>2</sub>O<sub>2</sub> (green).

Preliminary tests in HeLa cells have confirmed the uptake of the capsules into the cellular membrane. Analogue capsules, whose shell was build up using negative dextran sulfonate (Dex-S) and positive polyarginine (pArg) are currently under investigation to evaluate the



possibility to achieve a controlled release in an oxidative environment. In the future, indeed, these systems will be tested *in vitro*, within cells under oxidative stress.

## **4.7 Conclusions**

In conclusion of this part, a completely inorganic compound, a polyoxotungstate, containing a tetraruthenium core, has been studied as artificial catalase with possible application in Alzheimer's disease. Indeed, exploiting its high negative charge and the presence of exchangeable water ligands coordinating the Ru ions, amyloid peptides interact with the POM without starting the fibrillogenesis. The anti-amyloidogenic activity was demonstrated using fluorimetric techniques, circular dichroism and TEM analysis. A NMR analysis has confirmed that coordination of ruthenium with histidine may play a crucial role in limit amyloid toxicity, not only for the reduced aggregation, but also because the coordination of ruthenium avoid coordination of reactive metal centers like iron or copper, able to give enhanced ROS production once coordinated. Catalase activity has been studied in different buffered solution and has been compared with other complexes known in literature. The anti-ROS activity of RuPOM has been checked also in the presence of amyloids, and despite the lowered rate of dismutation, complete elimination of hydrogen peroxide could be reached. Biological experiments have confirmed the positive effect of POM also in cellular culture, showing low toxicity and great effects against amyloid cytotoxicity oxidative stress. Toxicity on isolated mitochondria is more relevant, and only very low concentrations of RuPOM are admissible, however it should be considered that the experiment was done on isolated organelles, not in a real condition. Furthermore measurements seem to confirm that RuPOM is able to enter in mitochondria, that have an high negative charge of their outer membrane and maybe also interact with ATPase and other inner membrane proteins. Finally, encapsulation of RuPOM into multilayered polymeric capsules has been considered for addressing the delivery issue.

## References

- <sup>1</sup> Pope M.T., Müller A., *Heteropoly and Isopoly Oxometalates*, Springer-Verlag, New York, **1983**.
- <sup>2</sup> Lipscomb W.N., *Inorg. Chem.*, **1965**, *4*, 132.
- <sup>3</sup> Illingworth J.W., Keggin J.F., *J. Chem. Soc.*, **1935**, 575.
- <sup>4</sup> Tezé A., Hervé G., Finke R.G., Lyon D.K., *Inorg. Synth.*, **1990**, *27*, 71.
- <sup>5</sup> Hill, C. L.; McCharta, C. M. *Coord. Chem. Rev.* **1995**, *143*, 407.
- <sup>6</sup> Bartis J., Dankova M., Lessmann J.J., Luo Q.H., Horrocks W. DeW. Jr., Francesconi L.C., *Inorg. Chem.*, **1999**, *38*, 1042.
- <sup>7</sup> Zhang C., Howell R.C., Luo Q.H., Fieselmann H.L., Todaro L.J., Francesconi L.C., *Inorg. Chem.*, **2005**, *44*, 3569.
- <sup>8</sup> Boglio C., Lenoble G., Duhayon C., Hasenknopf B., Thouvenot R., Zhang C., Howell R.C., Burton-Pye B.P., Francesconi L.C., Lacôte E., Thorimbert S., Malacria M., Afonso C., Tabet J.C., *Inorg. Chem.*, **2006**, *45*, 1389.
- <sup>9</sup> De Liang L., Tsunashima R., Cronin L., *Angew. Chem. Int. Ed.*, **2010**, *49*, 1736.
- <sup>10</sup> a) Wang J.P., Duan X.Y., Du X.D., Niu J.Y., *Crys. Grow. Des.*, **2006**, *6*, 2266. b) Wang J.P., Yan Q.X., Du X.D., Duan X.Y., Niu J.Y., *Inorg. Chim. Acta*, **2008**, *361*, 2701.
- <sup>11</sup> Crans D.C., Aureliano M., *J. Inorg. Biochem.*, **2009**, *103*, 536.
- <sup>12</sup> a) Nadjo L., de Oliveira P., Miron S., Craescu T.C., Keita B., Zhang G., *J. Phys. Chem.*, **2007**, *111*, 11253. b) Miron S., Craescu T.C., Nadjo L., de Oliveira P., Brochon J.C., Keita B., Zhang G., *J. Phys. Chem.*, **2007**, *111*, 1809.
- <sup>13</sup> a) Nadjo L., Keita B., Yao J., Zhang G., Ma Y., Zheng L., *Phys. Chem. Chem. Phys.*, **2010**, *12*, 1299. b) Miron S., Craescu T.C., Nadjo L., de Oliveira P., Keita B., Kortz U., Bassil B.S., Yao J., Zhang G., Ma Y., Zheng L., *Eur. J. Inorg. Chem.*, **2009**, *2009*, 5189. c) Nadjo L., de Oliveira P., Miron S., Craescu T.C., Keita B., Zhang G., *Biomacromolecules*, **2008**, *9*, 812.
- <sup>14</sup> Mark G., Klaus S., Graham H., *Photochem. Photob. S.*, **2008**, *7*, 6, 734.
- <sup>15</sup> Nair S.V., Lakshmanan V.K., Hussain F., Jayakumar R., Maya S., Narayanan S., Thomas T.R., Menon D., *Carbohydr. Polym.*, **2011**, *84*, 887.
- <sup>16</sup> Modak J.M., Pope M.T., Kortz U., Sarafianos S.G., *Biochem. J.*, **1996**, *319*, 619.
- <sup>17</sup> a) Hu M.K., Lin W.P., Wu K.H., Yang F.C., *Micropor. Mesopor. Mat.*, **2009**, *118*, 467; b) Chao, C.M., Wang G.P., Yang C.C., Yu P.Y., Wu K.H., *Polym. Degrad. Stabil.*, **2009**, *94*, 1411.
- <sup>18</sup> a) Parc-Vogt T.N., Bartik K., Proost P., Ly H.G.T., Moelants E., Stroobants K., *Chem. Eur. J.*, **2013**, *19*, 2848; b) Parc-Vogt T.N., Proost P., Moelants E., Absillis G., Stroobants K., *Chem. Eur. J.*, **2014**, *20*, 3894.
- <sup>19</sup> a) Schinazi R.F., Judd D.A., Hill C.L., Rhule J.T., *Chem. Rev.*, **1998**, *98*, 327; b) Cindric M., Novak T.K., Kraljevic S., Kralj M., Kamenar B., *Inorg. Chim. Acta*, **2006**, *359*, 1673; c) Pope M.T., Li B., Liu J., Yang Y., Li J., Liu J., Wang X., *J. Inorg. Biochem.*, **2003**, *94*, 279; d) Li R., Wang X., Zhang C., Li D., Zhai F., *Eur. J. Med. Chem.*, **2008**, *43*, 1911; e) Pope M.T., Liu S., Li F., Wang X., *J. Inorg. Biochem.*, **2005**, *99*, 452.
- <sup>20</sup> a) Eriguchi M., Yamase T., Hisa T., Kasano H., Yanagie H., Ogata A., Mitsui S., *Biomed. Pharmacol.*, **2006**, *60*, 353. b) Hongyou H., Xia L., Qiang G., Changgen F., *Chin. J. Chem.*, **2012**, *30*, 1589.
- <sup>21</sup> a) Judd A.D., Hill C.L., Rhule J.T., Schinazi F.R., *Chem. Rev.*, **1998**, *98*, 327. b) Yamase T., *J. Mater. Chem.*, **2005**, *15*, 4773.
- <sup>22</sup> Wang X., Liu J., Pope M.T., *Dalton Trans.*, **2003**, 957.
- <sup>23</sup> Wang X., Li F., Liu S., Pope M.T., *J. Inorg. Biochem.*, **2005**, *99*, 452.
- <sup>24</sup> a) Meißner T., Bergmann R., Oswald J., Rode K., Stephan H., Richter W., Zänker H., Kraus W., Emmerling F., Reck G., *Transition Metal Chemistry*, **2006**, *31*, 603. b) Menon D., Thomas R.T., Narayanan S., Maya S., Jayakumar R., Hussain F., Lakshmanan V.K., Nair S.V., *Carbohydr. Polym.*, **2011**, *84*, 887.
- <sup>25</sup> Patzke G., Geisberger G., Paulus S., Carraro M., Bonchio M., *Chem. Eur. J.*, **2011**, *17*, 4619.
- <sup>26</sup> Geisberger G., Paulus S., Besic Gyenge E., Maake C., Patzke G. R., *Small*, **2011**, *7*, 2808.
- <sup>27</sup> Nadjo L., de Oliveira P., Keita B., Yao J., Ma Y., Zhang G., Han F., Zheng L., Zhou Y., *Colloids and Surfaces A. Physicochem. Eng. Aspects*, **2011**, *151*, 97.
- <sup>28</sup> Qu X., Xu C., Duan T., Ren J., Dong K., Sun H., Gao N., *Nat. Commun.*, **2014**, *5*, 3422
- <sup>29</sup> a) Sartorel A., Carraro M., Scorrano G., De Zorzi R., Geremia S., McDaniel N.D., Bernhard S., Bonchio M., *J. Am. Chem. Soc.*, **2008**, *130*, 5006; b) Orlandi M., Argazzi R., Sartorel A., Carraro M., Scorrano G., Bonchio M., Scandola F., *Chem. Comm.*, **2010**, *46*, 3152. c) Puntoriero F., La Ganga G., Sartorel A., Carraro M., Scorrano G., Bonchio M., Campagna S., *Chem. Comm.*, **2010**, *46*, 4725.
- <sup>30</sup> Sartorel A., Miró P., Salvadori E., Romain S., Carraro M., Scorrano G., Di Valentin M., Llobet A., Bo C., Bonchio M., *J. Am. Chem. Soc.*, **2009**, *131*, 16051.
- <sup>31</sup> Sartorel A., Truccolo M., Berardi S., Gardan M., Carraro M., Toma F.M., Scorrano G., Prato M., Bonchio

- M., *Chem. Comm.*, **2011**, 47, 1716.
- <sup>32</sup> Oddo S., Green K.N., LaFerla F.M., *Nat. Rev.*, **2007**, 8, 499.
- <sup>33</sup> Selkoe D.J., Hardy J., *Science*, **2002**, 297, 353.
- <sup>34</sup> Andrisano V., Bartolini M., *ChemBioChem*, **2010**, 11, 1018.
- <sup>35</sup> Lashuel H.A., Lansbury P.T., *Nature*, **2006**, 443, 19, 774.
- <sup>36</sup> Stefani M., *Prog. Neurobiol.*, **2012**, 99, 226.
- <sup>37</sup> Ferguson S.J., Nicholls D.G., *Bioenergetics4*, **2013**, Academic Press.
- <sup>38</sup> Eckert A., Müller-Spahn F., Bonert A., Meier F., Rao S., Baysang G., Rhein V., *Cell. Mol. Neurobiol.*, **2009**, 29, 1063.
- <sup>39</sup> Atlante A., Lassandro R., Corsetti V., Valenti D., Amadoro G., Bobba A., *Mitochondrion*, **2013**, 13, 298.
- <sup>40</sup> Moraes C.T., Fukui H., *Trends neurosci.*, **2008**, 31, 5, 251.
- <sup>41</sup> Cassagnes L.E., Hervé V., Nepveu F., Faller C., Collin F., *Angew. Chem. Int. Ed.*, **2013**, 52, 11110.
- <sup>42</sup> Chakrabarti S., Banerjee A., Bhowmick P., Sinha M., *Free Radical Bio. Med.*, **2013**, 56, 184.
- <sup>43</sup> Beal M.F., Lin M.T., *Nature*, **2006**, 443, 787.
- <sup>44</sup> a) Faller P., Hureau C., *Biochimie*, **2009**, 91, 1212; b) Przybylski M., Mezo G., Petre B.A., Dragan E.S., Murariu M., Dragusanu M., Manea M., Drochioiu G., *Biophys. Chem.*, **2009**, 144, 9.
- <sup>45</sup> Ohyagi Y., Yamada T., Nishioka K., Clarke N.J., Tomlinson A.J., Naylor S., Nakabeppu Y., Kira J., Younkin S.G., *Neuroreport*, **2000**, 11, 167.
- <sup>46</sup> Li F., Calingasan N.Y., Yu F., Mauck W.M., Toidze M., Almeida C.G., Takahashi R.H., Carlson G.A., Beal M.F., Lin M.T., Gouras G.K., *J. Neurochem*, **2004**, 89, 1308.
- <sup>47</sup> Butterfield D.A., Aksenova M., Yatin S., Varadarajan S., *J. Struct. Biol.*, **2000**, 130, 184.
- <sup>48</sup> a) Larsson N.G., Bratic A., *J. Clin. Invest.*, **2013**, 123, 3, 951; b) Ugalde C., Martín A.M., Arenas J., Marín-Buera L., Moreno-Lastres D., Morán M., *Free Radical Bio. Med.*, **2012**, 53, 595.
- <sup>49</sup> IUPAC-IUB, *Eur. J. Biochem.*, **1984**, 138, 9.
- <sup>50</sup> Faller P., Hureau C., Berthoumieu O., *Inorg. Chem.*, **2013**, 52, 12193.
- <sup>51</sup> Nowick K.S., Eisenberg D., Zhao M., Liu C., Cheng P.N., *Nat. Chem.*, **2012**, 4, 927.
- <sup>52</sup> Lee M., Kim J.E., *Biochem. Biophys. Res. Co.*, **2003**, 303, 576.
- <sup>53</sup> Bolognesi M.L., Bazi R., Bartolini M., Cavalli A., Tarozzi A., Andrisano V., Minarini A., Rosini M., Tumiatto V., Bergamini C., Fato R., Lenaz G., Hrelia P., Cattaneo A., Recanatini M., Melchiorre C., *J. Med. Chem.*, **2007**, 50, 4882.
- <sup>54</sup> Kawashima H., Sohma Y., Nakanishi T., Kitamura H., Mukai H., Yamashita M., Akaji K., Kiso Y., *Bioorg. Med. Chem.*, **2013**, 21, 6323.
- <sup>55</sup> Lee H.H., Choi T.S., Lee S.J.C., Lee J.W., Park J., Ko Y.H., Kim W.J., Kim K., Kim H.I., *Angew. Chem. Int. Ed.*, **2014**, 53, 7461.
- <sup>56</sup> Zagorski M.G., Hou L., *J. Am. Chem. Soc.*, **2006**, 128, 29, 9260.
- <sup>57</sup> Viles J.H., Syme C.D., *Biochim. Biophys. Acta*, **2006**, 1764, 246.
- <sup>58</sup> Qu X., Wang E., Ren J., Li M., Geng J., *Angew. Chem. Int. Ed.*, **2011**, 60, 4184.
- <sup>59</sup> Gao N., Sun H., Dong K., Ren J., Duan T., Xu C., Qu X., *Nature Comm.*, **2014**, 5, 3422.
- <sup>60</sup> Orvig C., Scott L.E., *Chem. Rev.*, **2009**, 109, 4885.
- <sup>61</sup> a) Shi J., Dong H., Gong Q., Li F., *Curr. Pharma. Design*, **2012**, 18, 27; b) Liu R., Zhao M., Sun X., Du X., Zhang X., Wang Y., Yang S., Wang X., Feng Y., *Neurotoxicology*, **2009**, 30, 986.
- <sup>62</sup> a) Yazdanparast R., Bahraminkia S., *Int. J. Biol. Macromol.*, **2012**, 50, 187; b) Gheysarzadeh A., Yazdanparast R., Bahraminkia S., *Chem. Biol Drug. Des.*, **2012**, 80, 227.
- <sup>63</sup> Bonchio M., Kortz U., Nadjo L., Keita B., Dickman M.H., Bassil S., Scorrano G., Carraro M., Sartorel A., *Chem. Eur. J.*, **2009**, 15, 7854.
- <sup>64</sup> a) Syme C.D., Viles J.H., *Biochim. Biophys. Acta*, **2006**, 1764, 246; b) Gaggelli E., Janicka-Klos A., Jankowska E., Kozłowski H., Migliorini C., Valensin D., Vlensin G., Wieczerek E., *J. Phys. Chem. B.*, **2008**, 112, 100.
- <sup>65</sup> Takanashi T., Ogura Y., Taguchi H., Hashizoe M., Honda Y., *Invest. Ophthalm. Visual Sci.*, **1997**, 38, 13, 2721.
- <sup>66</sup> Leprotti S., Giannelli G., Ciccarella G., De Santis F., Baldassarre F., Vergarola V., *Curr. Pharmaceutical Desig.*, **2012**, 18.
- <sup>67</sup> Xu L., Mao B., Song Y., Kang Z., Wang E., Gao L., *J. Phys. Chem. B*, **2005**, 109, 16587.



## *5. Conclusions*

## *Conclusions*

**In conclusion, in this dissertation, some synthetic compounds, based on transition metals (Mn and Ru), have been evaluated as promising artificial catalase (CAT) and superoxide dismutase (SOD) mimicking, for their possible application as ROS scavengers in biological environment.** In particular, the following metal complexes and nanosystems were investigated:

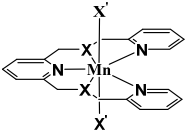
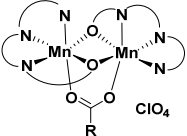
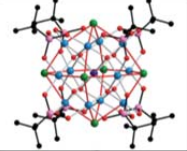
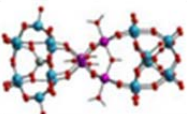
- I. **Mononuclear manganese complexes** bearing a tris-pyridyl pentadentate ligand with a NXNXN binding motif (X=N,O or S, Table 19, entry 1). **With respect to existing mononuclear Mn compounds, we found** (for X=S) an interesting yield and initial rate, with **an unprecedented dual CAT/SOD reactivity** and excellent stability, also in aqueous solution.
- II. **Dinuclear manganese complexes** with general formula  $[Mn_2L_2X]$  (Table 19, entry 2). In this case a comparison with other literature compounds was performed by analyzing enzymatic Michaelis-Menten parameters. In aqueous solution, **they result to be the best dinuclear complexes (not only of Mn) in terms of catalase reactivity, and they are also active in superoxide dismutation.** Toxicity tests, performed on isolated mitochondria, revealed no toxicity till  $50\mu M$  concentrations. **Modification of apical bridging carboxylate with mitochondriotropic functionalities was taken in account:** rhodamine derivatives and triphenylphosphonium salts were synthesized and characterized.
- III. **Multinuclear manganese oxoclusters** (Table 19, entry 3). The clusters have been **tested for the first time, as catalyst for  $H_2O_2$  dismutation,** showing an interesting reactivity in non-buffered water. Preliminary test as SOD mimics were also performed. However, the clusters precipitate from the reaction mixture and are deactivated by phosphate buffer. In this case, further experiments will be required to assess the nature of the active species and to increase their solubility/stability.
- IV. A fully inorganic **tetraruthenium substituted polyoxotungstate** (Table 19, entry 4). This POM, with known catalase activity has been **successfully used to contrast molecular events involved in Alzheimer's disease.** Indeed, thanks to its negative charge and to the presence of exchangeable water ligands on ruthenium atoms,  $\beta$ -amyloid can coordinate on the POM surface, resulting in a **decreased fibrillogenesis.** In addition, catalase activity was maintained in the presence of these peptides, allowing **reduction of  $A\beta$ -induced oxidative stress** within model neuronal cells. Experiments on isolated mitochondria suggest that probably RuPOM, despite its high negative charge, could enter in mitochondria and maybe

can interact with inner membrane proteins. Finally, the ruthenium polyoxometalate was **encapsulated into multilayered polymeric capsules for future delivery application.**

Among these compounds, the most promising ones are the dinuclear manganese complexes, that are very active, in buffered solution, toward hydrogen peroxide dismutation. The possibility of tuning dismutation efficiency and the insertion of targeting functionalities, modifying only carboxylate ligand, makes this complex even more appealing. Ruthenium polyoxometalate is another promising compound, in particular as anti-amyloidogenic and catalytic antioxidant.

Both species are definitely worth of further investigations, to confirm their reduced toxicity, the positive effects on cell protection against oxidative stress, and to enable their selective cell delivery.

**Table 19:** Collection of relevant results, obtained for the molecular metal complexes and nanosystems, described in this thesis.

Entry	Compound	Structure	N. Active Atoms	SOD	CAT
				$k_{M_2CF}$ ( $M^{-1}s^{-1}$ )	$R_0$ ( $\mu MO_2/s$ ), (Yield (%))
1	1-3 (MonoMn)		1	$2 \cdot 8 \cdot 10^6$	8-128 (0.6-14)
2	4-7 (DiMn)		2	$3.3 \cdot 10^7$	12-93 (50->99)
3	8-16 (PolyMn)		6-13-14	$>10^6$	5-17 (>90)
4	17 (RuPOM)		4	$5.5 \cdot 10^5$	7-25 (>99)





## *Conclusions*

## *6. Experimental Part*



## 6.1 Materials and methods

All commercially available reagents and solvents were used without further purifications.

MilliQ-deionized water (Millipore) was used for the reactions, buffers preparation and for spectrometric measurements.

Solvents and deuterated (d) solvents:

- diethyl ether, hexane, methanol, ethanol, chloroform, dichloromethane, acetonitrile, chloroform-d, acetonitrile-d<sub>3</sub>, methanol-d<sub>4</sub>, DMF-d<sub>7</sub>, DMSO-d<sub>6</sub>, D<sub>2</sub>O, dichloromethane-d<sub>2</sub> (Sigma-Aldrich);
- DMSO (Lab Scan);
- 1,2-dichloroethane, pyridine (Carlo Erba).

Reagents:

- Na<sub>2</sub>WO<sub>4</sub>·2H<sub>2</sub>O, KBr, Na<sub>2</sub>SiO<sub>3</sub>, RuCl<sub>3</sub>·xH<sub>2</sub>O, Mn(ClO<sub>4</sub>)<sub>2</sub>·xH<sub>2</sub>O, MnCl<sub>2</sub>·2H<sub>2</sub>O, Ni(NO<sub>3</sub>)<sub>2</sub>·6H<sub>2</sub>O, NaBH<sub>4</sub>, NaBH(OAc)<sub>3</sub>, NaBH<sub>3</sub>CN, KMnO<sub>4</sub>, CuCl<sub>2</sub>·2H<sub>2</sub>O, NaOH, NaHCO<sub>3</sub>, HCl (37%), HNO<sub>3</sub> (70%), H<sub>3</sub>PO<sub>4</sub> (85%) NaN<sub>3</sub>, 3-amino-1,2,4-triazole (ATZ), P<sub>2</sub>O<sub>5</sub>, CuSO<sub>4</sub>·5H<sub>2</sub>O, Na<sub>2</sub>C<sub>4</sub>H<sub>4</sub>O<sub>6</sub>·2H<sub>2</sub>O, *tert*-butylphosphonic acid, phenylphosphonic acid, di-2-pyridylketone, salicylaldehyde, rhodamine B, rhodamine B Base, *trans*-1,4-diaminecyclohexane, piperazine, succinic anhydride, zinc (powder), Al(CH<sub>3</sub>)<sub>3</sub> 2M (heptane solution), triphenylphosphine, bromovaleric acid, acetic acid, Tris, Hepes, Mops, EGTA, (CH<sub>3</sub>)<sub>2</sub>AsO<sub>2</sub>Na, ADP, FCCP, glutaraldehyde, cyclosporine A, antimycin A from *Streptomyces sp.*, 2-aminopyridine, 4-picoline, cytochrome c, tetrabutylammoniumchloride/bromide (TBAX), isonicotinic acid, 4,4'-trimethylenedipyridine (4,4'-TDP), 4-(3-phenylpropyl)pyridine, Mn(acac)<sub>3</sub>, Xanthine, Xanthine Oxidase, Cytochrome c, Nitro Blue Tetrazolium chloride (NBT), Catalase from bovine liver, polystyrenesulfonate (PSS), polyallylammonium (PAH), polyarginine (pArg), dextran sulfonate (Dex-S), dextran, dextra-FITC, dextran-RITC, hydrogen peroxide (30%), thioflavinT (ThT), Amberlite, Sephadex-G50™, Sephadex-G15™, 2',7'-dichlorofluorescein diacetate (DCF), (Sigma-Aldrich);
- NH<sub>4</sub>OAc, NaCl, KCl, K<sub>2</sub>CO<sub>3</sub>, CaCl<sub>2</sub>, MgSO<sub>4</sub>·xH<sub>2</sub>O, Na<sub>2</sub>SO<sub>4</sub>·xH<sub>2</sub>O, Na<sub>2</sub>HPO<sub>4</sub>·xH<sub>2</sub>O, NaH<sub>2</sub>PO<sub>4</sub>·xH<sub>2</sub>O, H<sub>3</sub>BO<sub>3</sub>, Na<sub>2</sub>B<sub>4</sub>O<sub>7</sub>·xH<sub>2</sub>O, benzoic acid, 4-carboxybenzaldehyde, sucrose, glucose, trimethylamine (Carlo Erba)
- Calcium Green N6 (Molecular Probe);
- Amyloid peptide 1-40, Amyloid peptide 1-42, Amyloid peptide 1-28 (Genscript).

## 6.2 Instruments

<sup>1</sup>H-NMR spectra were recorded with a Bruker Avance-DAX 200 spectrometer operating at 200 MHz. Chemical shift were determined using Si(CH<sub>3</sub>)<sub>4</sub> as reference ( $\delta$  <sup>1</sup>H-NMR=0 ppm). For the protonic spectra, the following symbols have been used: s: singlet, d: doublet, t: triplet, q: quartet, m: multiplet.

<sup>1</sup>H-NMR analysis of amyloid peptide was performed on a Bruker Avance 600 MHz.

FTIR spectra were recorded with a Nicolet 5700-Thermo Electron Corporation instrument. For FTIR spectra following symbols have been used: w: weak signal, m: medium signal, s: strong signal, b: broad signal.

UV-Vis spectra were recorded with a Varian Cary 50Bio spectrophotometer.

Fluorescence measurements were performed with a Perkin Elmer LS50B instrument with a cell length of 1cm.

ESI-MS spectra have been obtained with a Agilent LC/MSD Trap SL spectrometer, by using a capillary potential of 1500V. Solvent used: MeOH, ACN, H<sub>2</sub>O

MALDI-MS spectra were recorded with a MALDI TOF/TOF 4800 AB SCIEX instrument.

ICP-MS analysis were performed with a ICP-MS Agilent Technologies 7700xx instrument operating at 1550 W plasma power. Samples were diluted in 4 mL of HCl/HNO<sub>3</sub> 3:1 and mineralized in the Microwave Digestion System (CEM Explorer SP-D plus). The solution was then diluted in 100 mL of 5% *aqua regia* and analyzed. The instrument was calibrated by using Ru and W standard solutions diluted in 5% *aqua regia*.

Circular Dichroism (CD) spectra were recorded with a Jasco J-715 spectropolarimeter. Signal was mediated for 6 measure, 2mm cuvettes and a scan rate of 50nm/min were used.

Transmission electron microscopy (TEM) measurements were obtained using a FEI Tecnai G2 transmission electron microscope at Biology Department of University of Padova.

For catalytic experiments of hydrogen peroxide dismutation an home-made pressure transducer, with a septum for sample injection was used.

pH measurement was performed with a pH-meter HI 223 Hanna Instrument with a glass electrode. Calibration was carried out with Sigma-Aldrich buffers (pH 4-7-10).

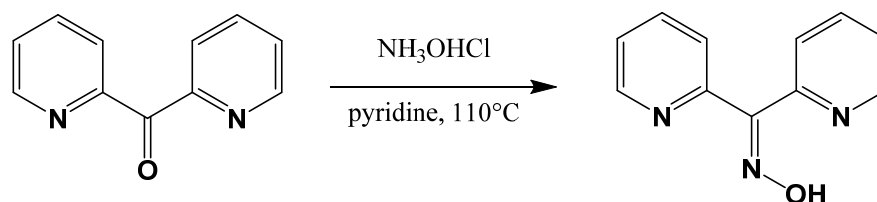
### 6.3 Synthetic procedures

#### -Seven coordinates complexes (1-3)

Synthesis of ligands and seven-coordinated complexes has been reported in Michaela Grau's PhD thesis, Imperial College, 2013.<sup>1</sup> Here is briefly reported the general synthesis for the metal complexes  $[\text{Mn}(\text{L})(\text{OTf})_2]$  used.

The relevant ligand L and 1 molar equivalent of  $[\text{Mn}(\text{MeCN})(\text{OTf})_2]$  were placed in different Schlenk flasks and dissolved in absolute tetrahydrofuran. After adding the solution of the ligand to the suspension of the metal precursor, the reaction mixture was stirred overnight at room temperature. The resulting solution was concentrated to one third of the initial volume. Diethyl ether was added to precipitate the product, which was dried under vacuum. If the complex already precipitated from the tetrahydrofuran solution during the reaction, the solvent was removed by filtration and the solid dried under vacuum.

#### -Synthesis of: di-2-pyridyl-ketoxime<sup>2</sup>



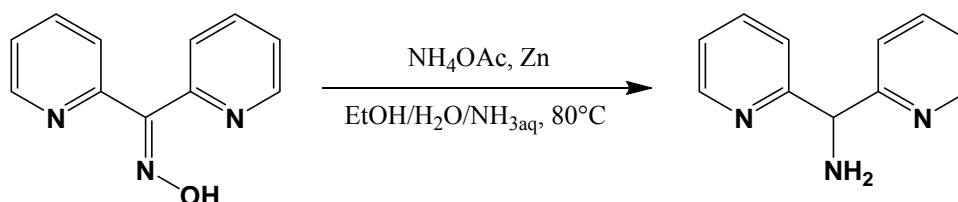
Di-2-pyridyl ketone (1.72g, 9.24mmol) and hydroxylamine hydrochloride (1.35g, 19.1mmol) were dissolved in 5ml of pyridine and heated at 110°C for 4-5 hours. After cooling to 0°C, 10ml of water were added and a white precipitate appeared (if not, scratch with a glass rod help the precipitation). Product was filtered on a gootch and washed abundantly with water and dried under vacuum. Yield: 1.84g (9.23mmol, 99%).

## Experimental Part

FTIR (KBr,  $\text{cm}^{-1}$ ): 3395 (s, br), 2996 (s, br), 2801 (s, br), 1621 (w), 1593 (s), 1566 (s), 1475 (s), 1432 (s), 1337 (m), 1282 (m), 1153 (m), 1096 (m), 1050 (w), 1017 (s), 999 (s), 949 (s), 904 (w), 791 (s), 758 (m), 690 (m), 659 (m), 622 (m), 580 (m), 495 (w).

$^1\text{H-NMR}$  (200MHz, MeOD)  $\delta$ : 7.34-7.49 (m, 2H), 7.62 (d, J: 7.9Hz 1 H), 7.80-7.99 (m, 3H), 8.43 (d, J: 4.8Hz, 1H), 8.60 (d, J: 4.3Hz, 1H) ppm.

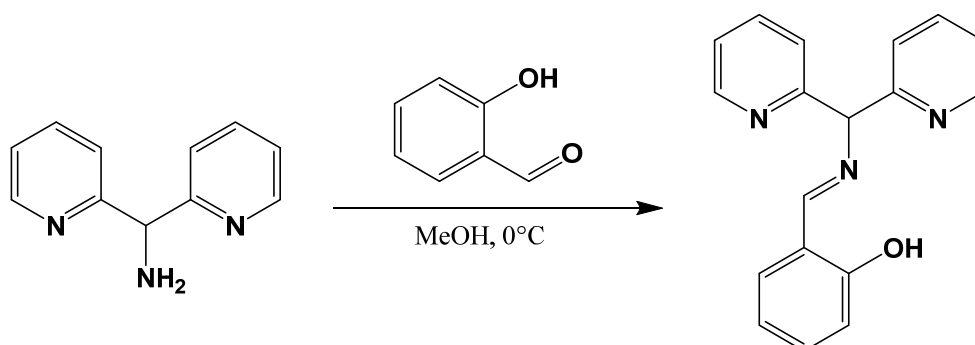
### -Synthesis of: di-2-pyridyl-methylamine<sup>3</sup>



Di-2-pyridyl-ketoxime (1.8g, 9.0mmol) was dissolved in a mixture of 17ml of ethanol, 10ml of water and 11ml of 28% aqueous  $\text{NH}_3$ .  $\text{NH}_4\text{OAc}$  (1.73g, 22.5mmol) was added and solution was heated to  $80^\circ\text{C}$ . Zinc powder (2.95g, 45.0mmol) was added in 30 minutes, then reaction was left refluxed for 4.5 hours. Solution was then filtered on paper, to remove residual solid, and concentrated under vacuum, until a white-yellow precipitate appeared. The resulting aqueous solution ( $\sim 5\text{ml}$ ) was basified with  $\text{NaOH}$  10M, solid disappeared and solution turned to yellow color. Basification continued until solution turned reddish-pink and a white precipitate appeared, then it was extracted with dichloromethane (5ml X 3). Organic fraction was washed with brine (5ml X 3) and water (5ml X 3), dried with  $\text{MgSO}_4$  and solvent was evaporated under reduced pressure. A yellowish oil was obtained. Yield: 1.25g (6.75mmol, 75%)

$^1\text{H-NMR}$  (200MHz,  $\text{CDCl}_3$ )  $\delta$ : 2.40 (br. s, 2H), 5.31 (s, 1H), 7.13 (ddd, J: 7.5-4.9-1.1 Hz, 2H, 2-H), 7.38 (d, J: 7.9Hz, 2H), 7.62 (dt, J: 7.7-1.8Hz, 2H), 8.56 (ddd, J: 4.9-1.5-0.8Hz, 2H) ppm.

### -Synthesis of: 2-((Di(2-pyridyl)methyl)imino)methylphenol<sup>4</sup>



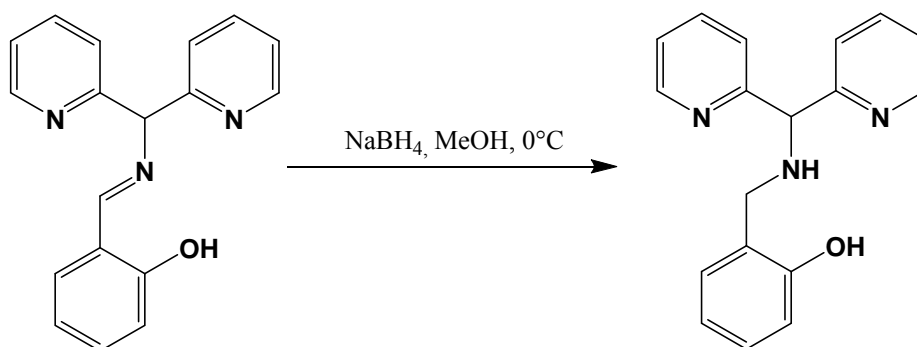


To a stirred solution of di-2-pyridyl-methylamine (1.25g, 6.75mmol) in 5 mL of methanol was added neat salicylaldehyde (0.84g, 6.8mmol). The solution immediately turned yellow. After stirring for about 5 min a yellow crystalline material appeared. The reaction mixture was cooled to 0°C and stirred for other 30 minutes. The solids were isolated by vacuum filtration, washed with ice-cold methanol and dried under vacuum. A yellow powder was obtained. Yield: 1.7g (5.9 mmol, 87%).

FTIR (KBr,  $\text{cm}^{-1}$ ): 3441 (w, br), 3046 (w), 3009 (w), 1626 (s), 1585 (s), 1498 (m), 1463 (s), 1431 (s), 1382 (w), 1312 (w), 1280 (s), 1216 (w), 1201 (w), 1152 (m), 1058 (m), 988 (m), 876 (w), 857 (w), 775 (s), 760 (s), 666 (w), 610 (m), 541 (m), 464 (m), 436 (w).

$^1\text{H-NMR}$  (200MHz,  $\text{CDCl}_3$ )  $\delta$ : 5.93 (s, 1H), 6.83-7.99 (m, 2H), 7.14-7.20 (m, 2H), 7.27-7.36 (m, 2H), 7.44 (dd, J: 7.8-0.5, 2H), 7.67 (dt, J: 7.7-1.7Hz, 2H), 8.49-8.61 (m, 2H), 8.63 (s, 1H) ppm.

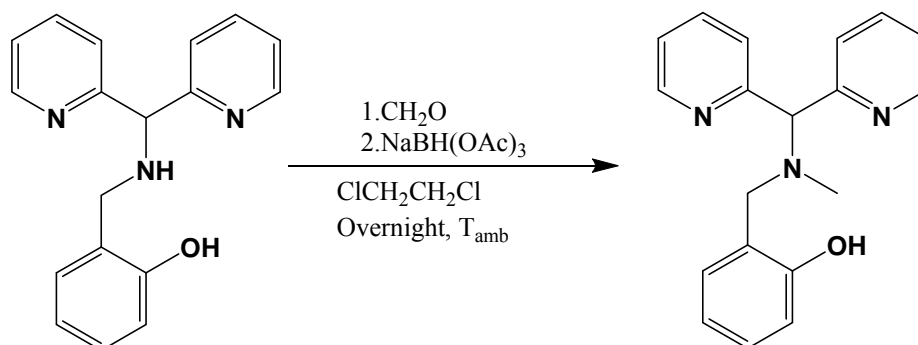
*-Synthesis of: 2-([Di(2-pyridyl)methyl]amino)methylphenol<sup>4</sup>*



To a stirred solution of 2-([di(2pyridyl)methyl]imino)methylphenol (1.7g, 5.9mmol) in 15 ml methanol at 0°C  $\text{NaBH}_4$  (227mg, 6.0mmol) was added in 3 portions during 15 min. The reaction mixture was stirred for 4 h. The mixture was then acidified with 2 M aq. HCl to pH 1 and stirred for 15 min. Subsequently the reaction was neutralized with 2 M aq.  $\text{NH}_3$  and 30 ml water was added (pH ~8), methanol was removed under reduced pressure and the mixture extracted with ethyl acetate (5ml X 3). The combined organic layers were dried with  $\text{Na}_2\text{SO}_4$  filtered and solvent was removed under vacuum to yield a reddish oil (it turned into a glass after several weeks). Yield: 1.61g (5.53mmol, 94%).

$^1\text{H-NMR}$  (200MHz,  $\text{CDCl}_3$ )  $\delta$ : 3.95 (s, 2H), 5.15 (s, 1H), 6.72-6.93 (m, 3H), 7.13-7.21 (m, 3H), 7.31-7.35 (m, 2H), 7.65 (dt, 2H, J: 7.7-1.7Hz, 2H), 8.58-8.60 (m, 2H) ppm.

-Synthesis of: 2-{{[Di(2-pyridyl)methyl](methyl)amino]methyl}phenol<sup>4</sup>

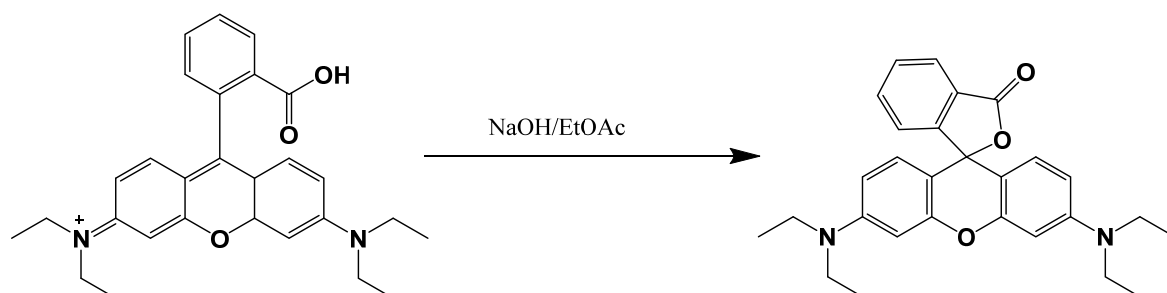


To a solution of 2-({[di(2-pyridyl)methyl]amino}methyl)phenol (1.61g, 5.53mmol) in 25mL of ClCH<sub>2</sub>CH<sub>2</sub>Cl was added aqueous 30% formaldehyde (650μl, 11.0mmol) and after 15 min of stirring NaBH(OAc)<sub>3</sub> (2.54g, 11.0mmol) was added in small portions during 20 minutes. Subsequently the reaction was vigorously stirred overnight. Dichloromethane (20 mL) was added and the organic layer was washed consecutively with 2 M aq. NH<sub>3</sub> (10ml X 2), and twice with water (10ml X 2). After drying with MgSO<sub>4</sub>, filtration and evaporation of the solvents under reduced pressure, the product was obtained as a sticky oil which was purified by chromatography on silica using diethyl ether. A white solid material was obtained. Yield: 1.38g, (4.46mmol, 81%).

FTIR (KBr, cm<sup>-1</sup>): 3048 (m), 3007 (m), 2970 (m), 2924 (m), 2849 (m), 2712 (m), 1607 (m), 1586 (s), 1490 (m), 1466 (s), 1432 (s), 1379 (w), 1330 (m), 1287 (m), 1257 (s), 1199 (m), 1149 (m), 1120 (m), 1102 (w), 1025 (m), 993 (m), 931 (m), 869 (w), 857 (w), 785 (m), 748 (s), 722 (m), 679 (w), 617 (m), 540 (w), 448 (w).

<sup>1</sup>H-NMR (200 MHz, CDCl<sub>3</sub>) δ: 2.22 (s, 3H), 3.67 (s, 2H), 4.98 (s, 1H), 6.71-6.98 (m, 3H), 7.14-7.23 (m, 3H), 7.53-7.57 (m, 2H), 7.66 (dt, J. 7.7-1.7Hz, 2H), 8.61 - 8.63 (m, 2H) ppm.

-Synthesis of: Rhodamine B Base<sup>5</sup>

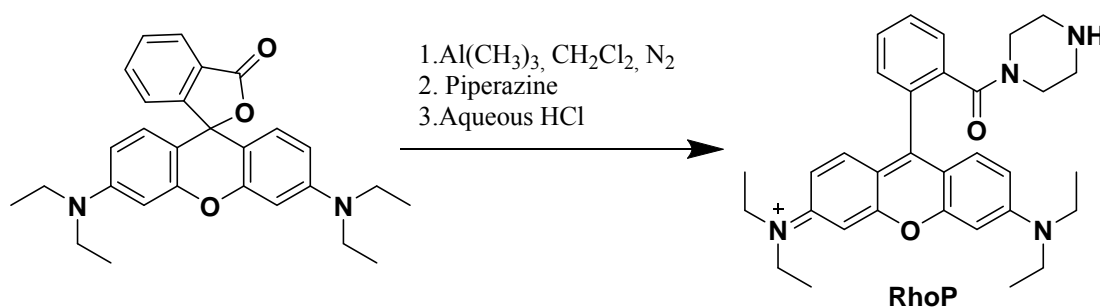


Rhodamine B (2.59g, 5.4mmol) was dissolved and partitioned between 1M NaOH aqueous solution (20ml, ~20mmol) and ethyl acetate. After isolation of organic layer,

aqueous part was washed with ethyl acetate (10ml X 2). The combined organic solution was washed with NaOH solution (10ml X 2), brine (10ml X 2) and water (10ml X 2), then dried with Na<sub>2</sub>SO<sub>4</sub>, filtered and concentrated under reduced pressure. A pink solid was obtained. Yield: 2.1g (4.75mmol, 88%).

<sup>1</sup>H-NMR (200 MHz, MeOD) δ: 2.22 (s, 3H), 3.67 (s, 2H), 4.98 (s, 1H), 6.71-6.98 (m, 3H), 7.14-7.23 (m, 3H), 7.53-7.57 (m, 2H), 7.66 (dt, J: 7.7-1.7Hz, 2H), 8.61 - 8.63 (m, 2H) ppm.

*-Synthesis of Rhodamine B piperazine amide (RhoP)*<sup>5</sup>



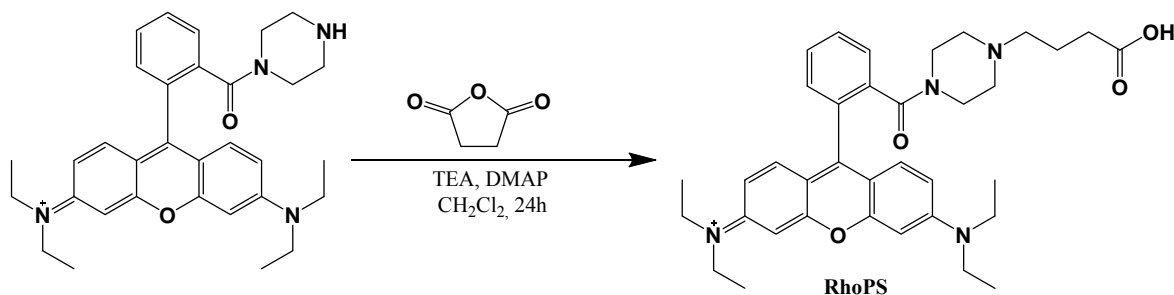
Al(CH<sub>3</sub>)<sub>3</sub> (8ml, 2M in heptane, 16.0mmol) was slowly added dropwise to a solution of piperazine (2.34 g, 27.1mmol) in 10ml of dry CH<sub>2</sub>Cl<sub>2</sub> under nitrogen. After 1 hour of stirring a white precipitate appeared. A solution of rhodamine B Base (3.0g, 6.8mmol) in 7ml of dichloromethane was added dropwise. Gas evolution was observed during the addition. After stirring at reflux for 24 hours, 0.1M aqueous HCl was added dropwise until gas evolution ceased. The heterogeneous solution was filtered and the solid was rinsed with dichloromethane and a 4:1 mixture of CH<sub>2</sub>Cl<sub>2</sub>/MeOH. The combined filtrate was concentrated and the residue was dissolved in dichloromethane, filtered again and solvent was evaporated under reduced pressure. Solid was partitioned between ethyl acetate and aqueous NaHCO<sub>3</sub> solution (0.1M). The aqueous layer was washed with ethyl acetate (10ml X 3), saturated with NaCl, acidified with 1M aqueous HCl and finally extracted with 2:1 mixture of *i*-propanol/dichloromethane (10ml X 5). The organic layer was dried with Na<sub>2</sub>SO<sub>4</sub>, filtered and solvent was evaporated under reduced pressure, obtaining a dark purple solid. Yield. 2.6g (4.9mmol, 72%)

FTIR (KBr, cm<sup>-1</sup>): 3422 (w, br), 2972 (w), 2713 (w, br), 1714 (w), 1647 (m), 1625 (m), 1588 (s), 1528 (w), 1467 (s), 1412 (s), 1337 (s), 1273 (m), 1245 (m), 1181 (s), 1132 (m), 1074 (m), 1009 (w), 974 (w), 921 (w), 819 (w), 682 (w), 577 (w).

<sup>1</sup>H-NMR (200 MHz, MeOD) δ: 1.30 (t, J: 7.0Hz, 12H), 3.13 (br s, 4H), 3.55-3.79 (m, 12H), 6.96-8.35 (m, 10H) ppm.

ESI-MS (m/z): 511.4 [M]<sup>+</sup>

-Synthesis of Rhodamine B 4-(3carboxypropionyl)piperazine amide (**RhoPS**)<sup>5</sup>



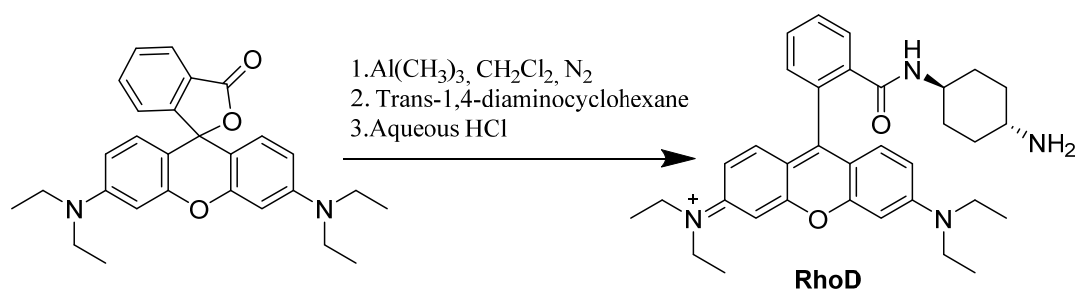
Triethylamine (0.56ml, 4.0mmol) was added to a stirred solution of rhodamine B piperazine amide (1.7g, 3.2mmol), succinic anhydride (0.35g, 3.5mmol) and DMAP (DiMethylAminoPiperazine, 0.41g, 3.4mmol) in 12ml of dichloromethane. Mixture was stirred 24 hour at room temperature then partitioned between ethyl acetate and 1M aqueous  $\text{K}_2\text{CO}_3$  solution. The aqueous layer was washed with 3 additional portion of ethyl acetate (10ml X 3), then saturated with NaCl and extracted with 2:1 mixture of *i*-propanol/dichloromethane (10ml X 5). The organic layer was dried with  $\text{Na}_2\text{SO}_4$ , filtered and concentrated under reduced pressure. The resulting solid was dissolved in chloroform and filtered again. Solvent was evaporated, obtaining a dark solid. Yield: 1.27g (2.1mmol, 66%)

FTIR (KBr,  $\text{cm}^{-1}$ ): 3426 (m, br), 2968 (w), 2726 (w, br), 1751 (w), 1634 (s), 1588 (s), 1510 (w), 1467 (s), 1413 (s), 1336 (s), 1273 (m), 1247 (m), 1179 (s), 1128 (m), 1072 (m), 1005 (m), 920 (w), 820 (w), 682 (w).

$^1\text{H-NMR}$  (200 MHz, MeOD)  $\delta$ : 1.31 (t, J: 7.0Hz, 12H), 2.38-2.44 (m, 2H), 5.51-2.59 (m, 2H), 3.31-3.43 (m, 8H), 3.69 (q, J: 7.0Hz, 8H), 6.82-8.01 (m, 10H).

ESI-MS (m/z): 611.4  $[\text{M}]^+$

-Synthesis of: Rhodamine B-trans-1,4-diaminocyclohexane amide (**RhoD**)<sup>6</sup>



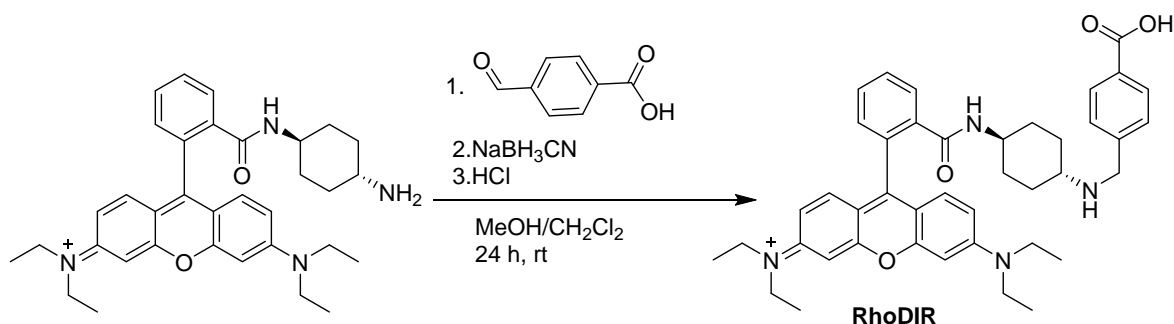
$\text{Al}(\text{CH}_3)_3$  (8ml, 2M in heptane, 16.0mmol) was slowly added to *trans*-1,4-diaminocyclohexane (3.1g, 27.1mmol) in 10ml of dry  $\text{CH}_2\text{Cl}_2$  under nitrogen. The mixture was stirred for 30 minutes then Rhodamine B (3.0g, 6.8mmol) in 7ml of  $\text{CH}_2\text{Cl}_2$  was added in one portion. Solution was refluxed for a minimum of 24 hours. After cooling to room temperature, 0.1M HCl was added dropwise in 20 minutes until effervescence ceased. Mixture was filtered and washed with  $\text{CH}_2\text{Cl}_2$  (100ml). Solution was concentrated under reduced pressure and the obtained solid was washed with 0.01M HCl, saturated with NaCl and extracted with a 4:1 mixture of *i*-propanol/dichloromethane (10ml X 3). The organic layer was dried with  $\text{Na}_2\text{SO}_4$ , filtered and solvents evaporated under reduced pressure. Product was purified by chromatography on silica using  $\text{CH}_2\text{Cl}_2/\text{MeOH}/\text{TEA}$  mixture (95/5/1), giving a pale pink solid. Yield: 1.2g (2.24mmol, 33%).

FTIR (KBr,  $\text{cm}^{-1}$ ): 3407 (s, br), 2940 (s, br), 2616 (s, br), 2458 (m, br), 1695 (s), 1613 (s), 1496 (s), 1470 (s), 1406 (s), 1359 (m), 1315 (s), 1270 (w), 1246 (m), 1174 (w), 1152 (w), 1115 (w), 1076 (w), 1056 (w), 1014 (m), 986 (m), 922 (w), 836 (w), 807 (w), 763 (m), 693 (w), 627 (w), 538 (w), 489 (w).

$^1\text{H-NMR}$  (200 MHz,  $\text{CDCl}_3$ )  $\delta$ : 0.80-2.00 (m, 20H), 2.26 (s, 2H), 3.08-3.18 (m, 1H), 3.61-3.80 (m, 8H), 4.02-4.13 (m, 1H), 7.12-7.38 (m, 5H), 7.73-7.83 (m, 4H), 8.00-8.09 (m, 1H) ppm.

ESI-MS ( $m/z$ ): 539 [ $\text{M}^+$ ]

*-Synthesis of: Rhodamine B-trans-1,4-diaminocyclohexane amide-4-carboxybenzyl (RhoDIR)*



Rhodamine B-*trans*-1,4-diaminocyclohexane amide (1.1g, 2.0mmol) was dissolved in 10ml of a mixture 1:1 methanol/dichloromethane. Triethylamine (0.835ml, 6.0mmol) and 4-carboxybenzaldehyde (0.306g, 2mmol) were added. After 10 minutes of stirring,  $\text{NaBH}_3\text{CN}$  (0.65g, 10.0mmol) was added and solution was stirred at room temperature. After 24 hours 0.1M aqueous HCl was added until effervescence stop (final pH  $\sim$ 2). The organic layer

## Experimental Part

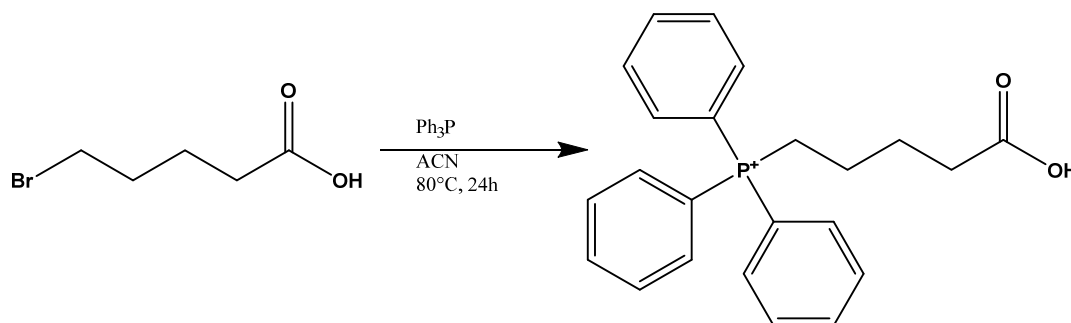
was separated and washed with 0.01M aqueous HCl. The combined aqueous solution was saturated with NaCl and extracted with a mixture 4:1 dichloromethane/*i*-propanol, dried with Na<sub>2</sub>SO<sub>4</sub>, filtered and concentrated. The obtained solid was dissolved in few ml (1-2) of methanol and filtered again to eliminate residues, then solvent was evaporated under reduced pressure. A pink solid was obtained. Yield: 1.0g (1.4mmol, 70%)

FTIR (KBr, cm<sup>-1</sup>): 3419 (s, br), 2979 (s, br), 2620 (s, br), 2457 (m, br), 2362 (m), 2339 (m), 1697 (s), 1685 (s), 1614 (s), 1590 (m), 1496 (s), 1471 (s), 1455 (s), 1408 (s), 1362 (m), 1328 (m), 1273 (w), 1247 (m), 1180 (m), 1152 (m), 1113 (m), 1076 (w), 1014 (m), 985 (m), 921 (w), 837 (w), 791 (w), 762 (m), 694 (w), 667 (w), 635 (w), 503 (w).

<sup>1</sup>H-NMR (200 MHz, CDCl<sub>3</sub>) δ: 1.27 (t, J: 7.0Hz, 12H), 2.28-2.69 (m, 4H), 3.38 (br s, 7H), 3.52-3.80 (m, 9H), 6.68-6.77 (m, 2H), 6.86-7.21 (m, 4H), 7.64-7.98 (m, 4H) ppm.

ESI-MS (m/z): 673.3 [M<sup>+</sup>] – 337.1 [M<sup>2+</sup>]

### -Synthesis of: (4-Carboxybutyl)triphenylphosphonium bromide (TPPAcV)<sup>7</sup>



To a solution of 5-bromovaleric acid (1.0g, 5.5mmol) in 10ml of acetonitrile, triphenylphosphine (1.6g, 6.1mmol) was added. The mixture was stirred at 80°C for 24 hours and then concentrated. The white residues was washed abundantly with benzene, hexane and finally diethyl ether. If there were still some reagent, the solid would be dissolved in 1-2ml of dichloromethane and precipitated with diethyl ether. The precipitation was repeated until the product was clean. Yield: 1.8g (5.0mmol, 92%)

FTIR (KBr, cm<sup>-1</sup>): 3428 (w, br), 2958 (m, br), 2902 (m), 2870 (w), 2590 (w, br), 2447 (w), 1990 (w), 1918 (w), 1838 (w), 1755 (s), 1712 (m), 1586 (m), 1484 (m), 1447 (s), 1437 (s), 1407 (8w), 1370 (m), 1354 (m), 1306 (m), 1212 (m), 1189 (m), 1110 (s), 1044 (w), 995 (m), 944 (m), 855 (w), 818 (w), 757 (s), 737 (s), 687 (s).

<sup>1</sup>H-NMR (200 MHz, CDCl<sub>3</sub>) δ: 1.62-1.80 (m, 2H), 1.86-1.97 (m, 2H), 2.62 (t, J: 6.8Hz, 2H), 3.54-3.69 (m, 2H), 7.69-7.82 (m, 15H) ppm.

ESI-MS(m/z): 363.2 [M<sup>+</sup>]

*-Synthesis of: General synthesis of compounds 4-7*

Ligand 2- $\{[[\text{Di}(2\text{-pyridyl})\text{methyl}](\text{methyl})\text{amino}]\text{methyl}\}$ phenol (0.2g, 0.66mmol) was dissolved in about 5ml of dry methanol in a 50ml round bottom flask under  $\text{N}_2$  and stirring. Then  $\text{Mn}(\text{ClO})_4 \cdot 6\text{H}_2\text{O}$  (0.24g, 0.66mmol) and apical carboxylate ligand (0.33mmol) were added to the solution. After complete dissolution of all solids trimethylamine (0.14ml, 0.99mmol) was added. Suddenly a precipitate appeared, and after 5 minutes of stirring, solution was heated to boiling and acetonitrile was added dropwise until solution became clear. Solution was left cool down slowly overnight and, in the case of acetate and benzoate, crystals appeared after few days. In the case of rhodamine derivatives, TPP and formylbenzoate, no crystals were obtained, the solids were filtered and washed abundantly with cold methanol and diethyl ether. Yield: 100-300mg (0.1-0.23mmol, 30-70% depending on carboxylate ligand).

FTIR **4 Formylbenzoate** (KBr,  $\text{cm}^{-1}$ ): 3443 (w, br), 3062 (w), 3012 (w), 2933 (w), 2814 (w), 1701 (m), 1597 (s), 1559 (s), 1481 (s), 1447 (s), 1408 (s), 1279 (s), 1202 (w), 1152 (w), 1086 (s), 1008 (m), 886 (m), 809 (w), 785 (m), 759 (s), 729 (w), 682 (w), 587 (w), 561 (w), 530 (m), 470 (w).

ESI-MS (m/z) **4 Formylbenzoate**: 867.1  $[\text{M}]^+$ , 763.2  $[\text{L}_2\text{Mn}_2(\text{O}_2\text{CH})]^+$ , 306.2  $[\text{L}]^+$

FTIR **4 Benzoate** (KBr,  $\text{cm}^{-1}$ ): 3428 (w, br), 3066 (w), 3012 (w), 2978 (w), 2931 (w), 2889 (w), 2854 (w), 2815 (w), 1597 (s), 1561 (s), 1481 (s), 1446 (s), 1412 (s), 1289 (s), 1280 (s), 1201 (w), 1153 (w), 1090 (s), 1012 (m), 889 (m), 791 (m), 762 (s), 736 (m), 697 (w), 676 (w).

ESI-MS (m/z) **4 Benzoate**: 839.1  $[\text{L}_2\text{Mn}_2\text{Bz}]^+$ , 763.2  $[\text{L}_2\text{Mn}_2(\text{O}_2\text{CH})]^+$ , 306.2  $[\text{L}]^+$ .

FTIR **4 Acetate** (KBr,  $\text{cm}^{-1}$ ): 3430 (w, br), 3063 (w), 3006 (w), 2976 (w), 2936 (w), 2881 (w), 2846 (w), 2806 (w), 1593 (s), 1574 (s), 1563 (s), 1479 (s), 1451 (s), 1421 (s), 1369 (w), 1291 (s), 1279 (s), 1235 (w), 1151 (w), 1096 (s), 1000 (m), 884 (m), 790 (m), 763 (s), 730 (w), 682 (w), 623 (m), 589 (w), 557 (w), 530 (m), 473 (w).

ESI-MS (m/z) **4 Acetate**: 777.3  $[\text{M}]^+$ , 763.2  $[\text{L}_2\text{Mn}_2(\text{O}_2\text{CH})]^+$ , 306.2  $[\text{L}]^+$ .

FTIR **5** (KBr,  $\text{cm}^{-1}$ ): 3440 (m, br), 3061 (w), 2971 (m), 2868 (w), 1683 (m), 1634 (m), 1615 (s), 1599 (s), 1548 (m), 1514 (m), 1480(s), 1444 (s), 1402 (s), 1332 (m), 1289 (m), 1275 (m), 1232 (w), 1218 (w), 1181 (w), 1153 (w), 1116 (s), 1014 (m), 886 (m), 819 (w), 787 (m), 758 (m), 702 (w), 623 (m), 557 (w), 531 (w).

ESI-MS (m/z) **5**: 664.2  $[\text{M}]^{2+}$ , 763.1  $[\text{L}_2\text{Mn}_2(\text{O}_2\text{CH})]^+$ , 611.3  $[\text{RhoPS}]^+$ , 359.1  $[\text{M-RhoDR}]^{2+}$ , 306.2  $[\text{L}]^+$ .

## Experimental Part

FTIR **6** (KBr,  $\text{cm}^{-1}$ ): 3432 (m, br), 3061 (w), 2973 (w), 2930 (w), 1647 (m), 1589 (s), 1528 (w), 1480(s), 1467 (m), 1452 (m), 1412 (m), 1336 (m), 1274 (m), 1246 (m), 1198 (w), 1181 (m), 1157 (w), 1084 (s), 1007 (m), 921 (w), 885 (w), 822 (w), 787 (w), 757 (m), 727 (w), 683 (m), 622 (m), 559 (w), 529 (w).

ESI-MS (m/z) **6**: 867.1  $[\text{M}-(\text{C}_{34}\text{H}_{42}\text{N}_3\text{O}_2)]^+$ , 763.1  $[\text{L}_2\text{Mn}_2(\text{O}_2\text{CH})]^+$ , 673.3  $[\text{RhoDIR}]^+$ , 443.2  $[\text{RhoDIR}-(\text{C}_{14}\text{H}_{17}\text{NO}_2)]^+$ , 359.1  $[\text{M-RhoDIR}]^{2+}$ , 306.2  $[\text{L}]^+$ .

FTIR **7** (KBr,  $\text{cm}^{-1}$ ): 3619 (w), 3335 (w, br), 3073 (w), 2995 (w), 2972 (w), 2949 (w), 2854 (w), 2802 (w), 1598 (s), 1568 (m), 1480 (s), 1452 (s), 1444 (s), 1420 (m), 1286 (s), 1273 (s), 1252 (w), 1151 (w), 1015 (w), 997 (m), 885 (m), 784 (m), 771 (m), 756 (s), 733 (w), 683 (w).

ESI-MS (m/z) **7**: 540.1  $[\text{M}]^{2+}$ , 763.2  $[\text{L}_2\text{Mn}_2(\text{O}_2\text{CH})]^+$ , 363.3  $[\text{TPPAcV}]^+$ , 306.2  $[\text{L}]^+$ .

*-Synthesis of:  $[\text{Mn}^{\text{II}}\text{Mn}^{\text{III}}]_{12}(\mu_4\text{-O})_8(\mu_4\text{-Cl})(\text{tert-butyl-PO}_3)_8$  $[\text{Mn}^{\text{II}}(\text{CH}_3\text{CN})_6]\text{Cl}_2 \cdot 6\text{CH}_3\text{CN} \cdot 5.25\text{H}_2\text{O}$  (**8**)*

$\text{MnCl}_2 \cdot 2\text{H}_2\text{O}$  (324mg, 2mmol), *tert*-butylphosphonic acid (138mg, 1mmol), isonicotinic acid (123mg, 1mmol),  $\text{KMnO}_4$  (33mg, 0.2mmol) and triethylamine (65 $\mu\text{l}$ , 0.5mmol) were dissolved in 25ml of  $\text{CH}_3\text{CN}$  and stirred for 3h. After addition of  $\text{CuCl}_2 \cdot 2\text{H}_2\text{O}$  (166mg, 1mmol), solution was stirred for other 2h, then it was filtered and left to evaporate at room temperature.

FTIR (KBr,  $\text{cm}^{-1}$ ): 3404 (m, br), 2975 (w), 1626 (m), 1480 (m), 1461 (w), 1396 (w), 1365 (w), 1026 (m), 986 (m), 924 (s), 830 (m), 670 (w).

*-Synthesis of:  $(\text{C}_5\text{H}_7\text{N}_2)_3[\text{Mn}^{\text{II}}_3\text{Mn}^{\text{III}}]_{10}(\mu_4\text{-O})_6(\mu_3\text{-O})(\mu_3\text{-OH})(\mu_4\text{-Cl})_4(\text{Cl})(\text{tert-butyl-PO}_3\text{H})(\text{tert-butyl-PO}_3)_9$  $\cdot 3\text{CH}_3\text{CN} \cdot 2\text{H}_2\text{O}$  (**9**)*

$\text{MnCl}_2 \cdot 2\text{H}_2\text{O}$  (162mg, 1mmol), *tert*-butylphosphonic acid (69mg, 0.5mmol), 2-aminopyridine (96mg, 1mmol) and  $\text{KMnO}_4$  (16mg, 0.1mmol) were dissolved in 20ml of  $\text{CH}_3\text{CN}$  and stirred for 5h at room temperature. Solution was then filtered and left to slowly evaporate.

FTIR (KBr,  $\text{cm}^{-1}$ ): 3395 (m, br), 3188 (m), 2972 (m), 2870 (w), 1666 (s), 1626 (m), 1479 (m), 1459 (w), 1393 (w), 1363 (w), 1326 (w), 1099 (m), 936 (s), 830 (m), 769 (m), 723 (w).



-Synthesis of:  $(C_5H_7N_2)_2[Mn^{II}_3Mn^{III}_{11}(\mu_4-O)_6(\mu_3-O)(\mu_3-OH)(\mu_2-OH)(\mu_4-Cl)_4$   
 $(tert\text{-butylPO}_3H)(tert\text{-butyl-PO}_3)_{10}(2\text{-aminopyridine})] \cdot 3CH_3CN \cdot 2H_2O$  (**10**)

MnCl<sub>2</sub>·2H<sub>2</sub>O (162mg, 1mmol), *tert*-butylphosphonic acid (69mg, 0.5mmol), 2-aminopyridine (191mg, 2mmol) and KMnO<sub>4</sub> (16mg, 0.1mmol) were dissolved in 20ml of CH<sub>3</sub>CN and stirred for 5h at room temperature. Solution was then filtered and left to slowly evaporate at room temperature.

FTIR (KBr, cm<sup>-1</sup>): 2971 (w), 1665 (m), 1617 (w), 1478 (m), 1452 (w), 1392 (w), 1362 (w), 1327 (w), 1095 (m), 938 (s), 831 (m), 771 (m).

-Synthesis of:  $[(Mn^{II}_{0.5}Mn^{III}_{0.5})Mn^{III}_{12}(\mu_4-O)_6(\mu-OH)_2(\mu-CH_3O)_4(CH_3OH)_2$   
 $(tert\text{-butylPO}_3)_{10}(4\text{-picoline})_4]Cl_{0.5} \cdot 1.5H_2O$  (**11**)

MnCl<sub>2</sub>·2H<sub>2</sub>O (162mg, 1mmol), *tert*-butylphosphonic acid (69mg, 0.5mmol), 4-picoline (200μl, 2mmol) and KMnO<sub>4</sub> (16mg, 0.1mmol) were dissolved in 20ml of CH<sub>3</sub>OH and stirred for 5h at room temperature. The solution was filtered and left to evaporate at room temperature.

FTIR (KBr, cm<sup>-1</sup>): 2949 (m), 2923 (m), 1618 (m), 1477 (m), 1456 (w), 1392 (w), 1361 (w), 1116 (s), 1054 (s), 998 (s), 978 (s), 833 (s), 806 (s), 723 (w), 667 (m).

-Synthesis of:  $[(Mn^{II}_{0.5}Mn^{III}_{0.5})Mn^{III}_{12}(\mu_4-O)_6(\mu-OH)_2(\mu-CH_3O)_4(CH_3OH)_2$   
 $(tert\text{-butylPO}_3)_{10}(4,4'\text{-TPD})_2]Cl_{0.5} \cdot 8CH_3OH$  (**12**)

(4,4'-TDP = 4,4'-trimethylenedipyridine)

MnCl<sub>2</sub>·2H<sub>2</sub>O (162mg, 1mmol), *tert*-butylphosphonic acid (140mg, 1mmol), 4,4'-trimethylenedipyridine (303mg, 1.5mmol) and KMnO<sub>4</sub> (34mg, 0.2mmol) were dissolved in 40ml of CH<sub>3</sub>OH and stirred for 5h at room temperature. Solution was then filtered and left to evaporate at room temperature.

FTIR (KBr, cm<sup>-1</sup>): 2949 (m), 1614 (m), 1477 (m), 1458 (w), 1424 (w), 1392 (w), 1361 (w), 1117 (s), 1065 (s), 978 (s), 832 (s), 808 (w), 754 (w), 666 (s).

-Synthesis of:  $[Mn^{III}_{13}(\mu_4-O)_2(\mu_3-O)_4(\mu_2-OH)_2(\mu_2-CH_3O)_4(C_6H_5PO_3)_{10}(C_5H_5N)_5Cl] \cdot 3H_2O$   
**(13)**

MnCl<sub>2</sub>·2H<sub>2</sub>O (162mg, 1mmol), phenylphosphonic acid (94mg, 0.6mmol) and KMnO<sub>4</sub> (39mg, 0.25mmol) were dissolved in 10ml of CH<sub>3</sub>OH(5ml)/CH<sub>3</sub>CN(5ml) mixture, the

### *Experimental Part*

1.2ml of pyridine were added and the solution was stirred for 5h. After filtration, solution was left to crystallize.

FTIR (KBr,  $\text{cm}^{-1}$ ): 3503 (w, br), 3055 (w), 1601 (w), 1485 (w), 1438 (m), 1139 (m), 1120 (s), 1084 (s), 1066 (s), 1032 (s), 1003 (s), 971 (s), 753 (s), 721 (m), 695 (s).

*-Synthesis of:  $[Mn^{III}_{13}(\mu_4-O)_2(\mu_3-O)_4(\mu_2-OH)_2(\mu_2-CH_3O)_4(C_6H_5CH_2PO_3)_{10}(C_5H_5N)_5Cl]$   
 $\cdot 5H_2O$  (14)*

MnCl<sub>2</sub>·2H<sub>2</sub>O (162mg, 1mmol), benzylphosphonic acid (102mg, 0.6mmol) and KMnO<sub>4</sub> (39mg, 0.25mmol) were dissolved in 10ml of CH<sub>3</sub>OH(5ml)/CH<sub>3</sub>CN(5ml) mixture, the 0.5ml of pyridine were added and the solution was stirred for 5h. After filtration, solution was left to crystallize.

FTIR (KBr,  $\text{cm}^{-1}$ ): 3423 (w, br), 3028 (w), 2918 (w), 2815 (w), 1601 (m), 1495 (m), 1446 (m), 1409 (w), 1240 (w), 1192 (w), 1132 (m), 1116 (s), 1080 (s), 1066 (s), 982 (s), 830 (m), 788 (m), 758 (w), 730 (w), 693 (s).

*-Synthesis of:  $[Mn^{III}_{13}(\mu_4-O)_2(\mu_3-O)_4(\mu_2-OH)_2(\mu_2-CH_3O)_4(C_6H_5CH_2PO_3)_{10}$   
 $(C_6H_5C_3H_6C_3H_4N)_5Cl] \cdot 5H_2O$  (15)*

MnCl<sub>2</sub>·2H<sub>2</sub>O (162mg, 1mmol), benzylphosphonic acid (102mg, 0.6mmol) and KMnO<sub>4</sub> (39mg, 0.25mmol) were dissolved in 20ml of CH<sub>3</sub>OH, then 4-(3-phenylpropyl)pyridine (1ml, 5mmol) was added and solution was stirred for 5h. After filtration, solution was left to crystallize at room temperature.

FTIR (KBr,  $\text{cm}^{-1}$ ): 3471 (w, br), 3060 (w), 3026 (w), 2921 (w), 2813 (w), 1615 (m), 1602 (m), 1558 (w), 1495 (m), 1453 (m), 1426 (w), 1240 (w), 1193 (w), 1133 (m), 1118 (s), 1082 (s), 1067 (s), 984 (s), 828 (m), 789 (m), 730 (w), 695 (s).

*-Synthesis of:  $TBA_2[Mn_6^{II}Mo_{10}^{VI}(O)_{12}(\mu_3-O)_4(tert-Butyl-PO_3)_6(Ac)_2(pyridine)_2(H_2O)_6]$   
(16)*

Manganese(III) acetylacetonate (177mg, 0.5mmol), TBA<sub>2</sub>Mo<sub>6</sub>O<sub>19</sub> (138mg, 0.1mmol), *tert*-butylphosphonic acid (71mg, 0.5mmol), TBABr (323mg, 1.0mmol) and pyridine (80μl) were dissolved in 25 ml of CH<sub>3</sub>CN and stirred at room temperature for 5h. Solution was filtered and left to crystallize.

FTIR (KBr,  $\text{cm}^{-1}$ ): 3444 (w, br), 2964 (m), 2872 (m), 1737 (w), 1660 (m), 1599 (w), 1563 (m), 1478 (m), 1443 (m), 1364 (w), 1311 (w), 1217 (w), 1101 (s), 1027 (w), 1003 (w), 972 (s), 945 (s), 892 (s), 832 (m), 795 (m), 764 (s), 700 (s), 659 (s).

-Synthesis of:  $\alpha_2\text{-K}_8\text{P}_2\text{W}_{17}\text{O}_{61}(\text{Ni}^{2+}\cdot\text{OH}_2)\cdot 17\text{H}_2\text{O}$  (NiPOM)<sup>8</sup>

In a 50ml round bottom flask,  $\alpha_2\text{-K}_{10}\text{P}_2\text{W}_{17}\text{O}_{61}\cdot 15\text{H}_2\text{O}^*$  (2.0g, 0.42mmol) was dissolved in 5ml of water at 90°C. A solution of  $\text{Ni}(\text{NO}_3)_2\cdot 6\text{H}_2\text{O}$  (0.138g, 0.47mmol) in 1ml of water was added under vigorous stirring, the solution turned pale green. After 15 minutes of stirring heating was stopped and solution was slowly cooled to 5°C for 5 hours. Light green crystals were collected by filtration, washed with water (10ml X 2) and dried under vacuum. Yield: 1.5g (0.31mmol, 74%).

FTIR (KBr,  $\text{cm}^{-1}$ ): 3543 (s, br), 1613 (s), 1085 (s), 945 (s), 915 (s), 779 (s), 526 (m).

UV-Vis:  $\epsilon_{680}$ :  $10\text{cm}^{-1}\text{M}^{-1}$

-Synthesis of:  $\text{K}_8[\beta\text{-SiW}_{10}\text{O}_{36}]$



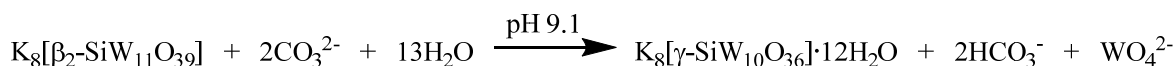
Sodium metasilicate (3.0g, 24,7mmol) was dissolved in 50ml of water. In a separated beaker sodium tungstate dehydrate (90.9g, 0.276mol) was dissolved in about 150ml of water and immersed in an ice/water bath at 5°C. to this solution 40ml of 4.1M HCl (0.16mmol) were added dropwise in about 40 minutes under vigorous stirring, in order to dissolve tungstic acid. When the solution returned to room temperature, metasilicate solution was added and pH was adjusted at 5.5 with 4.1M HCl. The pH was maintained by small addition of 4.1M HCl for 100 minutes than solid KCl (44.2g, 0.6mol) was added. After 15 minutes of stirring the white precipitate was collected by filtration through a sintered glass filter. Product was dissolved in 420ml of water filtered and precipitated again with KCl (39.4g, 0.5mol), filtered and washed with 2M KCl solution (15ml X 2) and dried under vacuum. Yield: 34.0g (11.4mmol, 46%)

FTIR (KBr,  $\text{cm}^{-1}$ ): 3423 (s, br), 1611 (s), 991 (s), 947 (s), 878 (s), 809 (s), 713 (s), 535 (m).

\*  $\alpha_2\text{-K}_{10}\text{P}_2\text{W}_{17}\text{O}_{61}\cdot 15\text{H}_2\text{O}$  was synthesized according to literature procedure (see ref.8).

## Experimental Part

### -Synthesis of: $K_8[\gamma\text{-SiW}_{10}\text{O}_{36}]$



This synthesis required an accurate control of the pH.

The fresh prepared potassium salt  $K_8[\beta\text{-SiW}_{10}\text{O}_{36}]$  (34.0g, 11.4mmol) was dissolved in 530ml of water and filtered to eliminate impurities. The pH of the solution was quickly adjusted to 9.1 by addition of 2M aqueous  $\text{K}_2\text{CO}_3$  solution and kept stable for 16 minutes.  $\text{KCl}$  (91.0g, 1.2mol) was then added to precipitate the potassium salt of  $\gamma$ - decatungstate. Solution was stirred for 10 minutes maintaining the pH at 9.1 by addition  $\text{K}_2\text{CO}_3$  solution. The solid was filtered, washed with 1M  $\text{KCl}$  solution and dried under vacuum.

Yield: 20.0g (7.6mmol, 66%)

FTIR (KBr,  $\text{cm}^{-1}$ ): 3461 (s, br), 1635 (m), 989 (m), 942 (s), 863 (s), 813 (s), 742 (s), 658 (m), 532 (w).

### -Synthesis of: $\text{Na}_{10}[\text{Ru}_4\text{O}_4(\text{OH})_2(\text{H}_2\text{O})_4(\gamma\text{-SiW}_{10}\text{O}_{36})_2]$ (RuPOM, **17**)<sup>9</sup>



In a round bottom flask,  $K_8[\gamma\text{-SiW}_{10}\text{O}_{36}] \cdot 12\text{H}_2\text{O}$  (1.0g, 0.38mmol) was dissolved in 16ml of water, then  $\text{RuCl}_3 \cdot x\text{H}_2\text{O}$  (0.153g, 0.74mmol) was added and solution was heated at  $70^\circ\text{C}$  for 1 hour (pH drop to 1.6). After cooling excess of  $\text{CsCl}$  (4.4g, 25mmol) was added to precipitate the cesium salt. Product was recovered by centrifugation and washed three time with cold water, then it was dissolved in about 100ml of water to prepare the sodium salt after cation exchange by eluting it through a cation exchange resin, charged with  $\text{Na}^+$ . Solvent was evaporated under reduced pressure and the black solid was dissolved in 5ml of water. Product was purified on a size exclusion column charged with Sephadex-G50<sup>®</sup> resin (10g). Solvent was evaporated and the purified sodium salt was obtained as a black solid. Yield: 0.8g (0.28mmol, 74%).

FTIR (KBr,  $\text{cm}^{-1}$ ): 3434 (s, br), 2923 (w), 2853 (w), 1622 (m), 1044 (w), 999 (w), 950 (s), 876 (s), 804 (s), 539 (w).

UV-Vis:  $\epsilon_{278}$ :  $69601\text{cm}^{-1}\text{M}^{-1}$ ,  $\epsilon_{453}$ :  $19116\text{cm}^{-1}\text{M}^{-1}$ .

### -Synthesis of capsules

Calcium carbonate ( $\text{CaCO}_3$ ) porous microparticles with size distribution around 2-3  $\mu\text{m}$  were obtained by mixing in a glass vial (6 mL) equal volumes (3.075ml) of aqueous solutions of  $\text{CaCl}_2$  (0.33 M) and  $\text{Na}_2\text{CO}_3$  (0.33 M) with 3.85ml of AM-dextran solution

conjugated to rhodamine (dextran-RITC) or fluorescein (dextran-FTIC) (fluorophore concentration  $\sim 50 \mu\text{M}$ ). The solution was left stirring for 30 s. Subsequently, the precipitate was separated from the supernatant by centrifugation (4500 rpm for 5 s) and washed three times with 1 mL of MilliQ water to remove unreacted species.

Particles were resuspended in 5 ml of 0.5 M NaCl solution containing the polyanion PSS (p-DexS) (2 mg/ml, pH = 6.5). The dispersion was initially left for 2 min in a sonication bath and was subsequently continuously shaken for 10 min to avoid precipitation and aggregation of the particles on the bottom of the tube. The excess polyanion was removed by three centrifugation/washing steps with 1 ml of MilliQ water (4500 rpm for 5 s). Subsequently 5 mL of a 0.5 M NaCl solution containing the polycation PAH (p-Arg) (2 mg/ml, pH = 6.5) was added to the particles and the dispersion was mixed as described above, followed again by three centrifugation/washing steps with 1 ml of MilliQ H<sub>2</sub>O (4500 rpm for 5 s). The particles were then incubated for 10 minutes in 5 ml of RuPOM solution (H<sub>2</sub>O, pH = 5.0, 2 mg/ml, 0.35 mM). The unbound molecules were removed by three centrifugation/washing steps with 1 mL of MilliQ water (4500 rpm for 5 s). As expected, the colour of the pellet changed to brown. Some other bi-layers of polymers were then adsorbed to complete the multilayer walls.

The CaCO<sub>3</sub> compartments were finally removed by complexation with EDTA buffer. To this aim coated CaCO<sub>3</sub> particles were shaken for 2 minutes with 5 ml of EDTA solution (0.2 M, pH = 7.0) followed by gentle centrifugation at 1200 rpm for 10 minutes in order to settle down the template-free capsules. After that, the supernatant was removed and the capsules were washed three times with 1ml MilliQ water by intermediate centrifugation steps at 1200 rpm for 8 min.

Finally, the capsules were stored as suspension in 500  $\mu\text{L}$  of MilliQ water at 4 °C. The capsule number per volume was determined by direct counting by a haemocytometer under a microscope. A drop of a diluted solution of capsules was added onto the chamber and the number of capsules in the volume defined by the haemocytometer was counted by using a 20X objective in phase contrast channel.

## 6.4 Catalytic measurements

### *-Hydrogen peroxide dismutation*

In a typical experiment 12ml (or 6ml) of buffer solution (phosphate, borate, Tris, Mops, Hepes, pure water or organic solvent) were placed in a thermostated reaction vessel. Mother commercially available H<sub>2</sub>O<sub>2</sub> solution (30%) was added to reach 33mM concentration (for Michaelis-Menten analysis, different H<sub>2</sub>O<sub>2</sub> concentrations were used). After 2 minutes of signal stabilization (not shown into kinetic traces), mother solution of catalyst was added through a septum to reach a final concentration of usually 15μM or 60μM. The head-space of the reactor for mole of oxygen calculation was 14,6ml (or 20,6ml). Ideal gas law was used to calculate the mole of oxygen produced at 25°C.

### *-SOD-test*

SOD-like activity of complexes was measured by inhibition of superoxide-dependent reduction of NBT (or cytochrome c) on a Cary 50 UV-Vis spectrophotometer. The superoxide radical anions, generated enzymatically by the xanthine/xanthine oxidase system, in phosphate buffer at pH 7.8, were detected at 550 nm measuring the reduction of NBT to blue formazan. Reaction mixture contained 50μM xanthine, 100μM NBT, 50 mM phosphate buffer and xanthine oxidase 0,0053 U/ml.

In the presence of a SOD mimic, the absorbance values of the blue formazan decrease with increasing concentration of complex, this is because the SOD mimic will compete with the NBT to scavenge the O<sub>2</sub><sup>-•</sup>, this then allows the SOD activity of the complex to be calculated. The indirect method assumes that there are no side reactions occurring and that only the catalytic superoxide dismutase reaction is taking place.<sup>10</sup> Mother catalyst solutions were prepared 2-0.2mM in water (or DMSO, not acetonitrile) and addition of 10, 20, 30 μL of prepared solution were done. Conditions were optimized to be close to IC<sub>50</sub>. Change in absorbance slope compared to the X/XO solution were determined in order to calculate the parameters. From IC<sub>50</sub> value it is possible to calculate kinetic constant of the catalyst for superoxide elimination ( $k_{McF} = k_{indicator}[\text{Indicator}]/IC_{50}$ ).

The calculated rates are more appropriate for a comparison of results with literature values, as IC<sub>50</sub> values will be smaller where a lower [NBT] has been used and the calculated rate is independent of both the nature and concentration of detector used.

*-Aggregation of A $\beta$ 40-42*

Amyloid peptide was dissolved in 1,1,1,3,3,3-Hexafluoro-2-propanol (HFIP) at a concentration of 1mg/ml and stirred 2 hours at 4°C. Solvent was evaporated with a gentle stream of N<sub>2</sub> and the peptide was re-dissolved in 10mM phosphate buffer at pH 7.4. Stock solution was divided in Eppendorf tube at concentration of 100 $\mu$ M, with or without RuPOM for CD and TEM measurement, and incubated at 37°C, for fixed time intervals.

*-<sup>1</sup>H-NMR of A $\beta$ 28*

Amyloid 1-28 were dissolved in phosphate buffer solution (10 mM, pH 7.4, H<sub>2</sub>O with 10% D<sub>2</sub>O) at 200  $\mu$ M concentration. NMR spectra were recorded before and after addition of 0.2-0.4 equivalents of RuPOM (stock solution 0.005 M in the same buffer).

*-Amyloid Fluorescence*

Quenching of tyrosine emission was followed at 305 nm, with excitation at 270nm and 5nm slit.

## **6.5 Biological tests**

*-Mitochondria preparation*

Fresh livers (1-3) from CD1 mice, grown in the biological department of University of Padova, have been extracted thanks to collaboration of Dr. Mauro Ghidotti.

Organs were put into a buffer solution (RLM: 250mM sucrose, 10mM Tris, 0.1mM EGTA, pH 7.4) and cut in small pieces, then homogenized. The homogenized was centrifuged at 700g for 4 minutes at 4°C. Supernatant was recovered and centrifuged at 7000g for 10 minutes, in order to separate mitochondria. Supernatant was eliminated and mitochondria *pellet* was washed with buffer solution, then was centrifuged again at 10000g for 5 minutes. After the elimination of supernatant, mitochondria were dispersed in few  $\mu$ l of buffer solution. Quantification of mitochondria concentration was assessed with Biuret method (20 $\mu$ l mitochondria in 1.5 ml biuret, 1ml H<sub>2</sub>O MilliQ and 500 $\mu$ l of 1%

## *Experimental Part*

deoxycholate solution (DOC); after heating of 2 minutes at 80°C, absorbance at 540nm is registered).<sup>†</sup> Mitochondria are to be used in the day.

### *-Mitochondrial respiration measurement*

Mitochondrial respiration was measured using a Clark-type electrode in the group of Prof. Paolo Bernardi, with the supervision Dr. Valeria Petronilli, in the Biology Department of University of Padova. Measurement were performed in a 2ml vessel containing the following buffer solution: 120mM KCl, MOPS 20mM, EGTA 10 $\mu$ M, P<sub>i</sub> 1mM at pH 7.4. Before each experiment the following solution were added by a syringe, to reach the concentration in the bracket: glutamate/malate (5/2.5mM) or succinate (5mM) and catalyst (2.5-100 $\mu$ M). Registration was started and after about 100s, fresh prepared mitochondria (1-2mg/ml) were added. ADP solution was added after 200s to reach 100 $\mu$ M concentration. When phosphorylation was finished FCCP (50nM) was added, at about 500s after registration started. Finally at about 650s antimycin A (0.5 $\mu$ M) and inhibitors (30mM) were added. Depending on mitochondrial respiration, addition could be done at different times. In the case of incubated mitochondria, they were incubated with and without RuPOM for 5 and 50 minutes then were injected into the vessel or prepared for TEM analysis. TEM samples were centrifuged for 5 minutes at 8000g, mitochondrial *pellet* was re-suspended in sodium cacodilate 0.1M at pH 7.3, with 1% of glutaraldehyde. Samples treated were further prepared for TEM by Dr. Caicci, Dr. Boldrin and Dr.ssa Moschin of Biology department of University of Padova.

### *-Calcium Retention Capacity (CRC) measurement*

Mitochondria were incubated in a buffered medium (120mM KCl, 20mM Mops, 20 $\mu$ M EGTA, 1mM P<sub>i</sub>, 5mM/2.5mM glutamate/malate, pH 7.4) at a concentration of 0.5mg/ml. Catalysts (RuPOM or [Mn<sub>2</sub>L<sub>2</sub>]) at different concentration were added before measurement was started. Calcium Green-5N (CaG, Molecular Probes:  $\lambda_{ex}$ :505nm,  $\lambda_{em}$ :535nm) was also added before starting at a concentration of 1 $\mu$ M. CaG is impermeable to the membrane and becomes fluorescent when complexes Ca<sup>2+</sup> ions (with a K<sub>D</sub> of 14 $\mu$ M). So it allows to monitor extra-mitochondrial calcium and follow release or accumulation of Ca<sup>2+</sup>.

---

<sup>†</sup> Biuret test allows to calculate mitochondria concentration, it is a mixture of strong base (usually NaOH), copper sulfate (CuSO<sub>4</sub>·6H<sub>2</sub>O) and sodium tartrate. In the presence of proteins, Cu<sup>2+</sup> is reduced to Cu<sup>+</sup> with an increase of absorbance at 540nm, that is proportional to mitochondrial concentration, obtained by a calibration curves with bovine serum albumin (BSA).



Fluorescence was measured by a Perkin-Elmer LS50B instrument at controlled temperature of 25°C and under magnetic stirring. Calcium chloride 2.5µM (mother solution 1mM) was added every minute until pore opening.

*-Cell viability*

The cell viability was measured by using the quantitative colorimetric MTT assay, showing the mitochondrial activity of living cells. Cells were incubated at 37°C under 5% CO<sub>2</sub> humidified air incubator for 72 h. After the first day of culture, the SH-SY5Y cells were treated with various concentrations (0–80µM) of POM. After treatment the medium was removed and 400µl of medium, containing 40µl of MTT solution (5 mg·ml<sup>-1</sup> in PBS), were added to each well and the cells were incubated at 37 °C. After 2 h of incubation at 37 °C, the reaction was stopped by adding 400µl of lysis buffer (10% SDS, 0.6% acetic acid in DMSO, pH 4.7). The quantity of formazan product was directly proportional to the number of metabolically active living cells. The optical density of each well was spectrophotometrically measured at 570nm. Results were expressed as the percentage of the control without treatment.

*-Apoptosis detection*

The apoptosis of cells was investigated by Annexin V-Apoptosis detection kit (Santa Cruz Biotechnology) and by investigating the expression of Caspase-3 by using Laser Scanning Confocal Microscope (LSCM). Normal viable cells in culture are negative for Annexin V-FITC and negative for PI. Cells that are induced to undergo apoptosis are positive for Annexin V FITC and negative for PI. Both cells in the later stages of apoptosis and necrotic cells are positive for Annexin V-FITC and PI. Controls and treated samples treated were rinsed and washed once with 500µl of 1× Assay Buffer per well. Following 100µl of Assay Buffer was added to each well, containing 1µg of Annexin V-FITC and 10µl of propidium iodide. After the incubation of cells for 15 min at room temperature in the dark, the fluorescence intensity of Annexin V-FITC and of propidium iodide was evaluated with LSCM. Data were analyzed and expressed as a percentage of the control. For the analysis of active N-terminal c-Jun protein kinase (p-JNK) and caspase-3 expression neuronal cells were rinsed with PBS, fixed for 15 min with paraformaldehyde (4%), permeabilized for 10 min with 0.25% Triton X-100 and subsequently blocked for 30 min with 1% BSA at room temperature. p-JNK expression was detected using anti-mouse monoclonal p-JNK antibody (1:250; Santa Cruz Biotechnology, CA) over night at 4 °C

### *Experimental Part*

and anti-mouse IgG Cy3-conjugated (1:400; Jackson Immunoresearch) for 60 min at room temperature. Caspase-3 expression was detected using rabbit anti-caspase-3 antibody (1:250; BD, Milan, Italy) over night at 4 °C and goat anti-rabbit IgG FITC conjugated (1:100; Invitrogen) for 60 min at room temperature. Nucleic acids were counterstained with DAPI30 (200ng/ml; Sigma, Milan Italy). Images were taken by using LSCM. Mitochondrial membrane potential (MMP) in cells was measured using a fluorescent probe, JC-1 (5,5',6,6'-tetrachloro- 1,1',3,3'-tetraethylbenzimidazolyl-carbocyanine iodide). Controls and cells treated with A $\beta$  alone or a mixture of A $\beta$  and POM at different concentrations were incubated with JC-1 staining solution (5 g/ml) for 20 min at 37 °C. The fluorescence intensity of both mitochondrial JC-1 monomers ( $\lambda_{\text{ex}}$ :514 nm,  $\lambda_{\text{em}}$ :529 nm) and aggregates ( $\lambda_{\text{ex}}$ :585 nm,  $\lambda_{\text{em}}$ :590 nm) were detected by using LSCM. The MMP of cells, for each treatment, was calculated as the fluorescence ratio of red to green.



## References

- 
- <sup>1</sup> Michaela Grau, PhD Thesis, Imperial College, London, **2013**.
- <sup>2</sup> Niemers E., Hiltmann R., *Synthesis*, **1976**, 593. Modified procedure.
- <sup>3</sup> Renz M., Hemmert C., Meunier B., *Eur. J. Org. Chem.*, **1998**, 1271.
- <sup>4</sup> Vicario J., Eelkema R., Browne W.R., Meetsma A., La Crois R.M., Feringa B.L., *Chem. Comm.*, **2005**, 3936.
- <sup>5</sup> Nguyen T., Francis M.B., *Org. Lett.*, **2003**, 5, 18, 3245.
- <sup>6</sup> Lee M., Grissom C.B., *Org. Lett.*, **2009**, 11, 12, 2499. Modified procedure.
- <sup>7</sup> de los Angeles Rey M., Martínez-Pérez J.A., Fernández-Gacio A., Halkes K., Fall Y., Granja J., Mouriño A., *J. Org. Chem.*, **1999**, 64, 3196.
- <sup>8</sup> Lyon D.K., Miller W.K., Novet T., Domaille P.J., Evitt E., Johnson D.C., Finke R.G., *J. Am. Chem. Soc.*, **1991**, 113, 7209.
- <sup>9</sup> Sartorel A., Carraro M., Scorrano G., De Zorzi R., Geremia S., McDaniel N.D., Bernhard S., Bonchio M., *J. Am. Chem. Soc.*, **2008**, 130, 5006. Modified procedure.
- <sup>10</sup> Goldstein S., Czapski G., *Free Radic. Res. Commun.*, **1991**, 12, 3, 5.





# *Appendix*



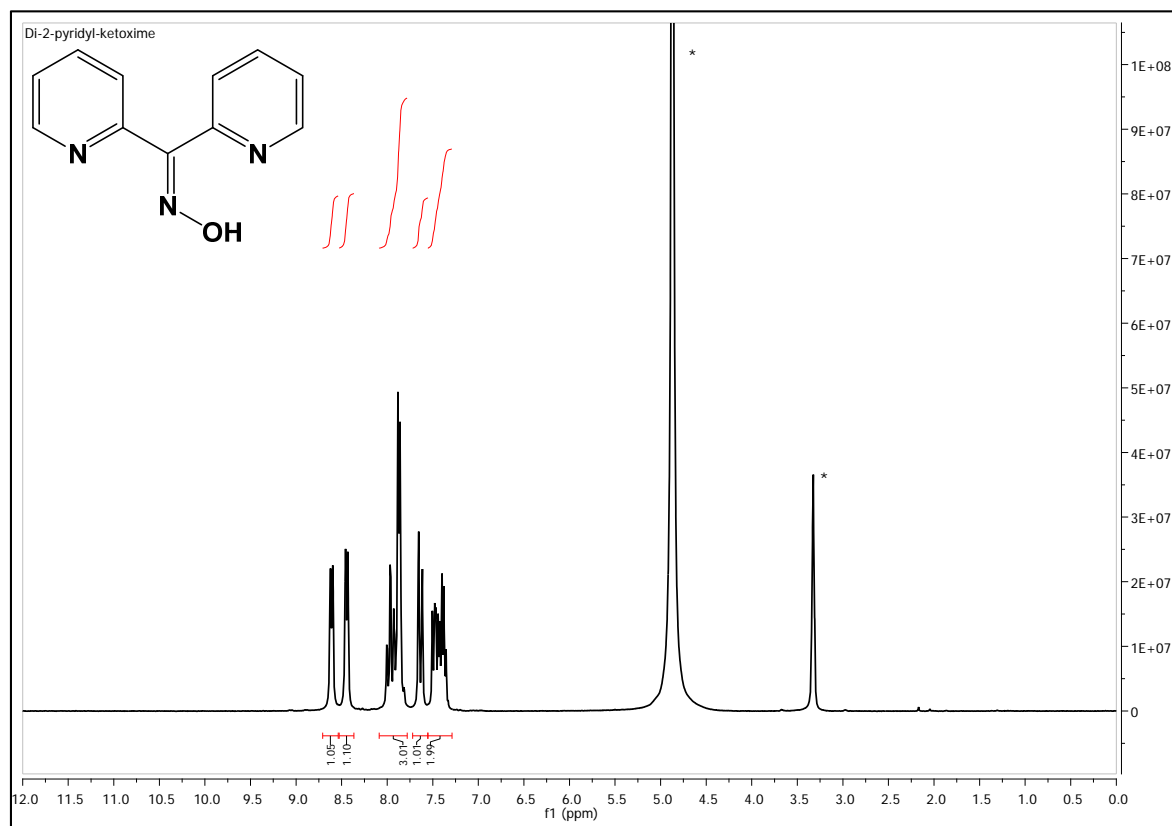


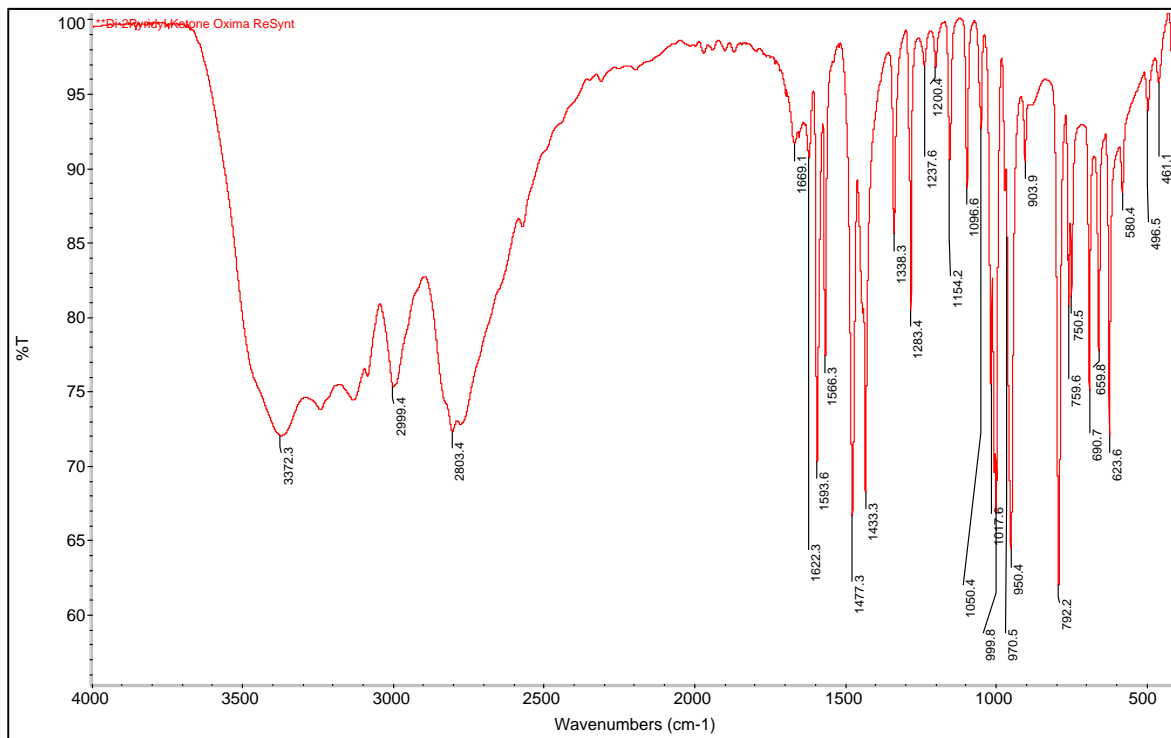
Natural aminoacids: name, three letter and one letter symbols

<i>Name</i>	<i>Symbol</i>	<i>One-Letter</i>	<i>Name</i>	<i>Symbol</i>	<i>One-Letter</i>
Alanine	Ala	A	Leucine	Leu	L
Arginine	Arg	R	Lysine	Lys	K
Asparagine	Asn	N	Methionine	Met	M
Aspartic Acid	Asp	D	Phenylalanine	Phe	F
Cysteine	Cys	C	Proline	Pro	P
Glutamine	Gln	Q	Serine	Ser	S
Glutamic Acid	Glu	E	Threonine	Thr	T
Glycine	Gly	G	Tryptophan	Trp	W
Histidine	His	H	Tyrosine	Tyr	Y
Isoleucine	Ile	I	Valine	Val	V

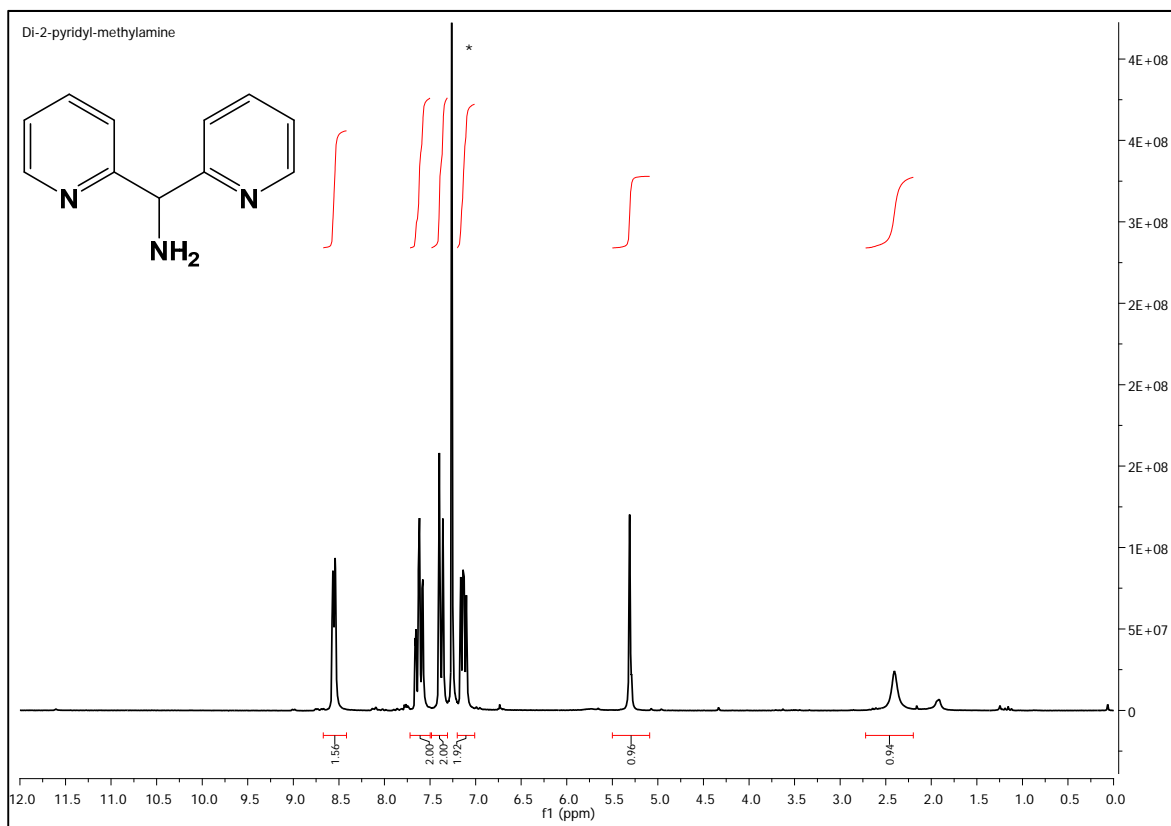
FTIR, NMR and UV-Vis spectra.

-Di-2-pyridyl-ketoxime

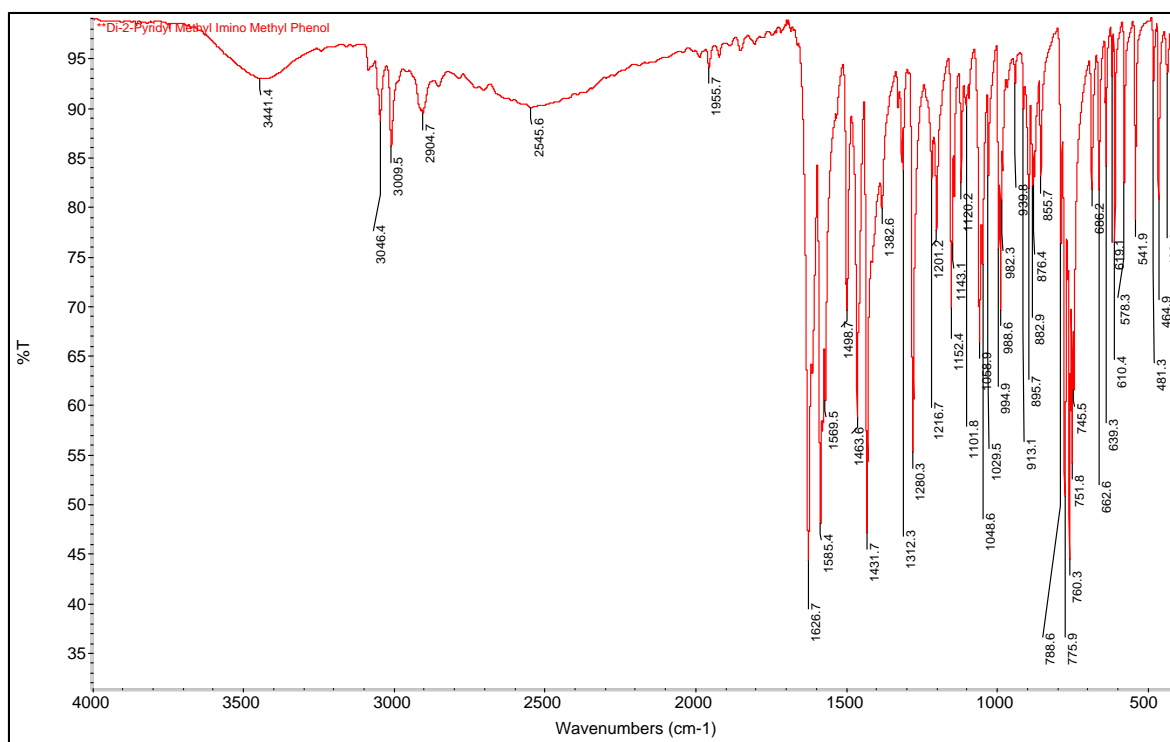
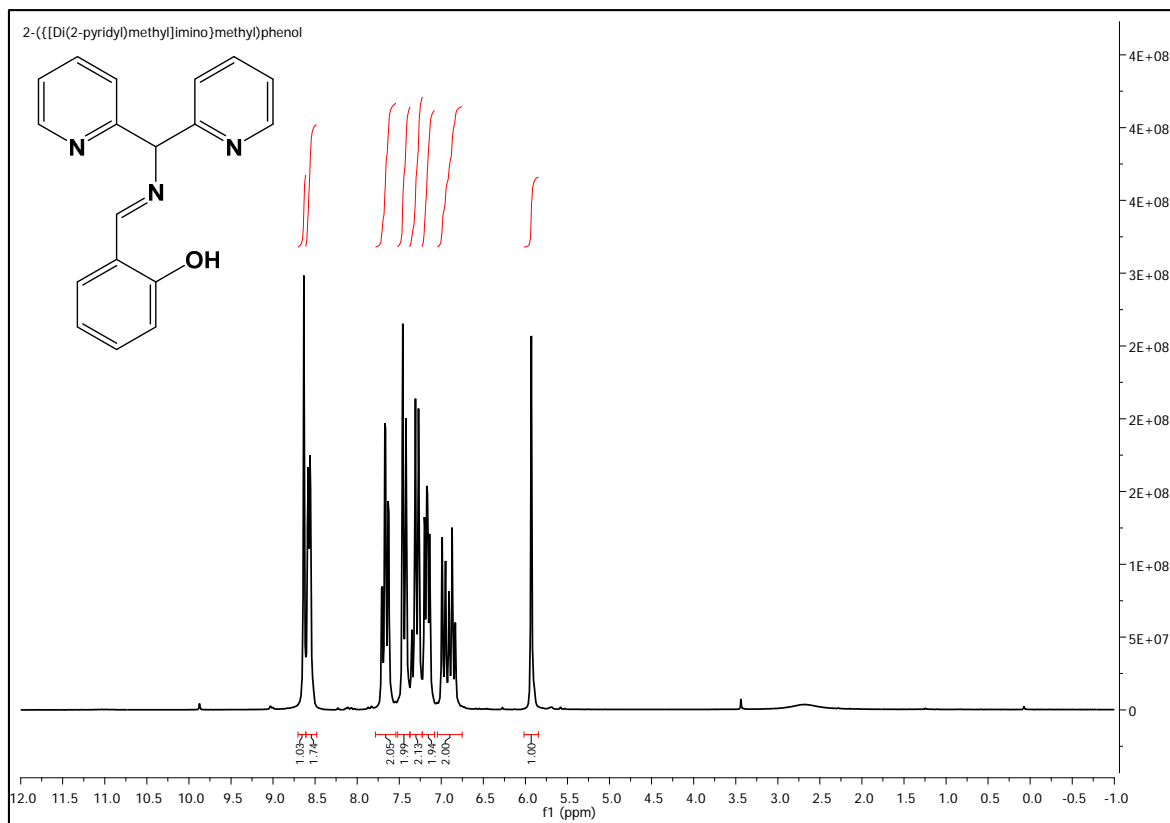




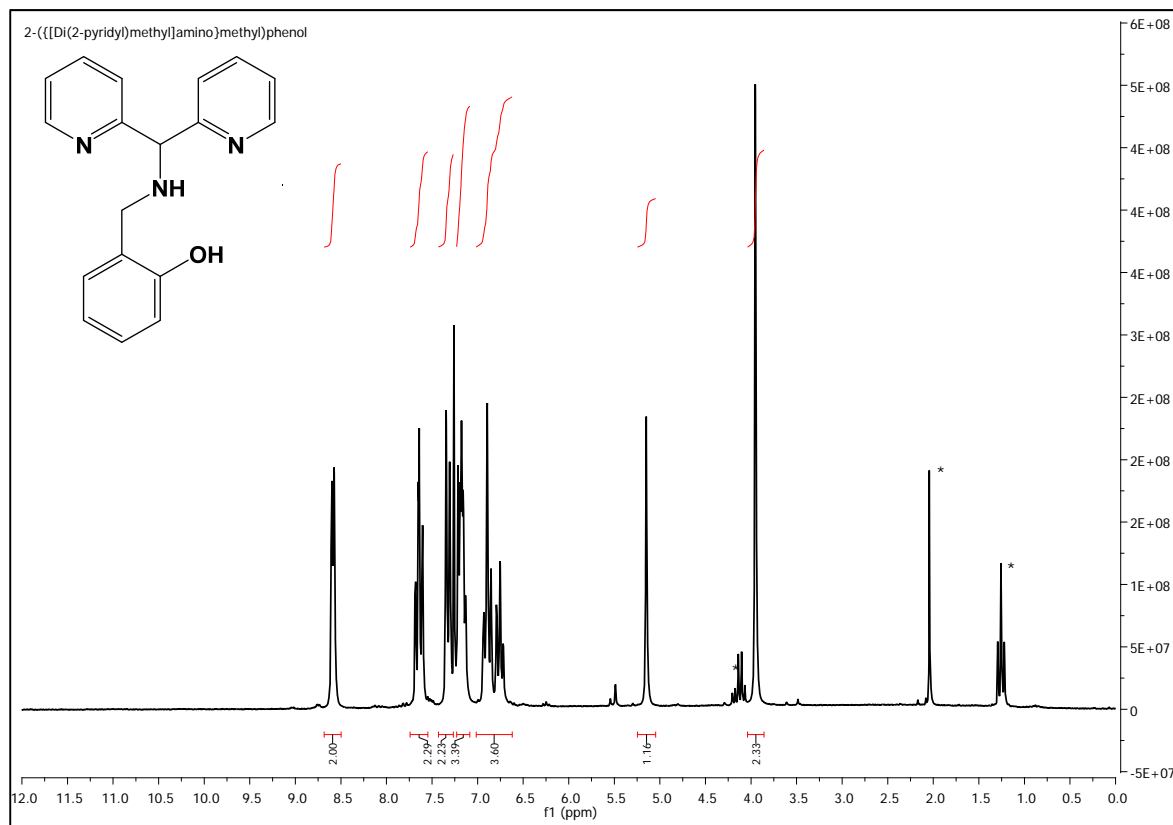
-Di-2-Pyridyl-methylamine



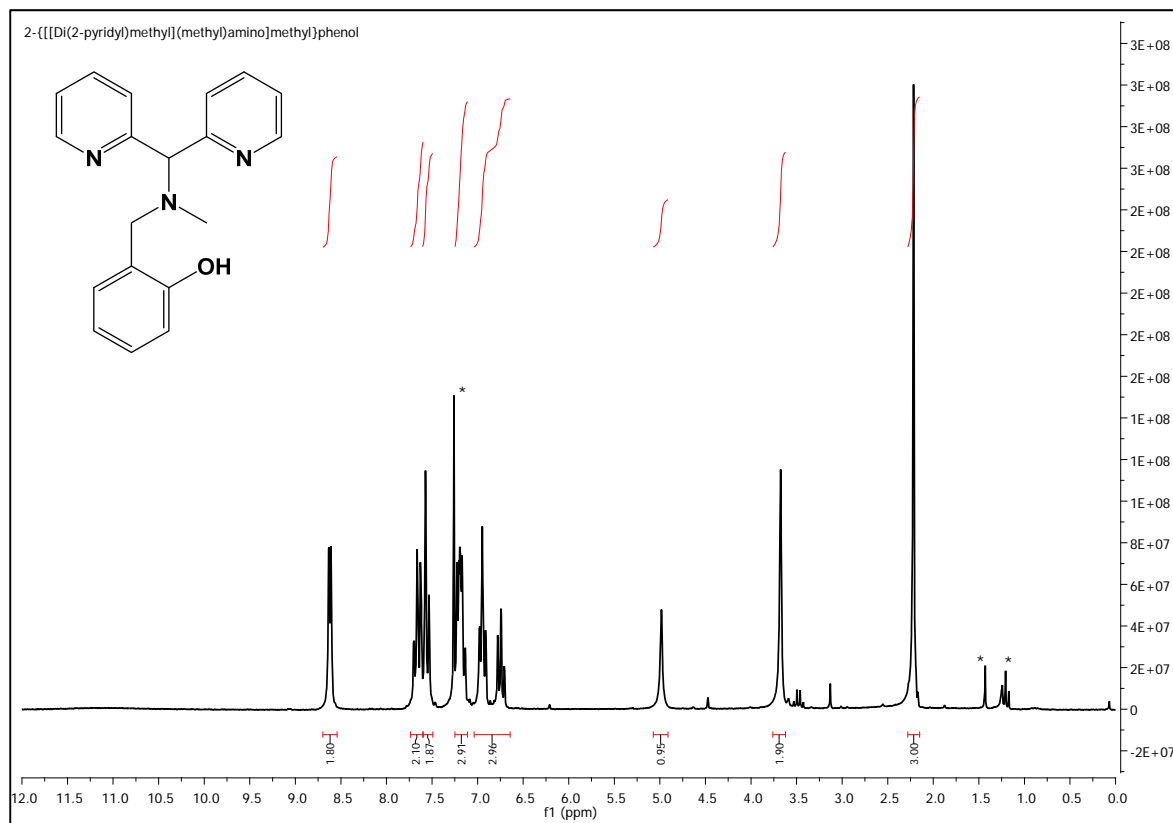
## -2-({[Di(2-pyridyl)methyl]imino}methyl)phenol

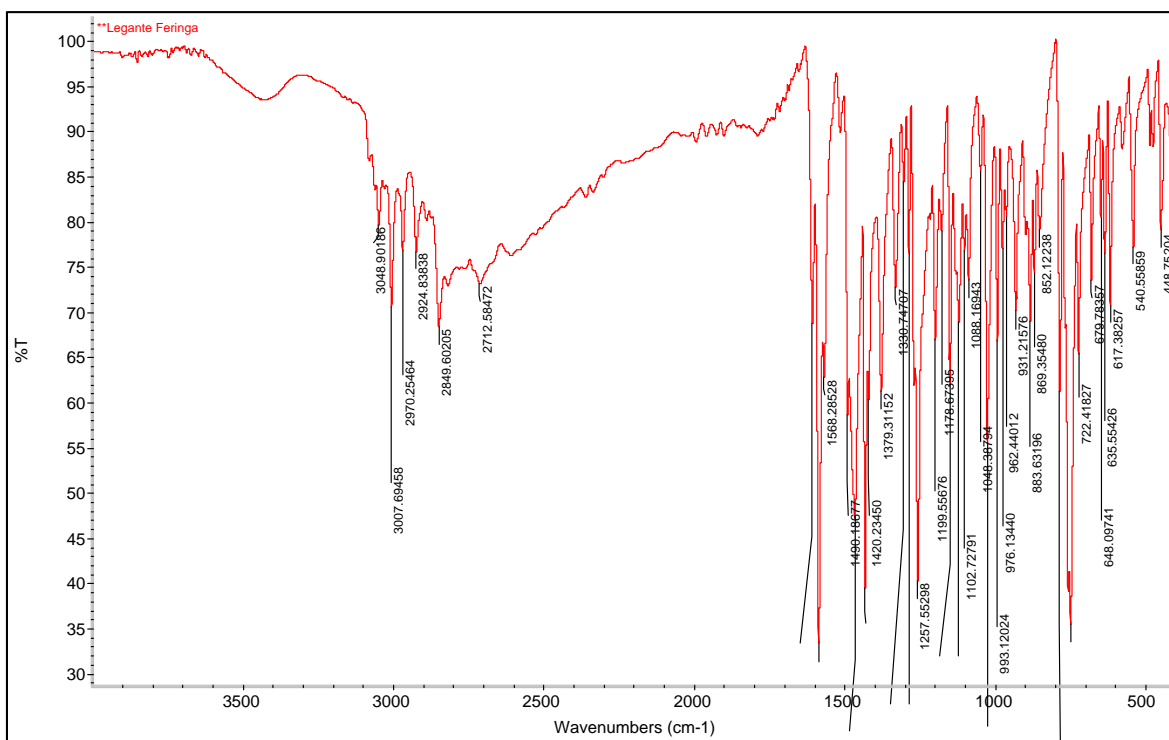


-2-({[Di(2-pyridyl)methyl]amino}methyl)phenol

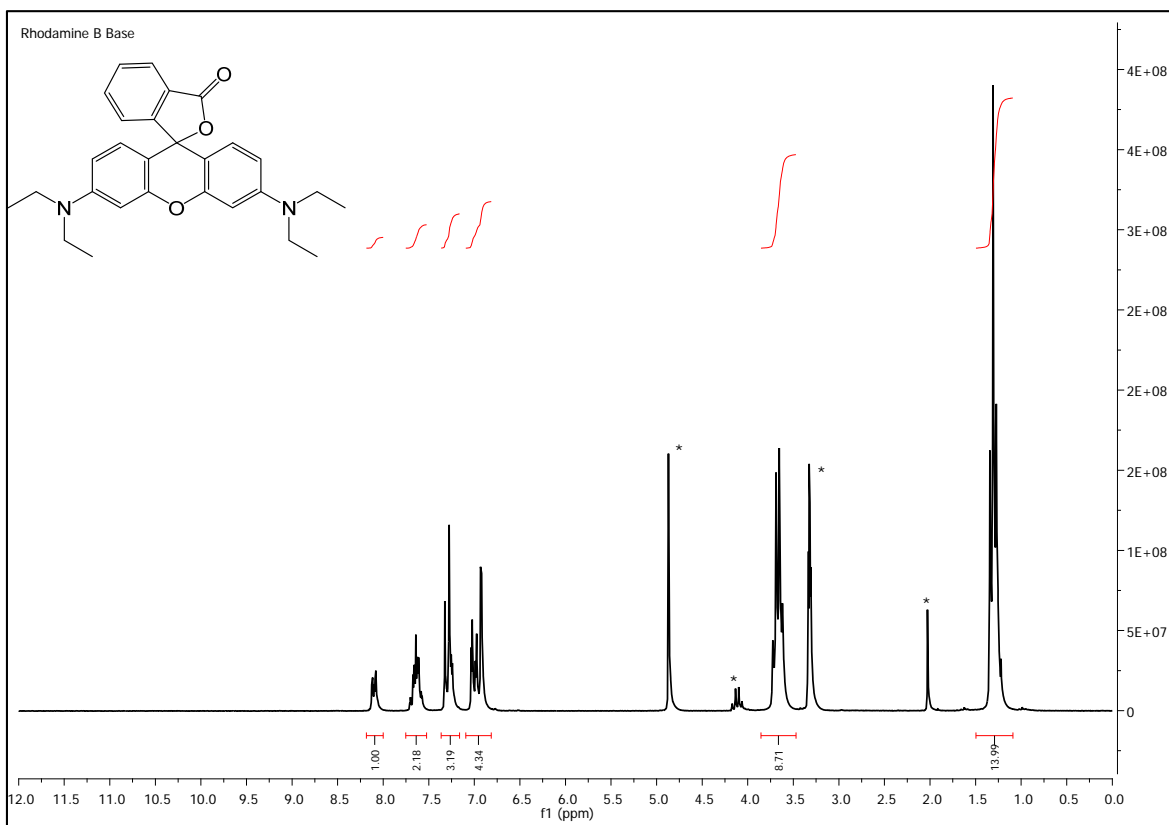


-2-({[Di(2-pyridyl)methyl](methyl)amino}methyl)phenol

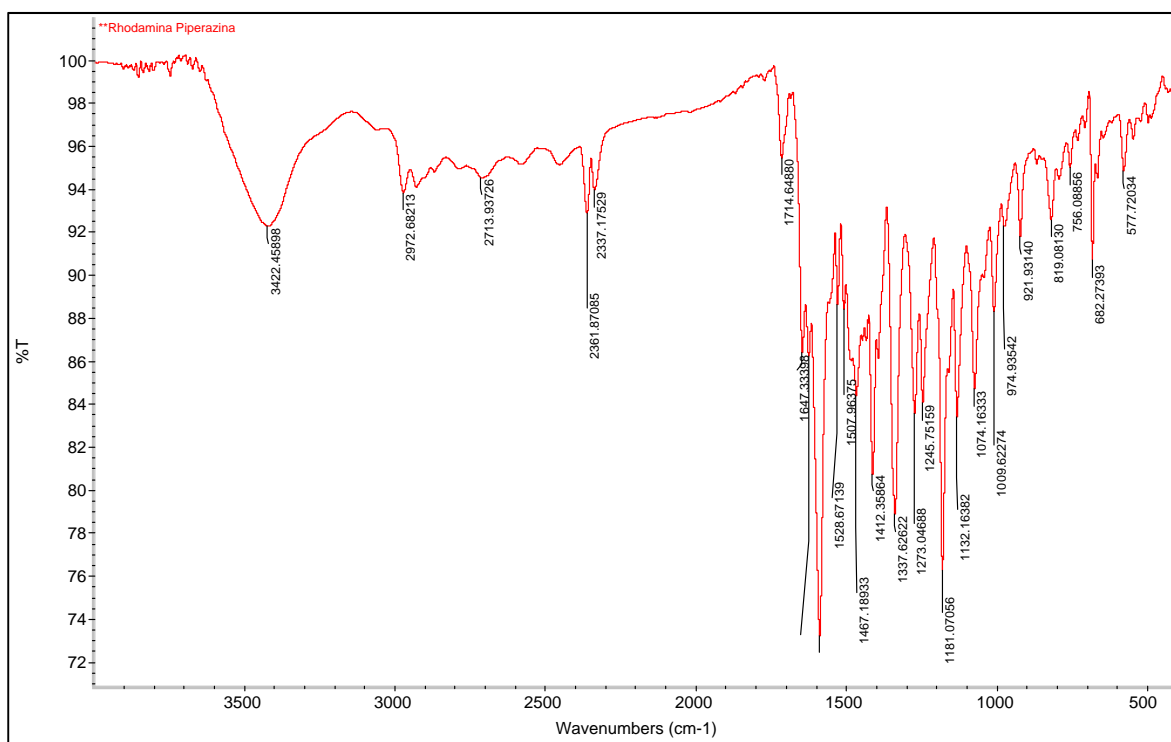
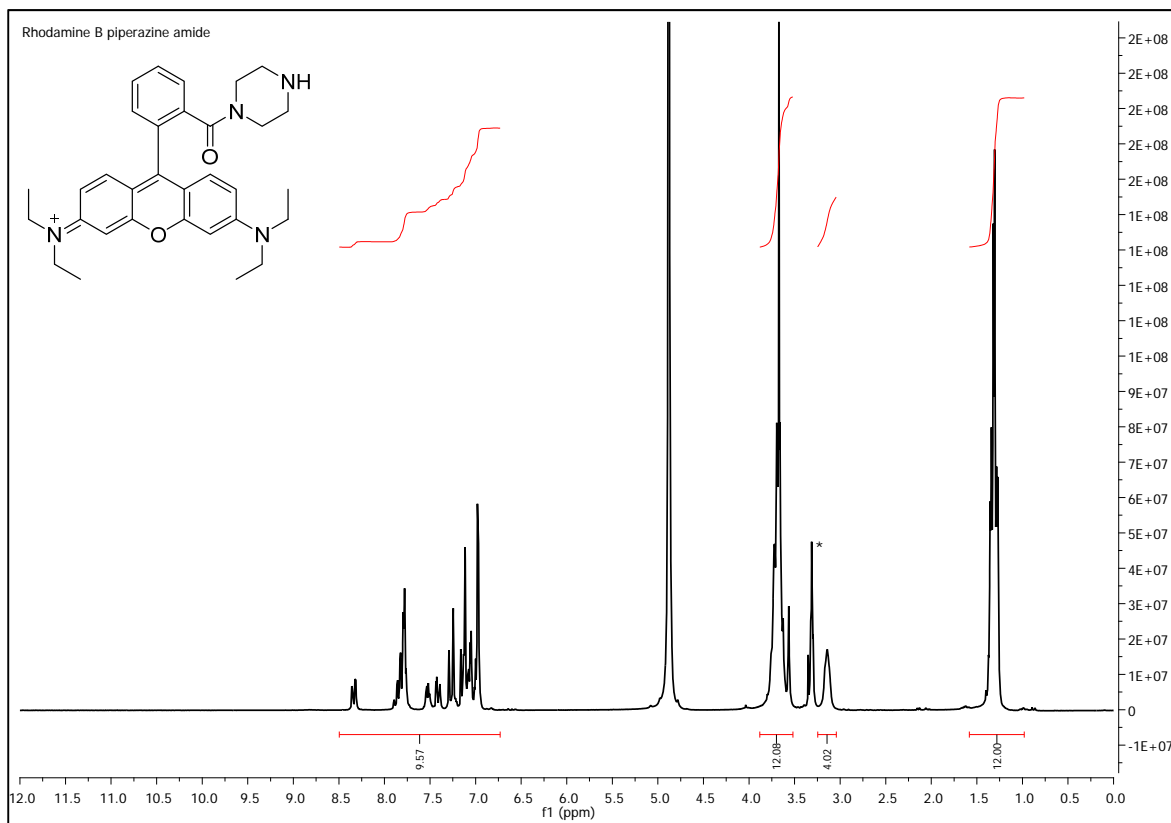




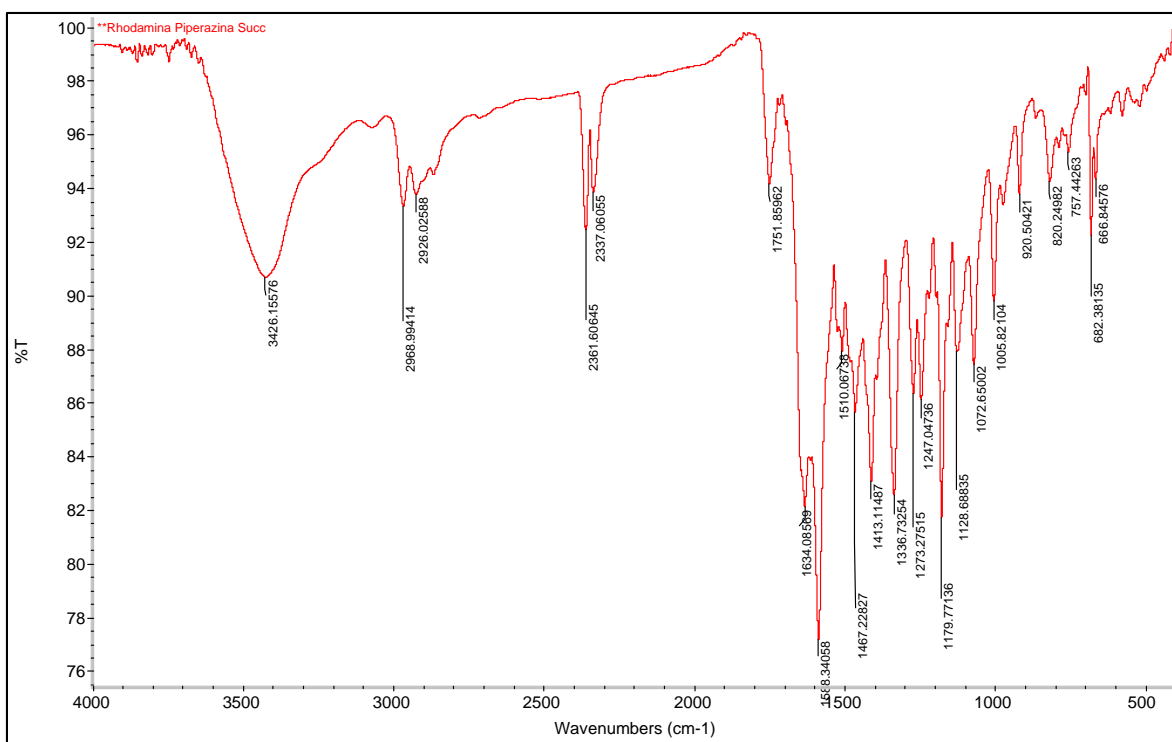
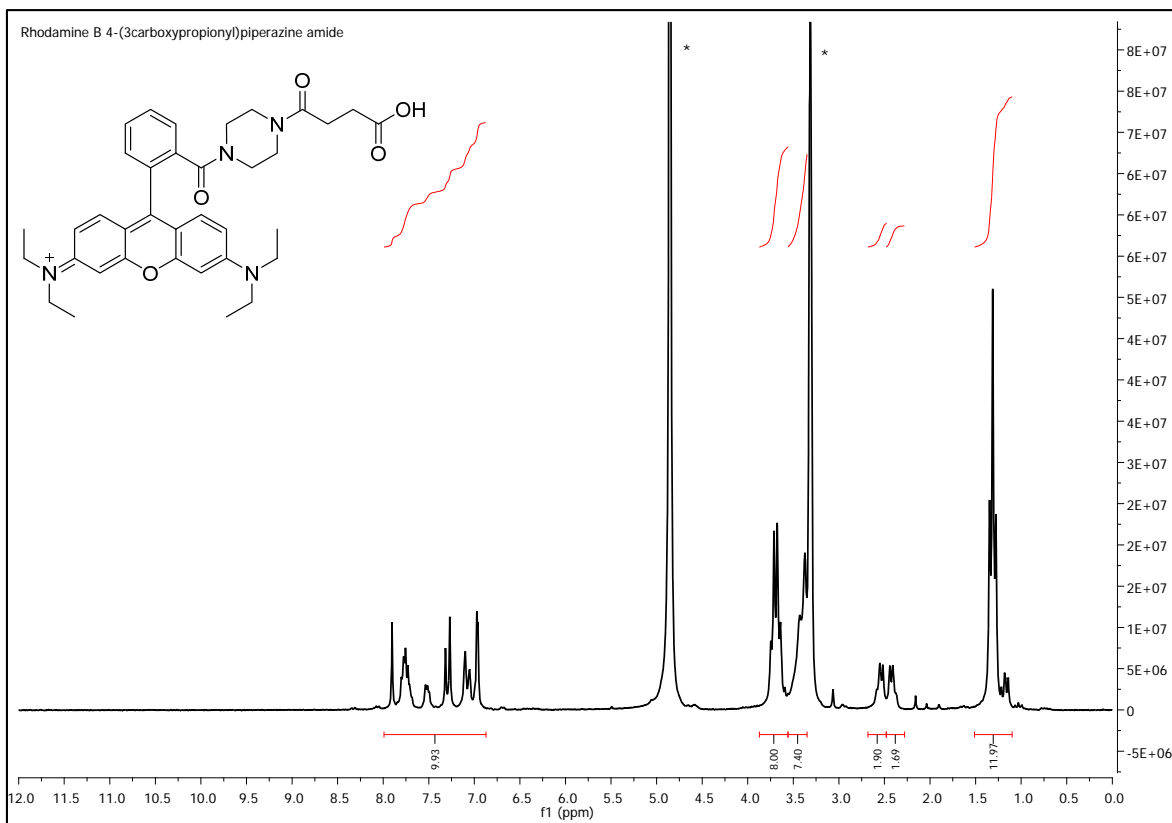
### -Rhodamine B Base



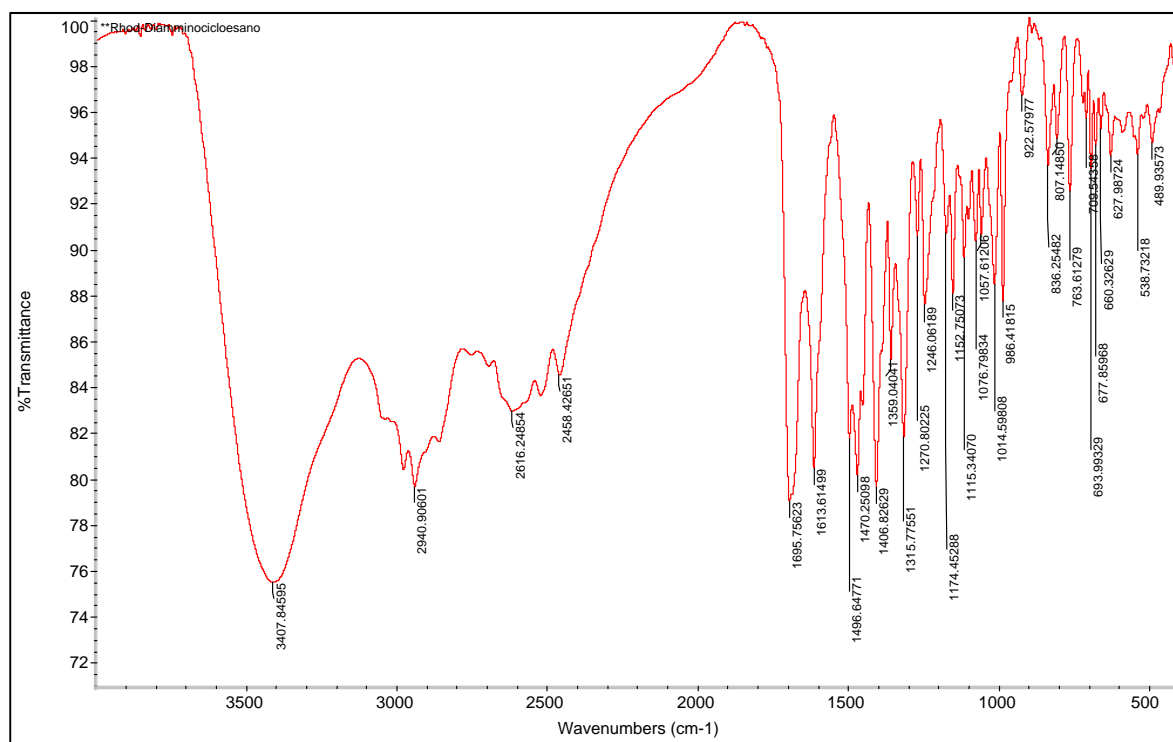
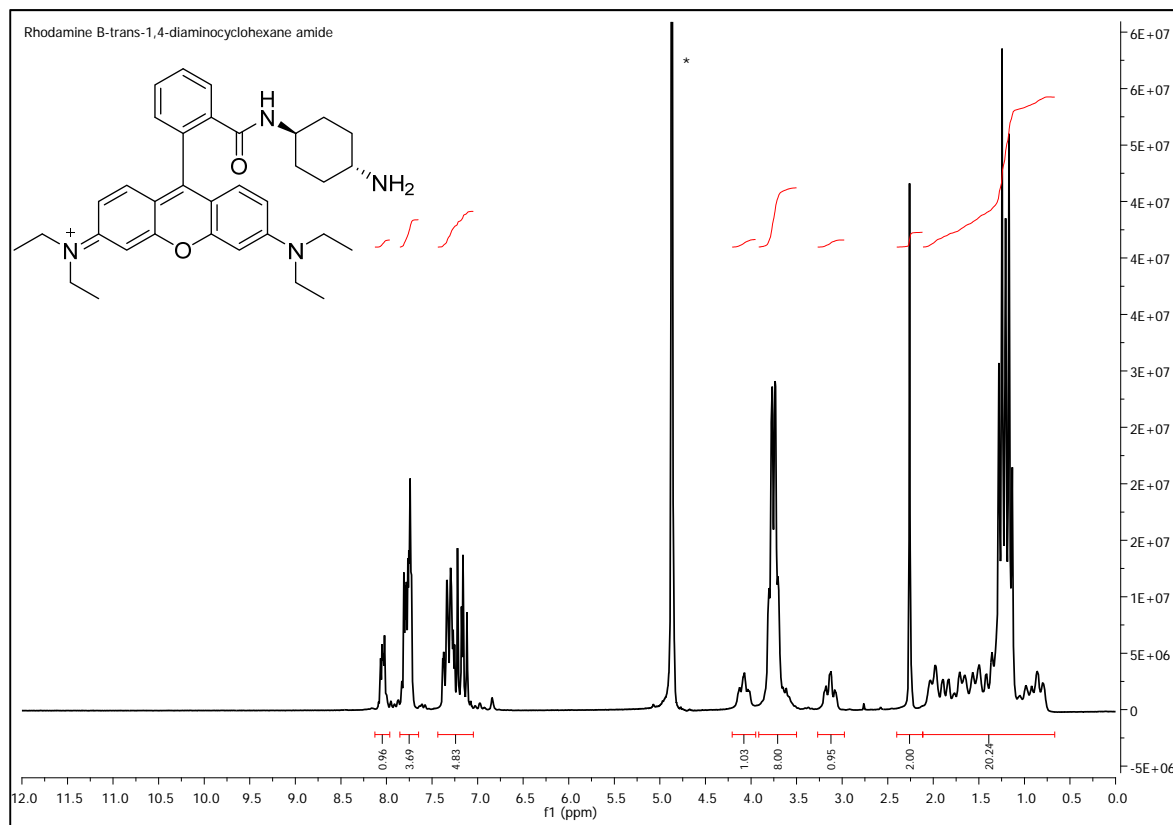
-Rhodamine B Piperazine Amide



## -Rhodamine B 4-(3carboxypropionyl)piperazine Amide

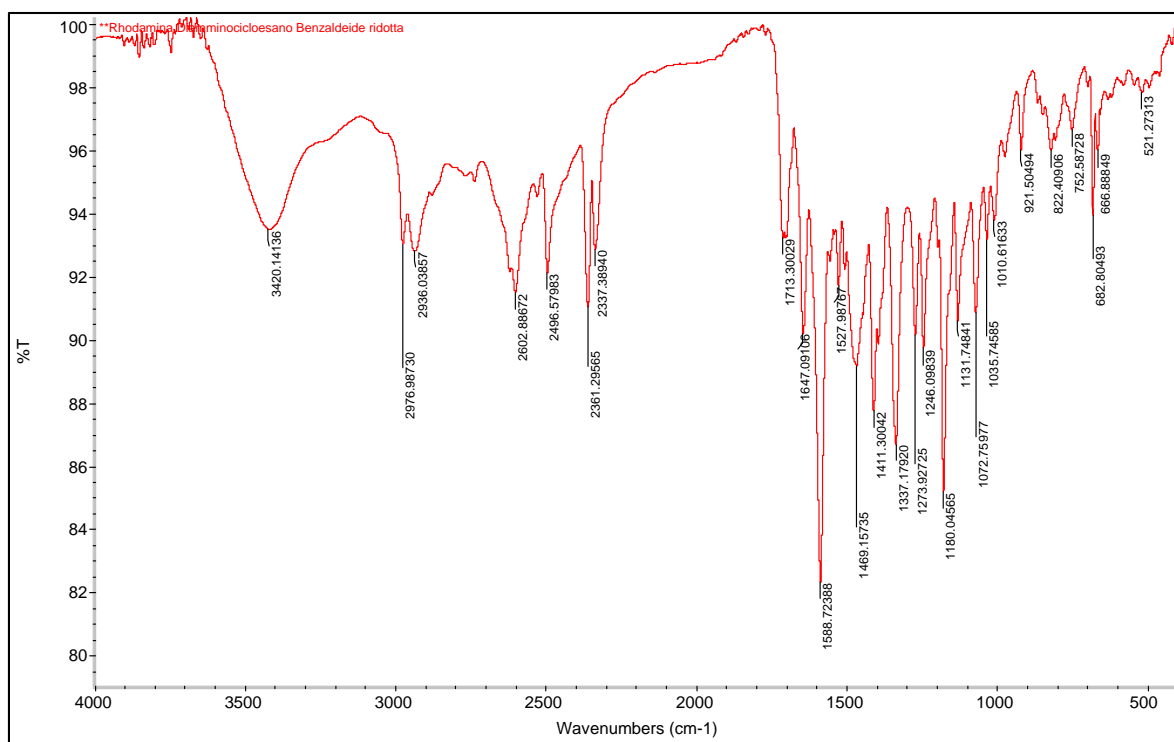
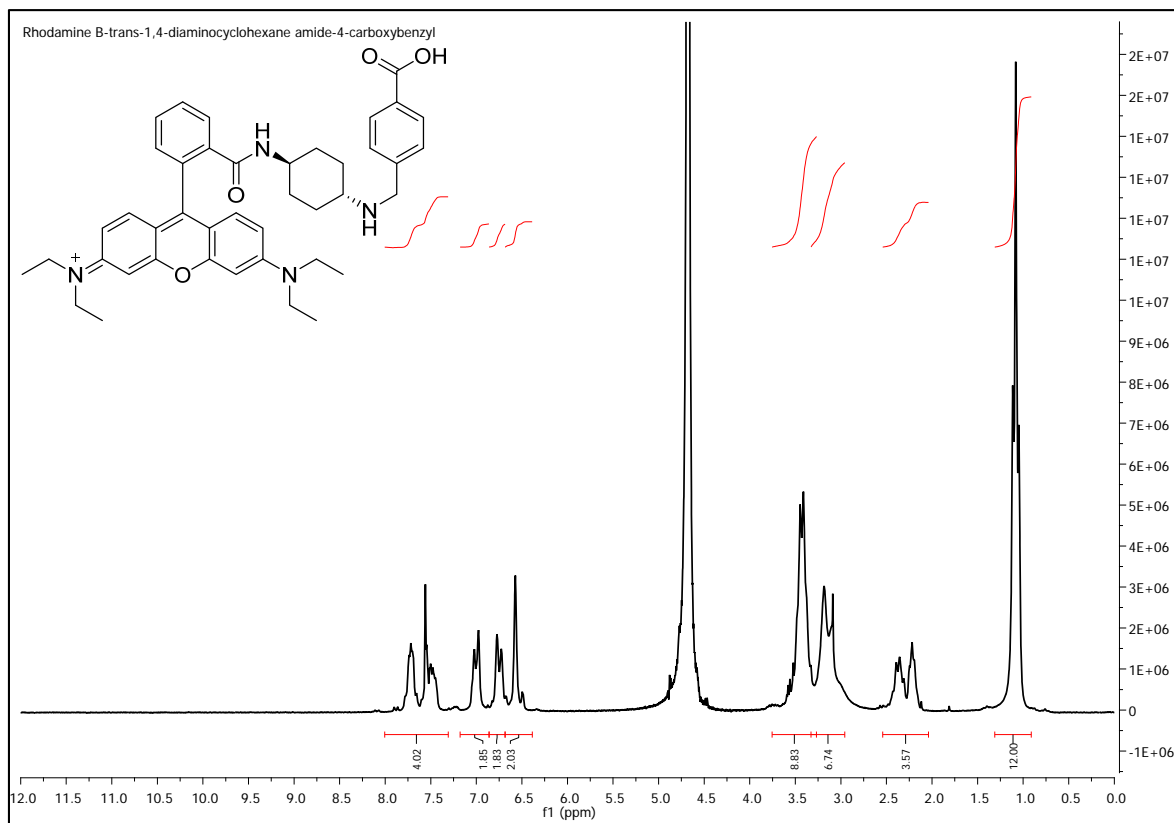


-Rhodamine B-trans-1,4-diaminocyclohexane Amide

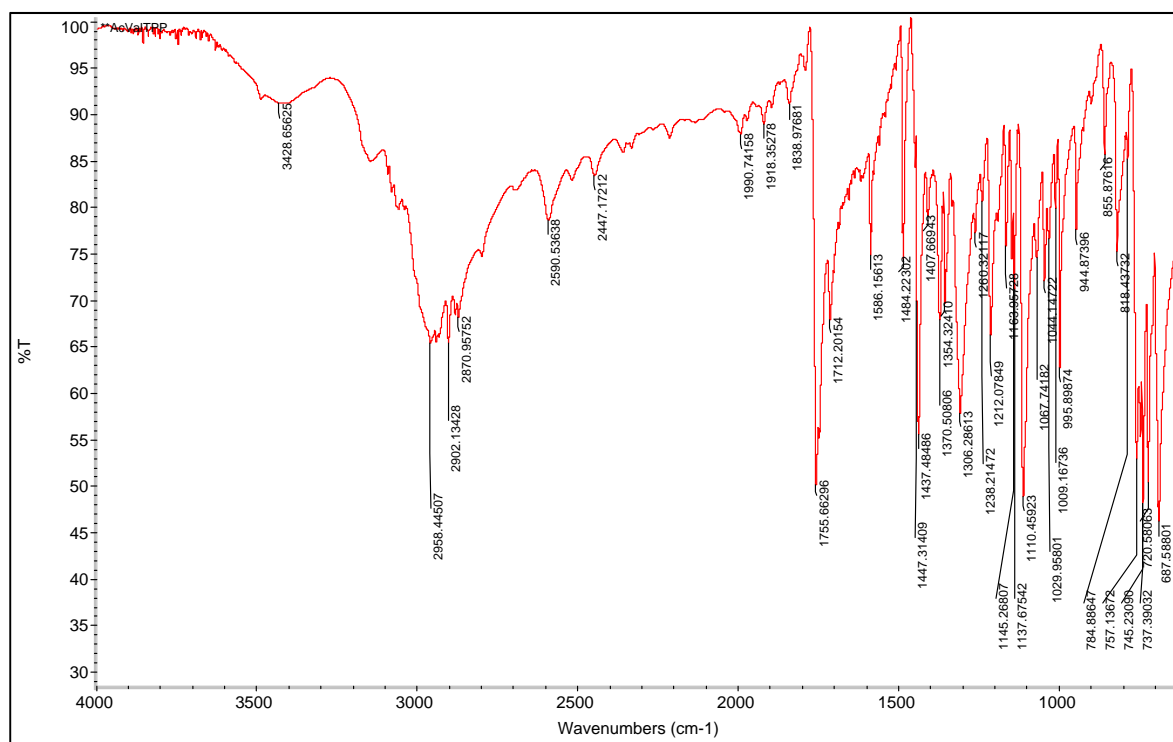
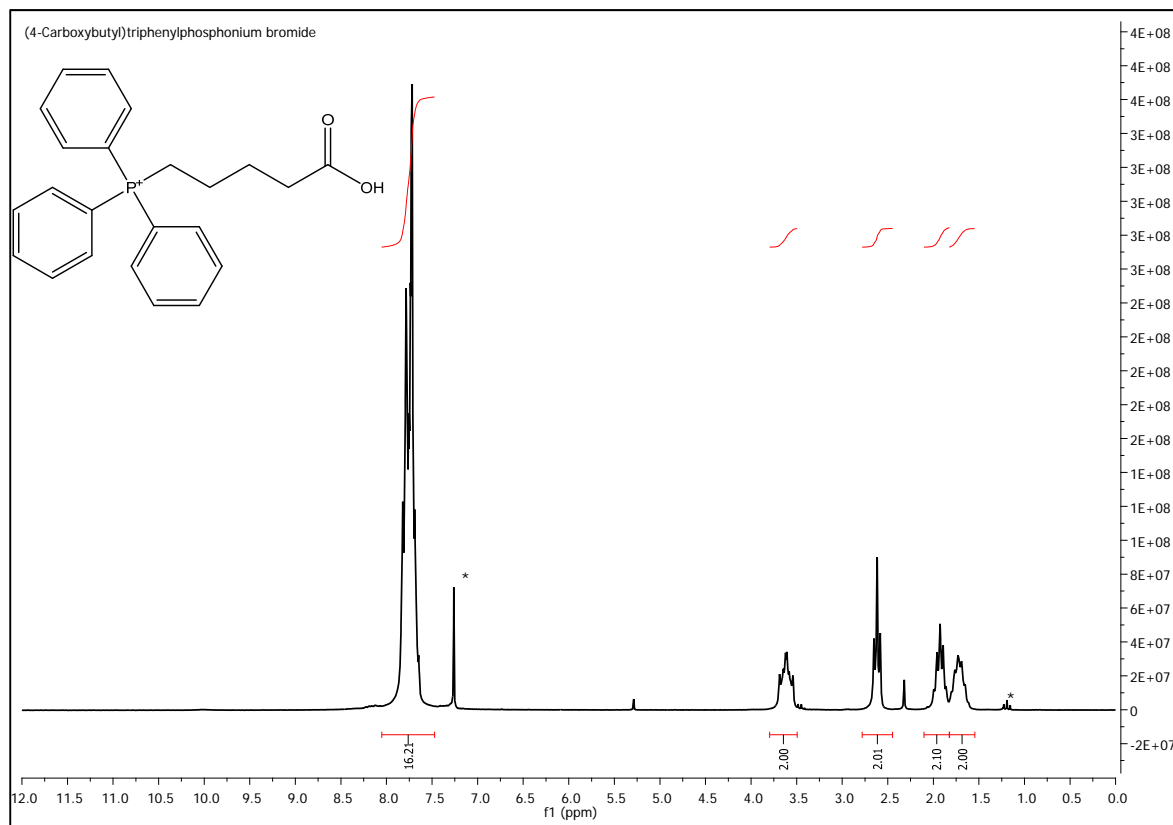




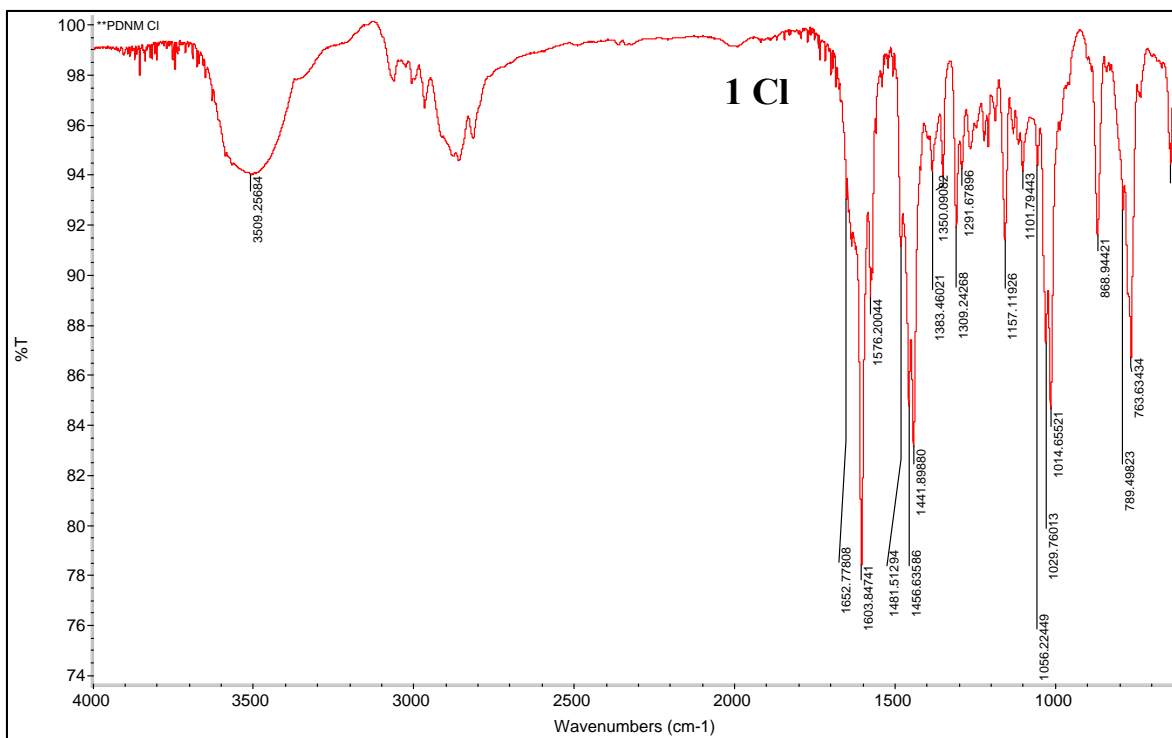
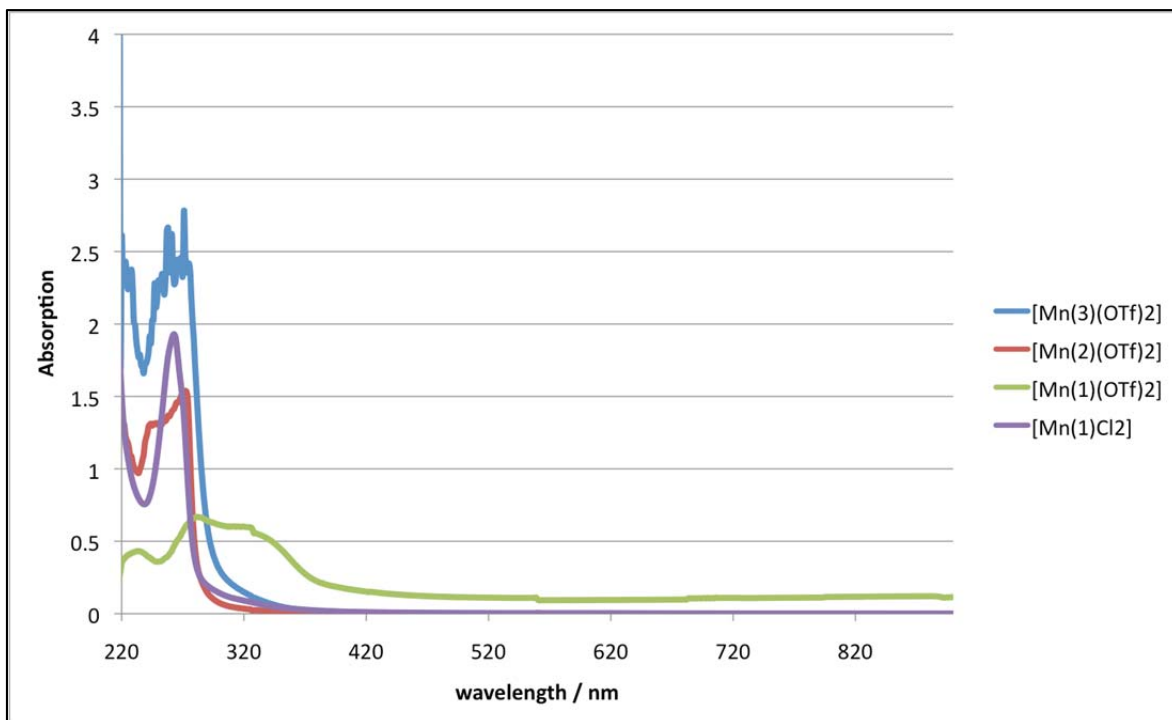
## -Rhodamine B trans-1,4-diaminocyclohexane Amide-4-carboxybenzyl

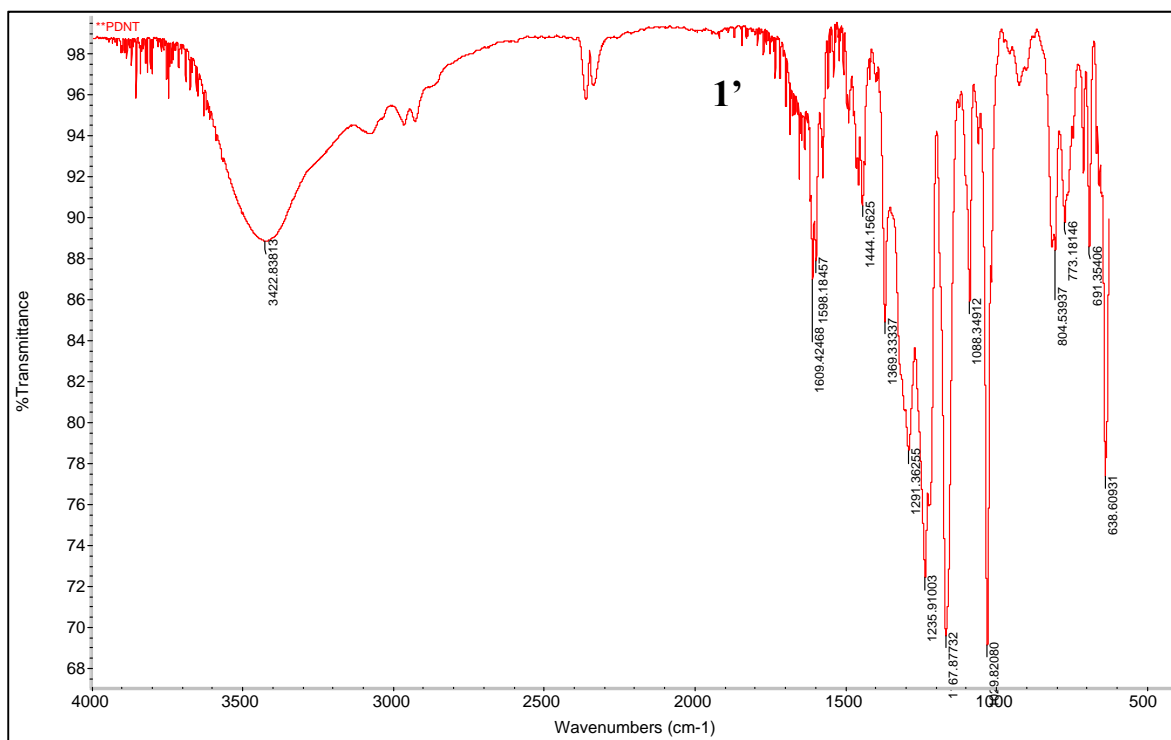
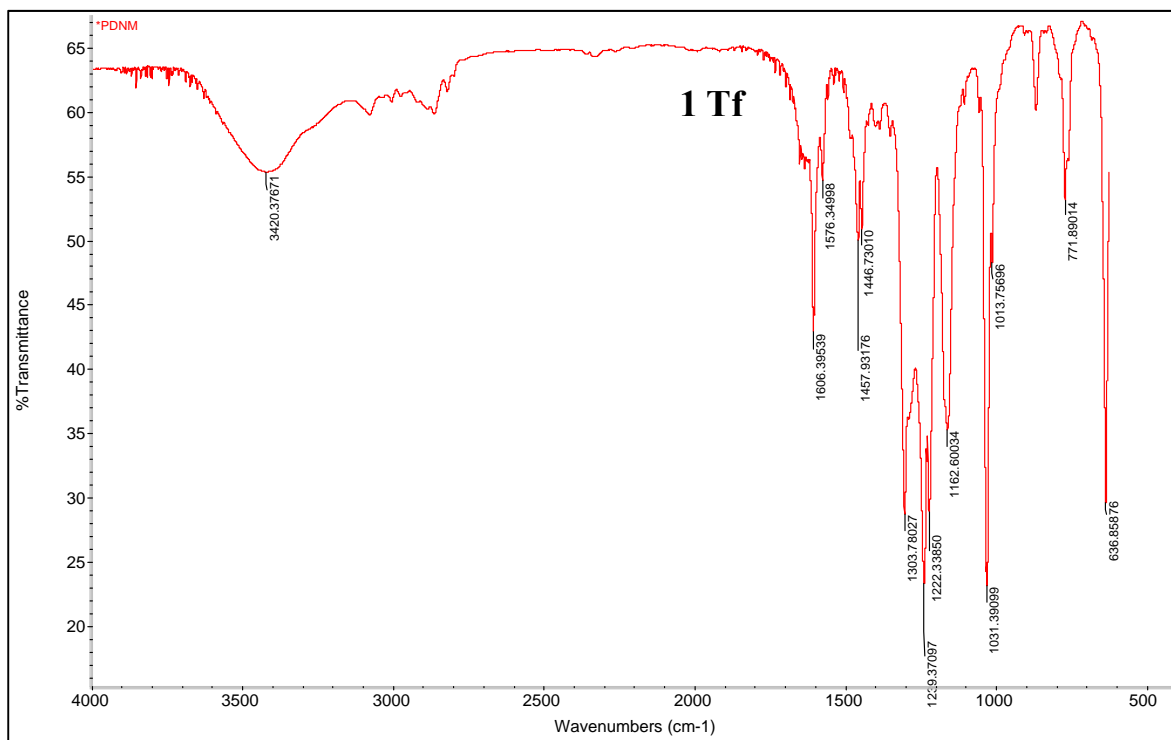


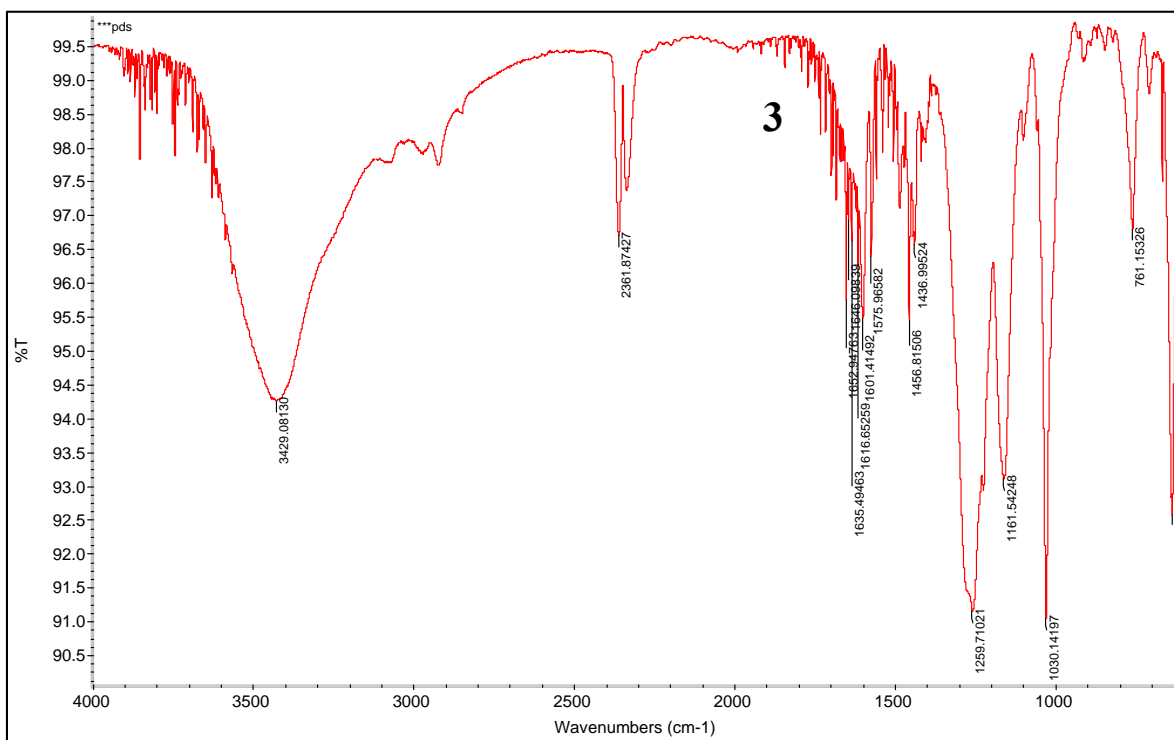
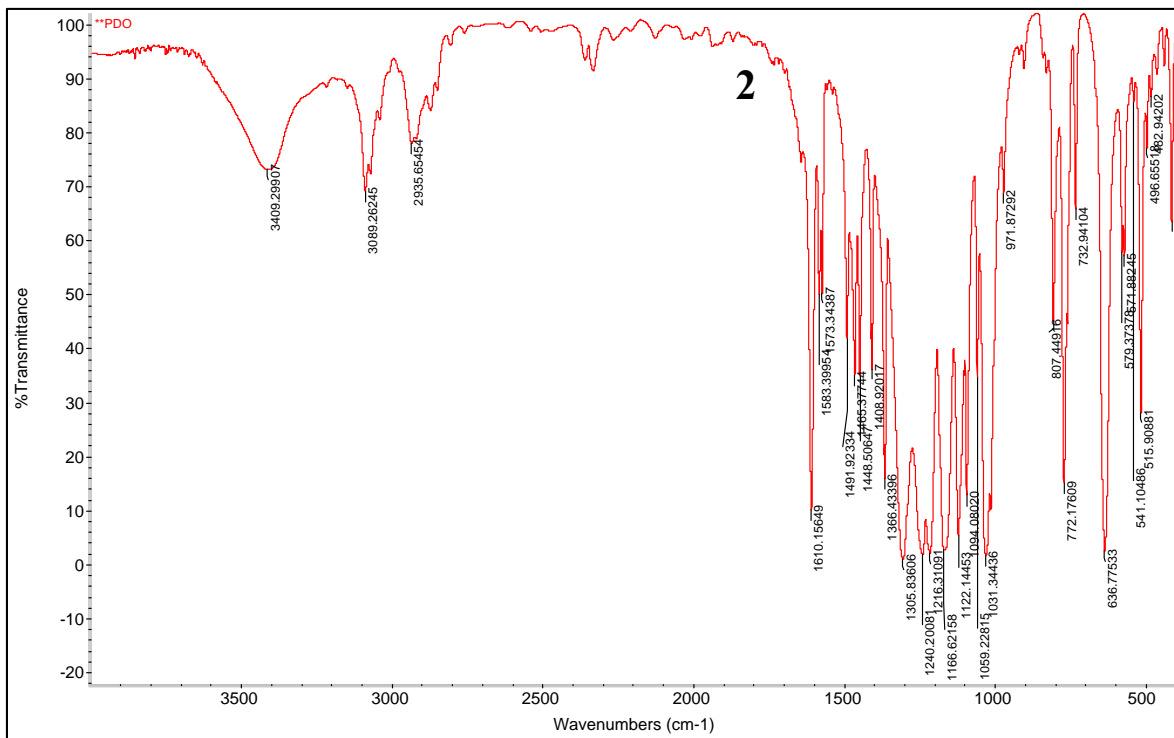
-(4-carboxybutyl)triphenylphosphonium bromide



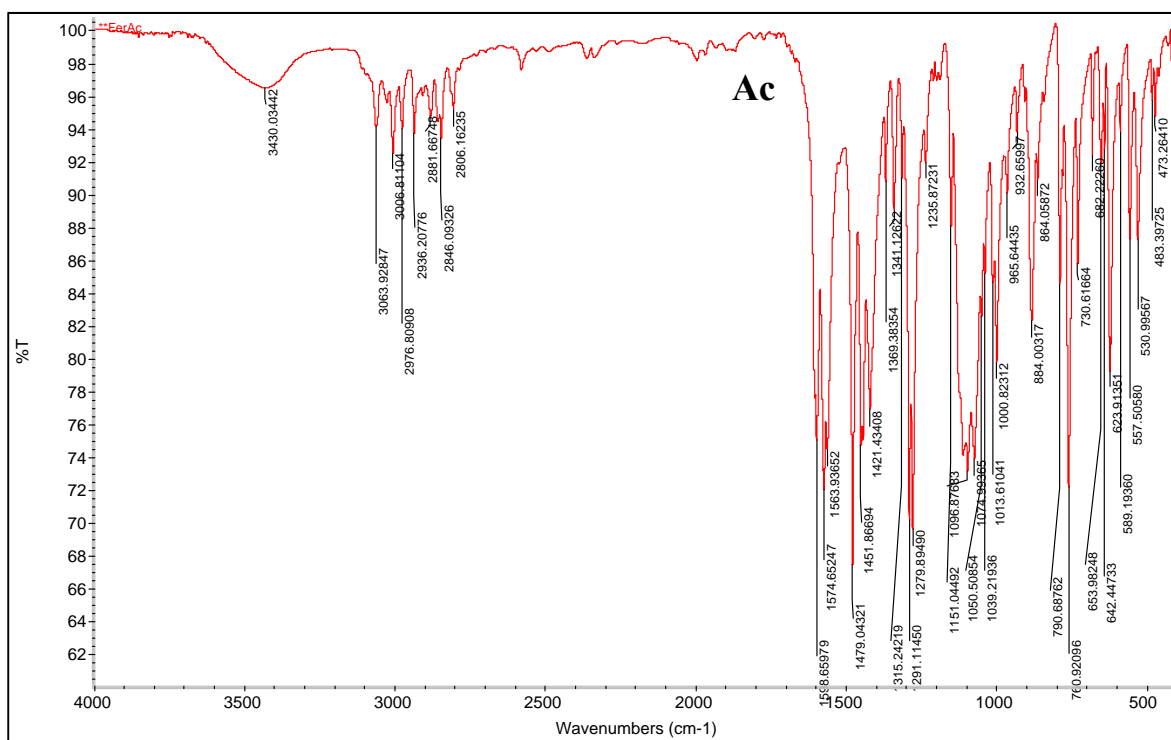
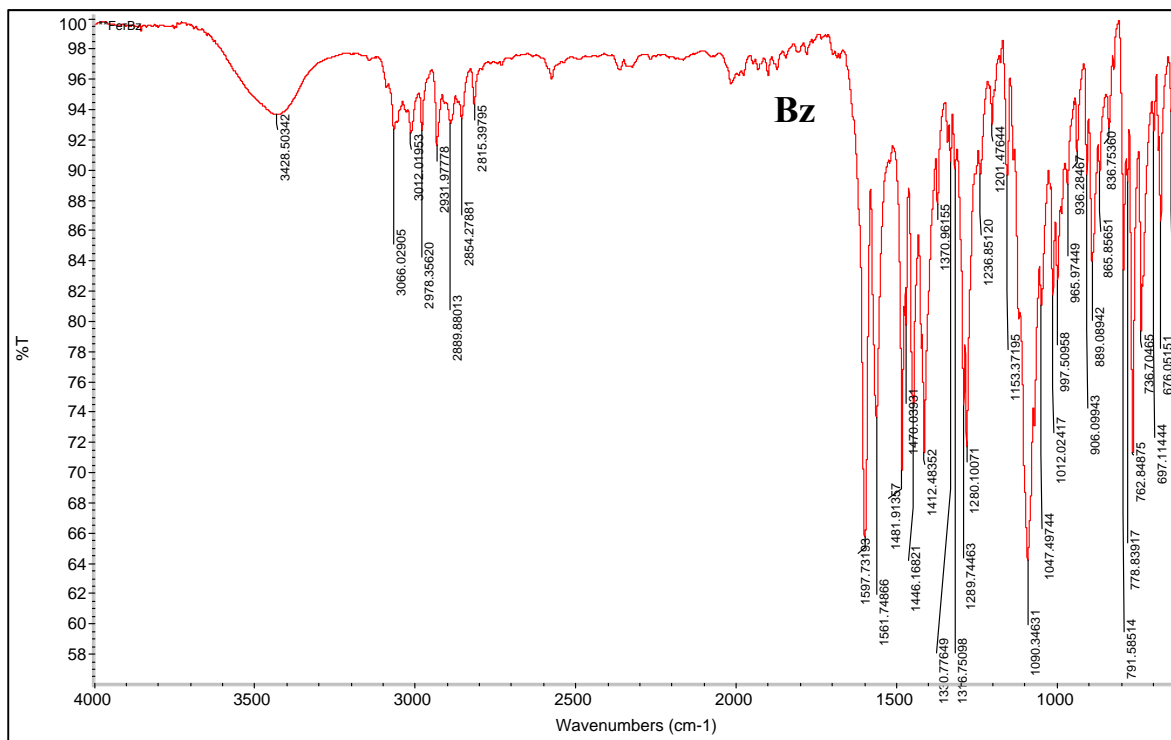
## -Compound 1-3

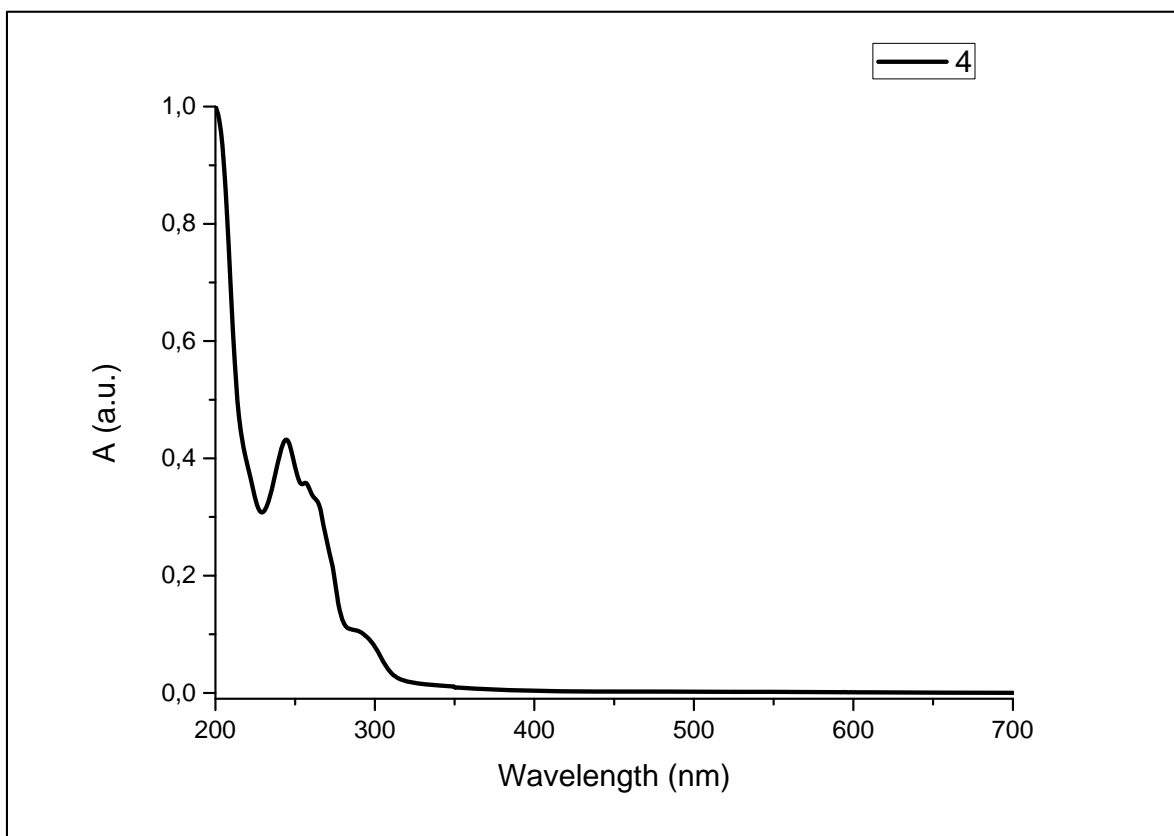
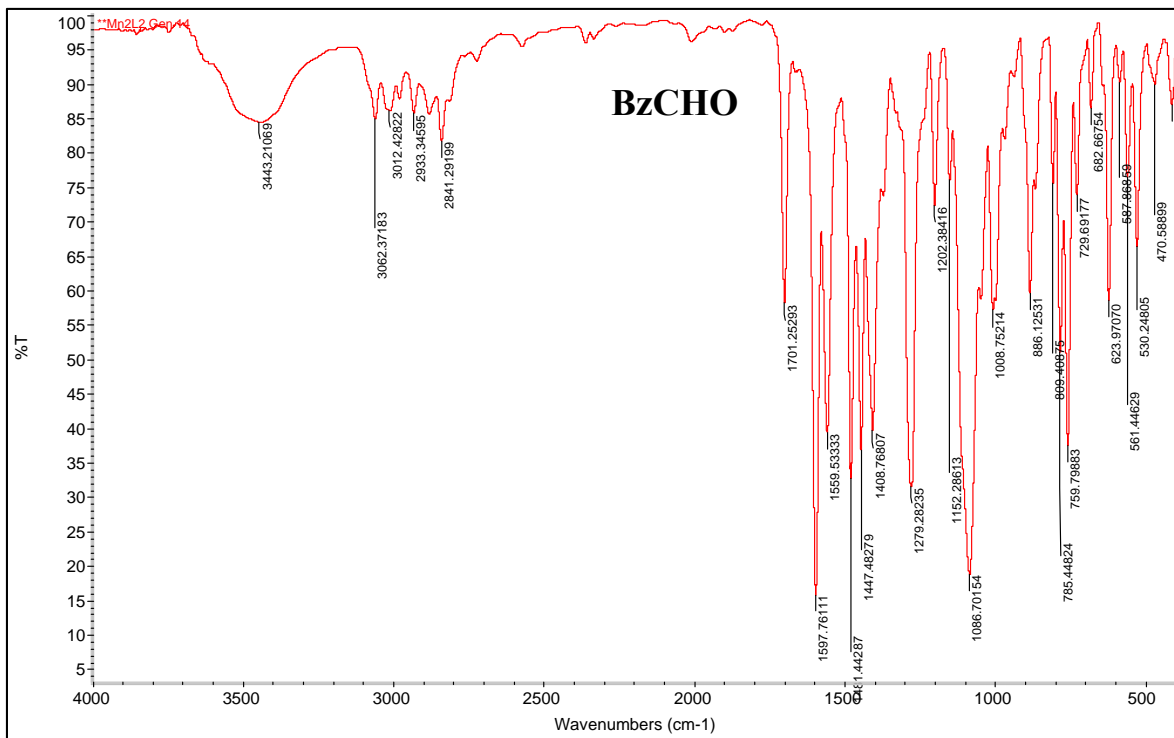


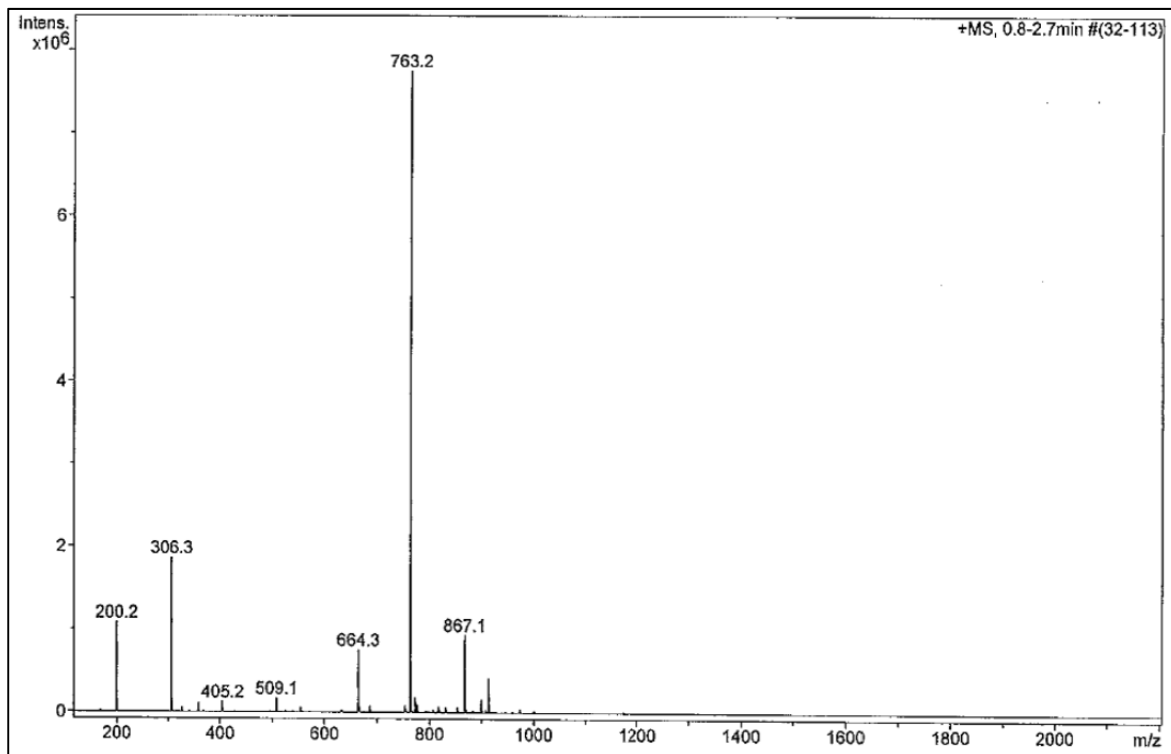




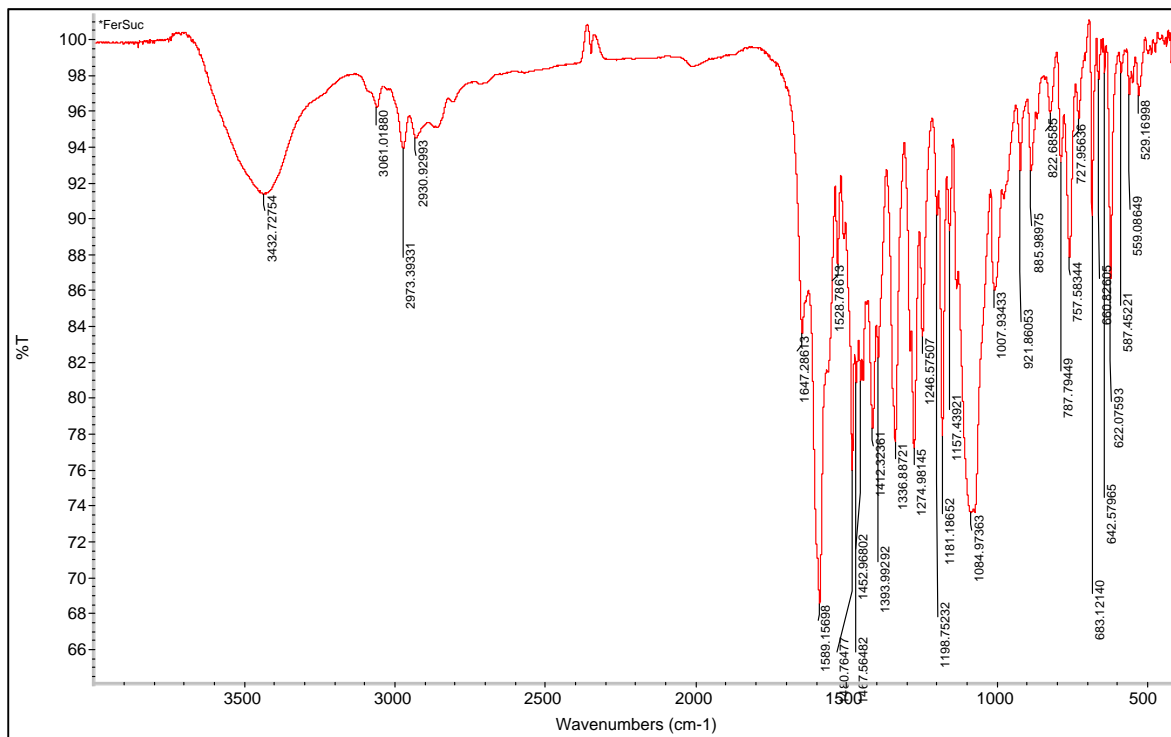
-Compound 4



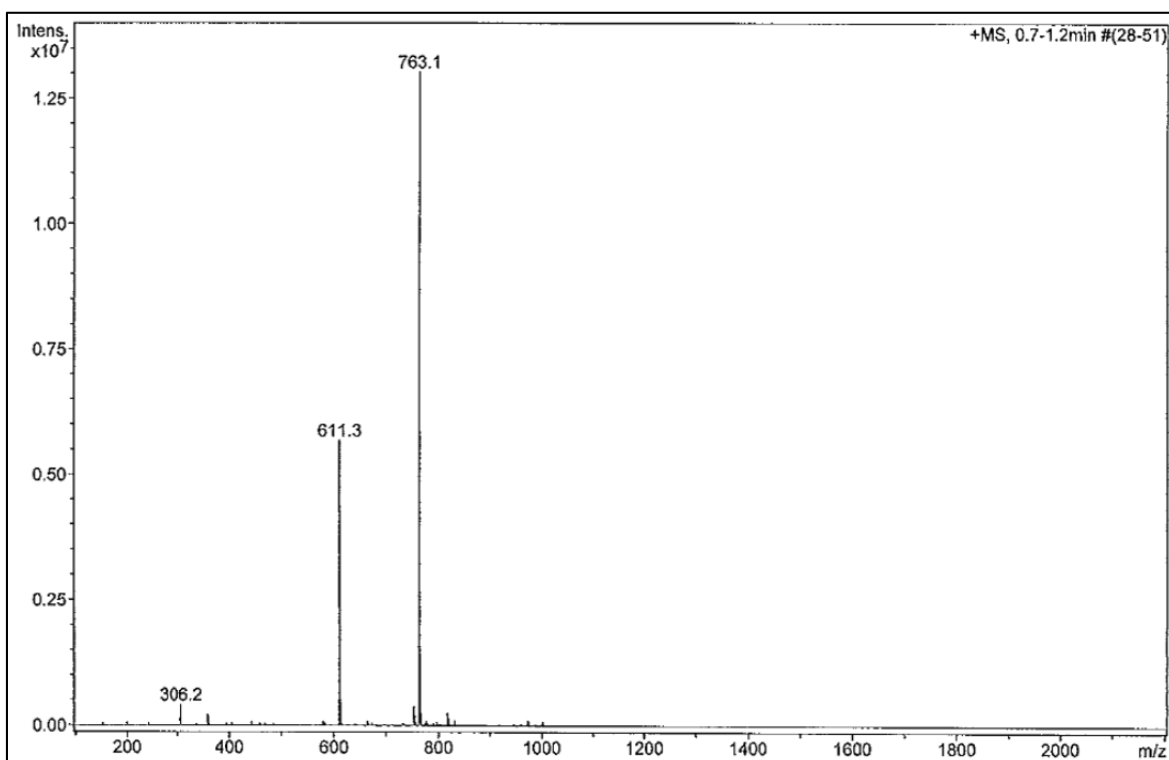
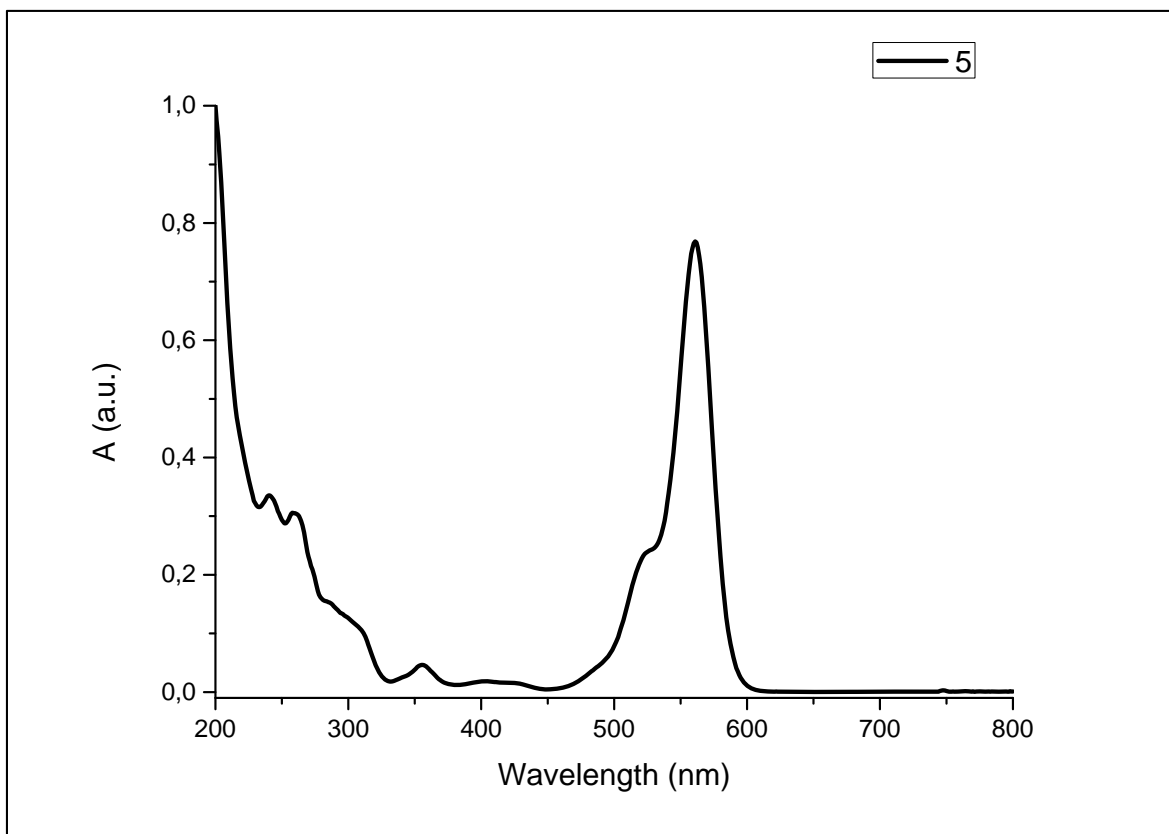




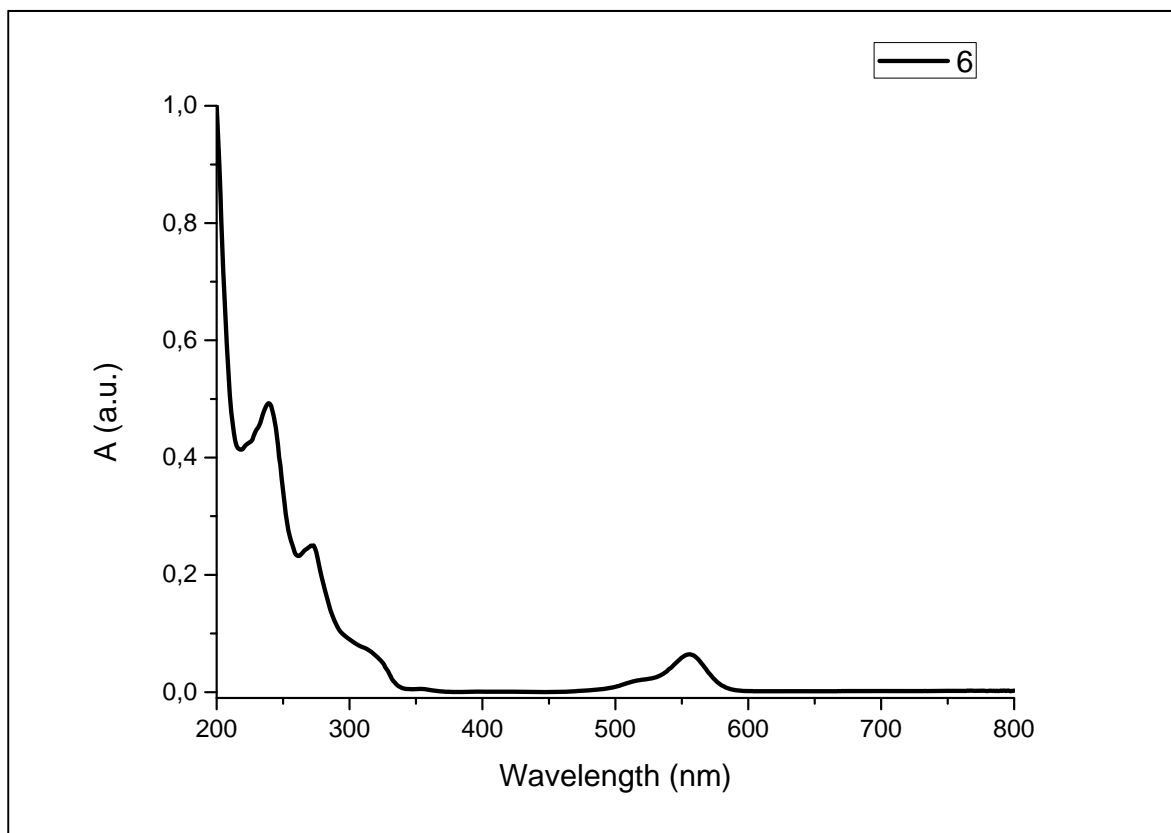
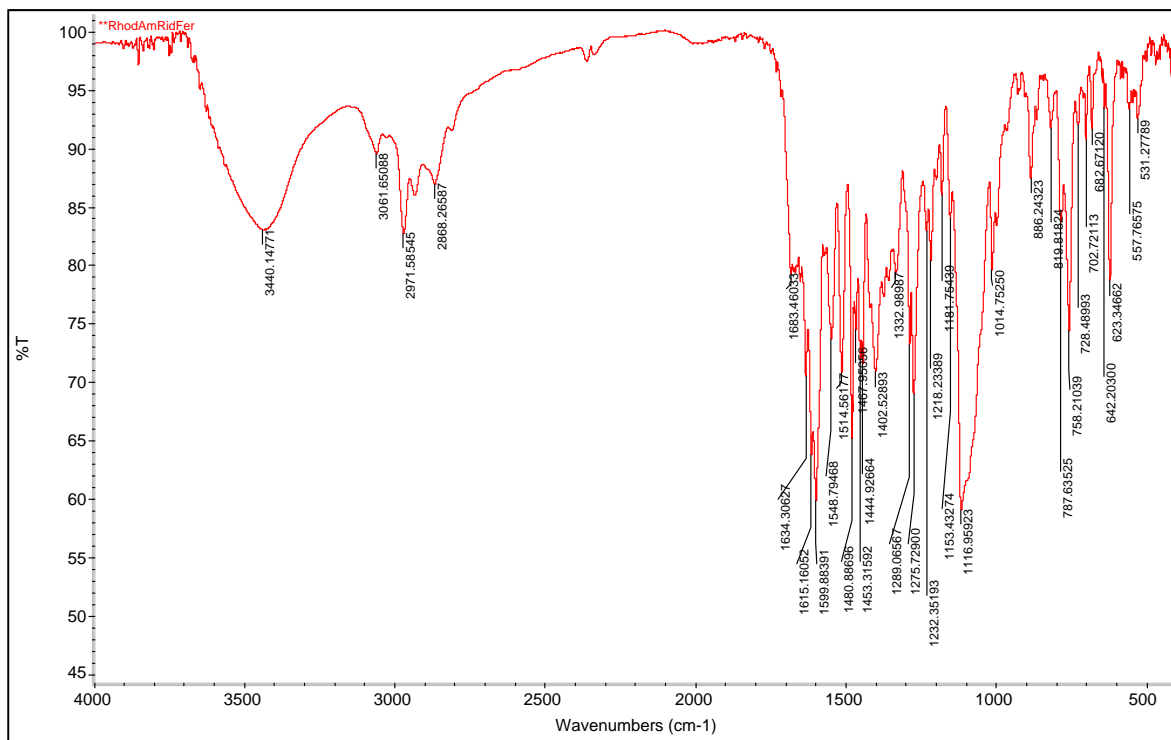
-Compound 5

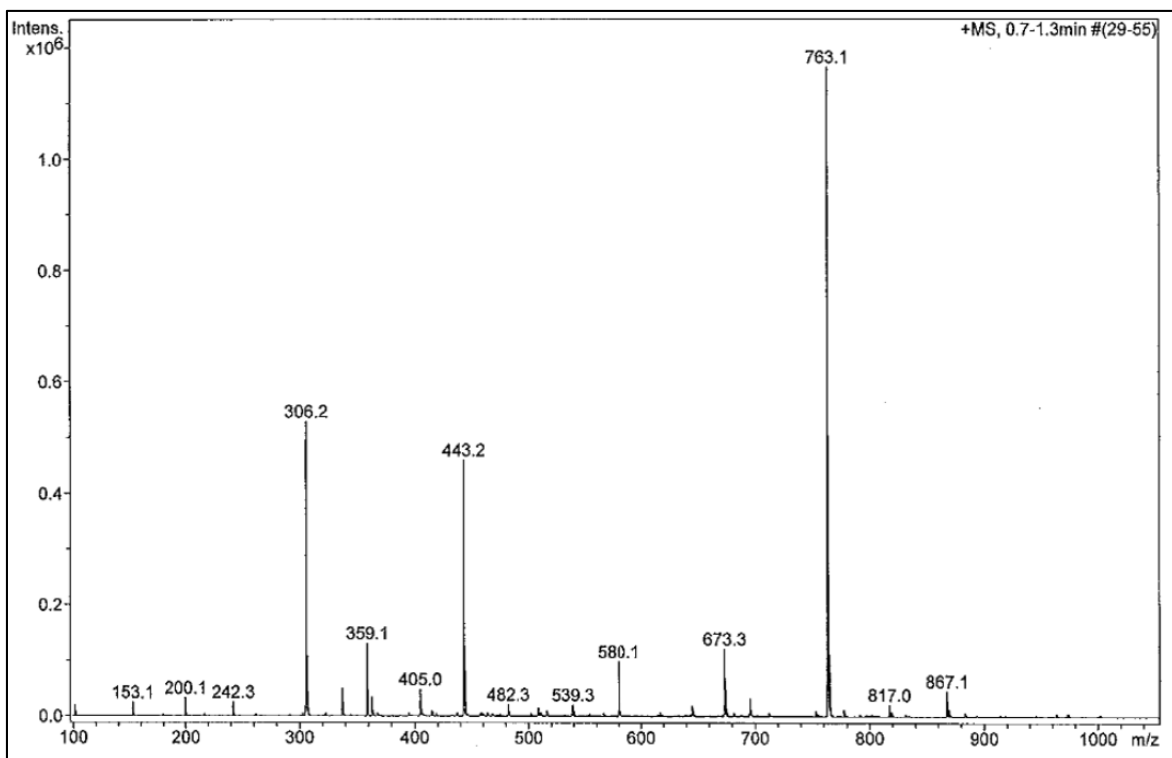




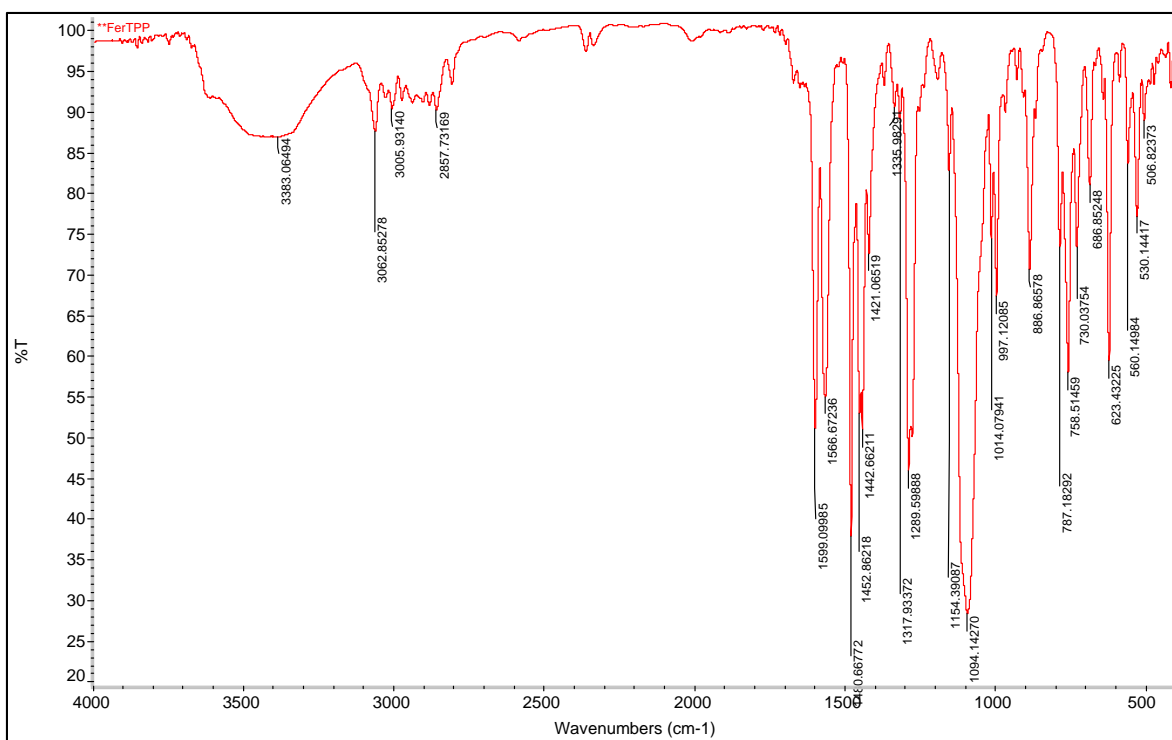


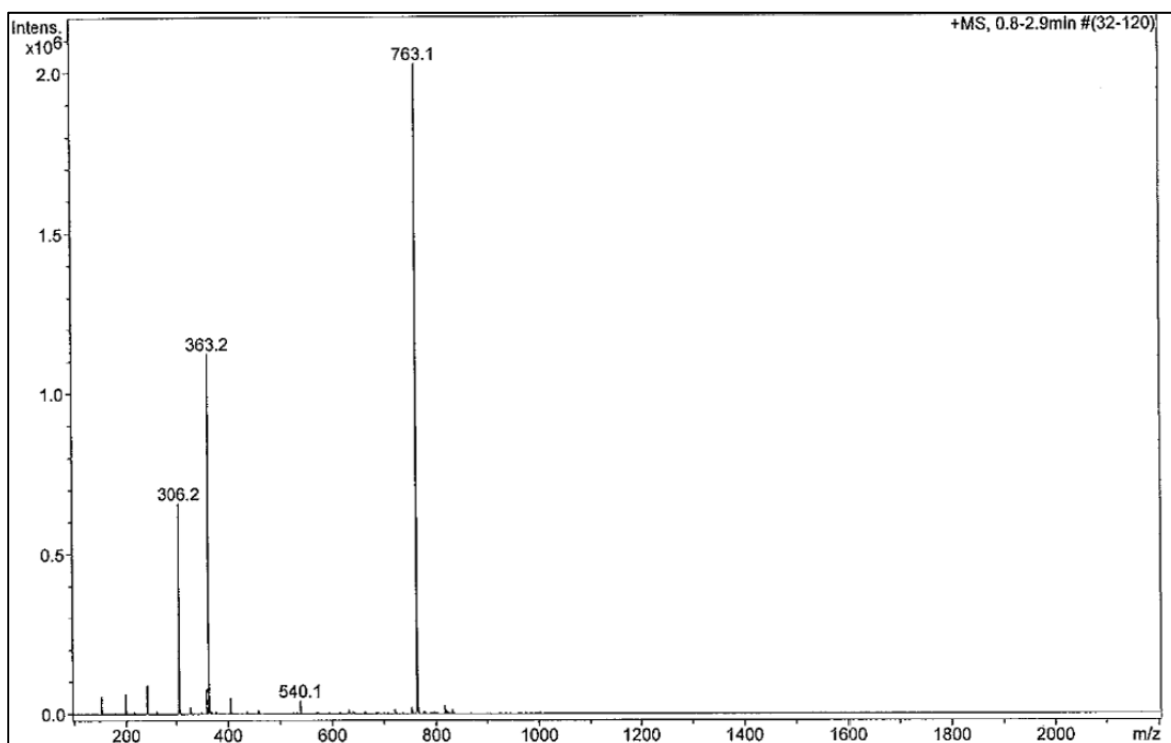
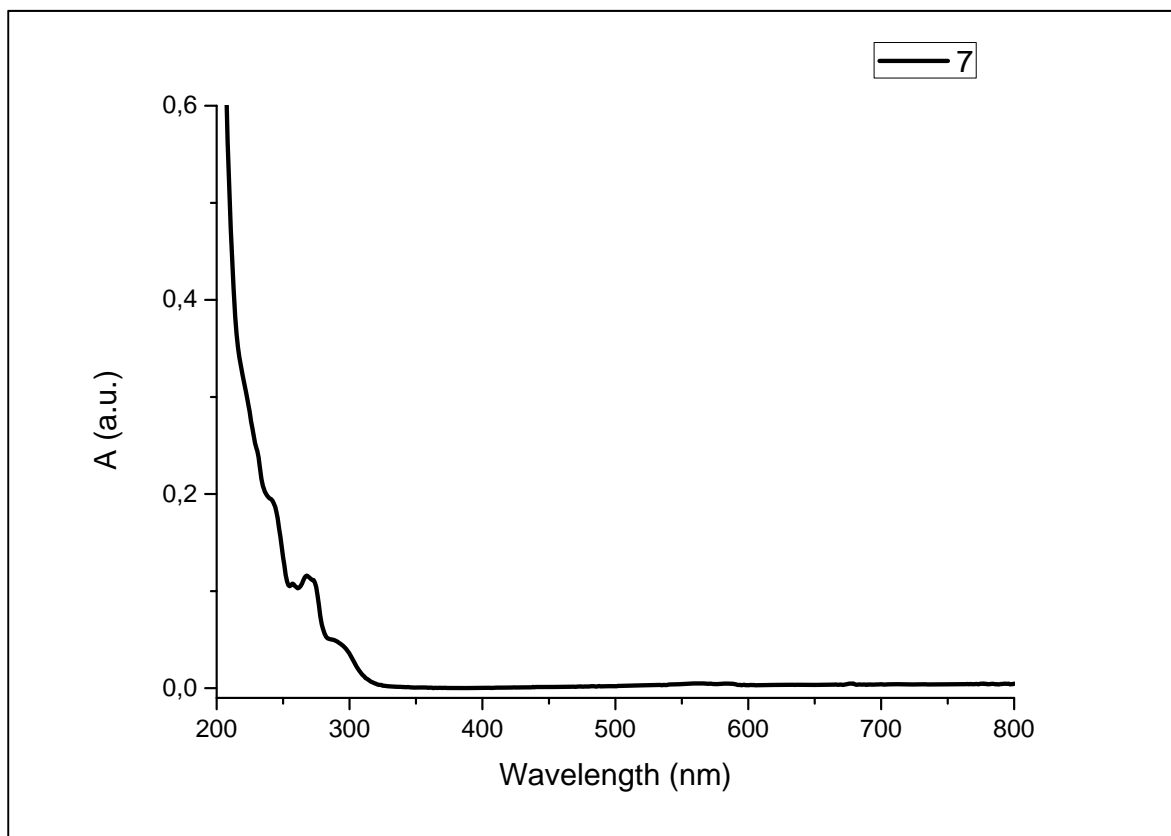
-Compound 6



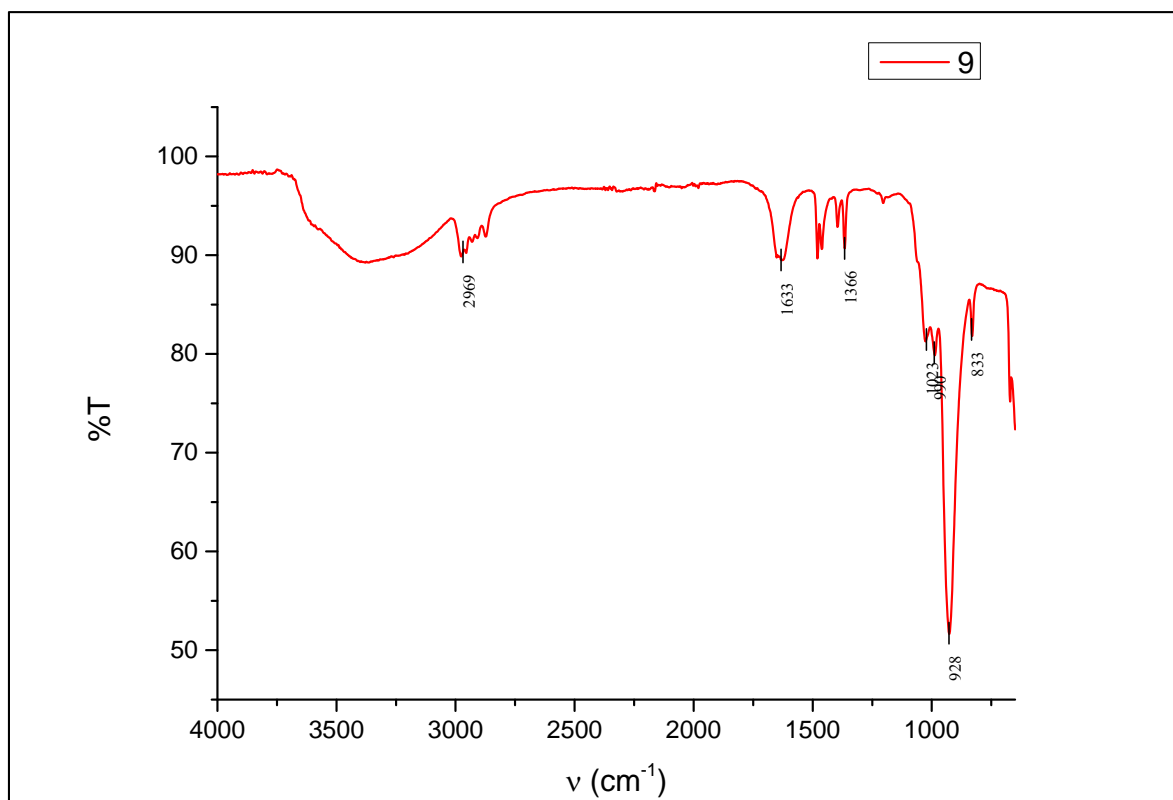


-Compound 7

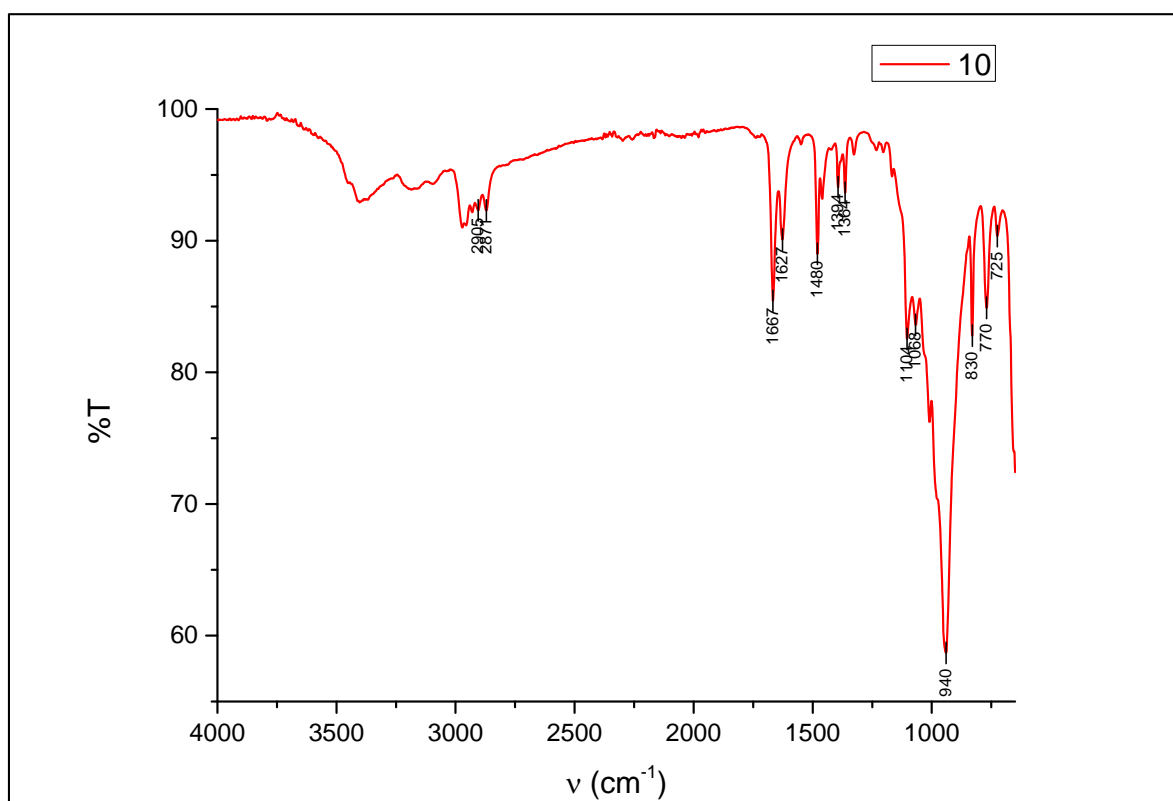




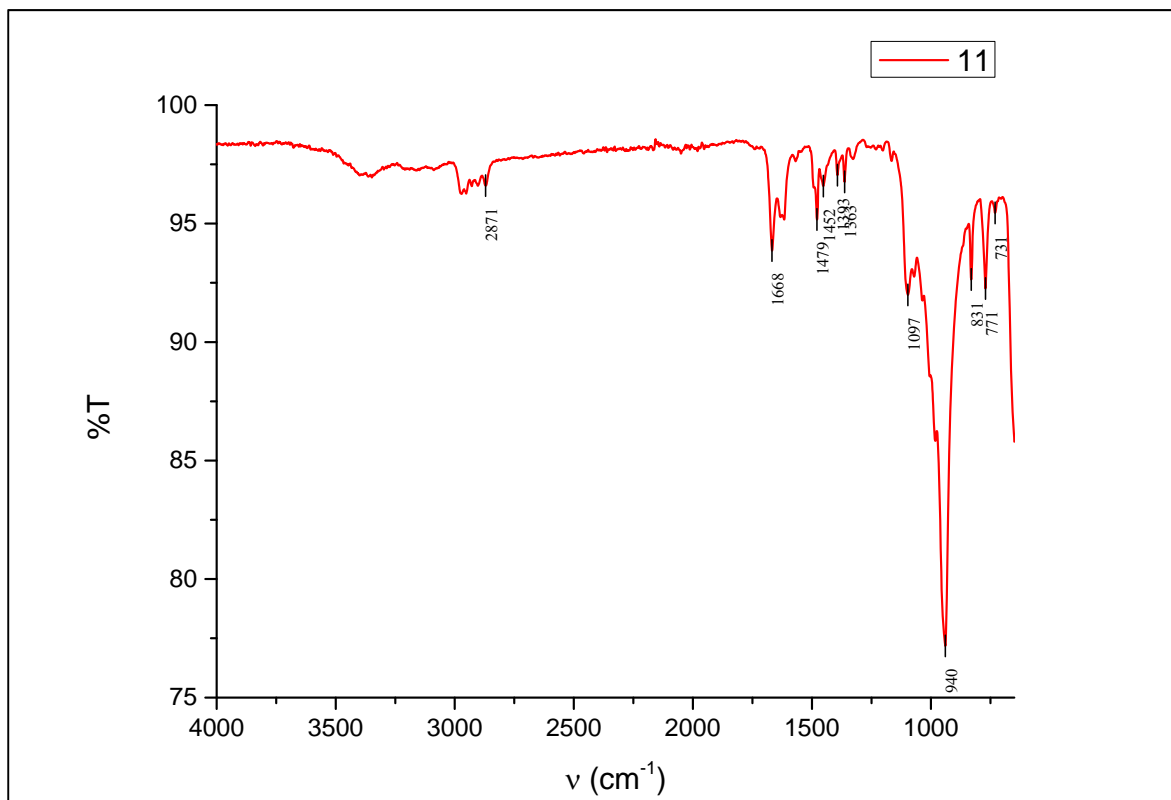
## -Compound 8



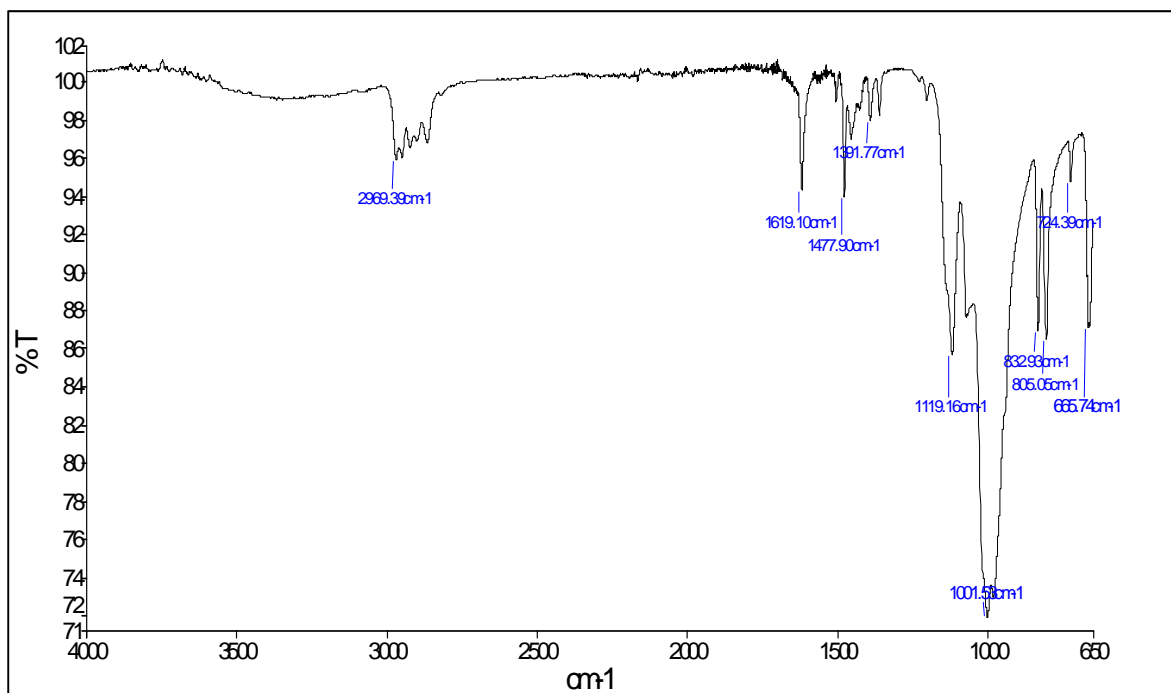
## -Compound 9



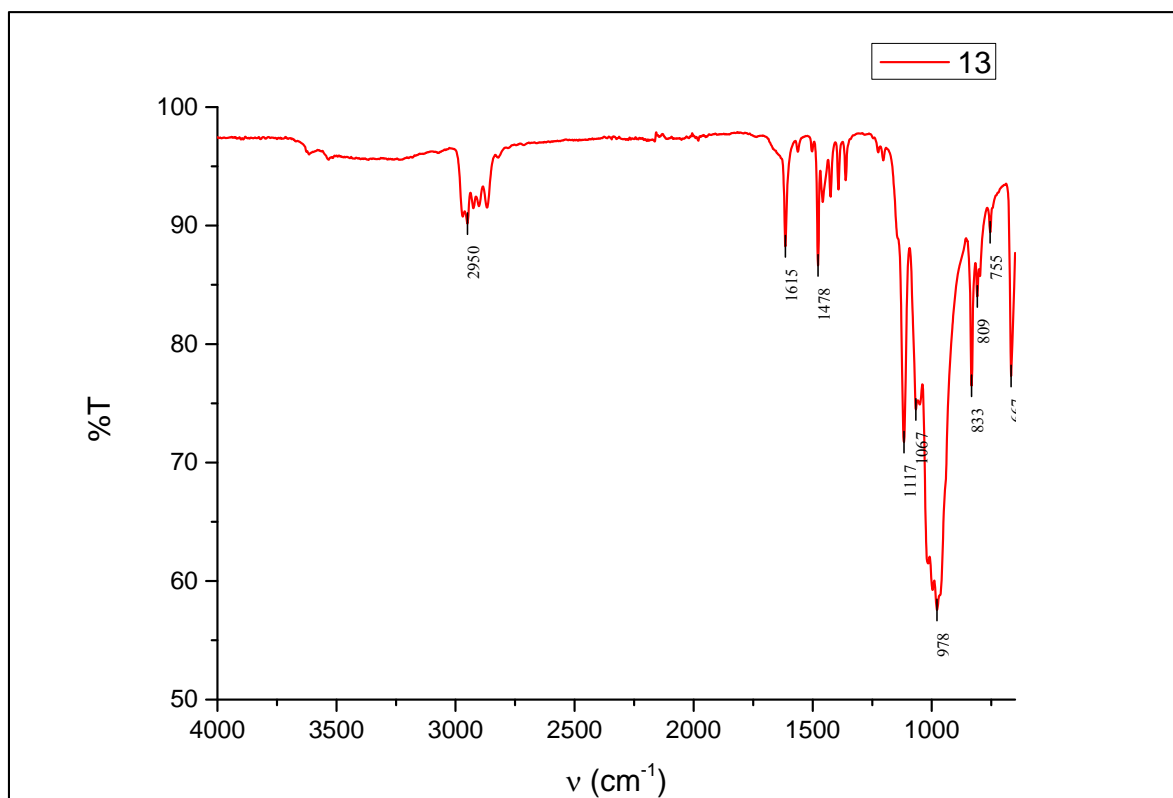
-Compound 10



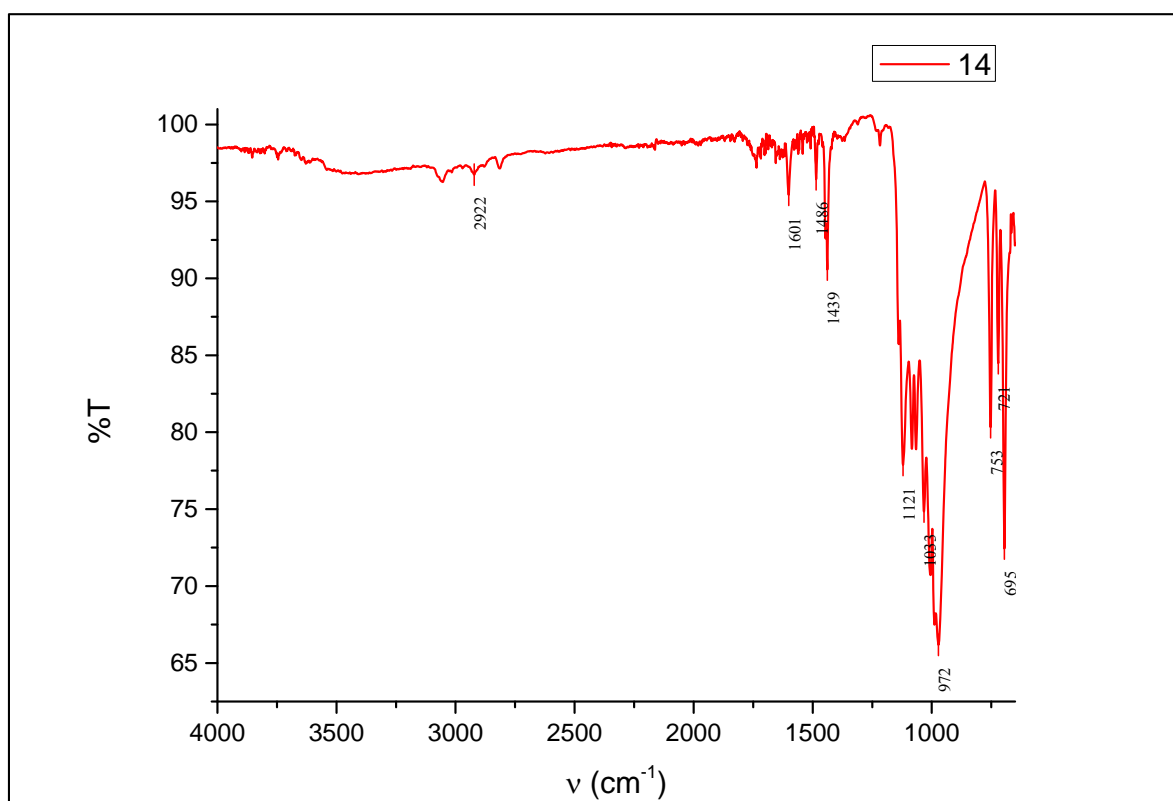
-Compound 11



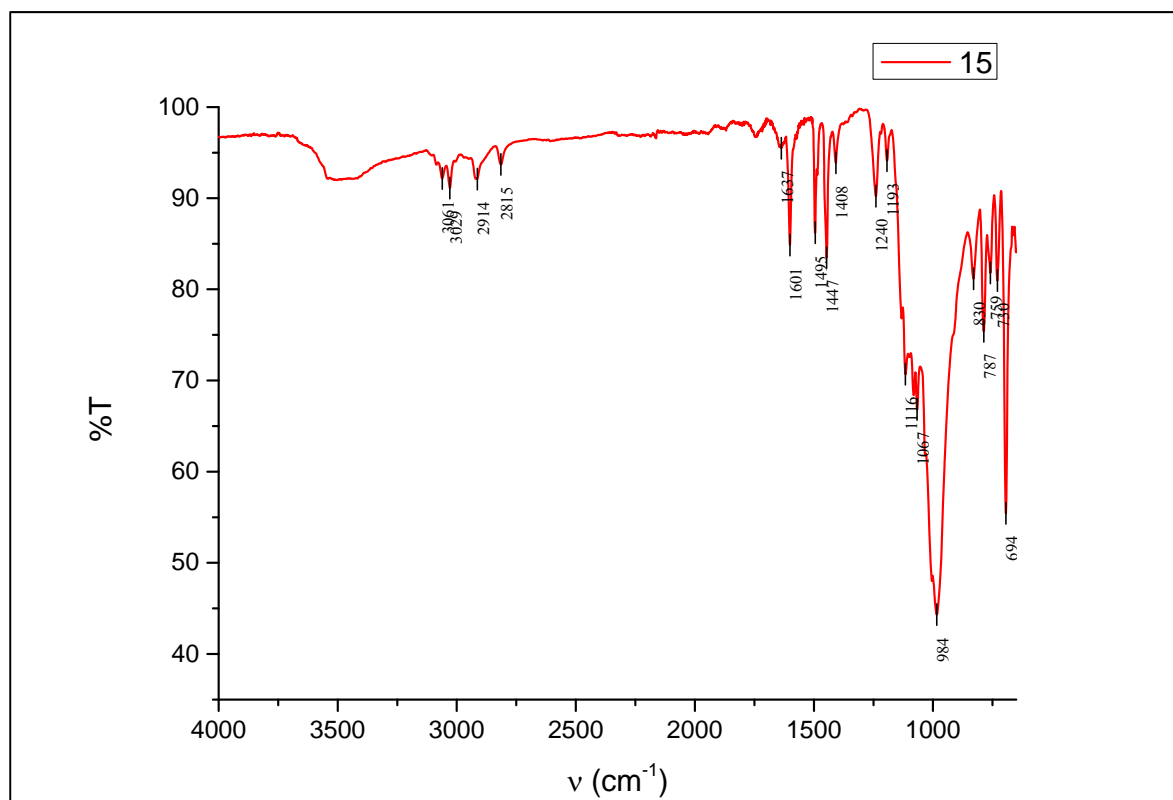
## -Compound 12



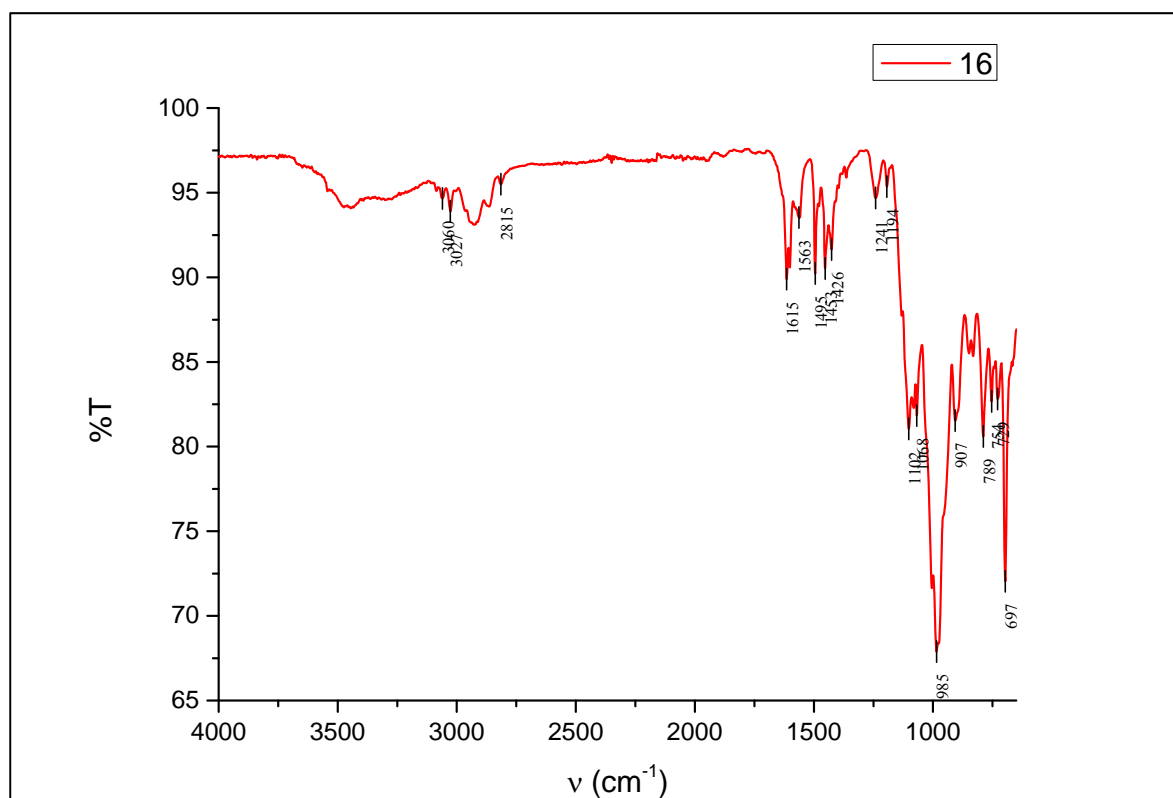
## -Compound 13



-Compound 14

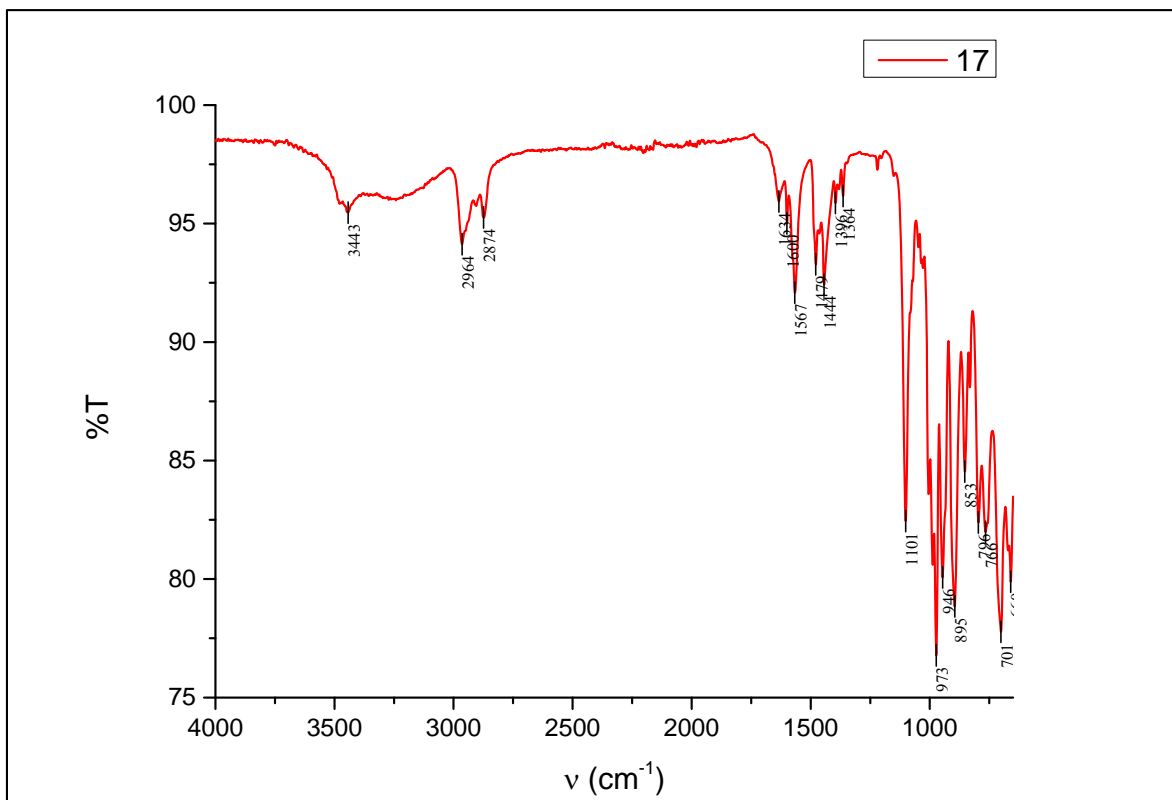


-Compound 15





## -Compound 16



## -Compound 17

